ANALYTICAL STUDY OF THE FATIGUE BEHAVIOR
OF A LONGITUDINAL-TRANSVERSE
STIFFENER INTERSECTION

APPROVED:

Karl A. Frank

Joseph A. Yura

To my parents,
Jack and Dolly, for their
love and support

ANALYTICAL STUDY OF THE FATIGUE BEHAVIOR OF A LONGITUDINAL-TRANSVERSE STIFFENER INTERSECTION

by

DAVID ALAN PLATTEN, B.S.C.E.

THESIS

Presented to the Faculty of the Graduate School of

The University of Texas at Austin

in Partial Fulfillment

of the Requirements

for the Degree of

MASTER OF SCIENCE IN ENGINEERING

THE UNIVERSITY OF TEXAS AT AUSTIN

May 1980

ACKNOWLEDGMENTS

The analytical study reported herein was conducted at the Phil M. Ferguson Structural Engineering Laboratory, Department of Civil Engineering, The University of Texas at Austin. The work was part of a study of the fatigue performance of structural steel bridge details sponsored by the Texas Department of Highways and Transportation under Study Number 3-5-79-247. The study was supervised by Professors Karl H. Frank and Joseph A. Yura.

The author is indebted to Dr. Karl H. Frank, the supervising professor, for his guidance and total involvement. Special thanks are also given to Dr. Joseph A. Yura for his helpful comments and suggestions.

Sincere thanks are due various support personnel of the Phil M. Ferguson Structural Engineering Laboratory. Mr. Richard Marshall and Mr. Dan Perez supervised and assisted in the building and maintenance of electronic data acquisition equipment. Mrs. Laurie Golding aided in the purchasing of the many items required for field testing. Mr. Gorham Hinckley and Mr. George Moden contributed suggestions which minimized unproductive efforts in the laboratory. Mrs. Maxine DeButts and Mrs. Tina Robinson carefully typed the manuscript.

Mr. Frank Endres developed the computer software needed to reduce large amounts of field test data, and the author is grateful to him.

Special thanks are given to Research Assistants Antonio Leite and Ashok Gupta for their assistance in the areas of computer work, laboratory work, and field testing.

D.A.P.

The University of Texas at Austin
January 1980

Results of finite element analyses performed on the longitudinal-transverse stiffener intersection detail are used to develop a preliminary design for an experimental test specimen. In the future, laboratory fatigue tests will be conducted with results being compared to those of the current study.

TABLE OF CONTENTS

Chapter Page

LIST OF TABLES

Table

Page

LIST OF FIGURES

Figure

Page

CHAPTER 1

INTRODUCTION

1.1 Current Bridge Fatigue Specifications

The fatigue behavior of a structural steel bridge detail is a function of the live load stress range at the detail, the frequency of occurrence of repetitive loadings, and the severity of the weld detail. The current American Association of State Highway and Transportation Officials (AASHTO) Specifications provide a means of classifying bridge details into various categories depending on the fatigue severity of the detail.

Over the past several years, a great deal of research has been conducted to determine the effects of cyclic loadings on highway bridges. Most of the work has been performed at Lehigh University in the form of a comprehensive study on "The Effect of Weldments on the Fatigue Strength of Steel Beams" [1,2]. The study was designed to determine the significance of the parameters believed to be important in fatigue behavior. Test results indicated that fatigue design could be based on a log-log relationship of stress range and cyclic life. In addition, a variety of welded bridge details were classified into categories according to their susceptibility to fatigue. Figure 1.1 summarizes these findings in the form of recommended design curves. The classification of structural details by stress categories essentially amounts to a classification by severity of local stress gradients. These provisions were first adopted by AASHTO in 1973, with minor revisions having been made in 1975, 1976, and 1977 in light of continuing laboratory studies.

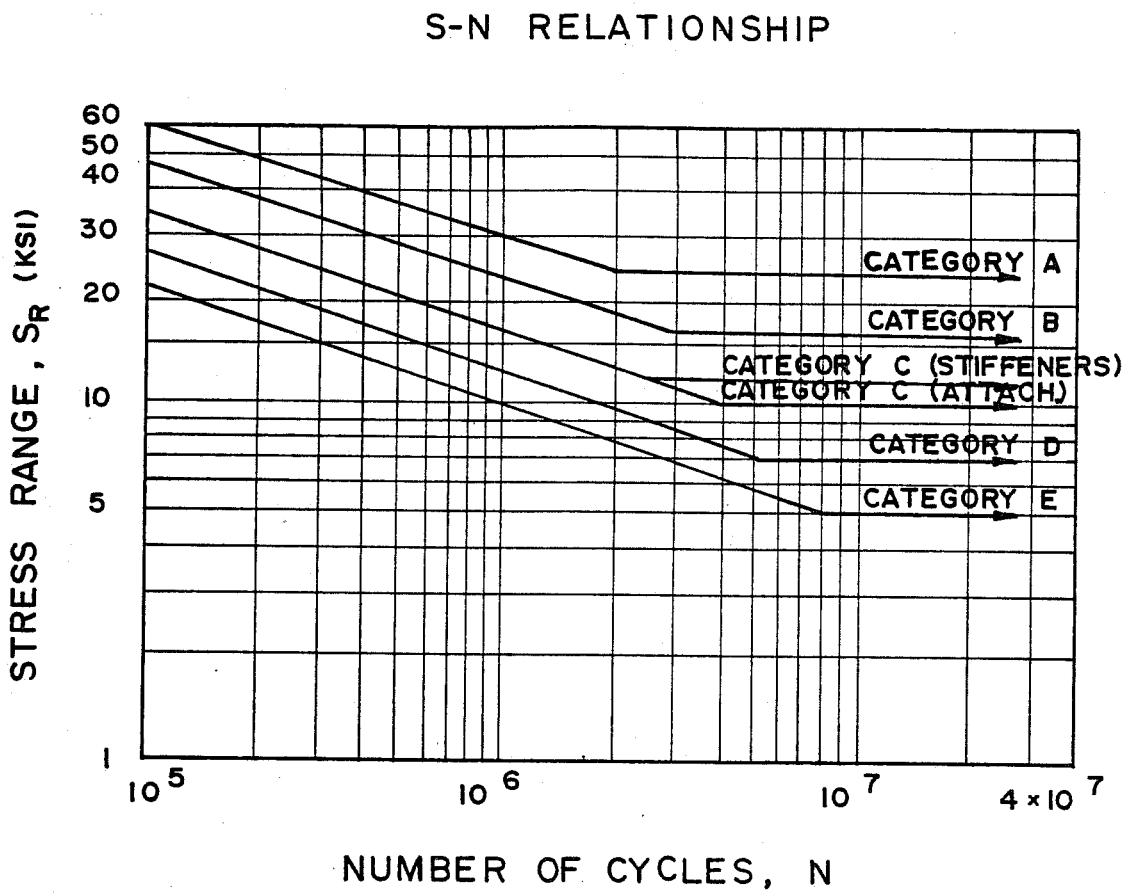

Fig. 1.1 Design stress range curves for Categories A through E

Recently, a new lower fatigue resistance category, Category E′, was established based on test results of cover plate details with flange thicknesses greater than 1.25 in. [3]. Figure 1.2 shows the relationship between Category E′ and the previous lower bound Category E. These findings establish a very important point. Although earlier studies classified many existing bridge details, many more details exist which are not covered by current specifications. Additional research is needed to attempt to categorize these details to provide an accurate determination of their fatigue lives.

1.2 Problem Statement

The University of Texas Phil M. Ferguson Structural Engineering Laboratory is currently conducting an evaluation of the fatigue life of various structural steel bridge details. The study is sponsored by the Texas Department of Highways and Public Transportation and the Federal Highway Administration. The steel bridges being studied contain details which have questionable fatigue resistance based on current specifications. The bridges were designed in the late 1960's, prior to the adoption of the new fatigue provisions which now appear in the AASHTO Bridge Specifications. Most of the bridges are twin girder spans with intersecting floor beams spaced 18 ft on center. The lack of redundancy of the structural framework results in a situation in which a fracture may cause serious damage or even failure of the structure. It is, therefore, apparent that an accurate determination of the fatigue lives of the existing bridge details is needed to establish the useful life of the bridge structure.

Among the various details under study, one detail stands out as a potential source of concern. This detail occurs repeatedly throughout the bridge structure at locations of longitudinal girder-to-floor beam connections. Sections A and B of Fig. 1.3 pinpoint

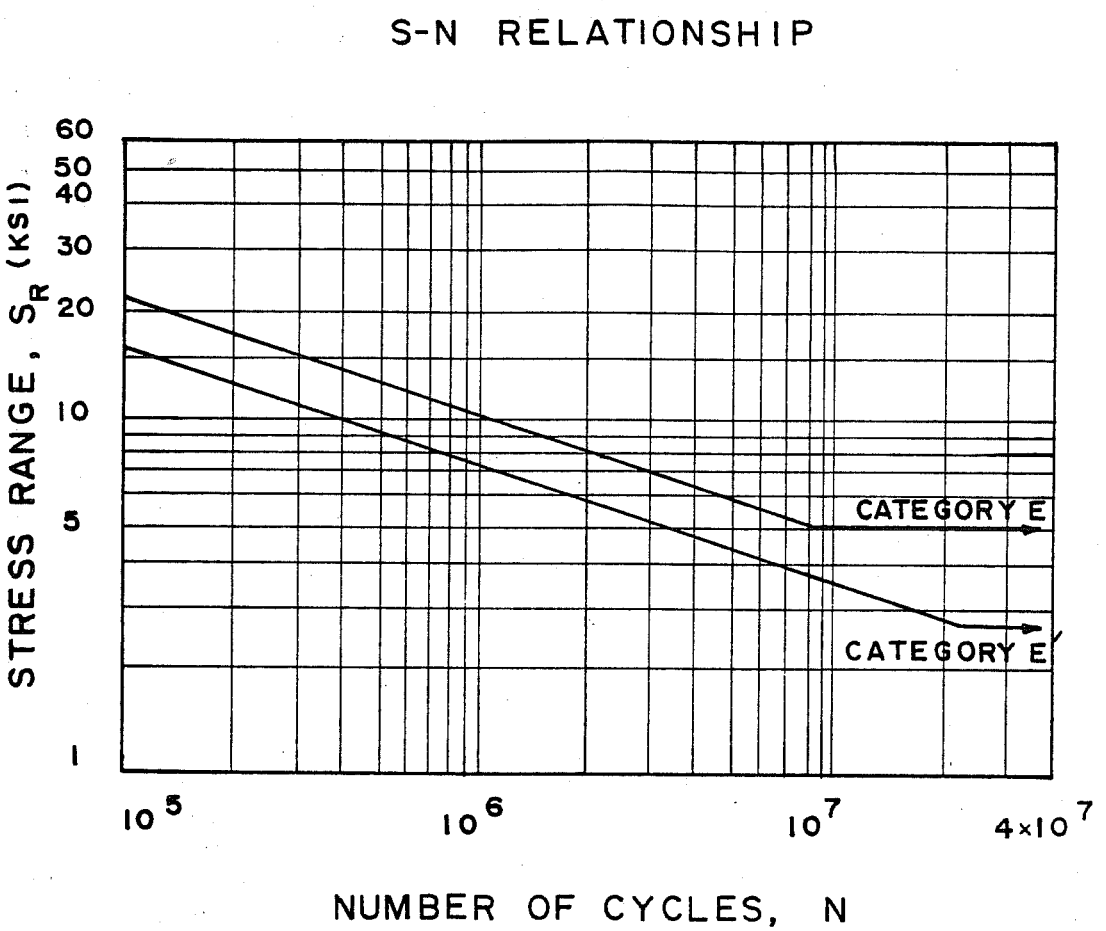

Fig. 1.2 Relationship between design stress range curves for Categories E and E′

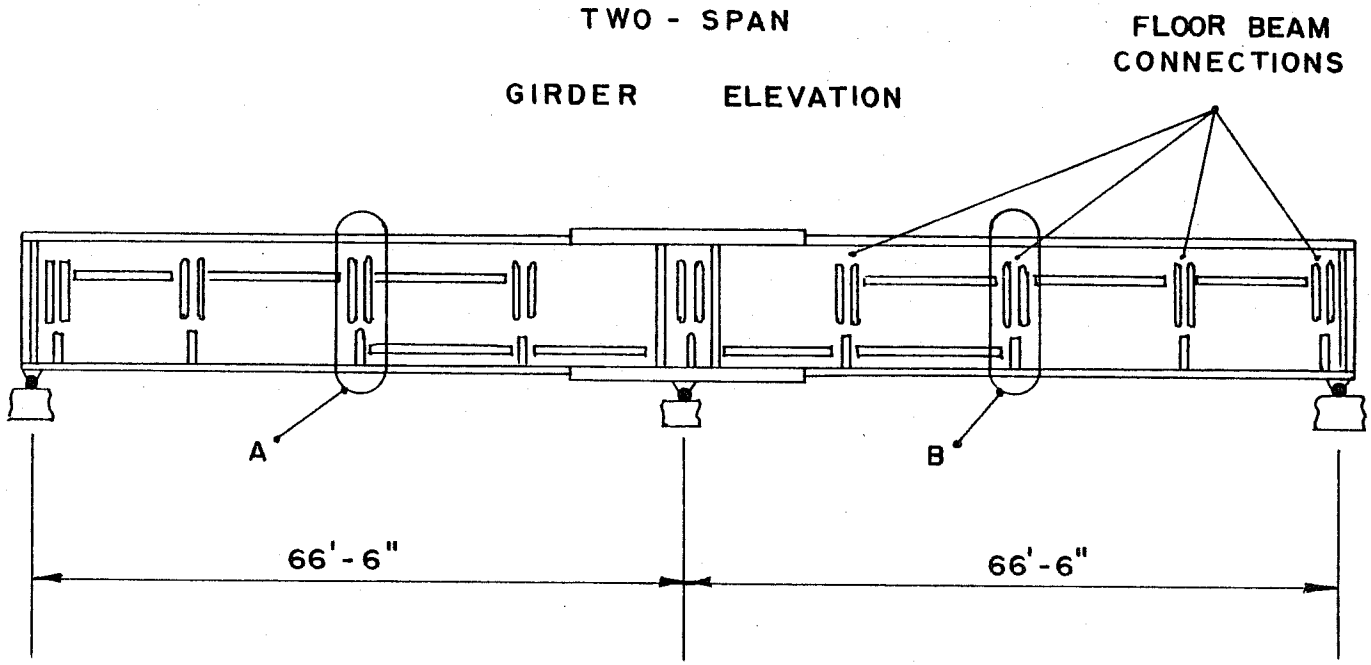

Fig. 1.3 Critical longitudinal-transverse stiffener intersection in a two-span bridge girder (Sections A and B)

the location of the detail in question within a typical two-span girder arrangement. Figure 1.4 shows the floor beam-to-plate girder connection in greater detail. Since attachments located in compressive stress regions are not fatigue critical, attention should be focused on areas subjected to tensile stresses. The span being considered is continuous; therefore, the possibility of some stress reversal at the detail does exist. However, these levels of stress can be assumed to be sufficiently small relative to levels of maximum stress. Therefore, the lower portion of the girder-floor beam detail should be examined for fatigue susceptibility. More specifically, the intersection of the transverse stiffener and the longitudinal stiffener shown in detail "A" of Fig. 1.4 needs to be evaluated.

When transverse and longitudinal stiffeners are used, each results in a weld termination as shown in Fig. 1.5. Since the transverse stiffener can be considered a short attachment in the direction of applied stress, it is governed by the Category C design condition. However, the longitudinal stiffener is a long attachment, the end of which is governed by the Category E design condition. A more desirable condition, shown in Fig. 1.6, is achieved if the transverse stiffener is placed on one side of the web and the longitudinal stiffener on the other. Category C still applies to the transverse stiffener, but the longitudinal stiffener welds are now continuous, in which case Category B is applicable. For the detail being considered, however, the presence of the floor beams on both sides of the girder web forced the undesirable situation depicted in Fig. 1.5, resulting in a longitudinal-transverse stiffener intersection.

Given the fact that a longitudinal-transverse stiffener intersection exists, current fatigue specifications recommend that fillet welds for longitudinal stiffeners be terminated short of

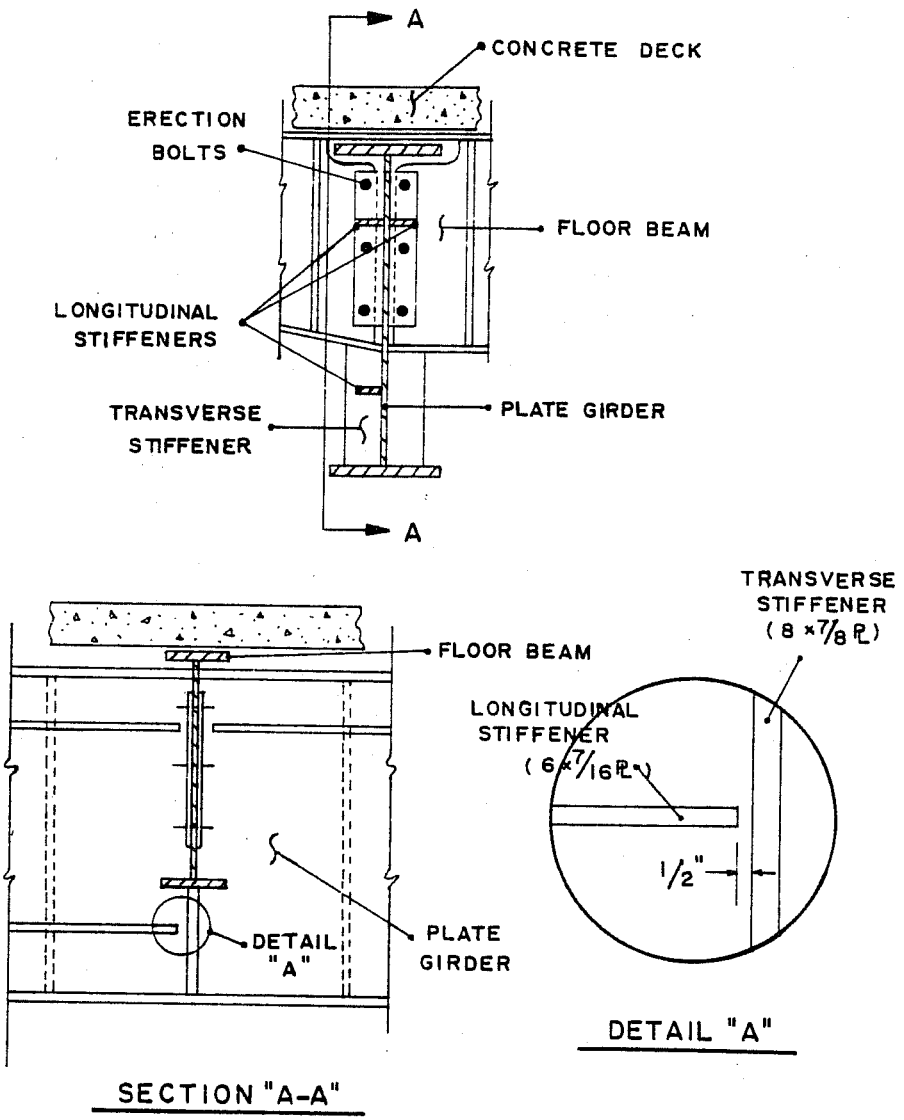

Fig. 1.4 Floor beam-to-plate girder connection

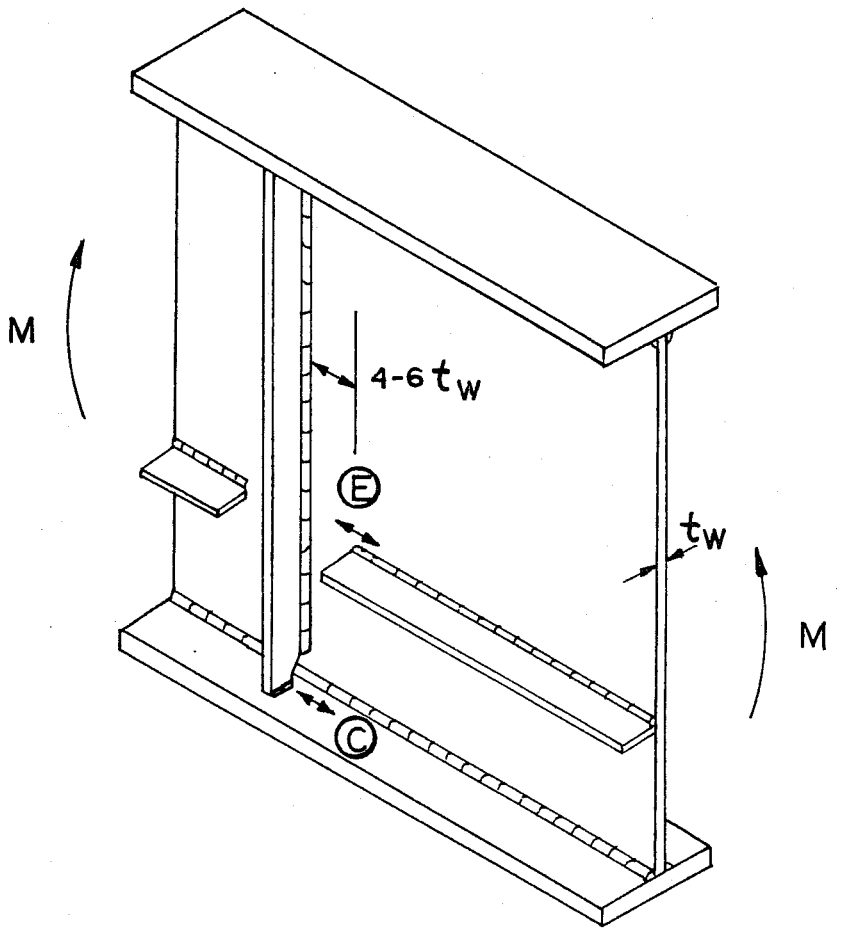

Fig. 1.5 Longitudinal and transverse stiffeners

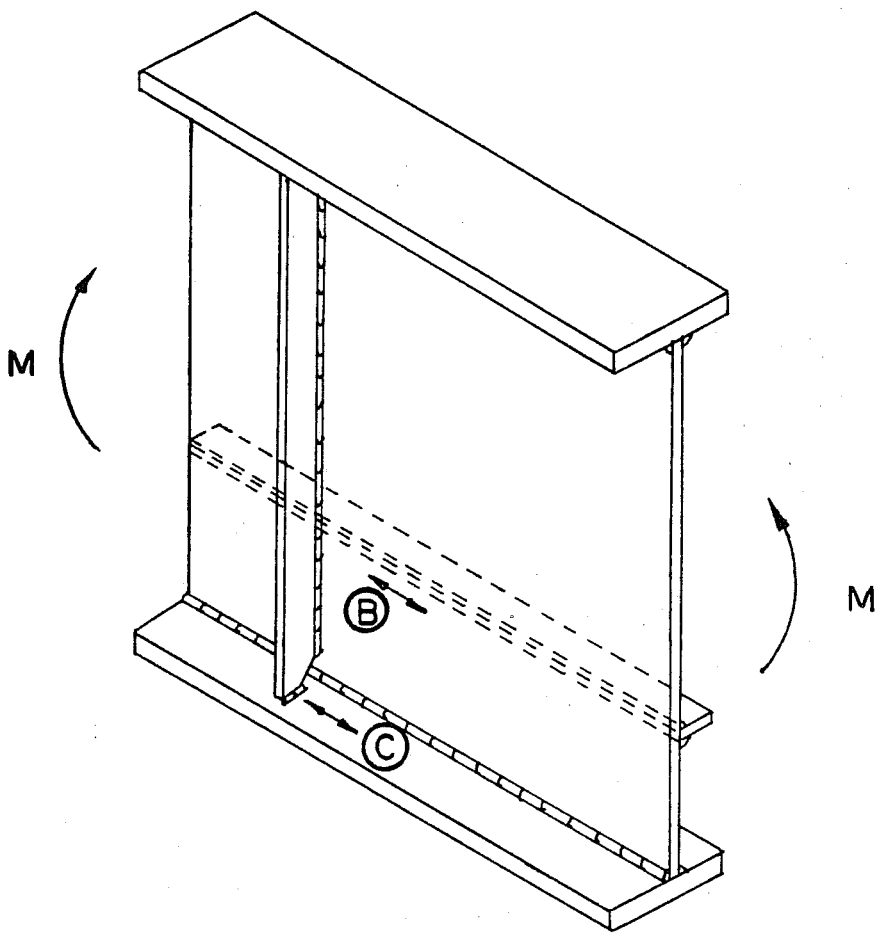

Fig. 1.6 Longitudinal and transverse stiffeners placed on opposite sides of girder web

web-to-transverse stiffener welds by a distance of at least four to six times the web thickness, as shown in Fig. 1.5. Previous tests [2] have indicated that failure to terminate longitudinal stiffener welds a suitable distance short of transverse stiffener welds can result in adverse behavior due to restraint stresses introduced by weld shrinkage. As can be seen in Fig. 1.4, the clear distance between the transverse stiffener and the longitudinal stiffener end is only 1/2 in. Considering the presence of the 5/16 in. web-to-transverse stiffener fillet weld and the 5/16 in. web-to-longitudinal stiffener fillet weld, it is observed that a weld overlap exists in the gap between the transverse and longitudinal stiffeners. This situation results in a possible stress concentration greater than that of a Category E detail. If this were the case, the existing bridge detail could exhibit a very low fatigue life. Clearly, the proximity of the longitudinal-transverse stiffener intersection raises a question with respect to the fatigue severity of the detail.

1.3 Objectives

The primary objective of this study is to establish an analytical estimate of the fatigue life of a longitudinal-transverse stiffener intersection bridge detail. A finite element model of the detail in question is utilized to determine the influence of geometry on the stress at the end of the longitudinal stiffener weld. Fracture mechanics principles are employed to achieve an estimate of the fatigue life of the structural steel bridge detail.

In addition to the primary objective, several secondary objectives are given significant consideration. Specifically, the current study strives to aid in the development of an experimental test specimen, to determine the adequacy of current fatigue design specifications, and to propose recommended design details for future use.

The analytical aspects with which this study deals are only a part of the previously mentioned research project being conducted at the Phil M. Ferguson Structural Engineering Laboratory. Eventually, laboratory fatigue tests will be conducted on test specimens which model the geometry of the details used on the twin girder bridge being studied. The results of such tests will be compared and combined with the analytical results of this study to yield data and information regarding detail fatigue life. The intent of this study is to provide information which will aid in the development of a test specimen that economically models the longitudinal-transverse stiffener intersection detail. Analytical results should provide geometric information which can be used to determine the scale and relative dimensions of an experimental test specimen. A comparison of field test data with analytical data can be expected to be useful in selecting an appropriate loading scheme to test the experimental model.

It has already been noted that current AASHTO fatigue specifications are limited in scope. Only those details which have been the subjects of recent research projects are treated. Many existing details resemble those currently covered by specification, but closer inspection of these details reveals inherent differences. The longitudinal-transverse stiffener intersection is an example of such a detail. This bridge detail appears to be a Category E detail at first glance. However, the narrow gap between the transverse stiffener weld and the longitudinal stiffener end does not conform to specifications. This study will strive to determine whether the current design specifications adequately cover the detail under consideration.

Finally, results of analytical investigations and field tests will be studied, with recommendations being made regarding the future design of longitudinal-transverse stiffener details.

Presently, this type of detail can be considered a Category E detail at best. This study will examine alternate methods of design and will propose recommended design details. Efforts will be concentrated on the potential effectiveness of a cope detail in which the longitudinal stiffener is actually welded to the transverse stiffener. This type of detail, illustrated in Fig. 1.7,is believed to fall somewhere between Category B and Category E with regard to fatigue severity. Analytical data will serve to clarify the degree of improvement, if any, in the fatigue performance of the longitudinal-transverse stiffener intersection modified by the cope detail.

1.4 Solution Approach

The fatigue resistance of a welded steel structure is affected by initial defects which are built into the structure during fabrication operations. Such defects can result from lack of fusion, porosity, toe cracks, or even a weld arc strike. Good fabrication and inspection practice can minimize the size and number of built-in discontinuities, but it cannot eliminate defects entirely. The manner in which such defects are modeled for purposes of fracture mechanics analysis, originally presented by Irwin [4], is to represent them as cracks. The quantitative measure of the severity of the crack is then given by the stress intensity factor, K, which serves to characterize the intensity of the stress field in a local region surrounding the leading edge of the crack. The stress intensity factor is a function of the applied stress, the crack size, and the geometric configuration of both the crack and the body in which the crack is located.

Two basic applications of linear elastic fracture mechanics exist relative to structural design. The first application involves designing against fracture by equating the value of K to

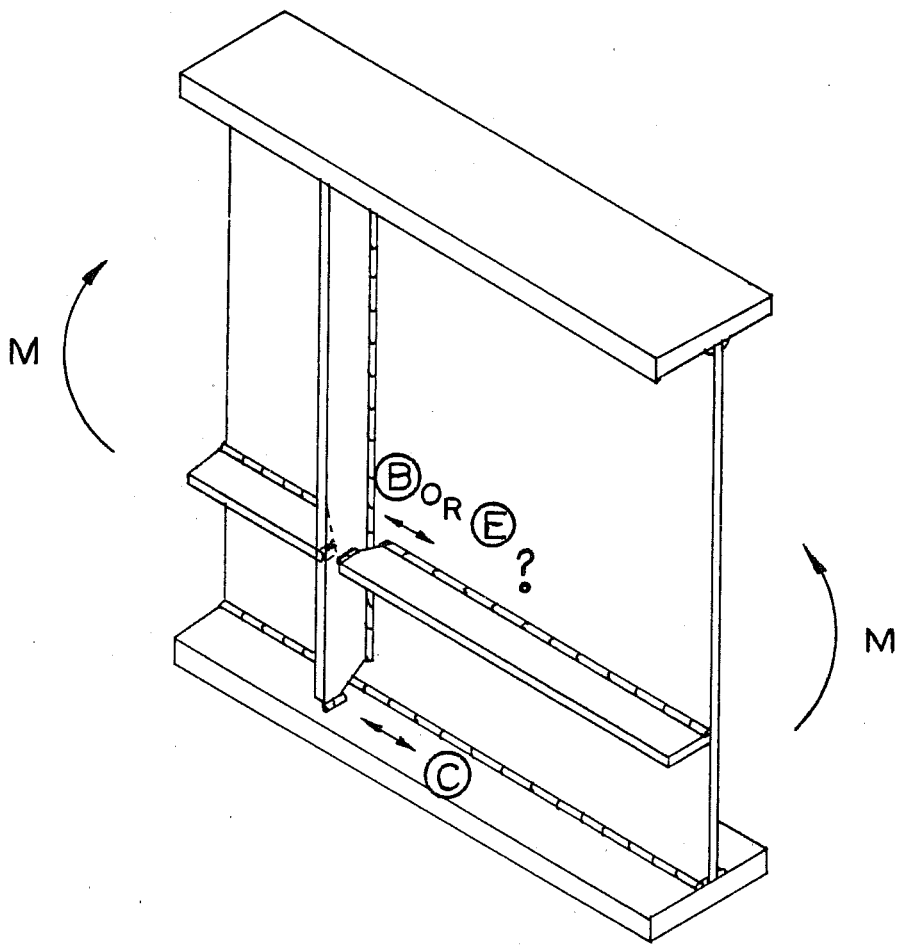

Fig. 1.7 Cope detail in which transverse and longitudinal stiffeners are welded together

to the critical value, K_C (a material property called fracture toughness), to determine those combinations of crack size and applied stress which result in sudden fracture. This study deals with the second application which involves fatigue crack growth. Under repeated load cycling, stable crack propagation occurs at values of K less than the critical value, K_C. The rate of crack propagation depends on ΔK, the range of the stress intensity factor. Crack growth per cycle, da/dN, can be empirically related to ΔK as follows:

$$da/dN = C(\Delta K)^n \tag{1.1}$$

where C and n are material constants. Equation 1.1 may be rearranged and integrated between the initial crack size, a_i, and the final crack size, a_f, as follows:

$$N = 1/C \int_{a_i}^{a_f} 1/(\Delta K)^n \, da \tag{1.2}$$

This produces a straight line on a log-log plot of stress range (S_r) vs number of cycles (N). Points of the S-N curve which deviate from the straight line relationship can be interpreted as variations in geometry and flaw size. The fatigue life, or the number of cycles required to propagate a crack from initial to final size, can thus be determined.

To utilize the fracture mechanics principles presented above, a means of computing the range of stress intensity must be selected. Several methods of obtaining K values are available. The compliance analysis method may be used to obtain an experimental determination of K values. Numerical techniques include closed-form analytical solutions, finite element techniques aided by special crack tip elements and solutions using the Green's Function [10] approach.

1.4.1 Compliance Analysis. The compliance analysis method [5,6] of determining stress intensity factors involves analyzing the results of an experimental test. A typical test specimen, the single edge-notch tension specimen, is shown in Fig. 1.8. Initially, a crack of length a_1 is introduced. A fixed load, P, is imposed and the corresponding displacement, ℓ_1, is measured. This procedure is repeated for a series of crack lengths. Load vs. displacement curves are plotted for each crack size, as shown in Fig. 1.8(a). The compliance of the specimen at each crack size is defined as the inverse of the slope of the corresponding load-displacement curve. A plot of compliance vs. crack size, shown in Fig. 1.8(b), may then be constructed. The strain energy release rate, G, may then be found as a function of dc/da, the slope of the compliance-crack size curve. Irwin presented a study which showed a direct relationship between G and K, the stress intensity factor [4]. As a result, K can be obtained based on data taken from a compliance analysis test specimen.

Recently, Frank [7] and Gurney [8] have applied finite element techniques to the compliance analysis problem. A finite element analysis, rather than an experimental test, is conducted for each crack length. Using the values of displacement generated by the finite element analysis, the strain energy release rate may be found as in the experimental approach. Since a finite element analysis is necessary for each crack size, this approach is potentially expensive in terms of computer time. In addition, new finite element mesh data must be generated for each crack size.

1.4.2 Closed-Form Solutions. Closed-form analytical solutions currently exist only for idealized geometries, such as a central crack in an infinite plate. This type of solution is difficult to obtain for most cracks because of geometric discontinuities. Changes in the cross-sectional dimensions of a

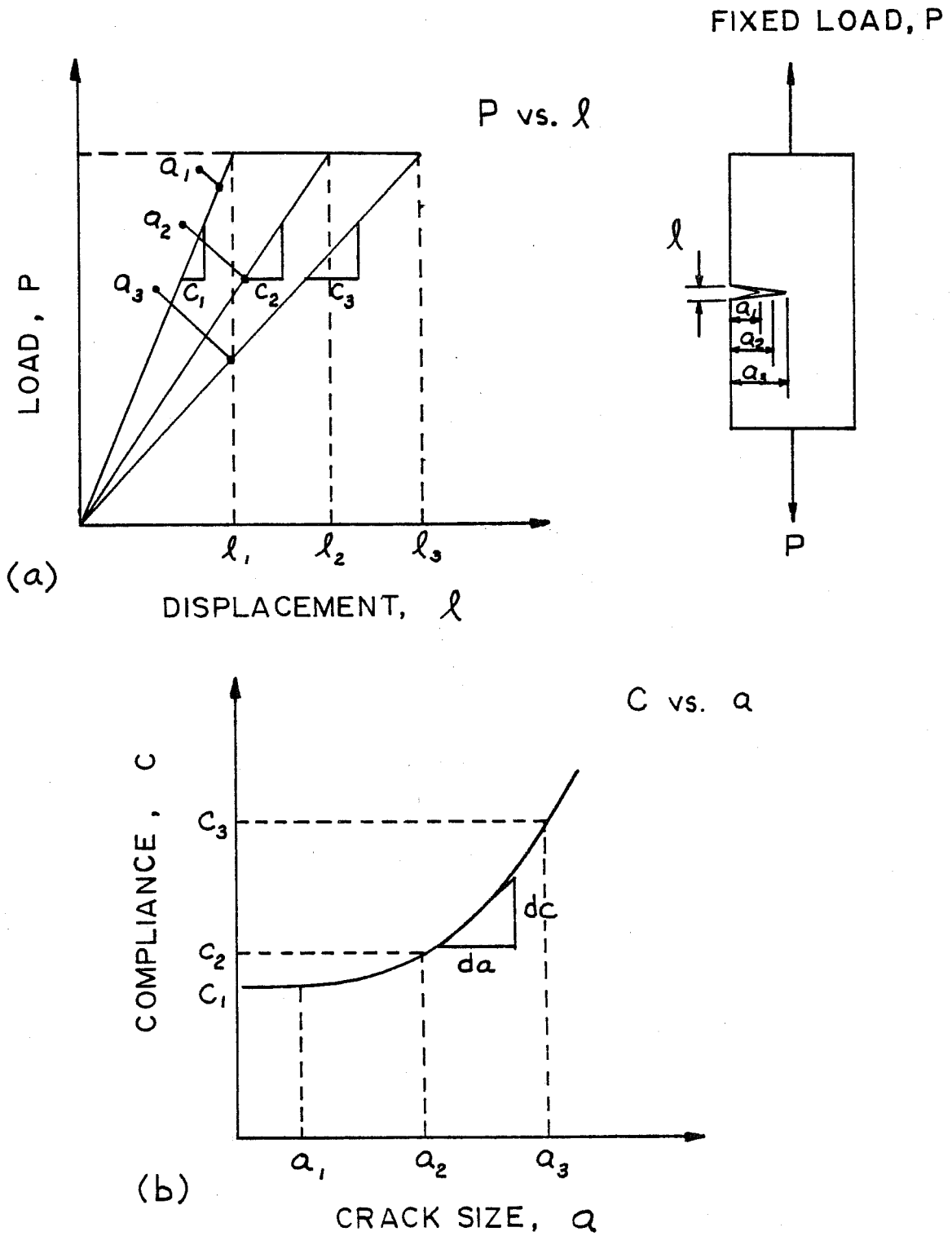

Fig. 1.8 Compliance analysis method

structural member produce nonuniform stress fields not related to the presence of a crack. Additional complications arise due to the three-dimensional aspect of both the structural configuration and the crack shape. Therefore, a numerical solution must be obtained for all practical problems.

1.4.3 Crack Tip Finite Elements. One numerical method of obtaining K values is the finite element technique aided by crack tip elements which possess inverse square root singularities. This method is similar to the finite element approach to the compliance analysis problem, except that the crack is modeled using crack tip elements. Stress and displacement near the crack tip are related to stress intensity which can be output directly from the finite element analysis. Unfortunately, the crack tip finite element method possesses disadvantages similar to those encountered when applying the finite element compliance analysis method. Preparation of lengthy input data along with the cost of required computer time make the solution of practical problems using the crack tip element method difficult to justify.

1.4.4 Green's Function Approach. The Green's Function technique was originally used by Kobayashi [9], who successfully estimated results of previous investigations. Subsequently, Albrecht [10] and Zettlemoyer [11,12] used the technique on fillet-welded joints and bridge details.

The Green's Function approach consists of a geometry correction factor which is added to accepted solutions for two-dimensional and three-dimensional crack problems in finite plates and bodies. The correction factor, F_g, accounts for the nonuniformity of the stress field at a structural detail. The procedure requires only a single finite element computation of stresses for the uncracked body. K values for any crack size may then be

determined by removing the normal stresses along the line where the crack is inserted.

In his work, Albrecht selected the Green's Function corresponding to the crack loading shown in Fig. 1.9(a) [10]. This configuration assumes a through-thickness crack located in an infinite plate subjected to two equal pairs of splitting forces, P, applied at $x = \pm b$. The stress intensity is given by:

$$K = \frac{2P}{\sqrt{\pi a}}\left(\frac{a}{\sqrt{a^2-b^2}}\right) \tag{1.3}$$

where $2/\sqrt{\pi a}\ (a/\sqrt{a^2-b^2})$ is the Green's Function. If the forces are distributed rather than concentrated, yet still symmetric with respect to the center of the crack, the splitting forces can be expressed as the sum of the stresses, σ_b, applied over an infinitesimal length, db, as illustrated in Fig. 1.9(b). The effect of distributed forces on K can thus be given by the integral:

$$K = \frac{2a}{\sqrt{\pi a}} \int_0^a \frac{\sigma_b}{\sqrt{a^2 - b^2}}\, db \tag{1.4}$$

Discretized stresses, σ_b, are obtained from a finite element analysis. Equation 1.4 can then be written as:

$$K = \sqrt{\pi a}\, \frac{2}{\pi} \sum_{i=1}^{n} \sigma_{b_i} \int_{b_i}^{b_{i+1}} \frac{1}{\sqrt{a^2 - b^2}}\, db \tag{1.5}$$

where the discrete stress, σ_{b_i}, is applied over the element width from b_i to b_{i+1}. Integrating Eq. 1.5 and factoring out the mean stress, σ, leads to:

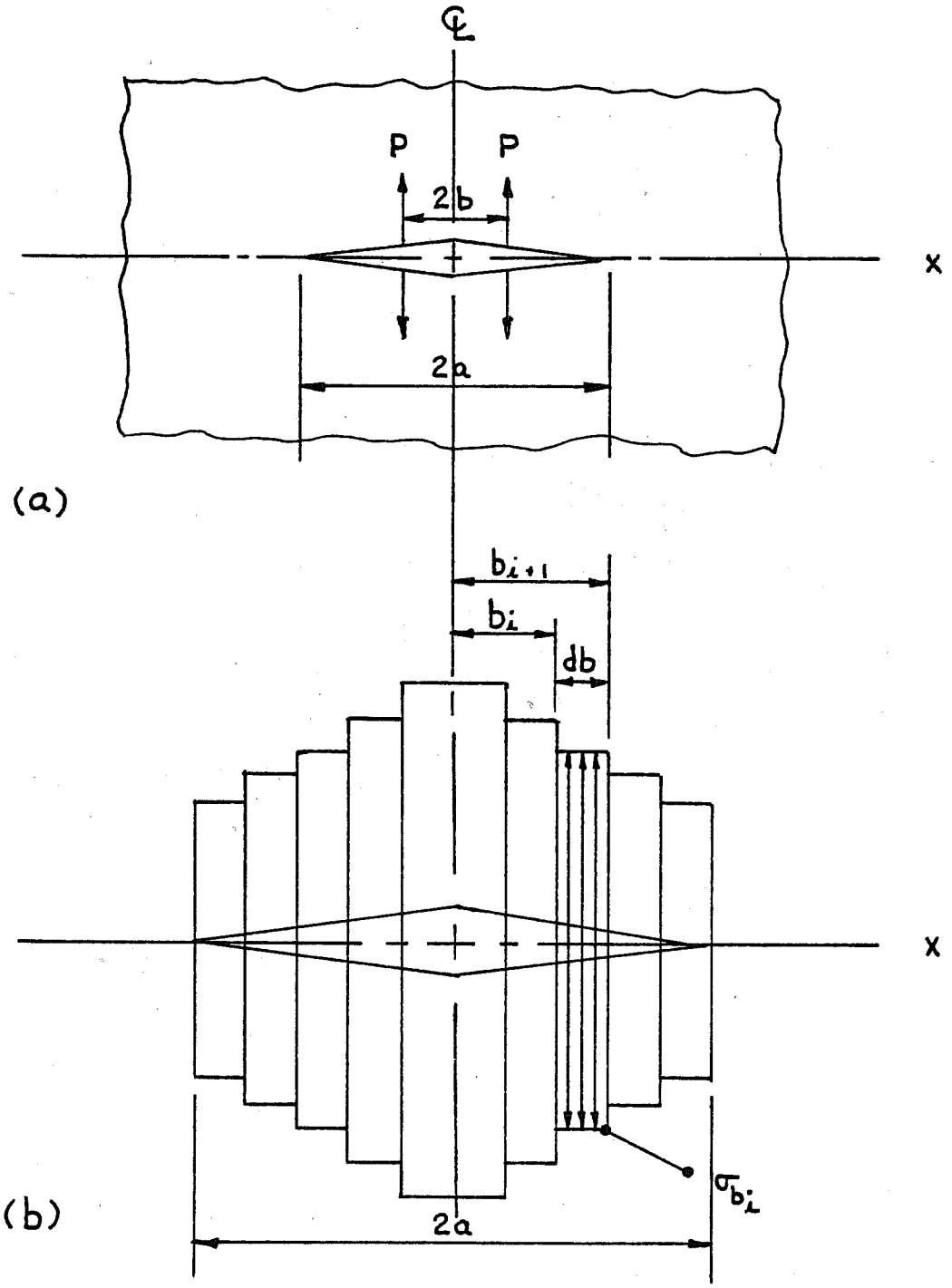

Fig. 1.9 Through-crack in an infinite plate subjected to: (a) two pairs of equal splitting forces, and (b) pairs of discrete stresses

$$K = \sigma \sqrt{\pi a} \frac{2}{\pi} \sum_{i=1}^{n} \frac{\sigma_{bi}}{\sigma} \left(\arcsin \frac{b_{i+1}}{a} - \arcsin \frac{b_i}{a} \right) \qquad (1.6)$$

Solutions for the stress intensity factor of a cracked body subjected to distributed stresses are written in the form:

$$K = F(a) \ \sigma \sqrt{\pi a} \qquad (1.7)$$

where F(a) is a correction function given by:

$$F(a) = F_e F_s F_w F_g \qquad (1.8)$$

where F(a) modifies K to account for effects of elliptical crack fronts, F_e, free surface, F_s, finite width, F_w, and nonuniform opening stresses, F_g. Of the many crack configurations with splitting forces possible, Albrecht chose a central crack in an infinite plate with two equal pairs of splitting forces because this configuration isolates the influence of stress gradient, F_g, from the other stress intensity correction factors, F_e, F_s, and F_w. It can thus be seen from Eq. (1.6) that:

$$F_g = \frac{2}{\pi} \sum_{i=1}^{n} \frac{\sigma_{bi}}{\sigma} \left(\arcsin \frac{b_{i+1}}{a} - \arcsin \frac{b_i}{a} \right) \qquad (1.9)$$

where F_g represents the ratio of the stress intensity factor for a nonuniform stress distribution along the line of the crack to the stress intensity factor for a uniformly distributed mean stress. F_g thus accounts for the effect on K of a stress concentration produced by a structural detail.

When applying Eq. (1.6) to the calculation of K for cracks at structural details, σ and σ_{bi} are defined as follows:

σ = normal stress in the member uniformly distributed over the thickness of the plate as computed using strength of materials formulas.

σ_{bi} = normal stresses in the finite element model of the structural detail where the crack will be inserted.

Due to its relative ease of application, the Green's Function approach for determining K values is used in this study.

CHAPTER 2

FINITE ELEMENT ANALYSIS

2.1 Introduction

The range of stress intensity, ΔK, at welded bridge details fluctuates depending on detail geometry and flaw characteristics. For a given detail, the stress intensity may be evaluated by applying a series of correction factors to a known closed-form analytical solution for K applicable to an idealized geometry. The correction factor which accounts for the stress gradient along the prospective crack path induced by detail geometry is called the stress gradient correction factor, F_g. If the stress distribution along the prospective crack path is known, the F_g factor may be established as a stress concentration decay function. The prospective crack path at the longitudinal-transverse stiffener intersection runs through the thickness of the girder web from the point at which the longitudinal stiffener is terminated. To determine the stress distribution through the girder web, the finite element technique was employed.

The analytical procedure utilized to obtain the stress gradient correction factor has been outlined in detail by Zettlemoyer [11,12]. Briefly, the procedure consists of subjecting the detail under study to a three-dimensional finite element analysis. Typically, as a means of reducing costs, this first level of investigation is only of sufficient accuracy to provide reasonable input to a more local, two-dimensional stress analysis. The two-dimensional mesh is subsequently refined until an

ultra-fine mesh very local to the weld toe is obtained. The element stresses along the prospective crack path of the uncracked body are thus obtained. The need for such an ultra-fine mesh can be explained as follows. The geometry at a weld toe creates a condition of elastic stress singularity. As a result, subsequent decreases in mesh size adjacent to the weld toe yield higher and higher stress values. However, the stresses somewhat removed from the weld toe become stabilized, with the distance to stabilization decreasing with decreasing mesh size. The major interest in a fracture mechanics analysis is in the accuracy of stresses beyond the initial crack size, a_i. It seems reasonable, then, to ensure that the mesh size be at least as small as the initial crack size. Past investigations have established a lower limit of initial crack size of 0.001 in. [13,14].

A general purpose finite element computer code, developed at The University of Texas at Austin, called TEXGAP [22], was used in this study. In all applications, material was considered to be isotropic and homogeneous. The value of Young's modulus was chosen to be 29,000 ksi, while Poisson's ratio was taken as 0.30.

2.2 TEXGAP Computer Program

The TEXGAP computer program is a linear elastic, static finite element code to be used for the analysis of two and three-dimensional structures. The three-dimensional element library consists of a variety of elements including quadratic isoparametric 20 node bricks, 15 node triangular prisms, 11 node tetrahedrons, and a degenerate form of the brick in which one edge is collapsed to a single node. Two-dimensional elements available to the user include an isotropic triangular element, and an isotropic quadrilateral element composed of four triangles.

Material models include isotropic, orthotropic, and anisotropic descriptions with options for transformation from local material axes to global axes. Permissible loadings and boundary conditions include uniform body and thermal forces over an element, pressure and traction on a surface, sliding and clamped surfaces, springs, and prescribed nodal point forces or displacements.

An outstanding feature of the TEXGAP program is the extensive preprocessor available for the definition of material properties, generation of the nodal points, and the definition of elements and boundary conditions. Also of value is an interactive graphics package that plots the elements defined in the program. This package permits a visual examination of the generated mesh eliminating the tedious process of checking the mesh by hand.

Several postprocessing options are also available to select points at which stresses and strains are to be calculated, to identify planes for plotting of stress and strain contours, to plot deformed grids and deformed planes, and to compute strain energy. In addition, the user may specify the rezoning of a grid in a local region of interest to obtain a more exact picture of the state of stresses.

2.3 Finite Element Solutions

The finite element analysis procedure utilized in this study is illustrated in Fig. 2.1. Stress is applied to a 3D coarse finite element grid simulating applied moment on the plate girder cross section. Nodal displacements from the 3D analysis are applied to the 2D fine grid model of the longitudinal-transverse stiffener intersection. Similarly, nodal displacements from the 2D fine grid model are applied to the 2D ultra-fine grid model

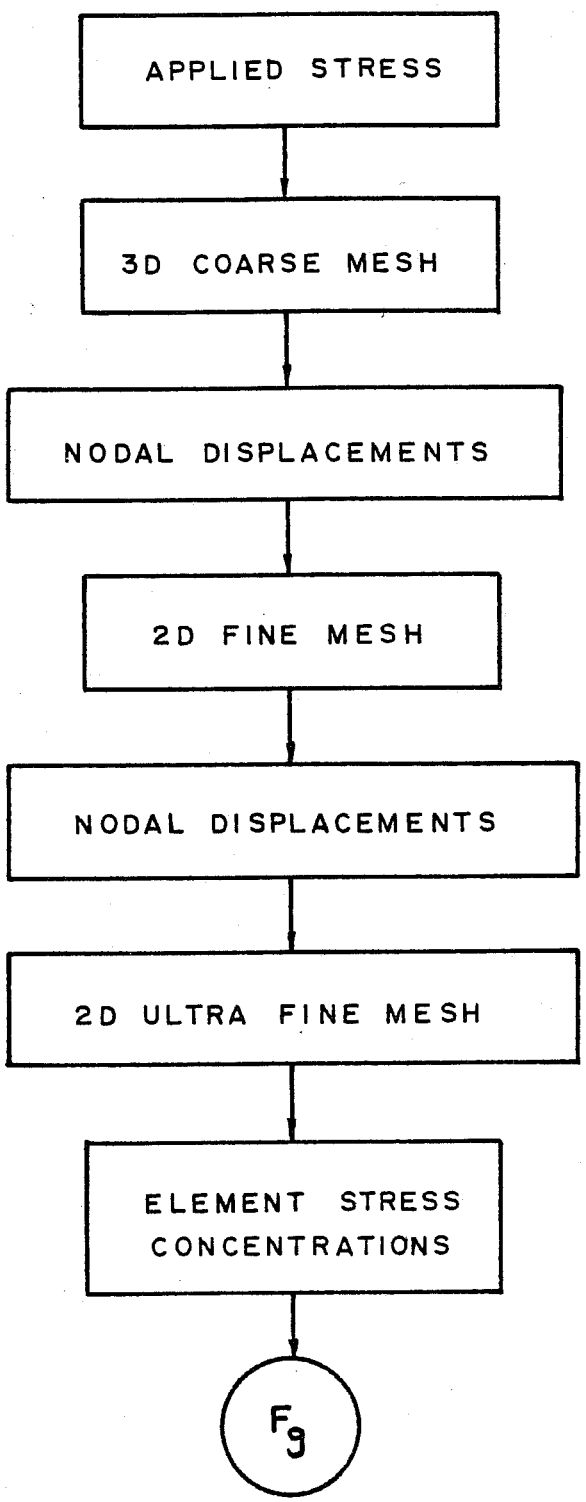

Fig. 2.1 Finite element analysis procedure

of the local weld toe area at the longitudinal stiffener end. Analysis of the 2D ultra-fine grid model results in the definition of the distribution of stress through the girder web necessary for the determination of F_g.

2.3.1 Longitudinal-Transverse Stiffener Intersection. The occurrence of the longitudinal-transverse stiffener intersection on the twin girder bridge under study is illustrated in the photographs of Fig. 2.2. Figure 2.2(a) shows the first of the two main girders in the foreground, the second main girder in the background, and the floor beams which connect the girders. The concrete bridge deck supported by the structural steel framework can also be observed. Figure 2.2(b) depicts the other side of the main girder to which transverse stiffeners are attached. The floor beam can also be seen framing into the plate girder in the center portion of the photograph.

The three-dimensional model of the longitudinal-transverse stiffener intersection consists of rectangular plate elements. Therefore, the 20 node brick element is used exclusively. For the two-dimensional analyses, both the 4 node quadratic element and the triangular element are utilized. These finite elements are shown in Fig. 2.3.

2.3.1.1 Geometry and Modeling. In modeling the longitudinal-transverse stiffener intersection detail, consideration must be given to the geometric portion of the floor beam and the girder which needs to be included in the finite element model.

The depth of the floor beam is just over one-half the depth of the main longitudinal girder. As a result, at the point of floor beam-girder intersection, a transverse stiffener runs from the lower flange of the floor beam to the lower flange of the girder. To simplify the finite element model and to reduce

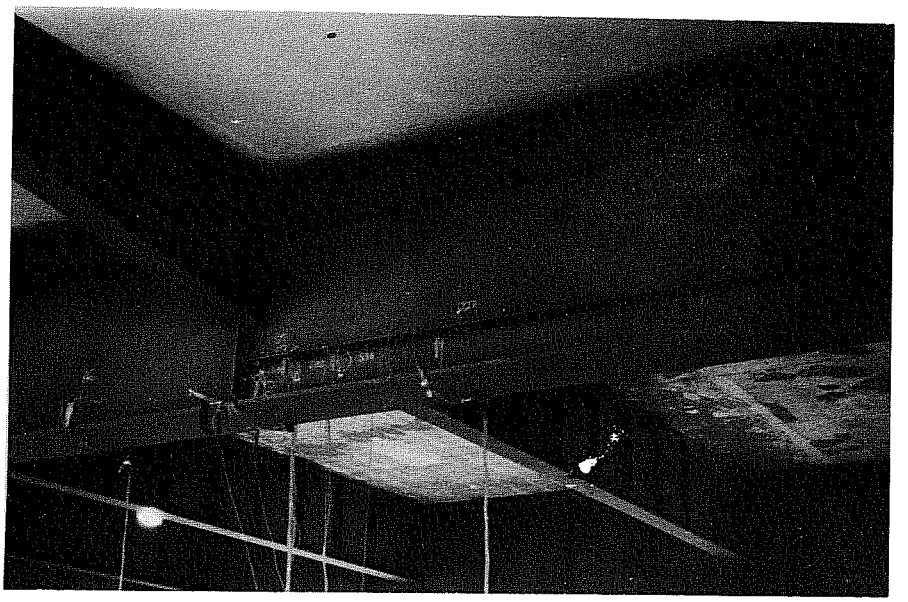

(a)

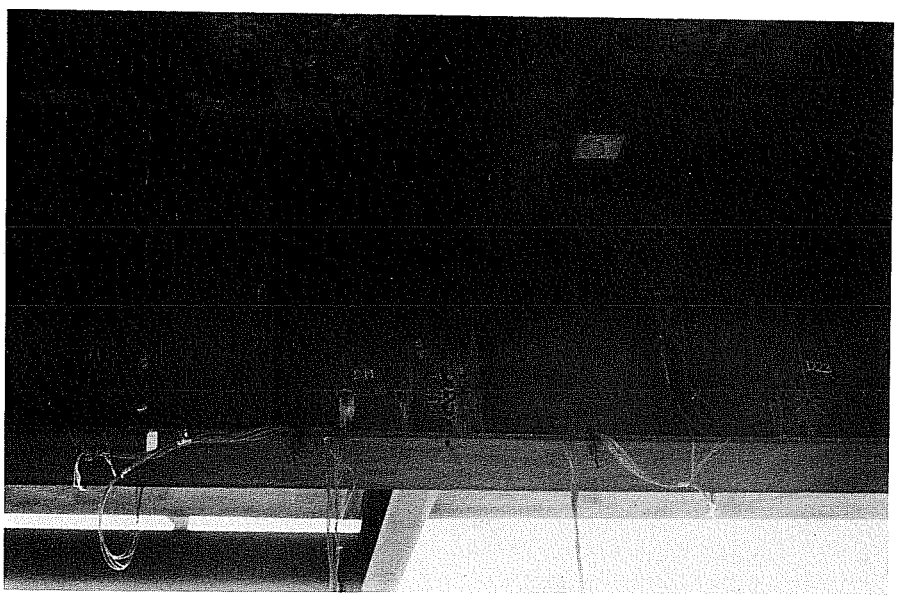

(b)

Fig. 2.2 Occurrence of the longitudinal-transverse stiffener intersection

20 NODE BRICK ELEMENT

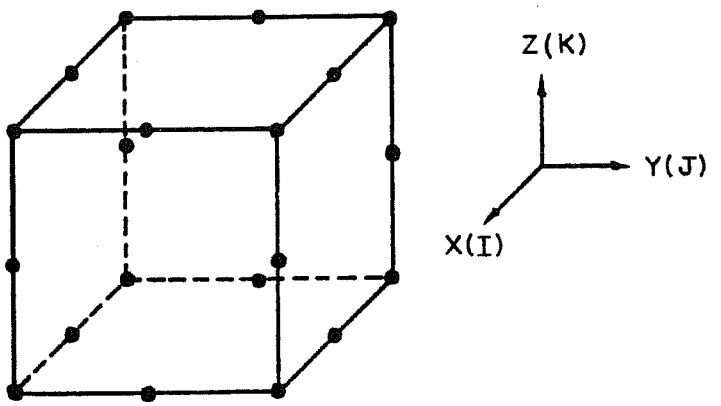

4 NODE QUADRILATERAL ELEMENT

TRIANGULAR ELEMENT

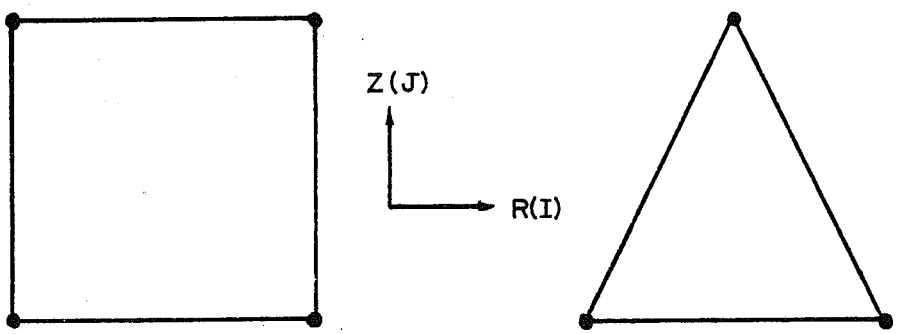

Fig. 2.3 Finite elements used to model the longitudinal-transverse stiffener intersection

computer solution time, it was assumed that the floor beam itself can be adequately modeled as a transverse stiffener on each side of the girder. In other words, the restraint to the girder provided by the floor beam is considered equivalent to that provided by a transverse stiffener. Therefore, the floor beam and the transverse stiffener located below the floor beam are represented by one continuous transverse stiffener in the three-dimensional finite element model.

The length of the girder to be modeled must also be determined. A portion of the girder sufficient to develop the stress in the longitudinal stiffener must be included to eliminate adverse effects on the state of stresses at the stiffener end. On the other hand, the overall length must be controlled to minimize computer costs. To eliminate a trial and error procedure of selecting the optimum length of girder to be modeled, results of field tests run on the twin girder bridge were utilized. To determine the distribution of stress through the girder, various cross sections were selected and instrumented. Based on the results of a computer analysis of the structure to determine locations of maximum moment, cross sections 6 ft on either side of the point of floor beam intersection were chosen for instrumentation. Figure 2.4 shows a typical girder with the location of the gaged sections indicated. The cross sections illustrated in Fig. 2.4 show the strain gage locations of each instrumented section. Of particular interest are gage numbers 11, 12, 13, and 14 of Section "B-B". These gages are mounted on the longitudinal stiffener which terminates at the point of floor beam intersection. Field test results consistently indicate similar readings for gages 11, 12, 13, and 14. It can, therefore, be concluded that the longitudinal stiffener stress is developed over a length of 6 ft or less. Thus, the length of the finite element model was chosen

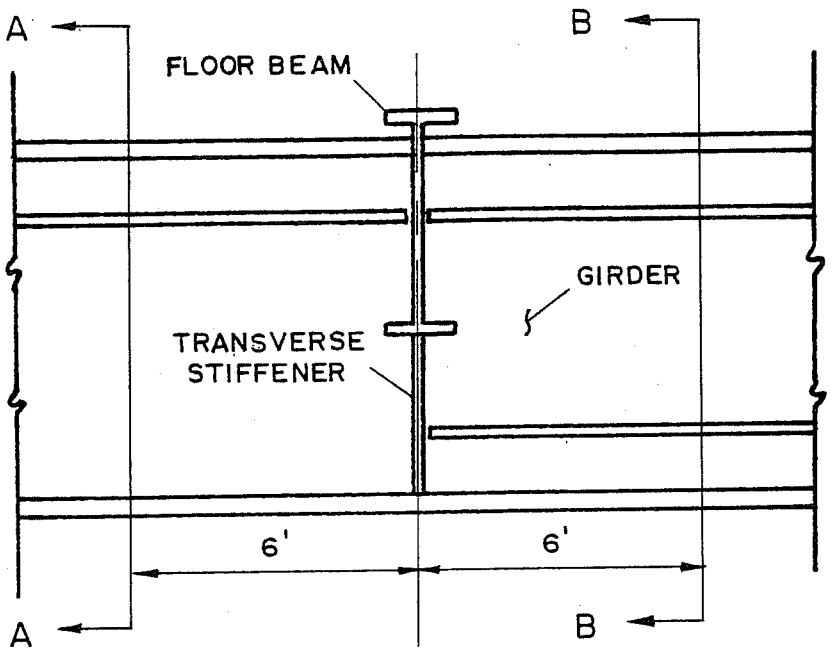

Fig. 2.4 Typical bridge girder with instrumentation shown

to be 12 ft, 6 ft on either side of the point of floor beam intersection. The resulting three-dimensional full-scale finite element model is shown in the isometric drawing of Fig. 2.5. A specific description of the dimensions of the full-scale model is presented in Fig. 2.6.

Once the dimensions of the finite element model are determined, boundary conditions must be established. It is important to select the boundary conditions carefully, since they determine the degree of accuracy obtained in representing an existing detail with a finite element model.

In determining the boundary conditions for the full-scale finite element model of Fig. 2.5, results of field tests on the twin girder bridge were found to be helpful. An important question had been raised regarding the location of the neutral axis of the plate girder model. If the girder and the concrete bridge deck were acting together compositely, the neutral axis of the composite section would lie above that of the girder alone. As a result, tensile stresses in the lower girder flange would be greater than compressive stresses in the upper flange. Field tests indicated, however, that levels of stress in the upper and lower girder flanges were similar in magnitude. Therefore, the neutral axis of the plate girder model was assumed at midheight and stress was applied to the model as shown in Fig. 2.7. The opposite end of the model was fixed in the direction of applied stress, creating a condition of constant moment along the length of the girder model. Figure 2.7 also shows the coarse grid used for the 3D detail investigation. Selection of the mesh consisting of 229 brick elements was made based on the geometry of the individual plate members of the girder model. In addition, an attempt was made to achieve element symmetry to avoid any error introduced due to an unsymmetrical grid pattern. Since the area of interest

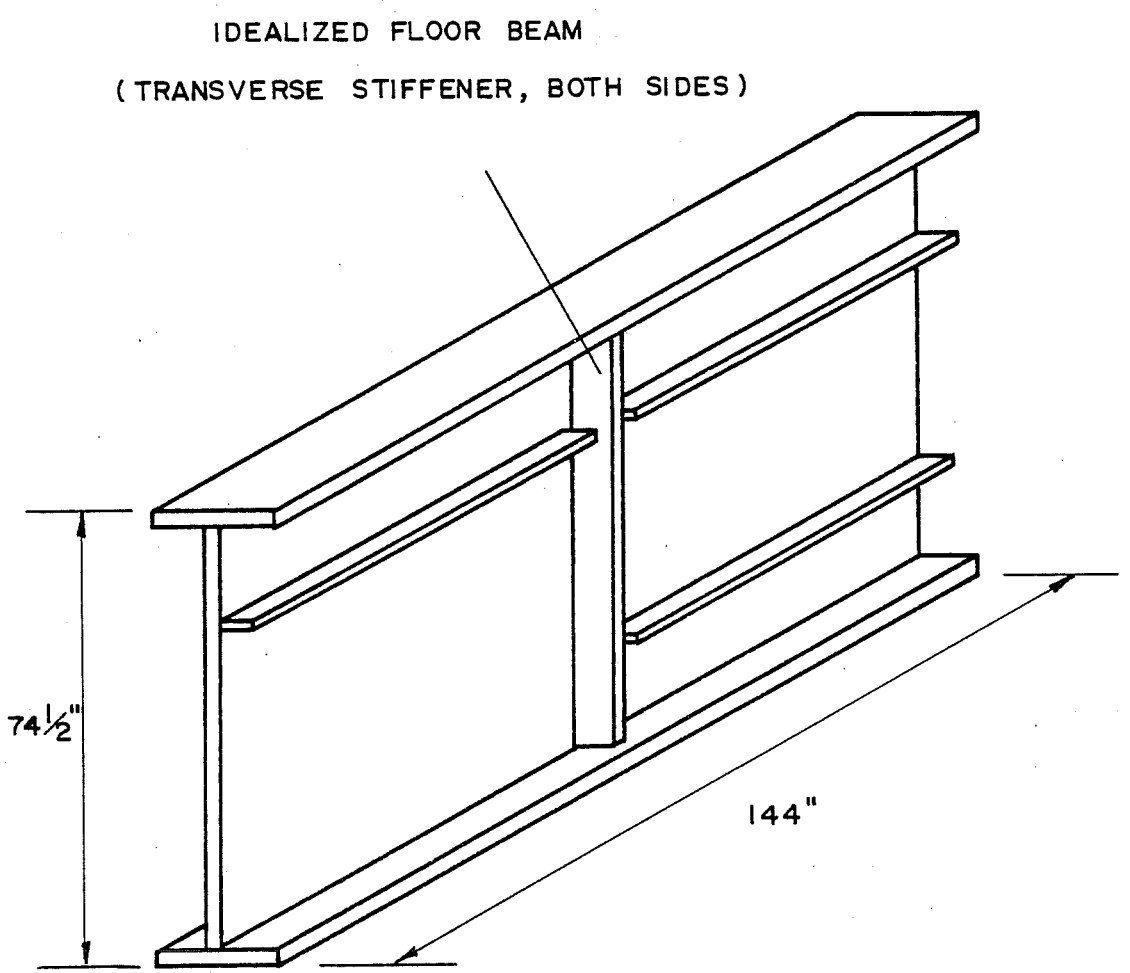

Fig. 2.5 Full-scale finite element model of longitudinal-transverse stiffener intersection detail

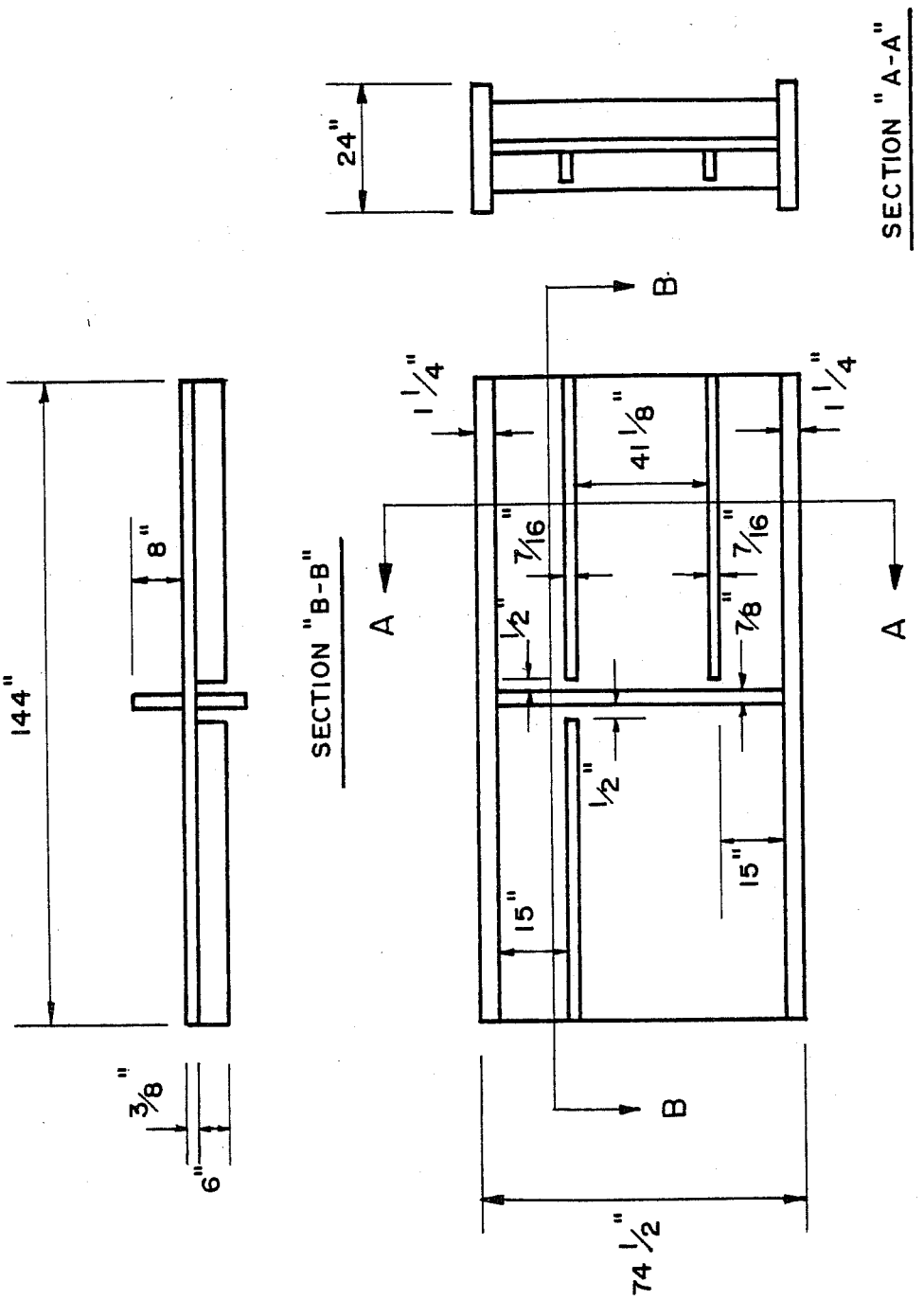

Fig. 2.6 Full-scale finite element model dimensions

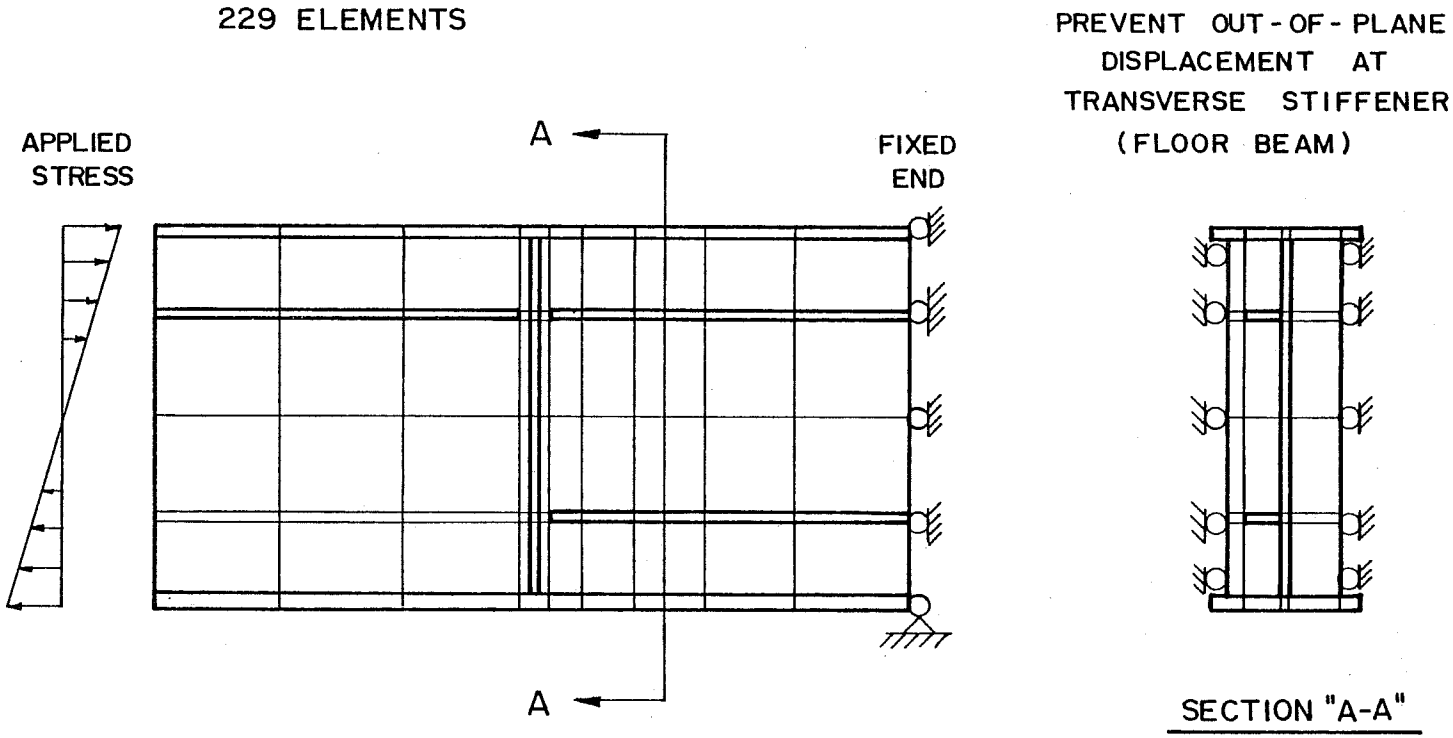

Fig. 2.7 Full-scale model mesh and boundary conditions

in the 3D analysis is located in the vicinity of the longitudinal stiffener end, a 4 to 1 gradient was utilized to generate the mesh along the longitudinal stiffener. (The last element along the longitudinal stiffener is 4 times as long as the first element.)

Field tests also revealed no detectible out-of-plane movement of the girder at the point of floor beam intersection. Therefore, out-of-plane displacement of the transverse stiffener used to model the floor beam was prevented, as shown in Fig. 2.7.

Initial analysis of the full-scale finite element model revealed the fact that an alternate approach would be necessary to perform the required computer analysis. The large number of elements required by the full-scale model resulted in heavy use of computer solution time. This would not present a great problem if the existing longitudinal-transverse stiffener intersection detail was the only detail being studied. However, the intent of this study was to also investigate variations in geometry of the longitudinal and transverse stiffeners (Sec. 2.3.2) and to determine the effectiveness of a cope detail for possible future use in design (Sec. 2.3.3). If all of the variations involved were studied using the full-scale model, practical limitations on computer solution time would be exceeded. Therefore, in an attempt to reduce the size of the finite element model, two planes of symmetry were established. This was made possible by assuming the existence of a fourth longitudinal stiffener located on the same side of the girder web as the three existing longitudinal stiffeners. The effect of this assumption was to change the problem from that of a longitudinal stiffener intersecting a transverse stiffener on one side only, to longitudinal stiffeners intersecting a transverse stiffener on both sides. Figure 2.8 illustrates this difference along with the location of the two planes of symmetry. The results obtained for each condition shown in Fig. 2.8

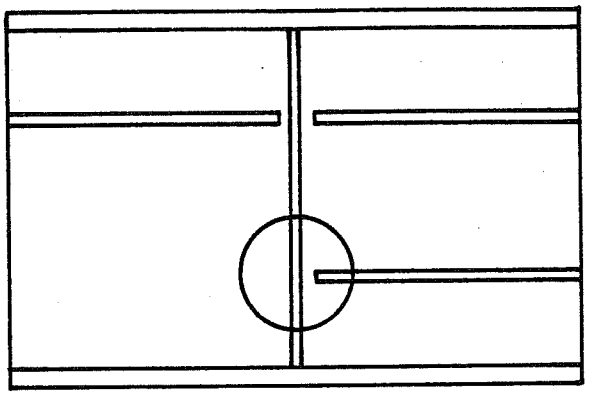

SINGLE STIFFENER INTERSECTION

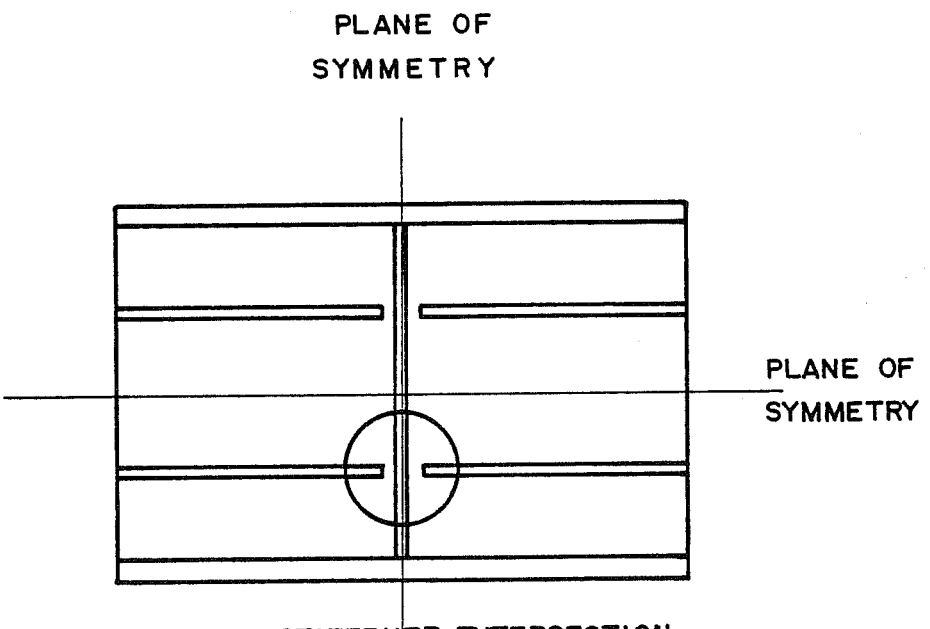

DOUBLE STIFFENER INTERSECTION

Fig. 2.8 Result of adding a fourth longitudinal stiffener to the problem, with two planes of symmetry

will be discussed and compared later (Sec. 2.3.1.2). The 1/4 symmetric finite element model obtained for subsequent use is shown in Fig. 2.9. Figure 2.10 illustrates the dimensions of the model.

Next, boundary conditions for the 1/4 symmetric model had to be determined. The necessary boundary conditions were inferred from those imposed on the full-scale model. Stress was applied in a similar fashion, and out-of-plane displacement at the point of floor beam intersection was prevented. Again, the end of the model opposite the loaded end was fixed in the direction of applied stress, representing the vertical plane of symmetry. Horizontal movement was prevented at the boundary which represents the horizontal plane of symmetry, or the neutral axis. The resulting finite element model consisted of 114 brick elements as opposed to 229 elements, which comprised the full-scale model, resulting in a 75 percent reduction in computer solution time. Figure 2.11 shows the above-mentioned boundary conditions as well as the coarse mesh used in the finite element analysis.

Before making the transition from the three-dimensional to the two-dimensional mesh, a horizontal section must be selected through the girder web and both the longitudinal and the transverse stiffeners. This section will be used as the basis for the two-dimensional mesh. Its location in the three-dimensional 1/4 symmetric model will determine which nodal displacements will be imposed on the two-dimensional fine mesh. Figure 2.12 illustrates the region of interest, including the girder web and both stiffeners. The "match section" to be used as the two-dimensional fine mesh is taken at the midheight level of the longitudinal stiffener, as shown in Fig. 2.12. Since the nodal displacements from the coarse mesh are to be imposed on the fine mesh, the length of the fine mesh in the longitudinal direction can be selected to be any convenient value.

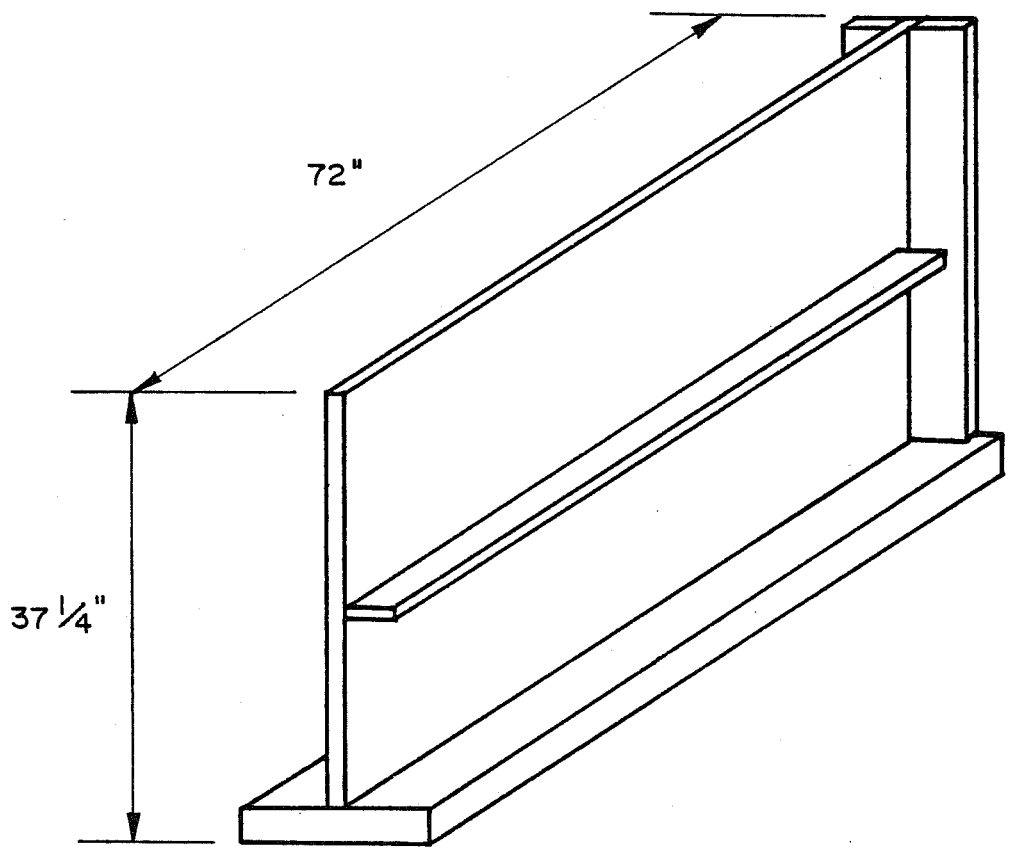

Fig. 2.9 Three-dimensional 1/4 symmetric finite element model

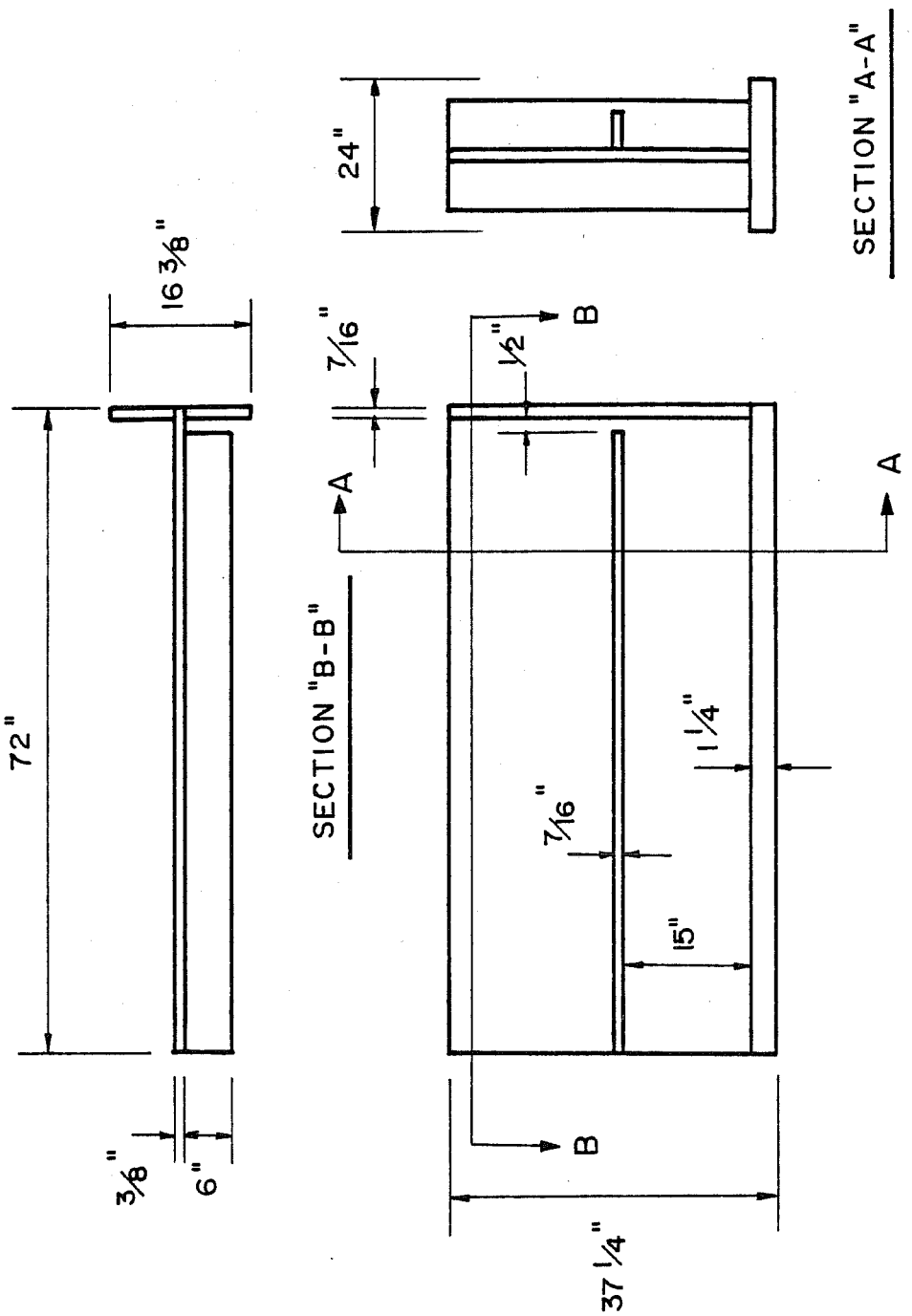

Fig. 2.10 One-quarter symmetric finite element model dimensions

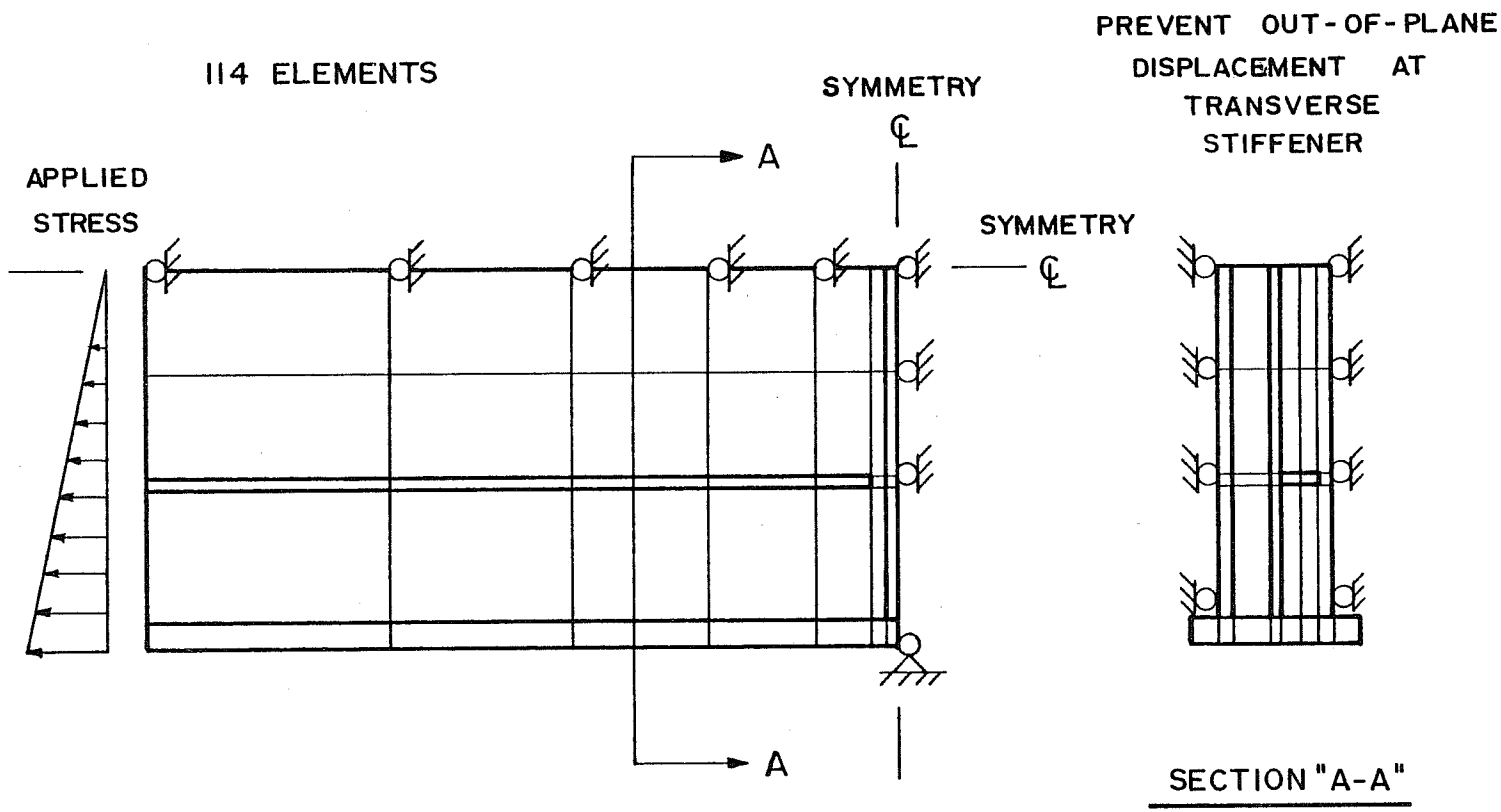

Fig. 2.11 One-quarter symmetric model mesh and boundary conditions

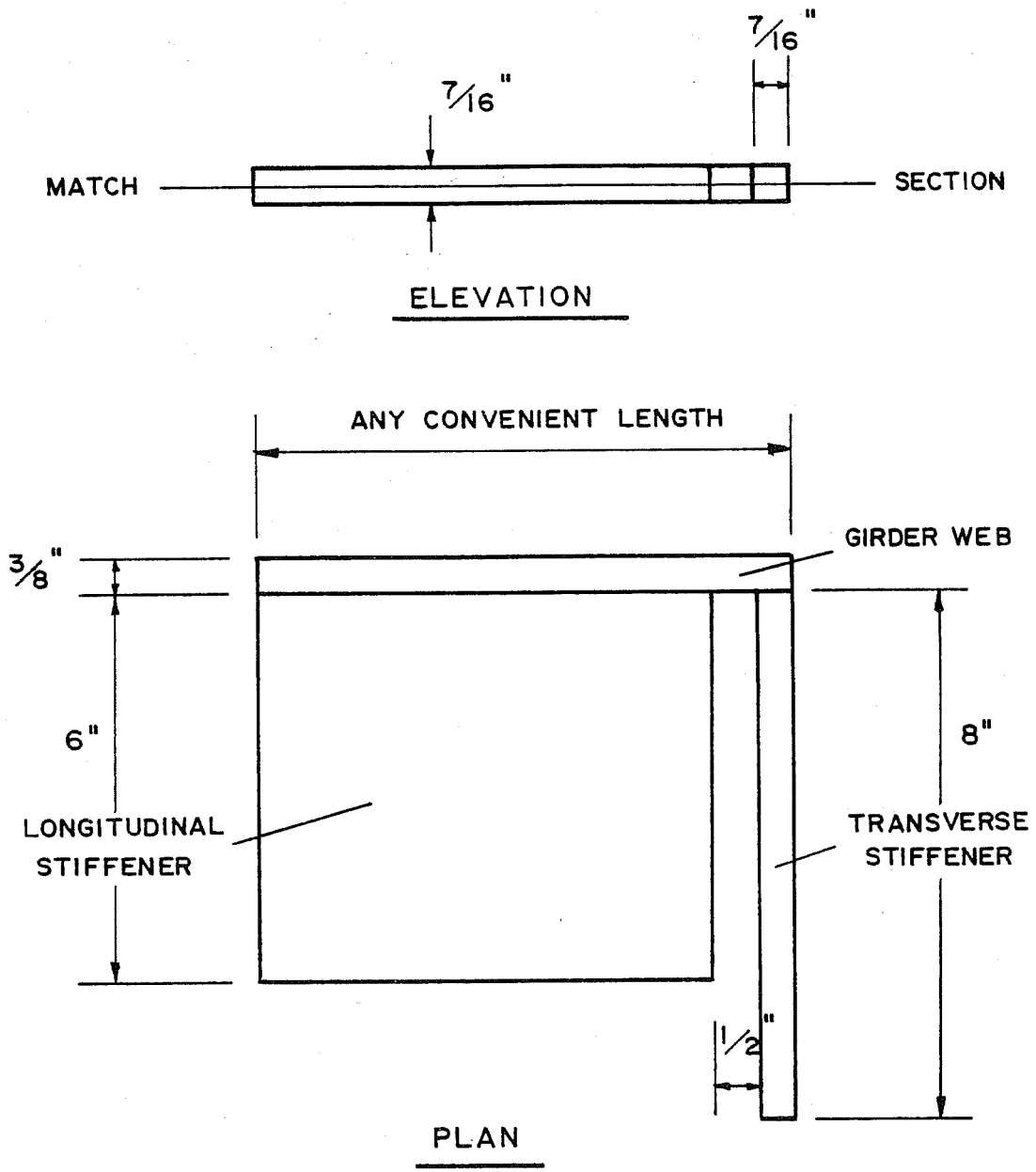

Fig. 2.12 Local region of interest of the 1/4 symmetric finite element model

In order to obtain an accurate set of nodal displacements to be imposed on the fine mesh, the three-dimensional coarse mesh was refined in the region of interest, as shown in Fig. 2.13. This was done using the rezone capabilities of the TEXGAP computer program previously discussed. As illustrated in Fig. 2.13, four elements of the coarse mesh were refined into 180 elements. The nodal displacements required by the fine mesh are thus easily obtained at the "match section" location in the rezoned coarse mesh.

The resulting two-dimensional fine mesh is shown in Fig. 2.14. As can be seen, the web-to-stiffener welds have been included in the fine mesh. Since the prospective crack path runs from the web-to-longitudinal stiffener weld toe through the girder web, the mesh in this area possesses a high degree of resolution. The length of the longitudinal stiffener included in the model, 4.2 in., was chosen based on the location of nodal lines in the coarse mesh. As a result, nodal displacements from the coarse mesh were imposed on the fine mesh in a convenient manner, as shown in Fig. 2.14.

In addition to nodal displacements at the longitudinal stiffener boundary of the fine mesh, remaining boundary conditions were established based on previous assumptions applied to the coarse mesh. The transverse stiffener is fixed against out-of-plane displacement as well as displacement in the longitudinal direction. Figure 2.14 illustrates these conditions.

When analyzing the fine mesh, a decision must be made to use either plane stress elements or plane strain elements. Zettlemoyer [15] found that results obtained assuming plane stress were very similar to plane strain results. However, the plane stress results were closer to the "correct" value established for

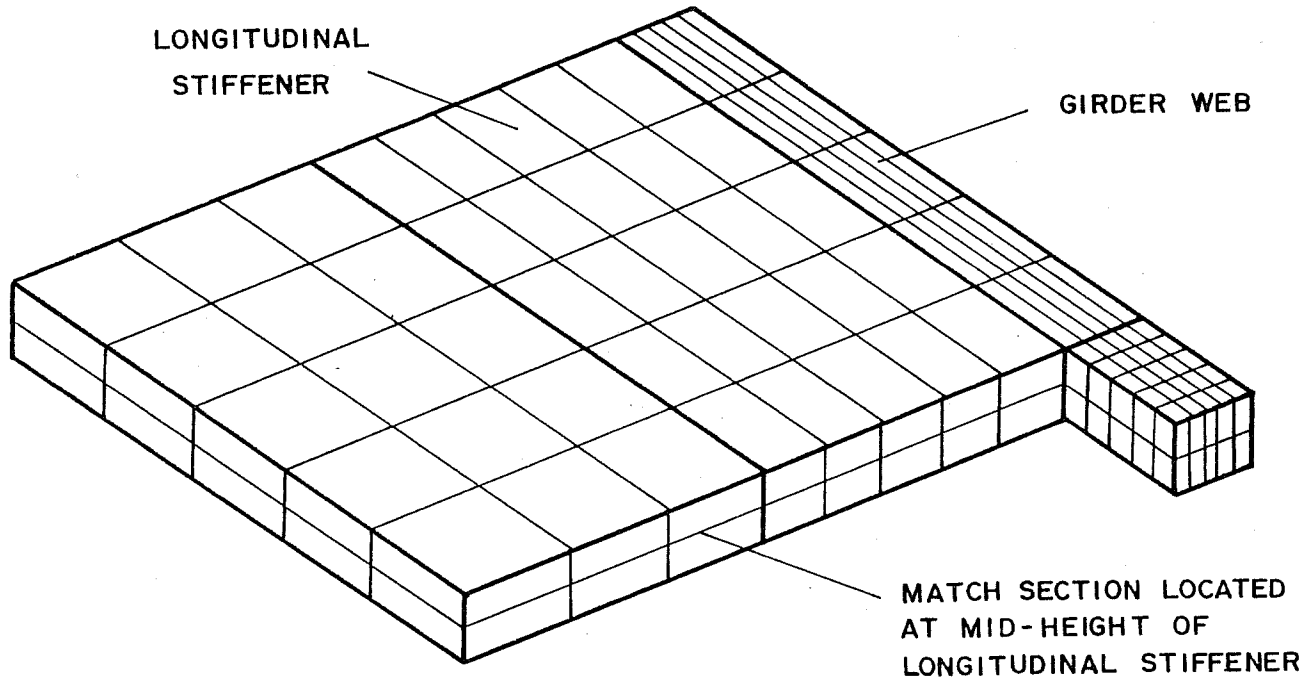

Fig. 2.13 One-quarter symmetric model grid refinement in the local region of interest with the "match section" shown

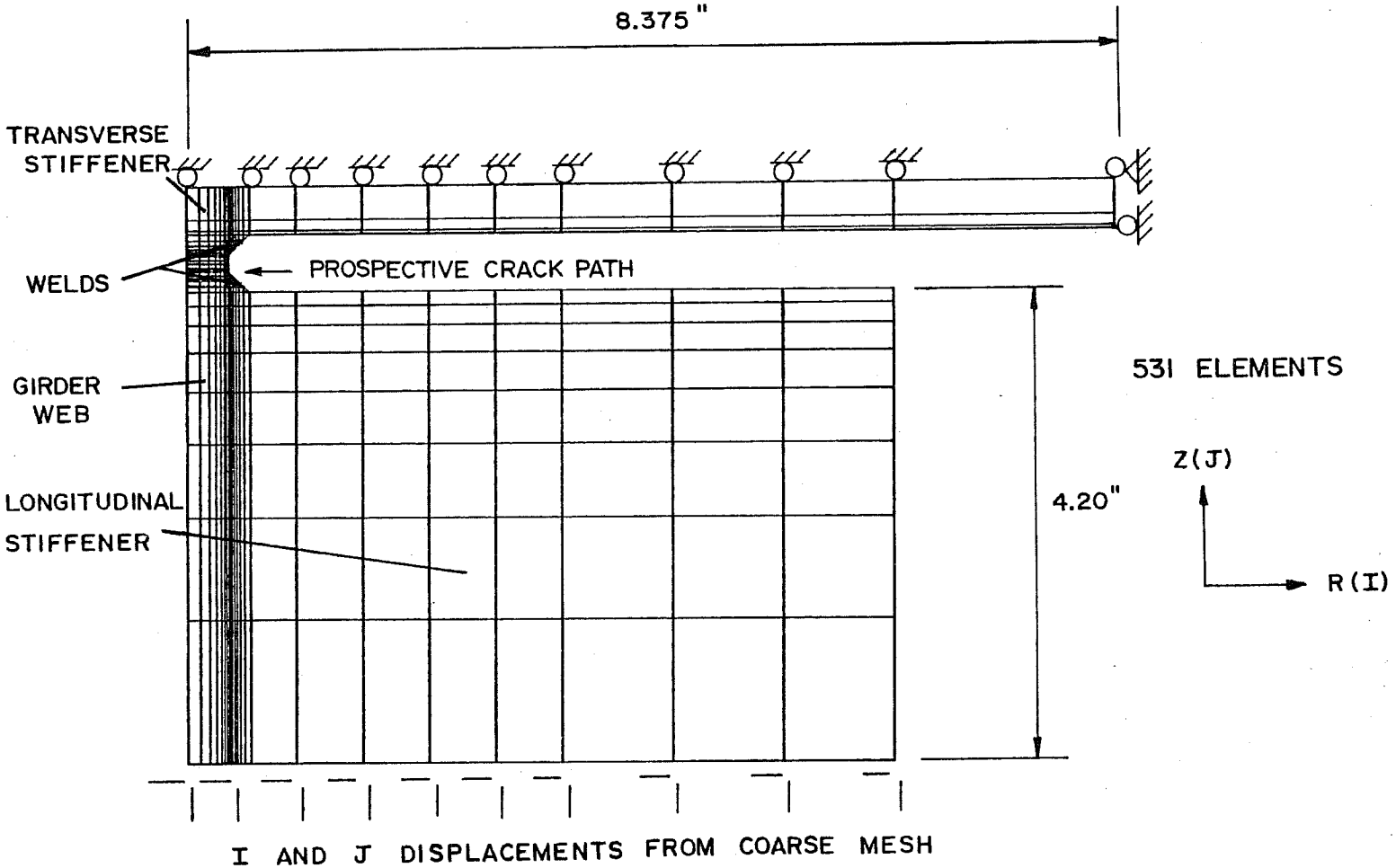

Fig. 2.14 Two-dimensional fine mesh with boundary conditions shown

comparison than were the plane strain results. Thus, Zettlemoyer assumed plane stress in his work on welded details. Plane stress is also assumed in this study.

To generate the ultra-fine mesh local to the longitudinal stiffener-to-web weld toe, the rezone feature of TEXGAP was again utilized. The rezone procedure involves imposing nodal displacements from analysis of the fine mesh on the boundaries which contain the ultra-fine mesh. When this was actually done, however, the dimensions of the TEXGAP computer program were exceeded. Two alternatives were available to solve this problem. First, a newer version of TEXGAP could be used to analyze the larger problem. This seems like the logical solution, but the new version of TEXGAP was not readily available to the author. Secondly, the coordinate system could be changed to solve the problem using the same version of TEXGAP. The program places limitations on the number of elements which can be rezoned in the I-direction, the direction parallel to the prospective crack plane along which an ultra-fine mesh is required. In the J-direction, however, gradients were used in the fine mesh which reduced the number of elements which needed to be rezoned. Therefore, if the mesh was rotated 90°, the analysis could be performed. In fact, this was done, but rather than reanalyze the entire fine mesh, the portion of the fine mesh located in the 1/2 in. gap between the longitudinal and transverse stiffeners was reanalyzed. The resulting fine mesh is shown in Fig. 2.15. The boundary conditions to the fine mesh were obtained from the results of the larger fine mesh of Fig. 2.14. The new fine mesh was thus rezoned in the area local to the longitudinal stiffener-to-web weld toe, as shown in Fig. 2.15. The resulting ultra-fine mesh and the corresponding element sizes are shown in Fig. 2.16. The web elements local to the weld toe are approximately 0.002 in. in the direction parallel

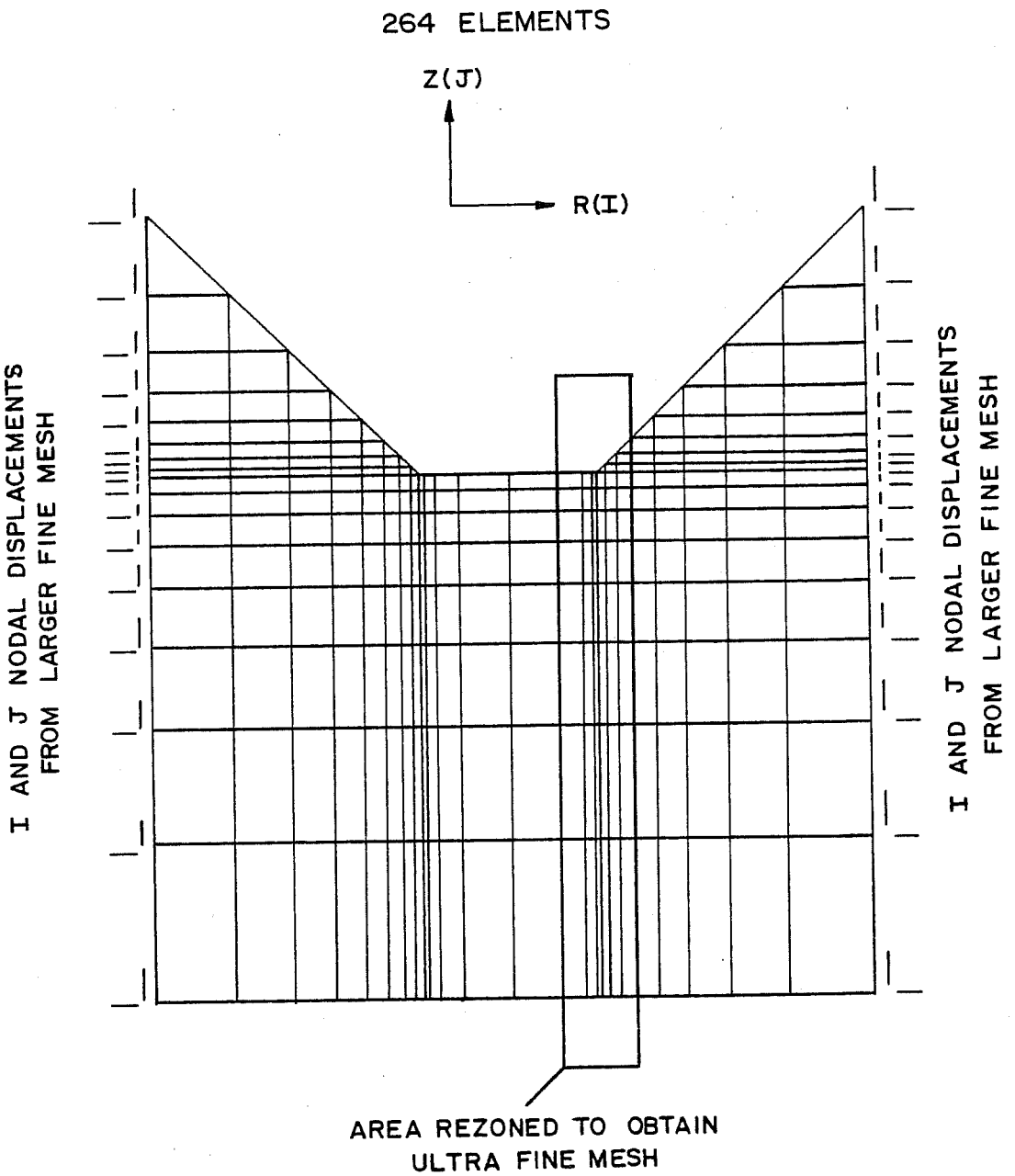

Fig. 2.15 Fine mesh located in the 1/2 in. gap between the longitudinal and transverse stiffeners

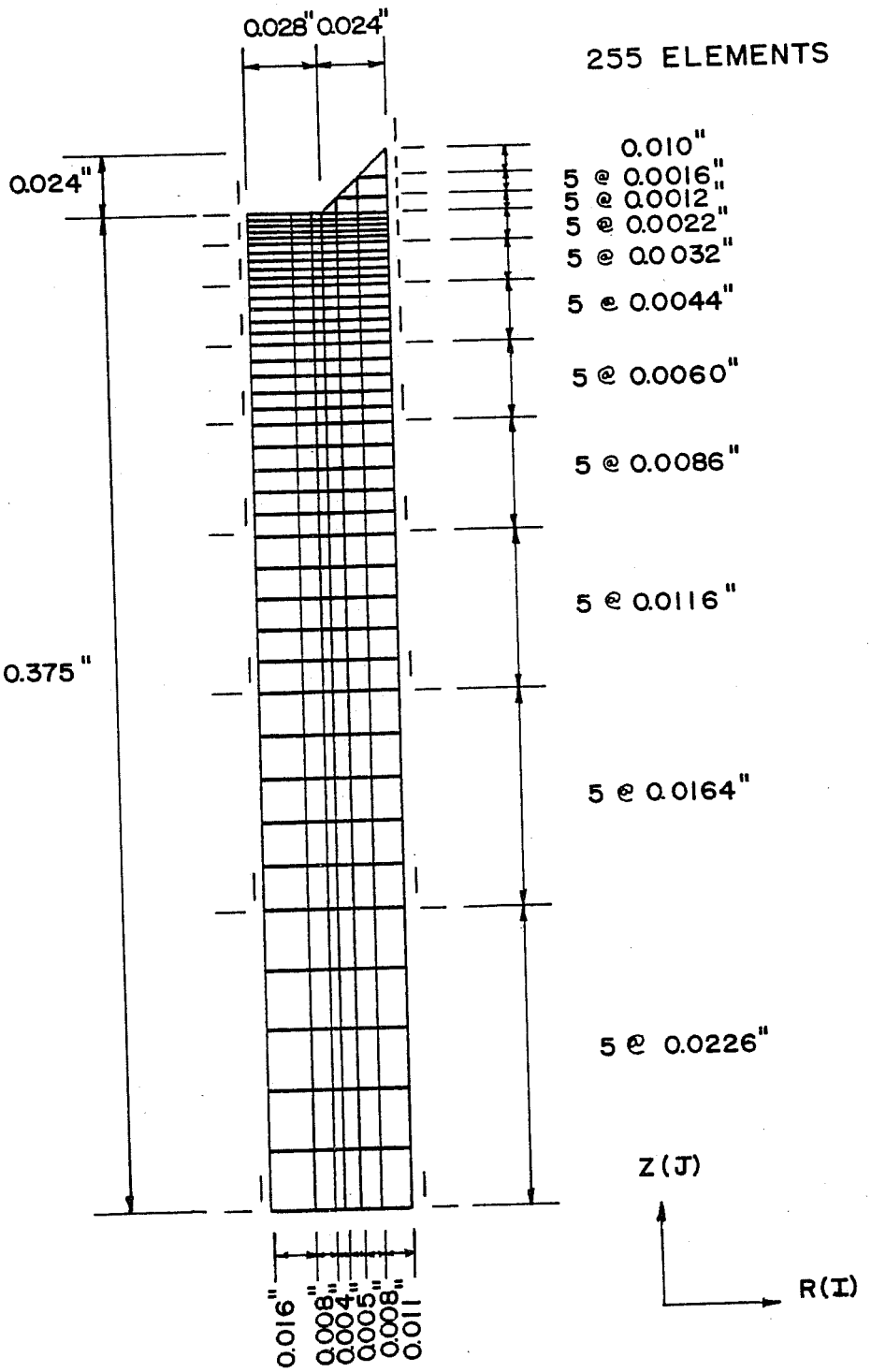

Fig. 2.16 Ultra-fine mesh for longitudinal-transverse stiffener intersection showing element sizes

to the prospective crack path. This value is very close to the absolute minimum initial flaw size of 0.001 in. previously discussed. Since the average initial crack size has been found to be about 0.003 in. [13,14], reasonable accuracy in F_g during the early stages of crack growth should be obtained.

2.3.1.2 Results. Using the results of the full-scale model analysis, the differences between the single stiffener and double stiffener intersection details, shown in Fig. 2.8, could be observed. The logical parameter to compare is the distribution of stress along the prospective crack path through the girder web. Since the full-scale model had a double stiffener intersection as well as a single stiffener intersection, the required comparison could be made. Figure 2.17 illustrates the results obtained from the full-scale model. Relative distance through the girder web, ℓ/T_w, is plotted against stress concentration factor, K_t. The stress distribution through the girder web is seen to be more severe for the double stiffener intersection, with the deviation from the values for the single stiffener intersection being significant. Although a difference in stress distribution exists between the single and double stiffener intersection, use of the double stiffener intersection for the purposes of analysis is a more severe condition and is certainly conservative. Subsequent analyses could thus be performed using the 1/4 symmetric finite element model.

To verify the accuracy of the 1/4 symmetric model, two parameters were studied and compared with those of the full-scale model previously analyzed. First, the distribution of stress along the longitudinal stiffener was plotted and compared to that of the full-scale model. As shown in Fig. 2.18, the results from the 1/4 symmetric model reproduce those of the full-scale model quite well. Further, the distribution of stress through the

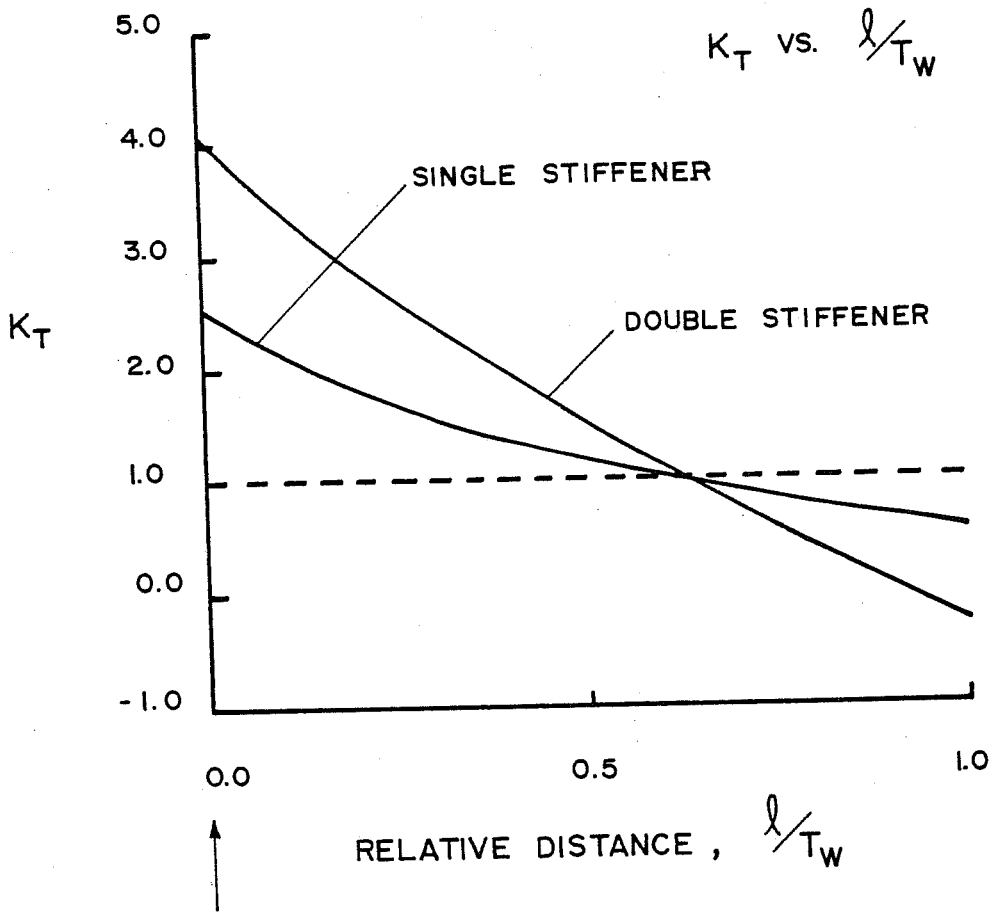

		ℓ/T_W		
		0	0.5	1.0
K_T	SINGLE STIFFENER	2.52	1.20	0.57
	DOUBLE STIFFENER	4.10	1.57	-0.30

Fig. 2.17 Comparison of stress distribution through the girder web for the single and double stiffener intersections

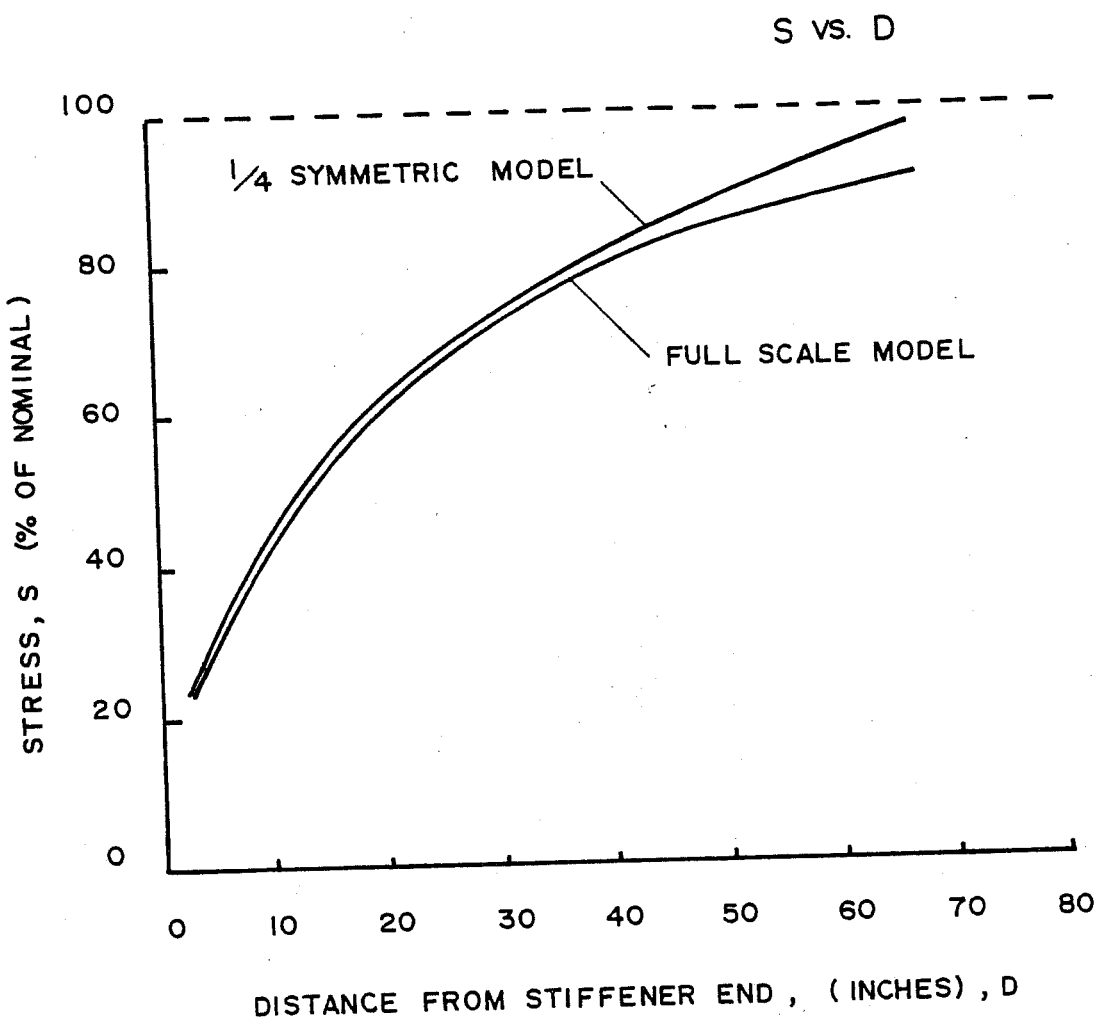

		D, (INCHES)				
		3.5	11.8	23.0	38.3	59.1
S, (%)	FULL SCALE MODEL	23	47	64	79	89
	1/4 SYMMETRIC MODEL	26	48	66	81	94

Fig. 2.18 Comparison of the distribution of stresses along the longitudinal stiffener of the full-scale model and the 1/4 symmetric model

girder web was compared for both models. Figure 2.19 illustrates the fact that both models gave essentialy identical results. It can, therefore, be concluded that the 1/4 symmetric model behaves like the full-scale model and can be used with confidence.

Once the analysis of the 1/4 symmetric model was performed, the three-dimensional mesh in the area of the longitudinal-transverse stiffener intersection was refined and reanalyzed. The purpose of this grid refinement was to obtain a complete set of nodal displacements to be applied to the two-dimensional fine mesh. As expected, analysis of the refined grid resulted in an increased stress concentration at the longitudinal stiffener-to-web weld toe. This is illustrated in Fig. 2.20, which compares the stress distribution through the girder web of the 1/4 symmetric model and the 1/4 symmetric refined model.

Table 2.1 lists the stress concentration factors obtained from analysis of the two-dimensional fine mesh. These values are plotted against the relative distance along the prospective crack path in Fig. 2.21. The figure shows a comparison of the fine mesh results to those of the 1/4 symmetric refined mesh. Again, it should be noted that as the elements local to the weld toe become smaller, the stress concentration at the weld toe becomes larger.

To obtain the required ultra-fine mesh, the fine mesh was rezoned in an area local to the prospective crack path through the girder web. Table 2.2 presents a listing of the resulting stress concentration factors. A comparison of the ultra-fine mesh results with the fine mesh results is made in Fig. 2.22. Several points should be made regarding the relationship between the results of the two analyses. First, for ℓ/T_w greater than 0.1, results of the fine mesh analysis and the ultra-fine mesh analysis are

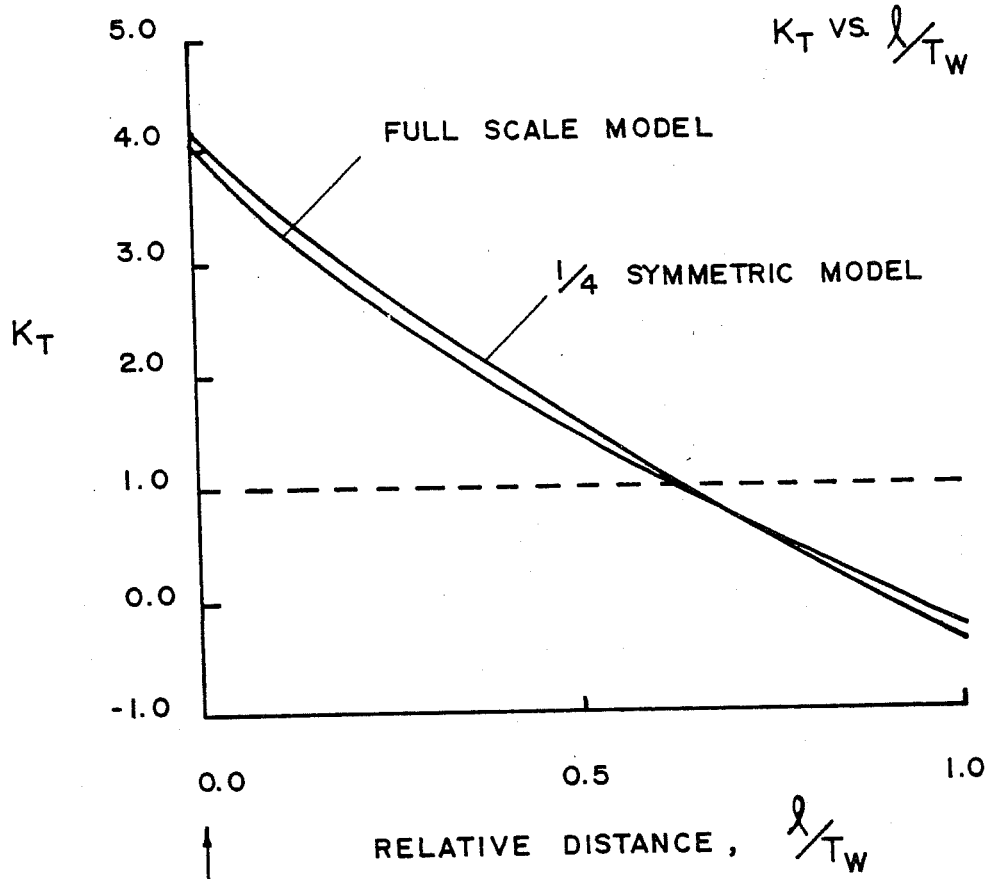

		ℓ/T_W		
		0	0.5	1.0
K_T	FULL SCALE MODEL	4.10	1.57	-0.30
	1/4 SYMMETRIC MODEL	4.19	1.59	-0.37

Fig. 2.19 Comparison of the stress distributions through the girder web of the full-scale model and the 1/4 symmetric model

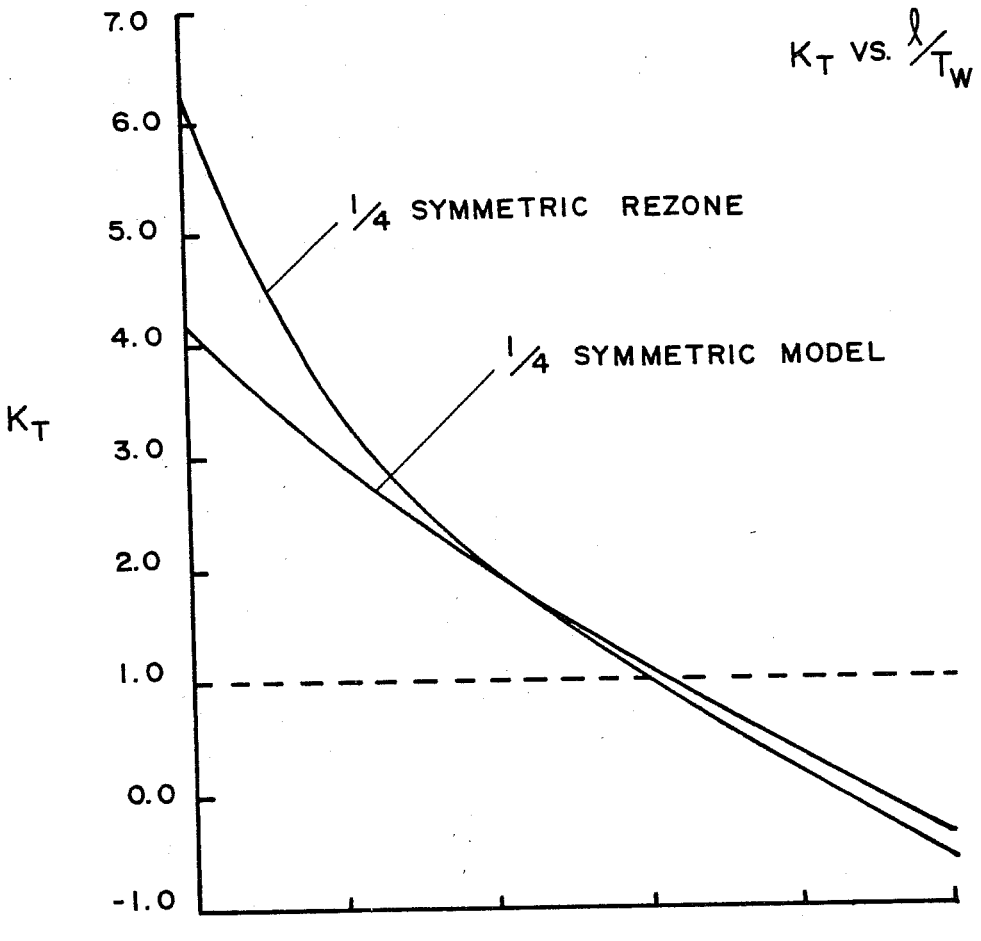

		ℓ/T_W						
		0	0.2	0.4	0.5	0.6	0.8	1.0
K_T	1/4 SYMMETRIC MODEL	4.19	-	-	1.59	-	-	-0.37
	1/4 SYMMETRIC MODEL	6.30	3.44	2.01	-	1.13	0.26	-0.66

Fig. 2.20 Comparison of the stress distributions through the girder web of the 1/4 symmetric model and the 1/4 symmetric refined model

TABLE 2.1 STRESS CONCENTRATION FACTORS ALONG THE PROSPECTIVE CRACK PATH FROM ANALYSIS OF THE TWO-DIMENSIONAL FINE MESH

z (in.)	ℓ (in.)	ℓ/T_w	K_t
0.375	0.0	0.0	18.0
0.364	0.011	0.03	8.04
0.348	0.027	0.07	5.73
0.326	0.049	0.13	4.61
0.296	0.079	0.21	3.65
0.253	0.122	0.33	2.67
0.195	0.180	0.48	1.60
0.113	0.262	0.70	0.38
0.0	0.375	1.00	-1.41

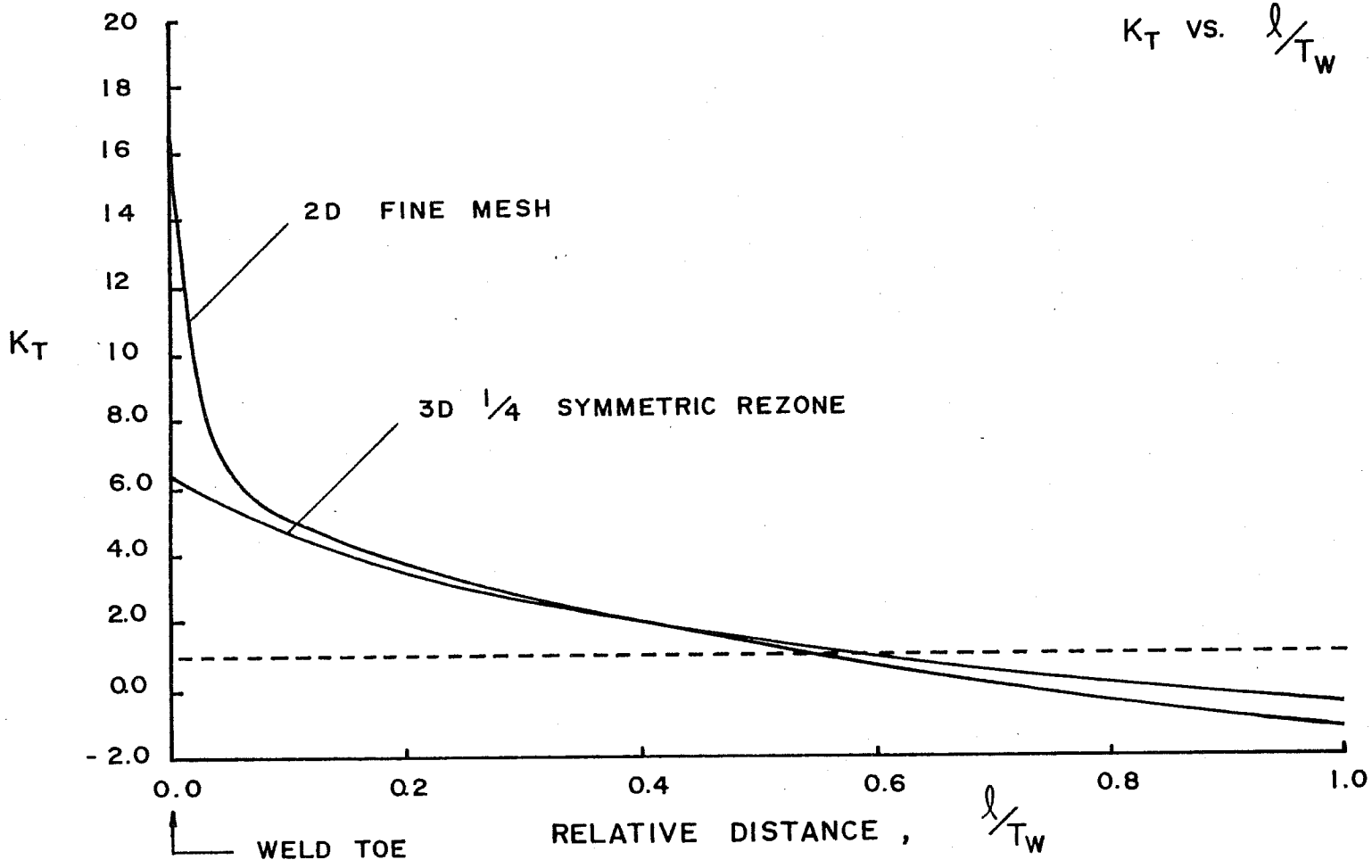

Fig. 2.21 Comparison of the stress distribution through the girder web of the two-dimensional fine mesh and the 1/4 symmetric refined mesh

TABLE 2.2 STRESS CONCENTRATION FACTORS ALONG THE PROSPECTIVE CRACK PATH FROM ANALYSIS OF THE ULTRA-FINE MESH

z (in.)	ℓ (in.)	ℓ/T_w	K_t	z (in.)	ℓ (in.)	ℓ/T_w	K_t
0.375	0.0	0.0	17.8	0.296	0.079	0.210	3.65
0.373	0.002	0.005	12.1	0.287	0.088	0.235	3.43
0.371	0.004	0.010	9.98	0.279	0.096	0.255	3.22
0.368	0.007	0.020	8.82	0.270	0.105	0.280	3.03
0.366	0.009	0.025	8.05	0.262	0.113	0.300	2.84
0.364	0.011	0.030	7.50	0.253	0.122	0.325	2.67
0.361	0.014	0.035	6.94	0.241	0.134	0.355	2.44
0.358	0.017	0.045	6.52	0.230	0.145	0.385	2.22
0.354	0.021	0.055	6.19	0.218	0.157	0.420	2.00
0.351	0.024	0.065	5.92	0.207	0.168	0.450	1.80
0.348	0.027	0.070	5.68	0.195	0.180	0.480	1.60
0.344	0.031	0.080	5.40	0.179	0.196	0.525	1.34
0.339	0.036	0.095	5.17	0.162	0.213	0.570	1.08
0.335	0.040	0.105	4.96	0.146	0.229	0.610	0.84
0.330	0.045	0.120	4.77	0.129	0.246	0.655	0.61
0.326	0.049	0.130	4.60	0.113	0.262	0.700	0.39
0.320	0.055	0.145	4.38	0.090	0.285	0.760	-0.10
0.314	0.061	0.160	4.18	0.068	0.307	0.820	-0.21
0.308	0.067	0.180	3.99	0.045	0.330	0.880	-0.57
0.302	0.073	0.195	3.82	0.023	0.352	0.940	-0.96
				0.0	0.375	1.0	-1.40

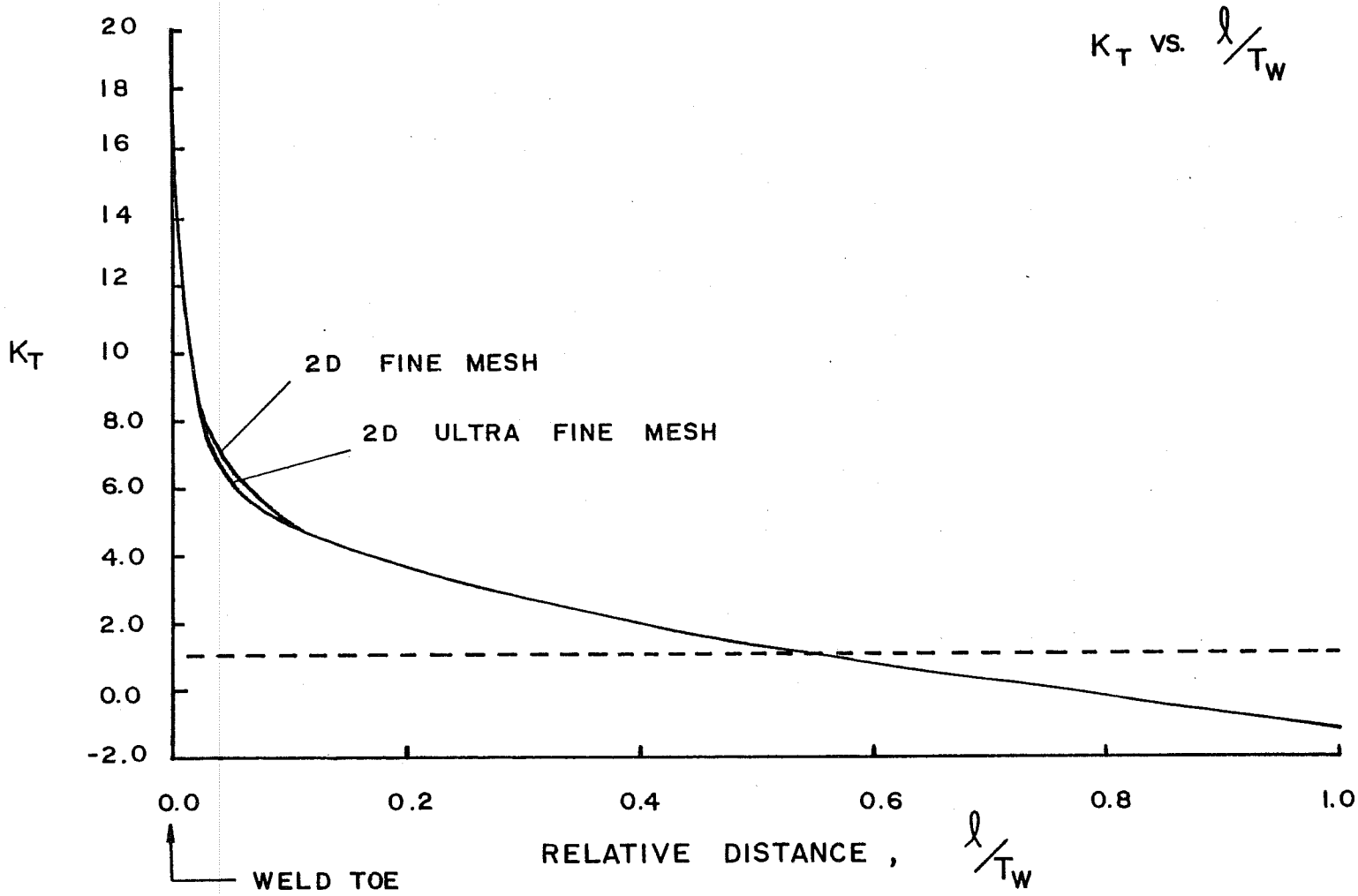

Fig. 2.22 Comparison of the stress distribution through the girder web of the ultra-fine mesh and the fine mesh

essentially identical. Also, the stress concentration at the weld toe is the same in both cases. For ℓ/T_w of zero to 0.1, results of the two analyses differ slightly. If the ultra-fine mesh was refined even further, this difference would be expected to become even smaller. In conclusion, the results of the ultra-fine mesh analysis seem to indicate that the mesh has been refined to the point at which stabilization of the stress distribution along the prospective crack path has taken place.

Figure 2.23 summarizes the results of all finite element analyses performed on the longitudinal-transverse stiffener intersection. The curves illustrate the progression toward a stable distribution of stress concentrations beginning with the three-dimensional 1/4 symmetric model and ending with the two-dimensional ultra-fine mesh.

2.3.2 Geometric Variations. In addition to performing finite element analyses on the existing longitudinal-transverse stiffener intersection detail, the effects of geometric variations of the existing detail were studied. The results of these studies are intended to serve two purposes. First, information obtained can be used to aid in the determination of an effective experimental test program. Secondly, results may be used to determine the importance of member geometries with regard to fatigue life. Although an attempt to categorize each geometric variation of the existing detail will not be made in this study, results may be used by the designer to determine the significance of geometric variations.

The cope detail, however, will be discussed later and will be analyzed in a manner similar to that of the longitudinal-transverse stiffener intersection detail. The usefulness of the cope detail as a design detail, or as a retrofit to the longitudinal-transverse stiffener intersection detail, will be investigated.

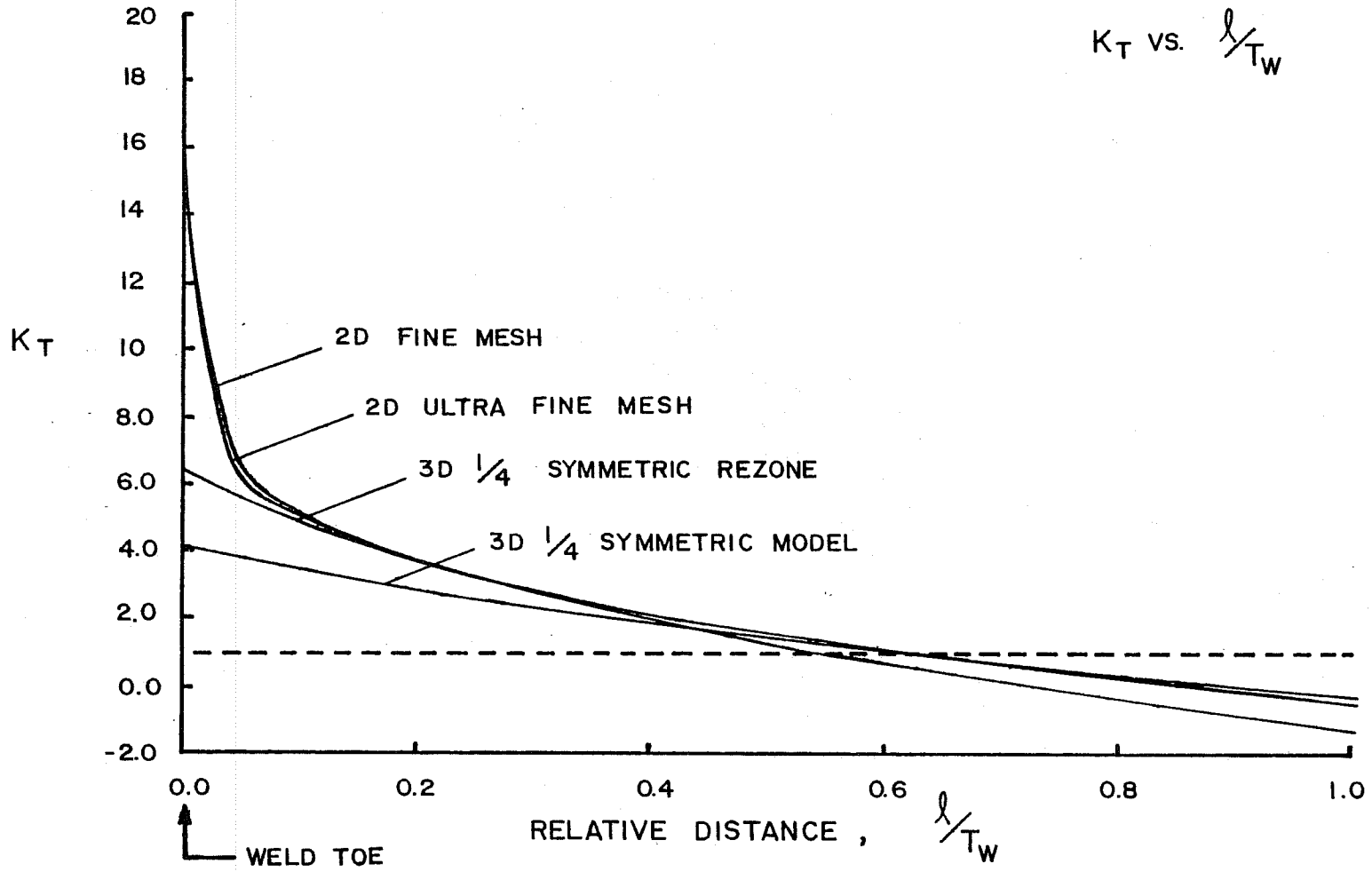

Fig. 2.23 Summary of the results of all analyses performed on the longitudinal-transverse stiffener intersection

2.3.2.1 Parameters. Several geometric parameters were thought to be important in determining the distribution of stresses along the prospective crack path through the girder web. These parameters include girder web thickness, longitudinal stiffener width, longitudinal stiffener thickness, and the size of the gap between the longitudinal stiffener and the transverse stiffener. Obviously, many combinations of these four parameters define unique details which could be analyzed. However, the purpose here is to change one parameter at a time in an attempt to isolate its effects on raising the nominal stress at the longitudinal stiffener-to-web weld toe. Therefore, a series of four finite element analyses were conducted. To investigate the effect of gap length, the two-dimensional fine mesh of the existing detail was modified and analyzed. For all remaining parameters, the three-dimensional 1/4 symmetric model was utilized. The thickness of the longitudinal stiffener of the existing detail was first increased, and an analysis of the modified detail was performed. This detail was further modified by increasing the longitudinal stiffener width, and a second analysis was conducted. Lastly, the girder web width was increased and a final analysis of the modified 1/4 symmetric model was performed.

To establish reasonable relationships between the geometric parameters involved, current AASHTO bridge specifications were followed. In all cases, the longitudinal stiffener was proportioned so that:

$$I \geq D\, t^3 \left[2.4 \left(\frac{d_o}{D}\right)^2 - 0.13\right] \qquad (2.1)$$

where I = the moment of inertia of the longitudinal stiffener about its edge in contact with the web plate

D = the unsupported distance between girder flange components, in.

d_o = the distance between transverse stiffeners, in.

t = thickness of the web plate, in.

The thickness of the longitudinal stiffener was controlled such that

$$t_s \geq \frac{b'\sqrt{f_b}}{2250} \tag{2.2}$$

where t_s = the thickness of the longitudinal stiffener, in.

b' = the width of the longitudinal stiffener, in.

f_b = the calculated compressive bending stress in the flange, psi

The stress in the stiffener was conservatively taken as F_b, the allowable bending stress. Table 2.3 summarizes the values of the four geometric parameters for each of the analyses performed.

2.3.3.2 Results. For the first finite element analysis, the existing 1/4 symmetric model was modified by increasing the longitudinal stiffener thickness, T_s, from 7/16 in. to 7/8 in.. The results of this analysis are compared to those of the existing detail in Fig. 2.24. It can be seen that doubling T_s results in an increase in the stress concentration at the weld toe of approximately 50 percent. This can be expected, since as the size of the longitudinal stiffener increases, more stress must be transferred to the girder web at the stiffener end, resulting in higher stress concentrations.

The second analysis uses the same geometry as the first analysis, except that the longitudinal stiffener width, B_s, is increased from 6 to 8 in. The results of both analyses are compared in Fig. 2.25. Increasing B_s by 33 percent resulted in an increase in the stress concentration at the weld toe of approximately 30 percent. Again, the increase can be attributed to the larger amount of stress being transferred into the girder web.

TABLE 2.3 SUMMARY OF THE COMPUTER ANALYSES PERFORMED TO INVESTIGATE GEOMETRIC VARIATIONS

Analysis Number	Stiffener Thickness T_s (in.)	Stiffener Width B_s (in.)	Girder Web Thickness T_w (in.)	Gap Size G (in.)
Existing detail	0.4375	6.00	0.375	0.50
1	0.875	6.00	0.375	0.50
2	0.875	8.00	0.375	0.50
3	0.875	8.00	0.75	0.50
4	0.4375	6.00	0.375	2.00

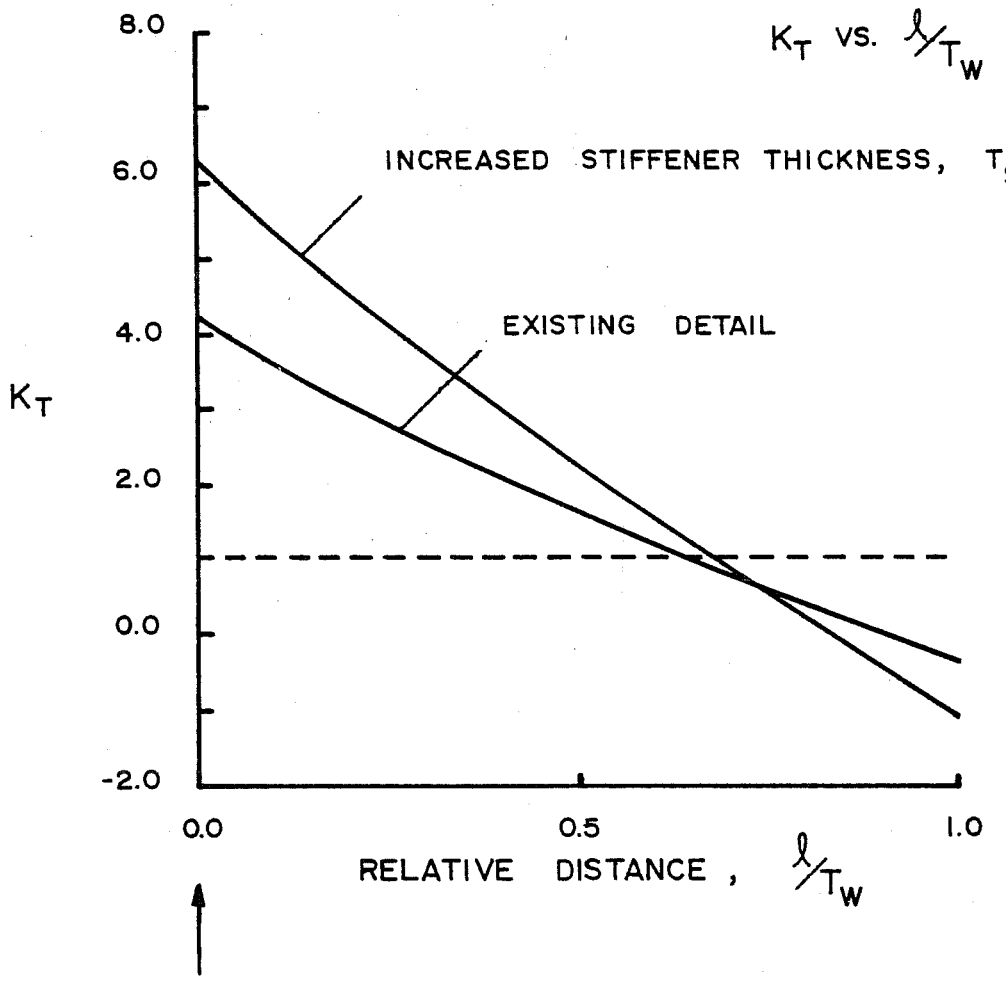

		ℓ/T_W		
		0	0.5	1.0
K_T	EXISTING DETAIL	4.19	1.59	-0.37
	INCREASED T_S	6.20	2.30	-1.10

Fig. 2.24 Effect of increasing longitudinal stiffener thickness on K_t

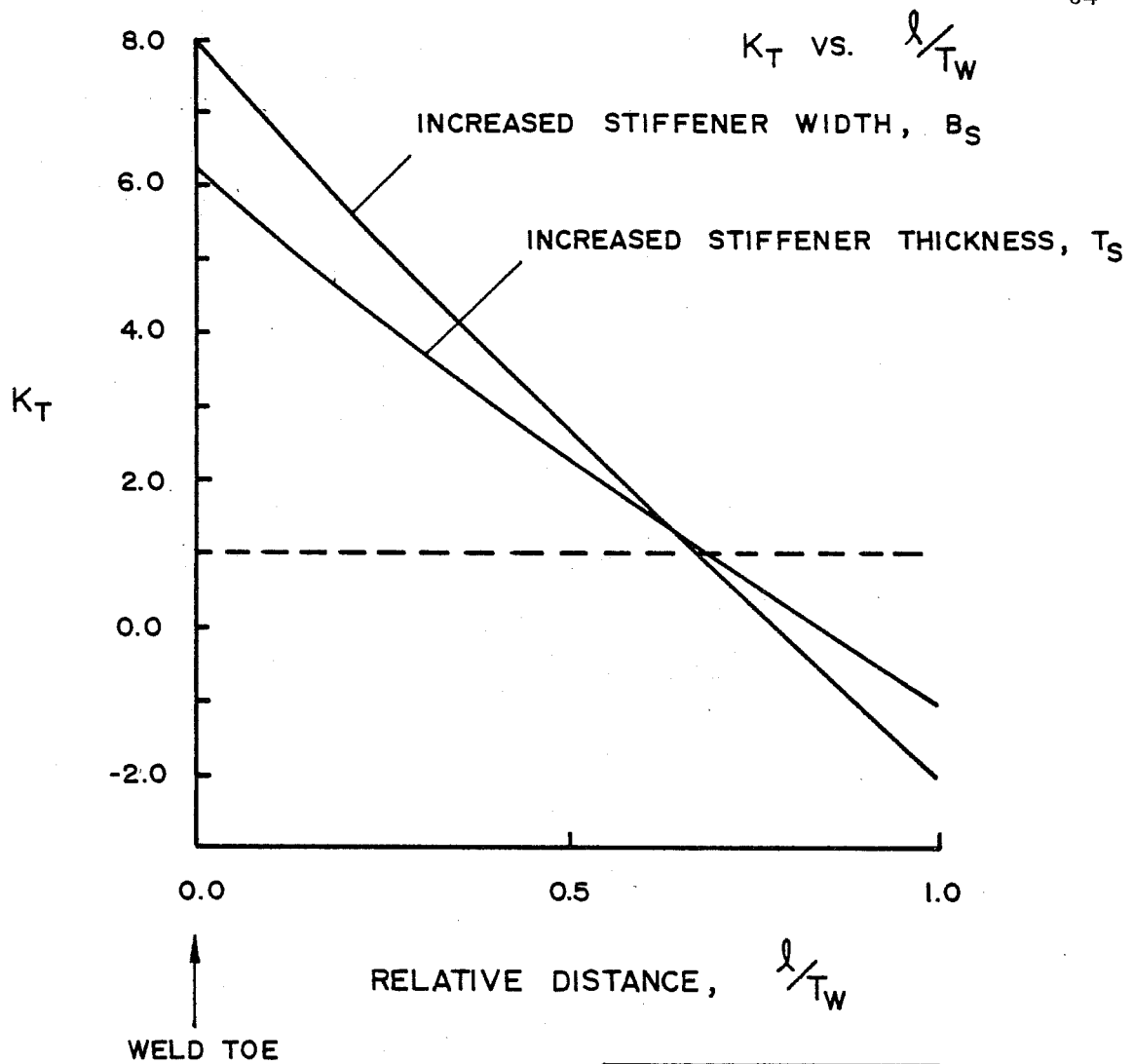

		ℓ/T_W		
		0	0.5	1.0
K_T	INCREASED T_S	6.20	2.30	-1.10
	INCREASED B_S	7.93	2.69	-2.06

Fig. 2.25 Effect of increasing longitudinal stiffener width on K_t

Figure 2.26 illustrates the effect of increasing the girder web thickness, T_w. The results from the model in which T_w was 3/8 in. are compared to those from the model in which T_w was increased to 3/4 in. With T_w doubled, the stress concentration at the weld toe decreases approximately 40 percent. Since a greater web cross section is available to handle stress due to the stiffener cutoff, a decrease in stress concentration is realized.

Figure 2.27 serves to summarize the results of analyses performed using the 1/4 symmetric finite element model. The stress distribution along the prospective crack path for the existing detail is compared to those resulting from increases in T_s, B_s, and T_w. Increasing T_s and B_s (the size of the longitudinal stiffener) results in a distribution of stress concentrations of greater severity. Increasing T_w reduces the magnitude of the stress distribution along the prospective crack path.

Although the AASHTO bridge specifications do not specify minimum and maximum values for the gap length, G, between longitudinal stiffener end and transverse stiffener, Fisher [1] has recommended using 4 to 6 times the girder web thickness. For the existing detail, G is equal to 1/2 in. If the recommended 4 to 6 times T_w were applied, minimum G would be 1-1/2 in., while maximum G would be 2-1/4 in. To determine the effect of increasing G, the two-dimensional fine mesh of the existing detail was utilized. The fine mesh was modified by increasing G from 1/2 in. to 2 in. The results of this modification are tabulated in Table 2.4 and displayed in Fig. 2.28. It can be seen that increasing G has a very beneficial effect of the severity of the stress distribution along the prospective crack path. This points out the fact that a major problem with the existing detail is the small gap length of 1/2 in.

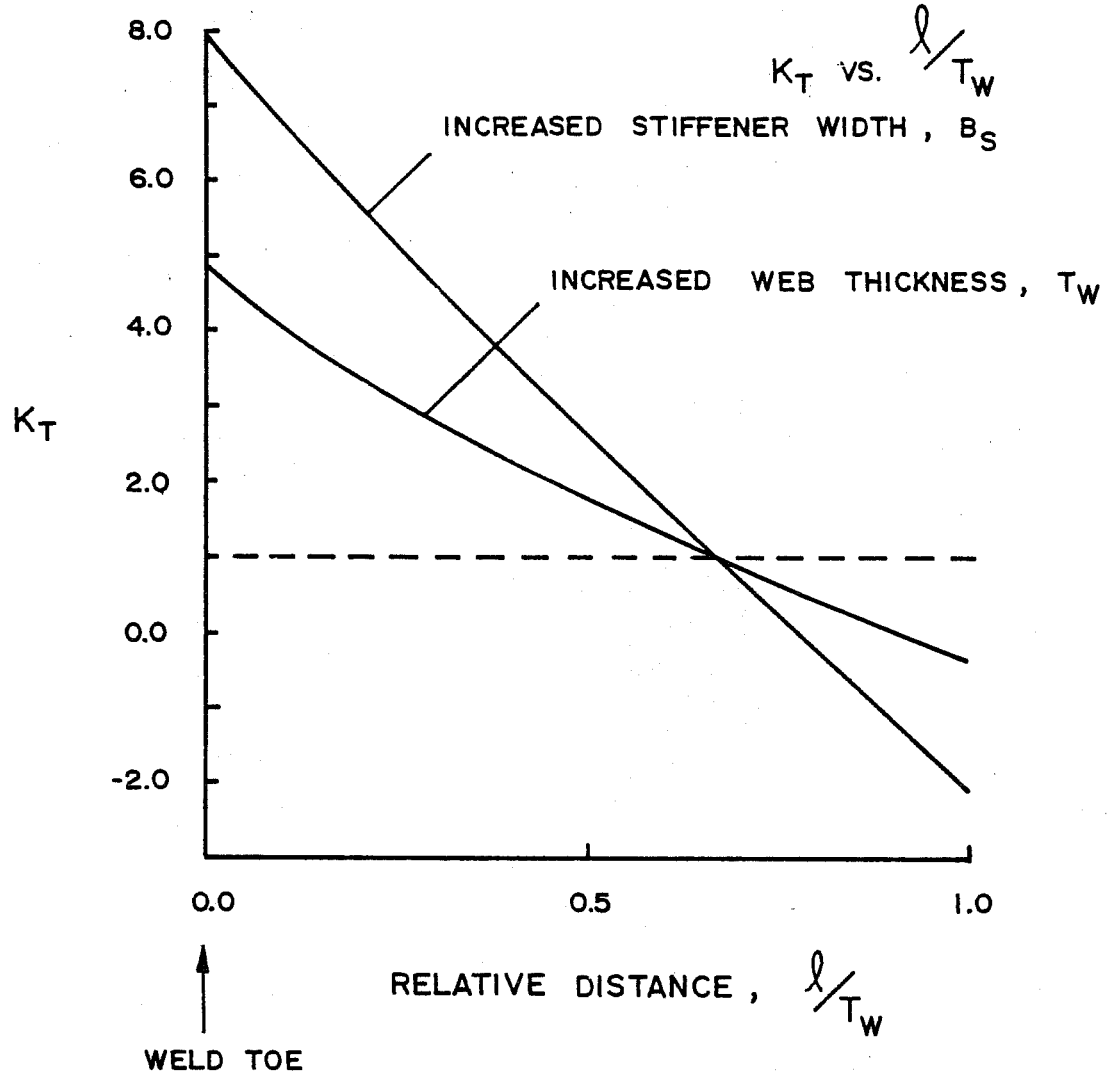

		ℓ/T_W		
		0	0.5	1.0
K_T	INCREASED B_S	7.93	2.69	-2.06
	INCREASED T_W	4.90	1.74	-0.35

Fig. 2.26 Effect of increasing girder web thickness on K_t

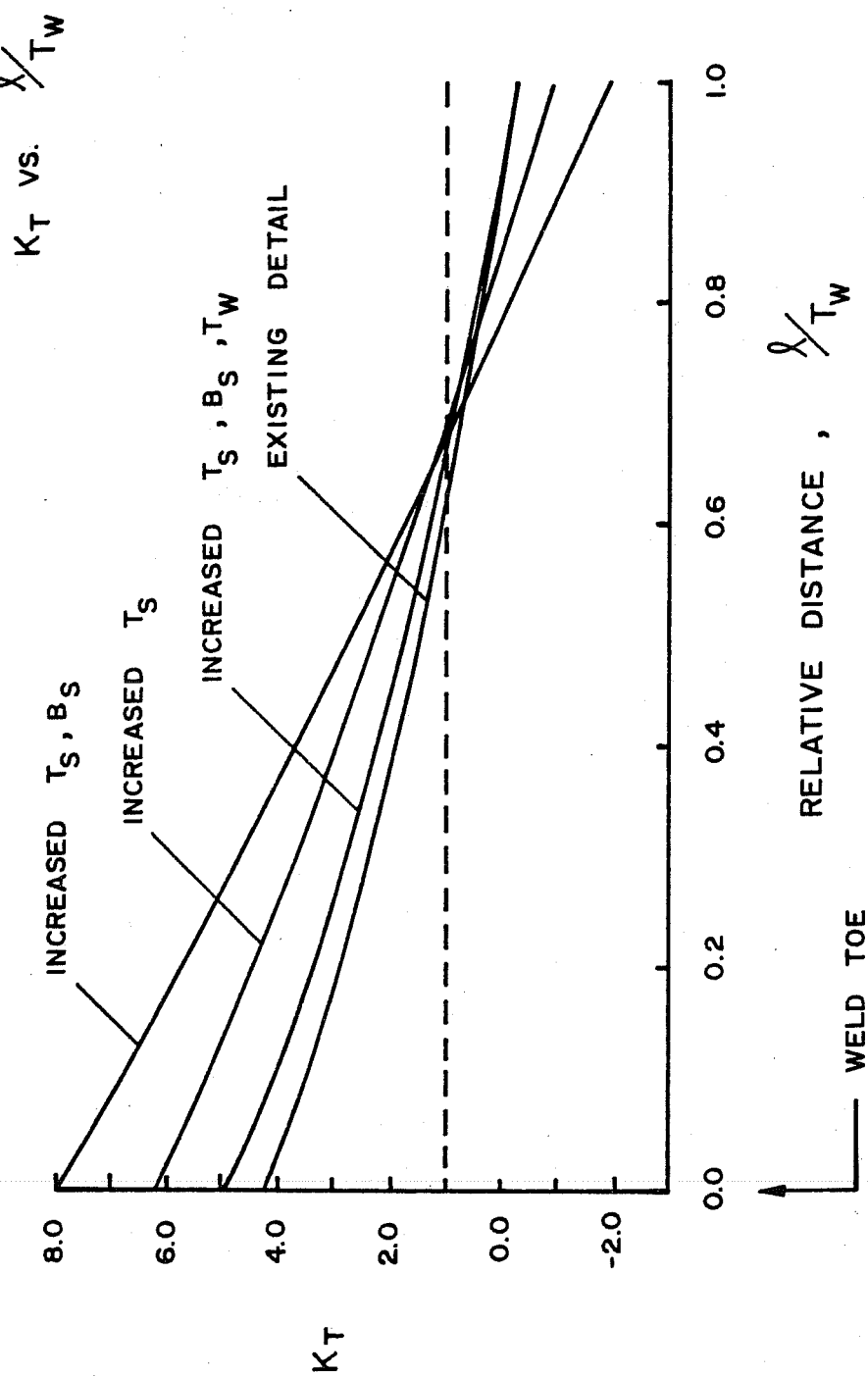

Fig. 2.27 Summary of the effect of T_s, B_s, and T_w on stress concentration, K_t

TABLE 2.4 STRESS CONCENTRATION FACTORS ALONG THE PROSPECTIVE CRACK PATH OF THE FINE MESH FOR G = 2 in.

z (in.)	ℓ (in.)	ℓ/T_w	K_t
0.375	0.0	0.0	6.44
0.364	0.011	0.03	3.66
0.348	0.027	0.07	2.79
0.326	0.049	0.13	2.26
0.296	0.079	0.21	1.90
0.253	0.122	0.33	1.57
0.195	0.180	0.48	1.22
0.113	0.262	0.70	0.77
0.0	0.375	1.00	0.06

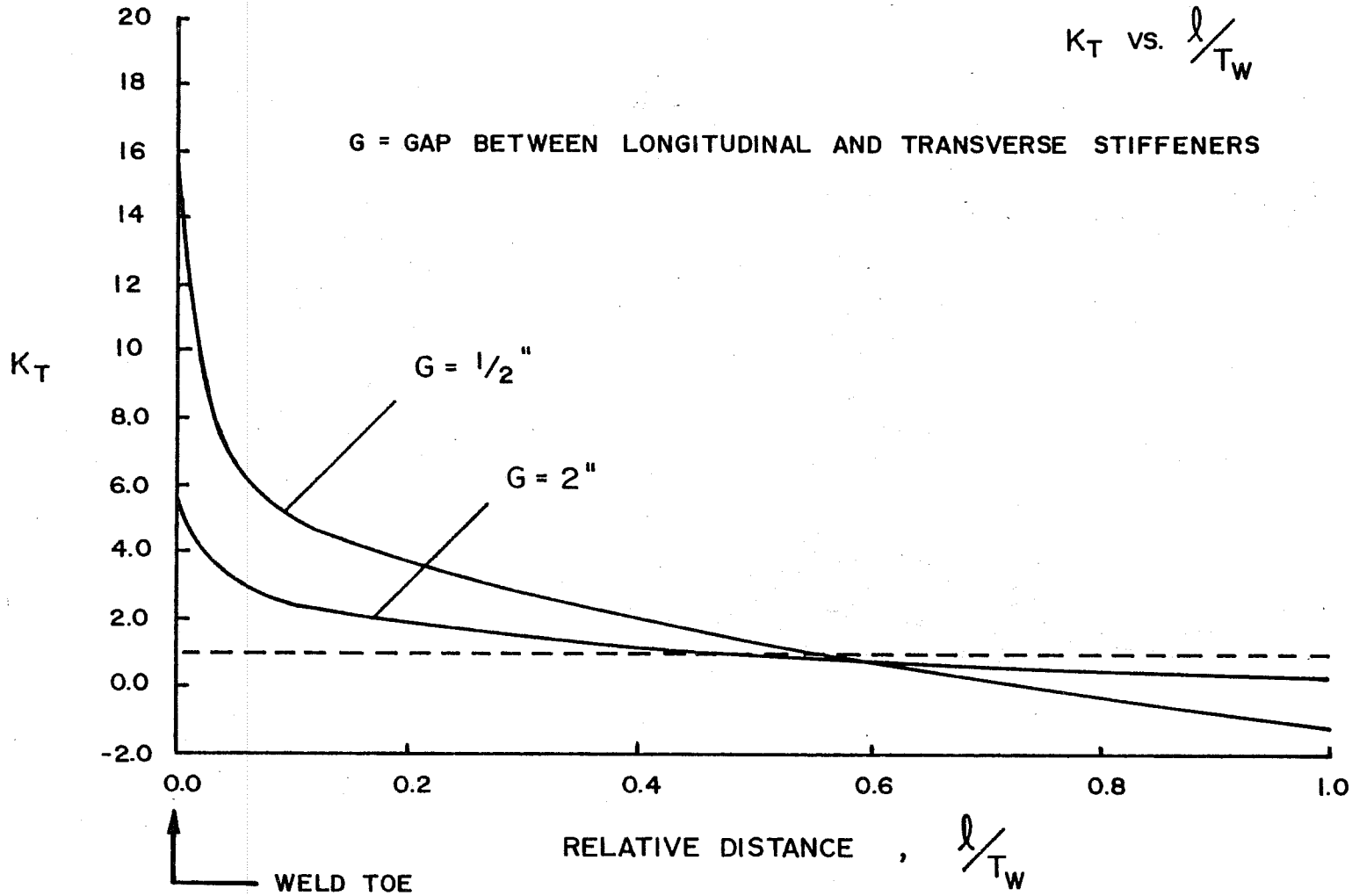

Fig. 2.28 Effect of increasing the gap length, G, on K_t

2.3.3 Cope Detail. To investigate the effectiveness of the cope as a possible means of retrofitting the existing detail, finite element analyses were performed in a manner similar to that used for the longitudinal-transverse stiffener intersection detail. The fatigue lives of both details will be estimated using principles of fracture mechanics, with comparisons and relevant recommendations being made in a later chapter.

2.3.3.1 Geometry and Modeling. Based on the results obtained from analysis of the longitudinal-transverse stiffener intersection, it was decided that a three-dimensional full-scale model of the cope detail was not needed. The accuracy of the 1/4 symmetric model had already been established. Therefore, the 1/4 symmetric model of the existing detail was modified by the addition of a 3 in. cope at the longitudinal-transverse stiffener intersection. In modeling the cope, the 15 node prism element was used along with the 20 node brick elements of the remaining portion of the model. Figure 2.29 illustrates the 1/4 symmetric model of the cope detail. The dimensions of the model are shown in Fig. 2.30.

Boundary conditions for the 1/4 symmetric model of the cope detail were the same as those used on the model of the existing detail. Tensile stress was applied, as shown in Fig. 2.31, and out-of-plane displacement at the transverse stiffener was prevented. The unloaded end of the model was fixed in the direction of applied stress. Horizontal movement was prevented at the boundary which represents the neutral axis of the girder. Figure 2.31 shows the mesh used in the model which consisted of 115 brick elements and one prism element.

As was done for the existing detail, the 1/4 symmetric model of the cope detail was refined in the region of the

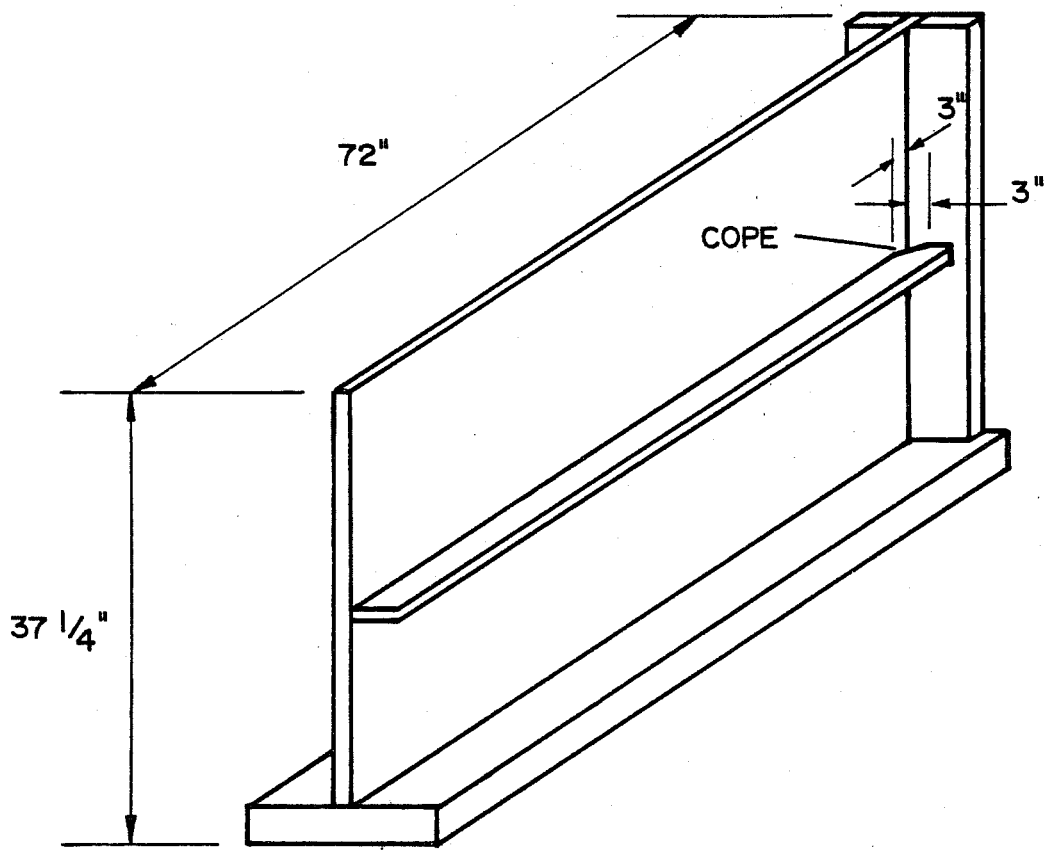

Fig. 2.29 Three-dimensional 1/4 symmetric model of the cope detail

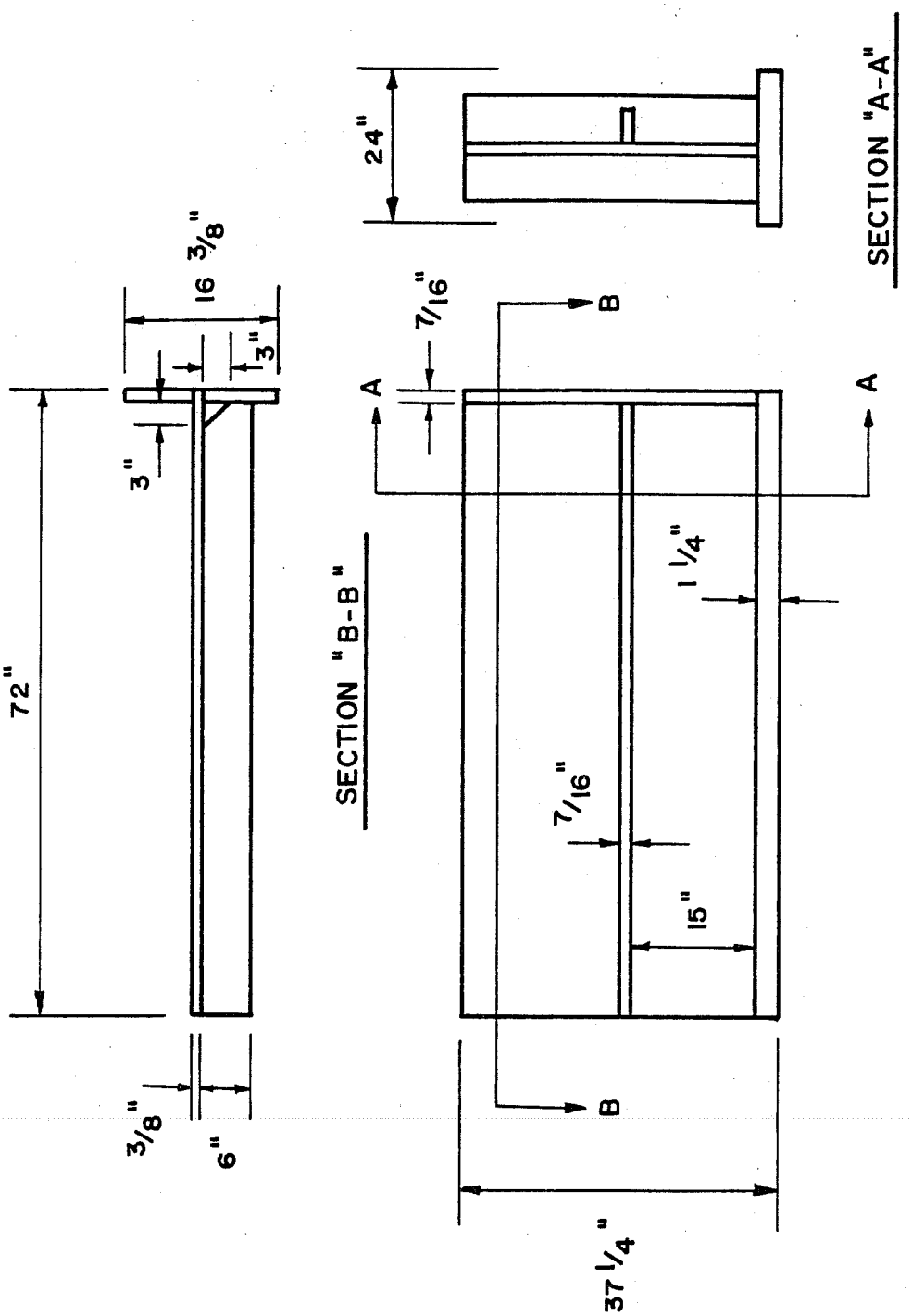

Fig. 2.30 Dimensions of the 1/4 symmetric cope detail model

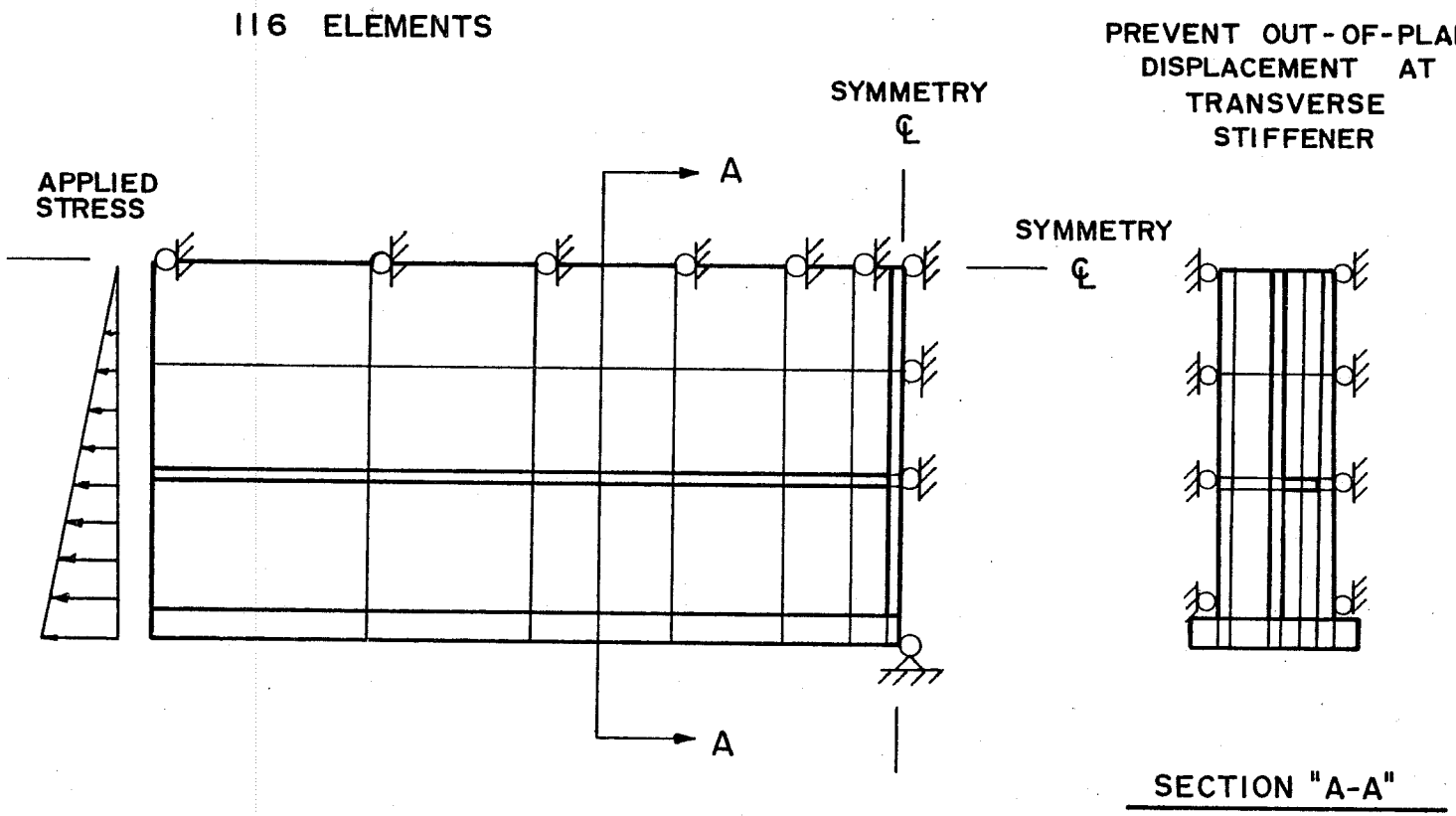

Fig. 2.31 One-quarter symmetric cope detail model mesh with boundary conditions shown

longitudinal stiffener end to obtain an accurate set of nodal displacements to be imposed on the fine mesh. To minimize computer solution time, only the two elements of the longitudinal stiffener were refined. This gives the required nodal displacements, but does not provide any additional information regarding the stress distribution along the prospective crack path. Figure 2.32 illustrates the grid refinement of the 1/4 symmetric model of the longitudinal stiffener end. Also shown in Fig. 2.32 is the "match section" used as the basis for the grid definition of the two-dimensional fine mesh. The location of the "match section" also determines which nodal displacements are to be applied to the fine mesh.

The resulting two-dimensional fine mesh is shown in Fig. 2.33. Again, the model uses 4 node quadratic elements as well as triangular elements. The web-to-longitudinal stiffener weld was modeled, as shown in Fig. 2.33. To minimize the need for additional elements in the fine mesh, the web-to-transverse stiffener weld was not included. Since this weld is significantly removed from the prospective crack path, effects due to its elimination should be negligible. As in the existing detail fine mesh, the cope detail fine mesh possesses a high degree of resolution local to the prospective crack path.

Boundary conditions for the fine mesh were based on those of the three-dimensional model. In addition to the application of the nodal displacements from the coarse mesh, the transverse stiffener was again fixed against out-of-plane displacement as well as displacement in the longitudinal direction. These conditions are illustrated in Fig. 2.33.

To generate the ultra-fine mesh local to the web-to-longitudinal stiffener weld toe, experience gained from analysis

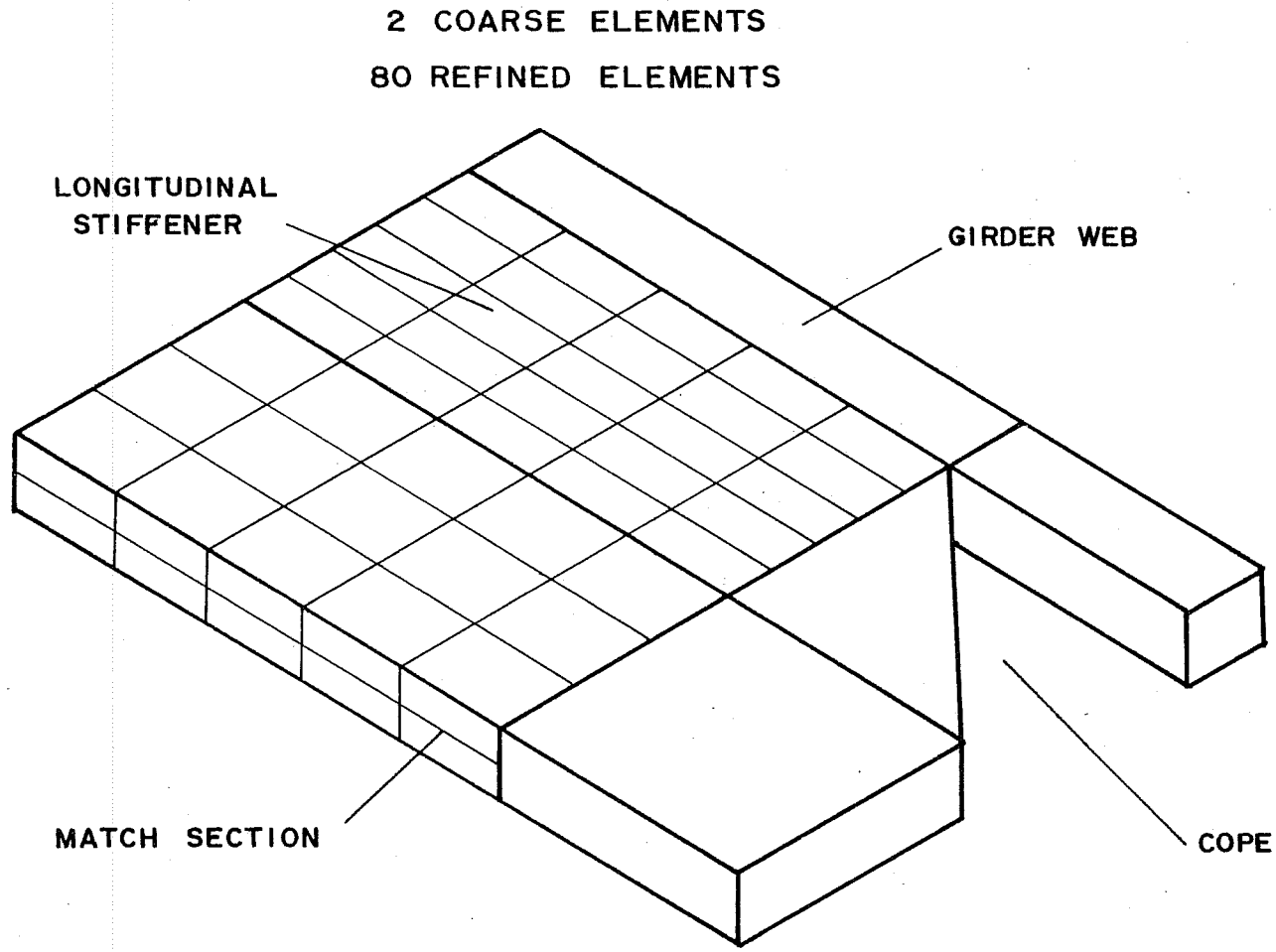

Fig. 2.32 One-quarter symmetric cope detail model grid refinement in the local region of interest showing "match section"

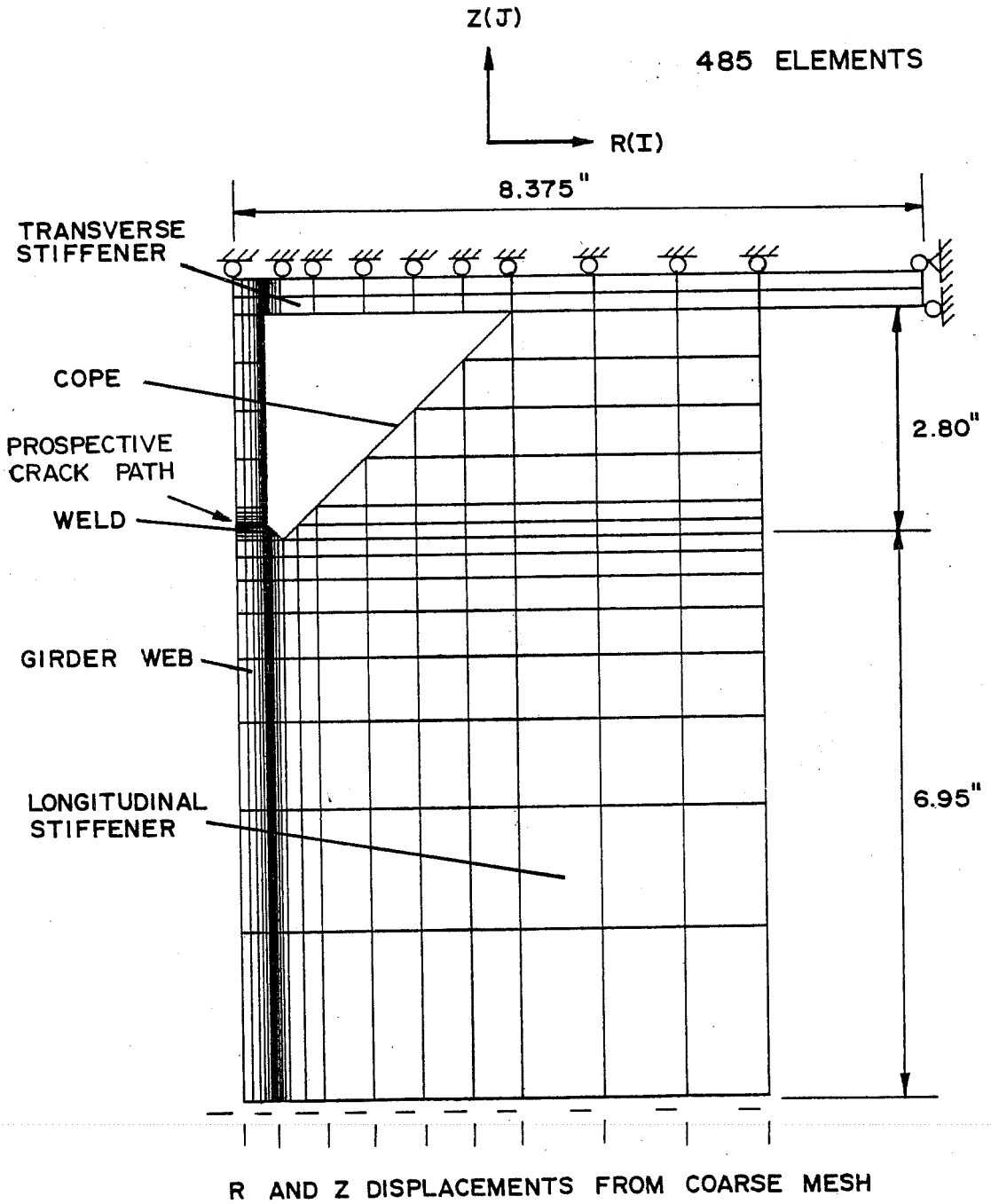

Fig. 2.33 Two-dimensional fine mesh for the cope detail with boundary conditions shown

of the existing detail was utilized. Once again, to avoid exceeding the dimensions of the TEXGAP computer program, the fine mesh was rotated 90°. To minimize computer solution time, the rotated fine mesh was generated only for the area local to the prospective crack path, as shown in Fig. 2.34. Boundary conditions for the rotated fine mesh were obtained from analysis of the large fine mesh shown in Fig. 2.33. The ultra-fine mesh was then obtained by rezoning the rotated fine mesh in the area local to the web-to-longitudinal stiffener weld. Figure 2.35 illustrates the ultra-fine mesh with corresponding element sizes. The sizes of the elements in the direction parallel to the prospective crack path were the same as those used for the existing detail. As a result, reasonable accuracy in F_g during the early stages of crack growth should be obtained.

2.3.3.2 Results. The results of the analysis of the three-dimensional 1/4 symmetric model of the cope detail are shown in Fig. 2.36.

Table 2.5 lists the stress concentration factors obtained from analysis of the two-dimensional fine mesh of the cope detail. Table 2.6 lists these factors resulting from analysis of the ultra-fine mesh. Results of both analyses are plotted and compared in Fig. 2.37. For the most part, the stress distributions are identical. Only for values of ℓ/T_w between 0.03 and 0.07 do the values of K_t deviate from one another. As was the case with the analysis of the existing detail, analysis of the cope detail indicates that the ultra-fine mesh has been refined a sufficient amount to stabilize the stress distribution along the prospective crack path.

Figure 2.38 summarizes the results of all finite element analyses performed on the cope detail. In a manner similar to that of the existing detail, the curves progress toward a stable

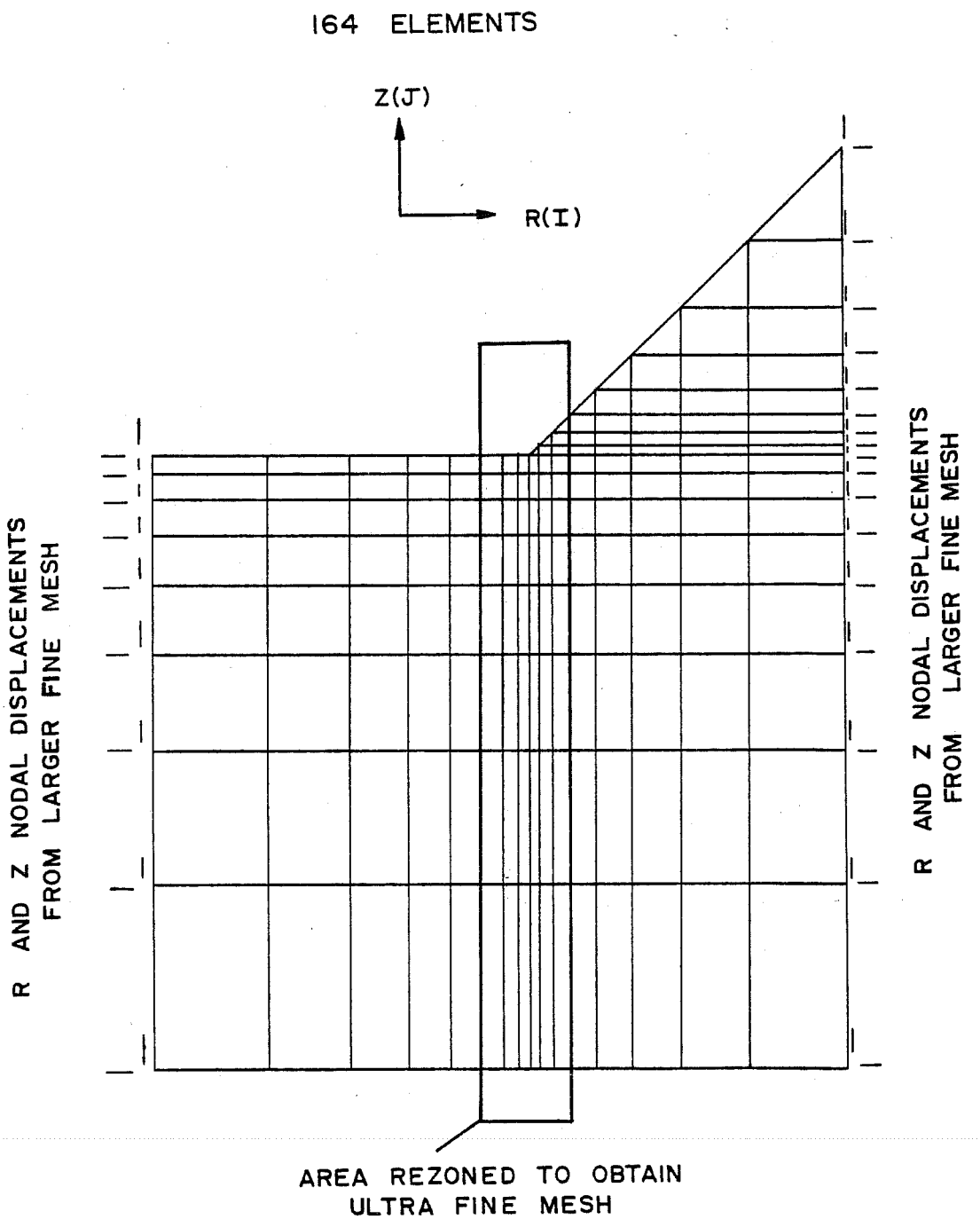

Fig. 2.34 Fine mesh in local area of the longitudinal stiffener-to-web weld

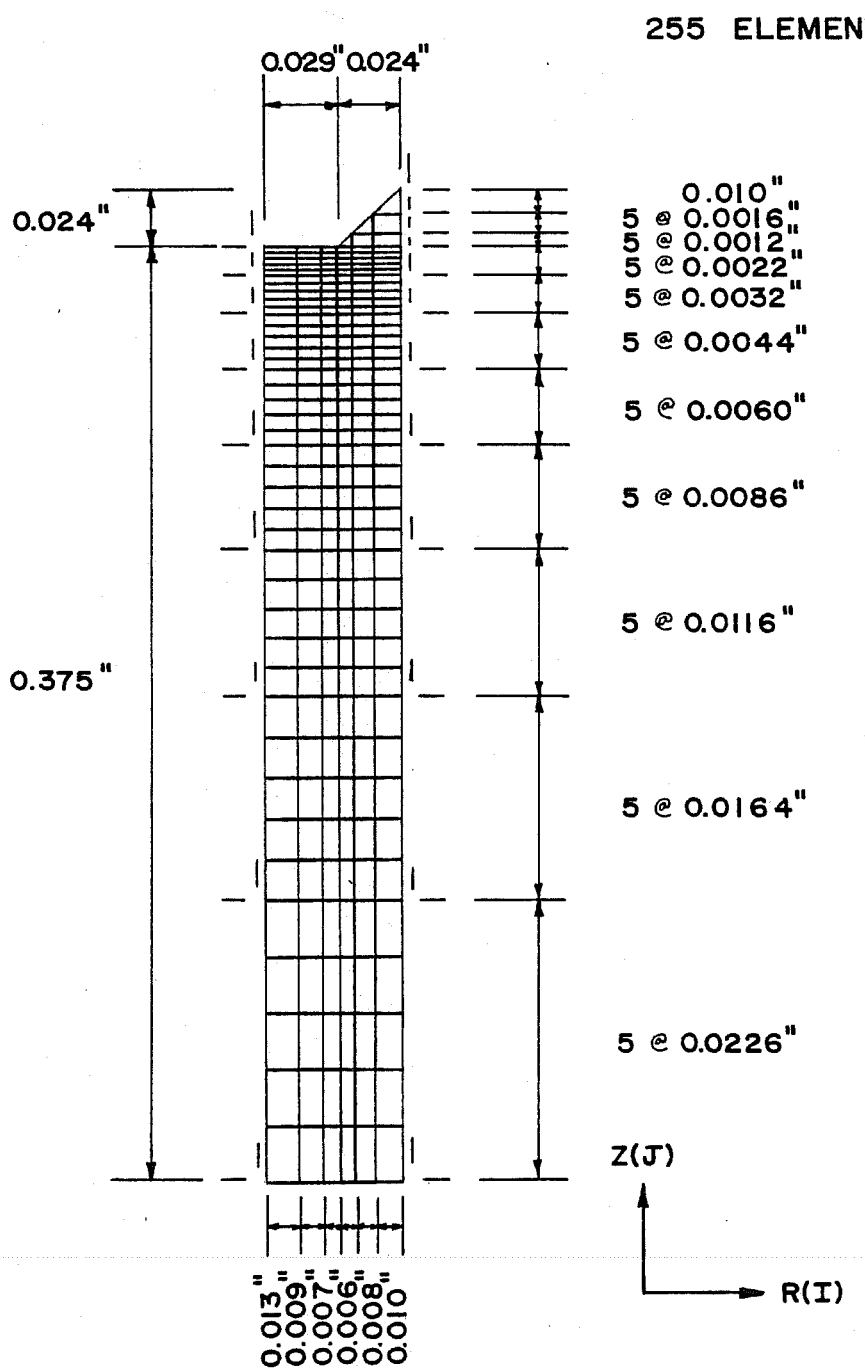

Fig. 2.35 Ultra-fine mesh for cope detail showing element sizes

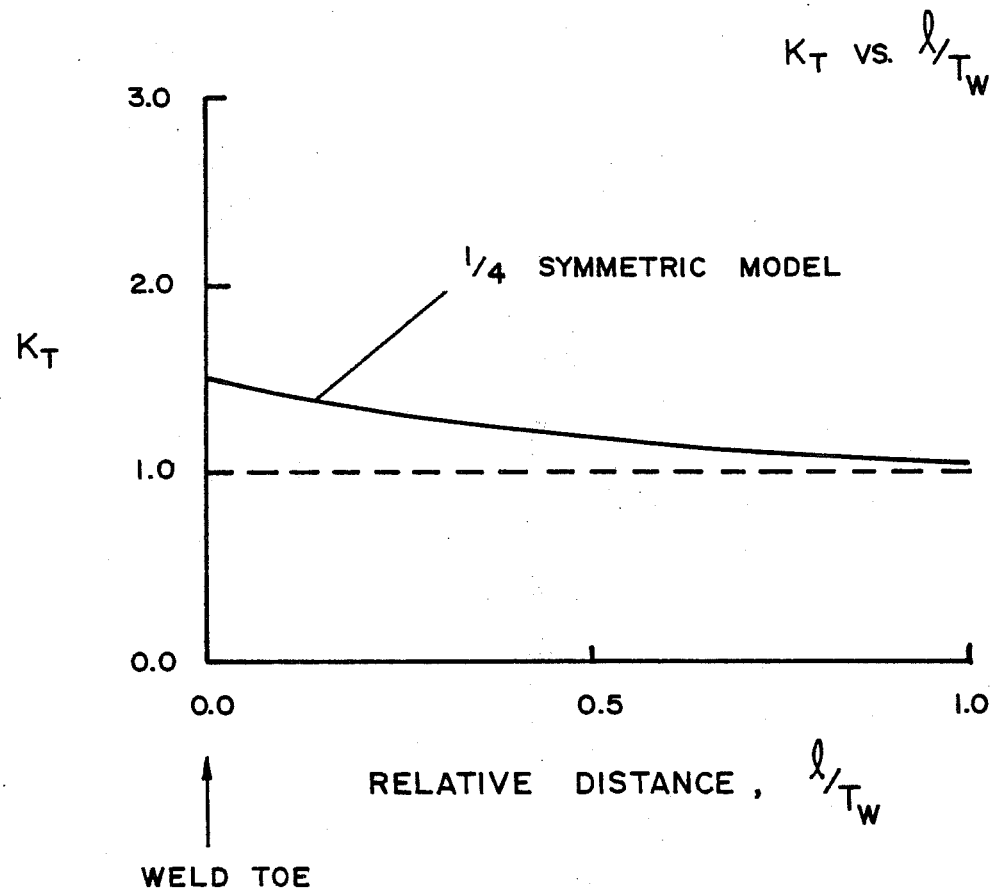

		ℓ/T_W		
		0	0.5	1.0
K_T	1/4 SYMMETRIC MODEL	1.51	1.18	1.06

Fig. 2.36 Distribution of stress through the girder web of the cope detail for the 1/4 symmetric model

TABLE 2.5 STRESS CONCENTRATION FACTORS ALONG THE PROSPECTIVE CRACK PATH OF THE COPE DETAIL FROM ANALYSIS OF THE FINE MESH

z (in.)	ℓ (in.)	ℓ/T_w	K_t
0.375	0.0	0.0	6.55
0.364	0.011	0.03	3.46
0.348	0.027	0.07	2.64
0.326	0.049	0.13	2.29
0.296	0.079	0.21	2.06
0.253	0.122	0.33	1.85
0.195	0.180	0.48	1.62
0.113	0.262	0.70	1.39
0.0	0.375	1.00	1.03

TABLE 2.6 STRESS CONCENTRATION FACTORS ALONG THE PROSPECTIVE CRACK PATH OF THE COPE DETAIL FROM ANALYSIS OF THE ULTRA-FINE MESH

z (in.)	ℓ (in.)	ℓ/T_w	K_t	z (in.)	ℓ (in.)	ℓ/T_w	K_t
0.375	0.0	0.0	6.51	0.296	0.079	0.210	2.06
0.373	0.002	0.005	5.10	0.287	0.088	0.235	2.01
0.371	0.004	0.010	4.33	0.279	0.096	0.255	1.96
0.368	0.007	0.020	3.87	0.270	0.105	0.280	1.92
0.366	0.009	0.025	3.55	0.262	0.113	0.300	1.88
0.364	0.011	0.030	3.33	0.253	0.122	0.325	1.85
0.361	0.014	0.035	3.11	0.241	0.134	0.355	1.80
0.358	0.017	0.045	2.95	0.230	0.145	0.385	1.75
0.354	0.021	0.055	2.82	0.218	0.157	0.420	1.70
0.351	0.024	0.065	2.72	0.207	0.168	0.450	1.66
0.348	0.027	0.070	2.63	0.195	0.180	0.480	1.62
0.344	0.031	0.080	2.54	0.179	0.196	0.525	1.57
0.339	0.036	0.095	2.46	0.162	0.213	0.570	1.52
0.335	0.040	0.105	2.40	0.146	0.229	0.610	1.48
0.330	0.045	0.120	2.35	0.129	0.246	0.655	1.43
0.326	0.049	0.130	2.30	0.113	0.262	0.700	1.39
0.320	0.055	0.145	2.23	0.090	0.285	0.760	1.34
0.314	0.061	0.160	2.18	0.068	0.307	0.820	1.27
0.308	0.067	0.180	2.14	0.045	0.330	0.880	1.20
0.302	0.073	0.195	2.09	0.023	0.352	0.940	1.12
				0.0	0.375	1.0	1.03

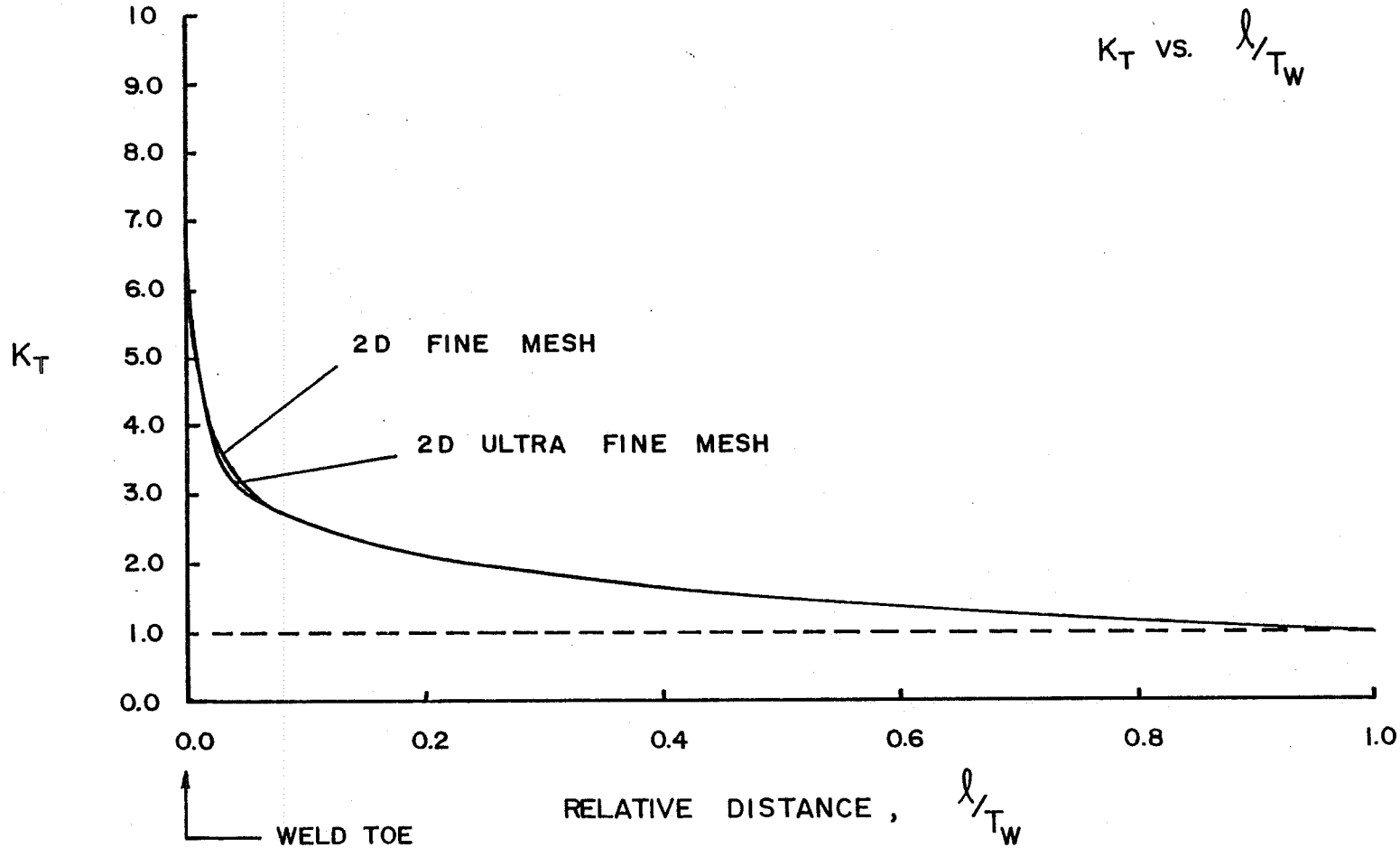

Fig. 2.37 Comparison of the stress distribution through the girder web of the cope detail for the fine mesh and the ultra-fine mesh

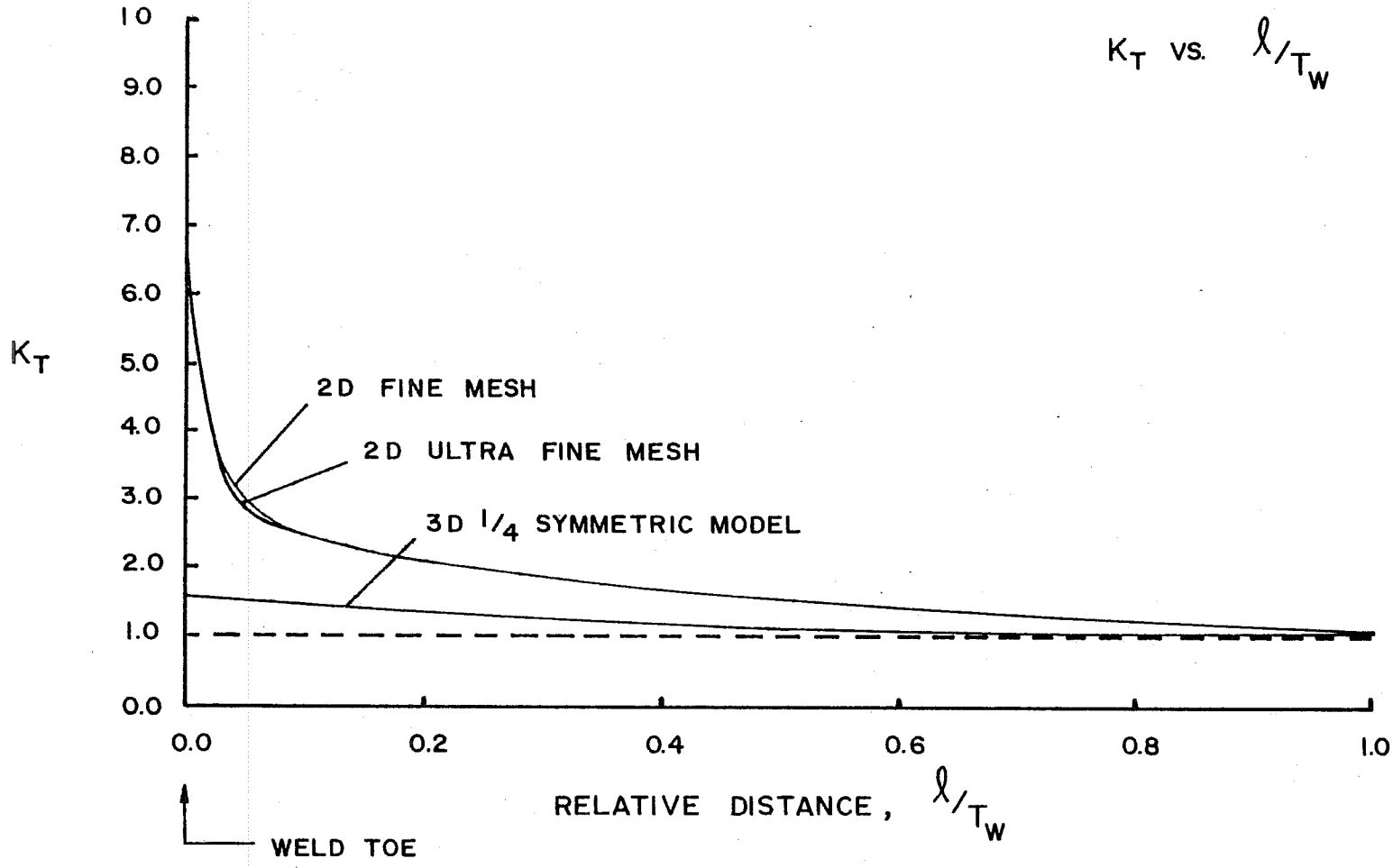

Fig. 2.38 Summary of the results of all analyses performed on the cope detail

distribution of stress concentrations beginning with the three-dimensional 1/4 symmetric model and ending with the two-dimensional ultra-fine mesh.

Figure 2.39 indicates that the stress distribution through the girder web of the cope detail is much less severe than that of the existing detail. These differences should be reflected in the estimation of fatigue lives for the two details.

2.4 Bridge Test Results

Field tests were conducted as a means of verifying the accuracy of the finite element model utilized in the analysis of the longitudinal-transverse intersection detail. A strain-gaging scheme, shown in Fig. 2.40, was designed to serve two main purposes. First, gages were mounted along the longitudinal stiffener in an attempt to describe the development of stress in the stiffener. Secondly, gages were mounted vertically on the girder web in the vicinity of the longitudinal stiffener end in an attempt to isolate stress concentrations.

Data obtained from the longitudinal stiffener gages are depicted in Fig. 2.41. Results are presented in a plot of percent of nominal stress, S, vs. distance from stiffener end, D. The plot serves to describe the buildup of stress in the longitudinal stiffener and to compare directly to results obtained using the finite element model. Since the field test data points represent stresses relative to the nominal stress (the stress in the girder at the level of the longitudinal stiffener based on known stresses in the girder flanges and the assumption that plane sections remain plane), the points had to be obtained by looking at an instantaneous scan of all strain gages. This was made possible by the high speed data acquisition equipment used to conduct the field tests. The equipment electronically scans at a rate of

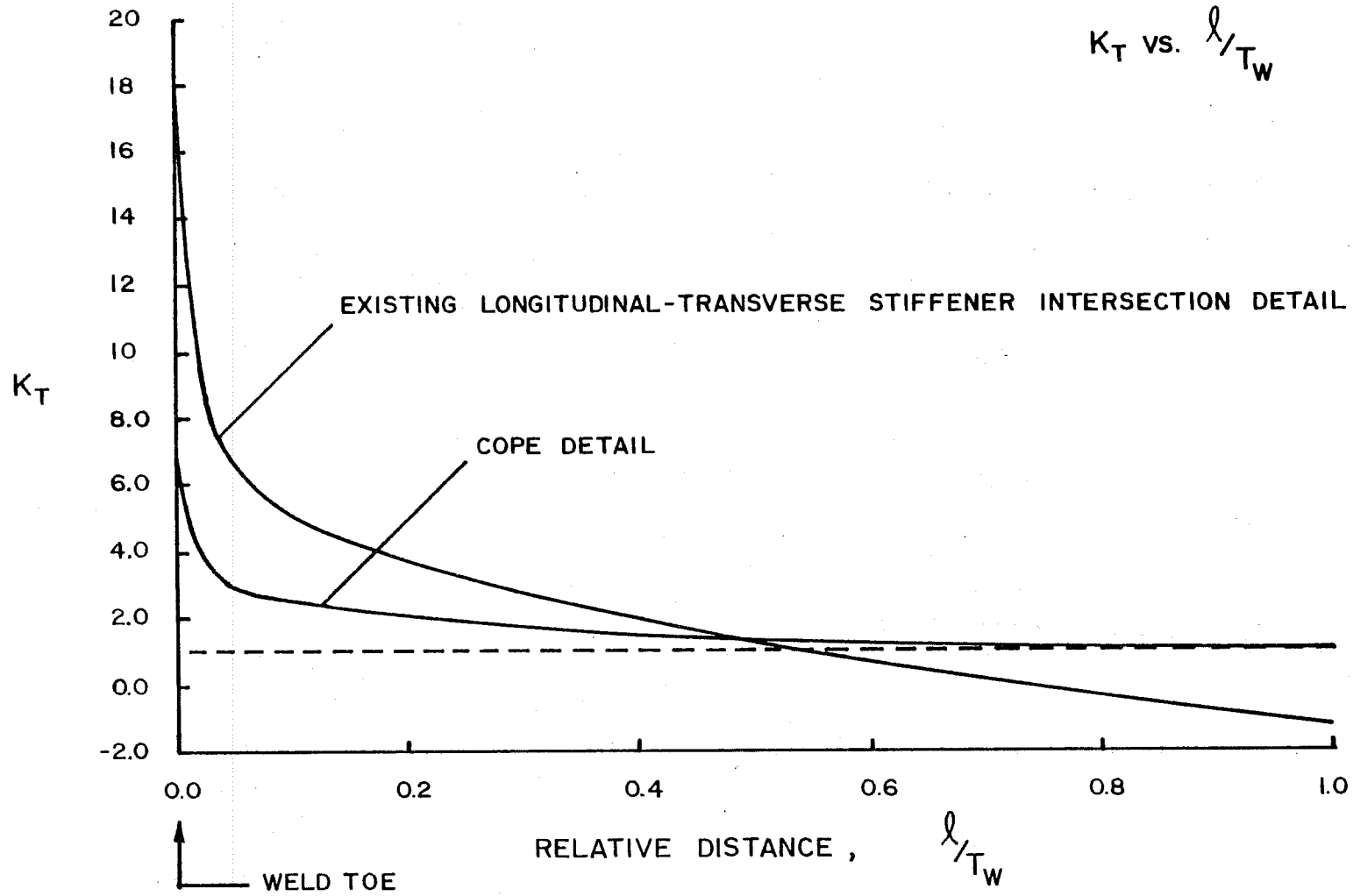

Fig. 2.39 Comparison of the stress distribution through the girder web of the cope detail and the existing detail

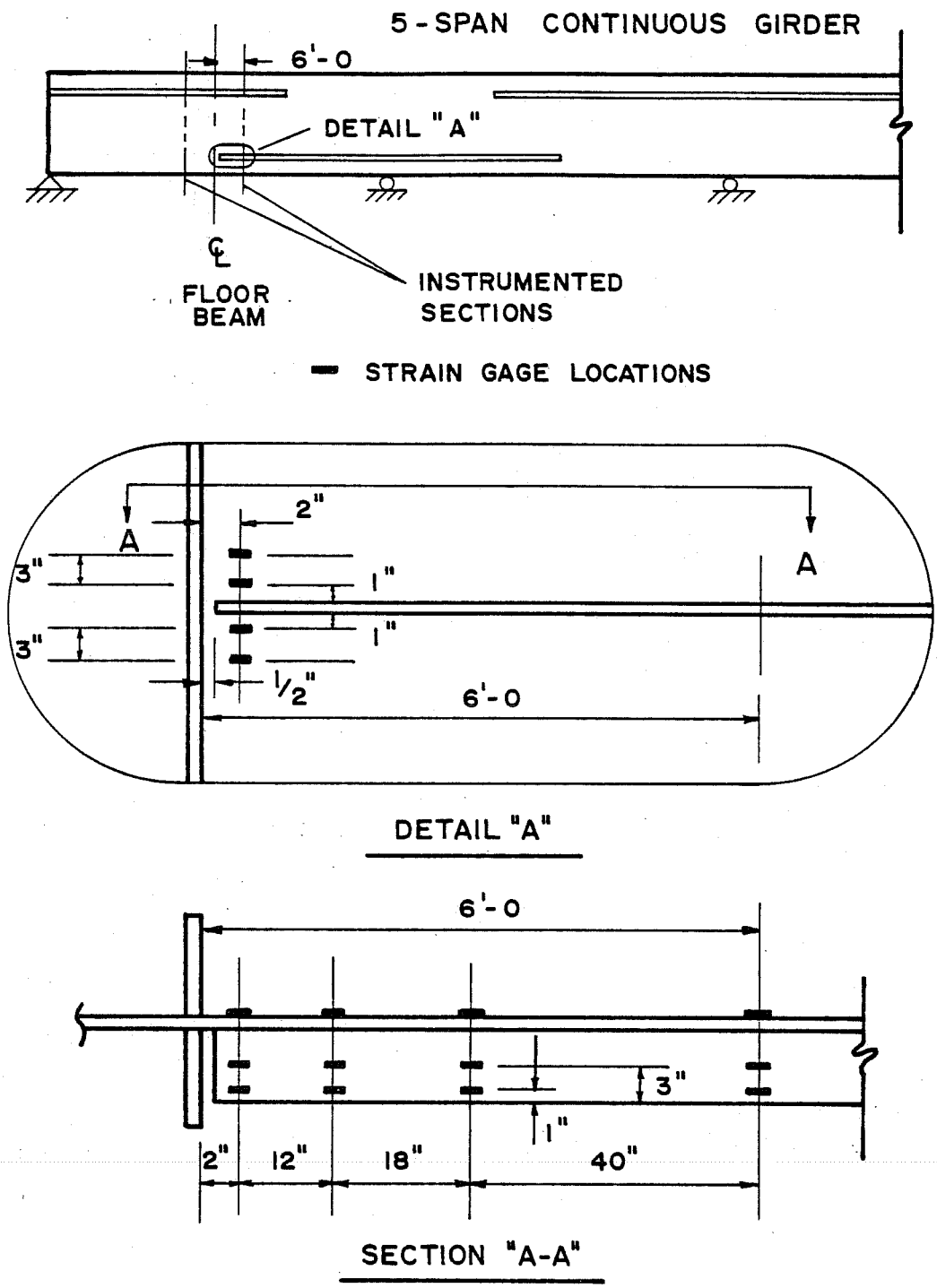

Fig. 2.40 Gaging scheme for longitudinal-transverse stiffener intersection

10,000 channels per second, recording all data on magnetic tape for subsequent computer processing. An instantaneous scan can thus be analyzed with the relative values of each strain gage being computed. Each data point at a particular gage location in Fig. 2.41 represents one instantaneous scan. Two points are plotted for each gage location, one point being obtained from a single scan of one test, and one point from a single scan of a second test. This serves to give an indication of the scatter obtained in the field test data. The smooth curve of the S vs. D plot was obtained from the full-scale finite element computer model. It can be seen that field test results correlate quite well with the predicted results using the finite element model. This is very important in assuring that the computer model accurately depicts actual conditions.

The gages mounted vertically on the girder web in the vicinity of the longitudinal stiffener end did not indicate the presence of a stress concentration. Again, stresses were computed relative to the nominal stress. In addition, since the gages were mounted vertically and their distances to the neutral axis varied, values were normalized to a common distance from the neutral axis to facilitate comparison. A plot of percent of nominal stress vs vertical distance from stiffener end is shown in Fig. 2.42. It can be seen that no evidence of a stress concentration is present in the data. This could be the result of several factors. First, the stress concentration at the stiffener end is likely to be very localized in the area of the gap between the transverse and longitudinal stiffeners. Mounting of strain gages in this localized region was found to be virtually impossible. Secondly, the type of strain gages used to instrument the bridge were quite large (approximately 1/2 in. in length), making detection of a localized stress concentration very difficult. Lastly, the levels

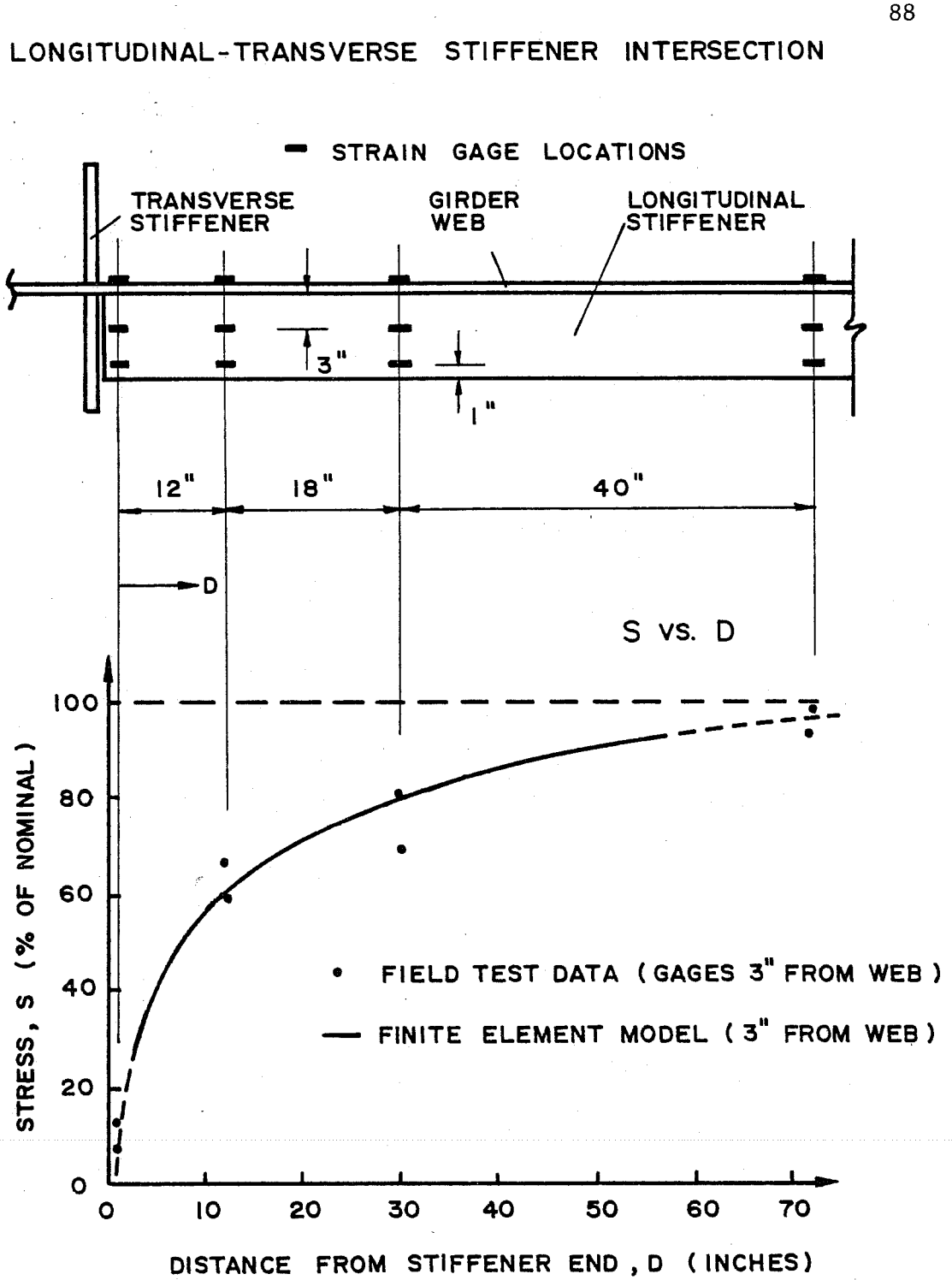

Fig. 2.41 Comparison of field test data with the computer finite element model

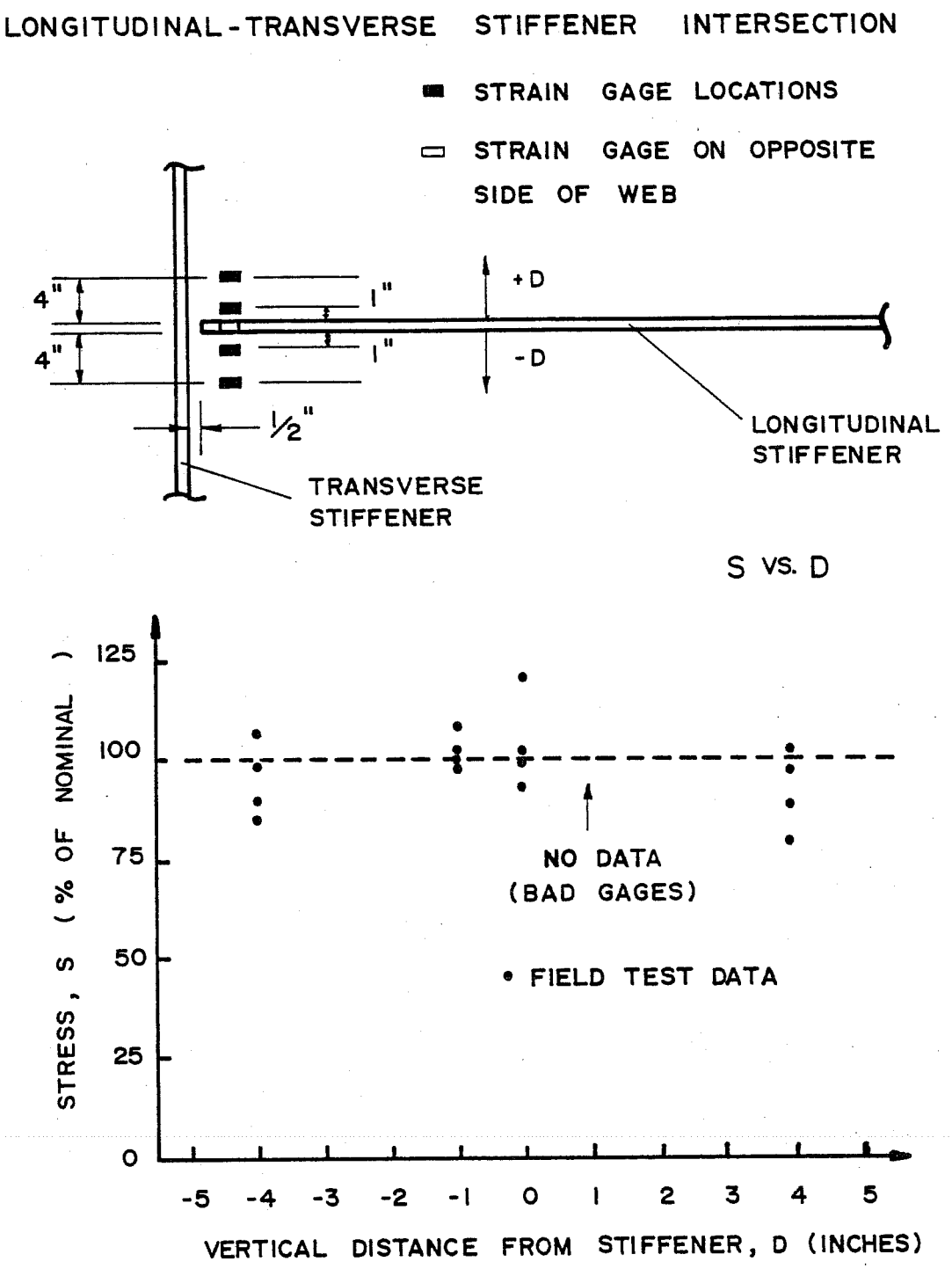

Fig. 2.42 Field data indicating no evidence of a stress concentration

of stress being measured were very small (1 to 2 ksi). As a result, normal scatter in the measured data could potentially cover up evidence of a stress concentration.

2.5 Recommended Test Specimen

An experimental determination of the fatigue life of the longitudinal-transverse stiffener intersection detail requires load cycling which will produce tensile stresses at the longitudinal stiffener end. These stresses could be obtained using a direct tension test specimen, or a beam test specimen. Figure 2.43 illustrates the geometric differences between the two types of test specimens. The transverse floor beam connection in both test specimens is represented using a transverse stiffener in a manner similar to that used in the analytical studies.

The tension test specimen would be much more economical to use than the beam test specimen. However, loading the tension specimen would seemingly be quite difficult. Tension would have to be applied uniformly to the longitudinal stiffener and web plate at one end of the specimen, while the other end would have to be fixed. The resulting unsymmetrical loading would generate out-of-plane movement which may adversely affect experimental results. It, therefore, seems questionable that this type of specimen could accurately simulate actual field conditions. Alternatively, the beam test specimen could be conveniently loaded and could reproduce field conditions with greater certainty. Obviously, this type of specimen would be larger and more costly to fabricate.

In deciding which type of specimen to use, results of the analytical work performed in this study can be utilized. Finite element computer analyses have indicated that out-of-plane displacements exist due to unsymmetrical loading on the plate girder

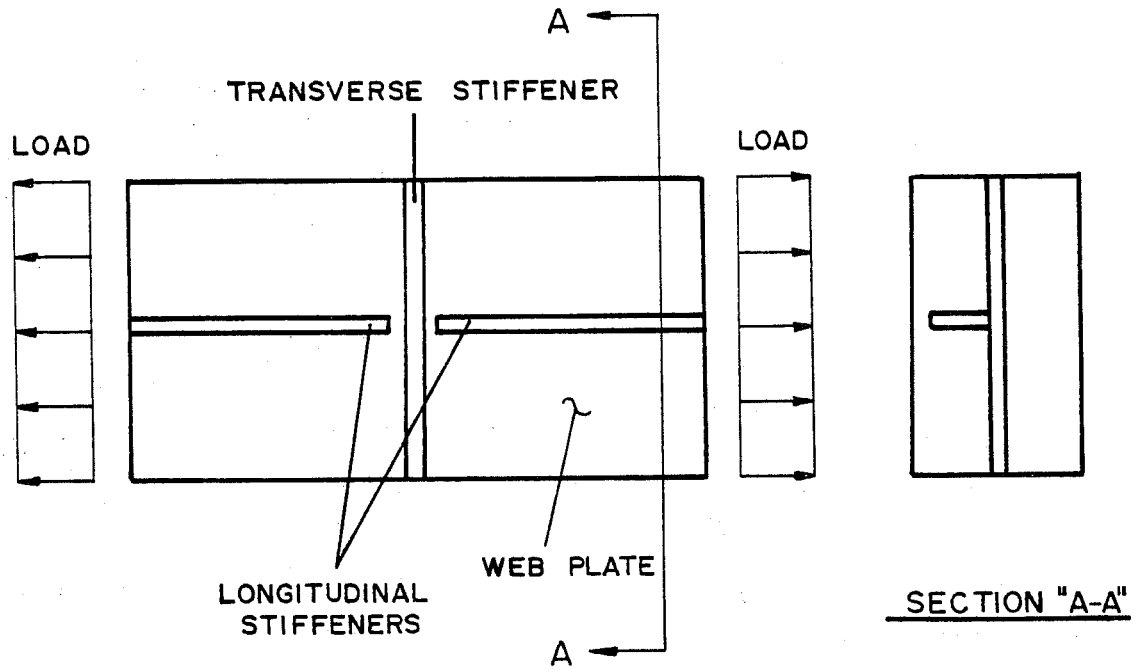

DIRECT TENSION TEST SPECIMEN

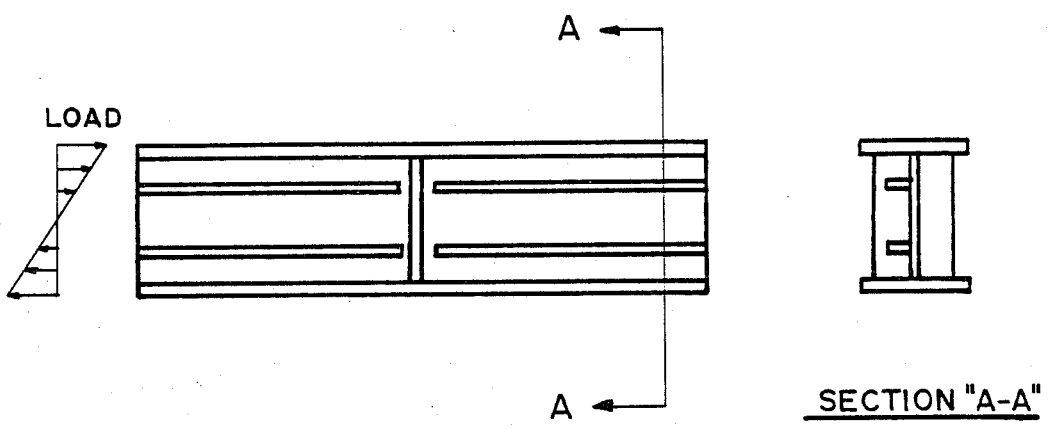

BEAM TEST SPECIMEN

Fig. 2.43 Two possible types of test specimens

(longitudinal stiffeners located on one side of the girder web only). These displacements are very small at the longitudinal stiffener end, since out-of-plane restraint is provided in this region by the floor beam. Moving away from the stiffener end, the stress in the stiffener increases, and so do the out-of-plane displacements. The resulting deflected shape of the girder web at the longitudinal stiffener for a double stiffener intersection is shown in Fig. 2.44(a). Use of the tension specimen would seemingly result in an opposite condition. That is, out-of-plane displacements would be restricted at the ends of the specimen, and unrestricted at the stiffener intersection, as shown in Fig. 2.44(b). One may then ask whether the two situations depicted in Fig. 2.44 are opposite. Indeed, they may produce the same end result, since the deflected shapes are similar in both cases. It seems that this question is worthy of study beyond the scope of this work. Although the tension test specimen would be more economical, the above dilemma still raises questions with regard to the specimen's ability to reproduce field conditions. Therefore, it seems conservative at this point to recommend that the beam test specimen be selected.

2.5.1 Geometry and Loading. Testing a full-scale model of the detail as it exists in the field is obviously not practical. A scale model of the detail, however, would seem to result in a usable test specimen. Although actual design of a test specimen and a corresponding test setup is beyond the scope of this study, consideration will be given to various parameters thought to be of importance.

In choosing the scale of the beam specimen, practical limitations on overall beam size should be adhered to. A larger specimen is more expensive and more difficult to work with in the laboratory. For example, a 1/2-scale beam would have a web height

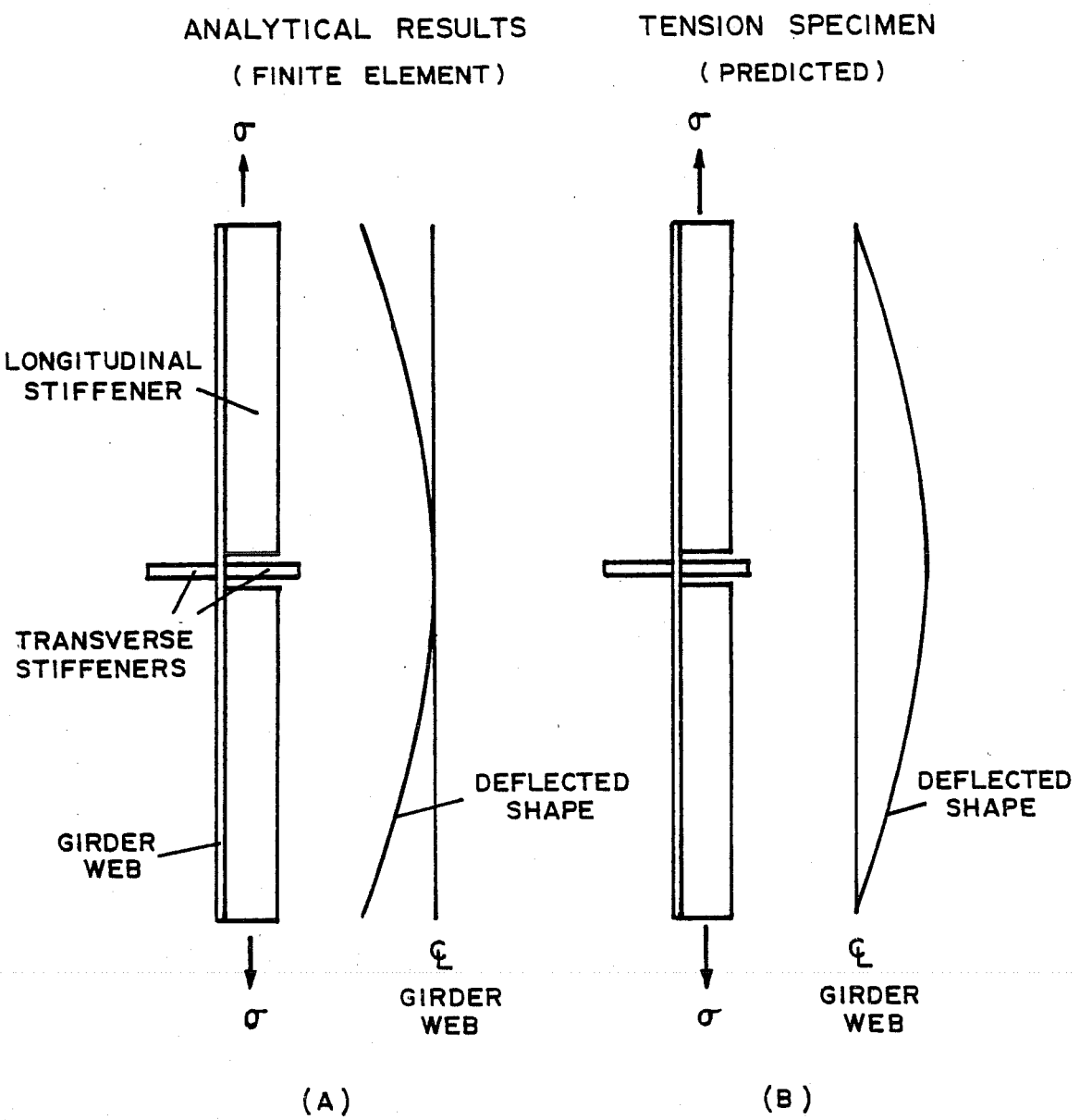

Fig. 2.44 Comparison of out-of-plane displacements from analytical results and for the tension test specimen

of 36 in., still quite large for experimental use. A more realistic beam size may be a 1/4-scale model in which the web height would be equal to 18 in.

To obtain a condition of constant moment in the region of the longitudinal-transverse stiffener intersection, two equal concentrated loads may be placed symmetrically on the simple beam test specimen. The distance between the concentrated loads, along with the overall length of the beam specimen, can be established using analytical results as guidelines. For the full scale model, analytical studies showed that the stress in the longitudinal stiffener reached nominal value at a distance, d_s, of about 6 ft from the longitudinal stiffener end. This length is approximately equal to the overall depth of the girder, and is independent of the scale of the girder model in this respect. Therefore, if the model is 1/4 scale, d_s would be equal to 18 in. The two concentrated loads would thus be placed at least 18 in. on either side of the longitudinal-transverse stiffener intersection. If the loads were placed at the one-third points of the beam test specimen, an overall beam length of about 9 ft would result. Figure 2.45 shows the dimensions and loading arrangement for the 1/4-scale model.

The magnitude of the load, P, will depend on the desired value of stress range imposed at the longitudinal stiffener level. Table 2.7 lists several possible values of stress range at the longitudinal stiffener level, $S_{R_{st}}$, and the corresponding values of P required to produce such stress ranges for the 1/4-scale model. A zero to P load cycle is assumed. The intent of the table is to present a general range of P values which could be expected to be seen by the girder specimen. This will become very important in the final design of the test specimen, since shear, web crippling, and vertical buckling must be considered.

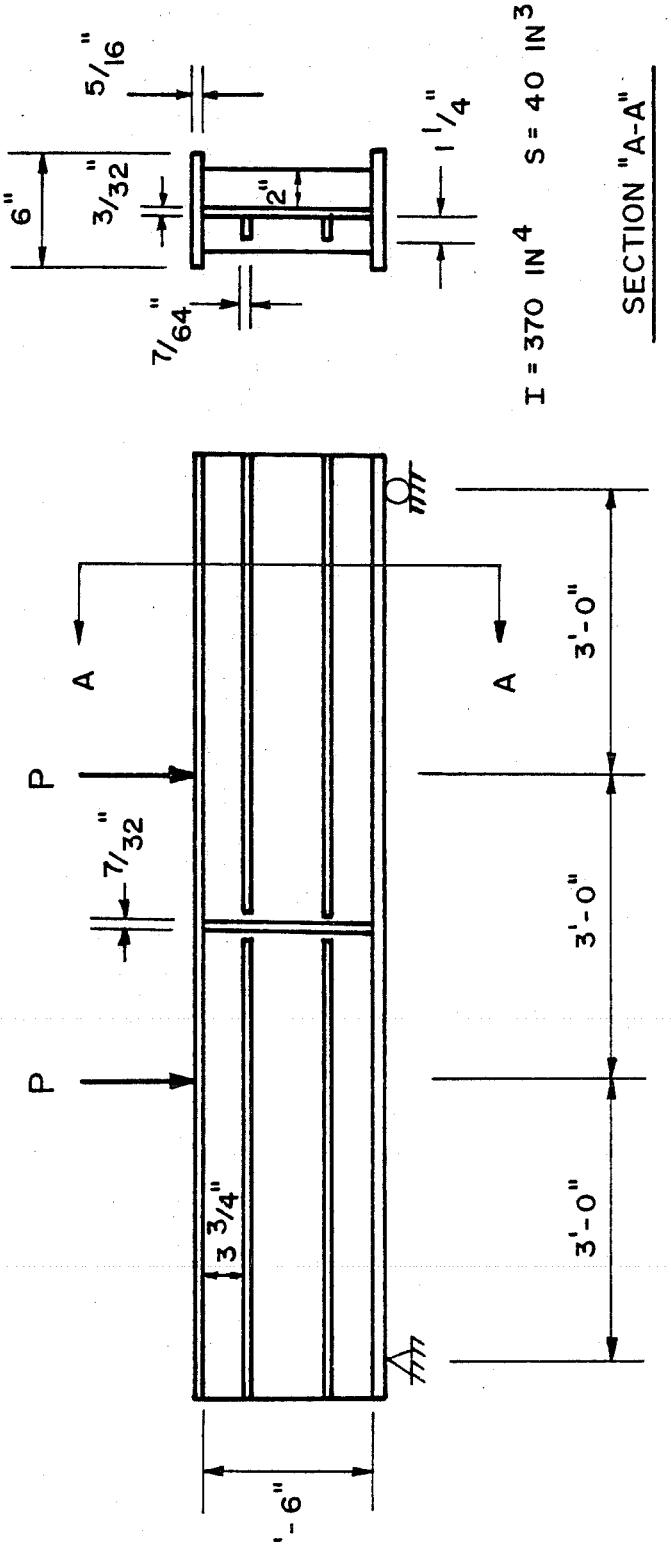

Fig. 2.45 One-quarter scale model dimensions and loading arrangement

TABLE 2.7 MAGNITUDE OF LOAD, P, AS A FUNCTION OF STRESS RANGE IMPOSED AT THE LONGITUDINAL STIFFENER LEVEL, $S_{R_{st}}$

$$S_{R_{st}} = \frac{MC_{st}}{I} \qquad S_R = \frac{MC}{I}$$

$$\frac{S_{R_{st}}}{C_{st}} = \frac{S_R}{C}$$

$$S_{R_{st}} = \frac{C_{st}}{C} S_R \qquad S_{R_{st}} = \frac{5.195}{9.3125} S_R$$

$S_{R_{st}} = 0.56\ S_R$ $\quad S = 40\ \text{in.}^3$ $\quad P = M/a$ $\quad a = 36$ in.

(1)	(2)	(3)	(4)
$S_{R_{st}}$ (ksi)	S_R (1) ÷ 0.56 (ksi)	M_{max} (2) × S (in.-k)	P (3) ÷ a
20.0	35.7	1430	38.3
18.0	32.1	1290	34.5
16.0	28.6	1140	30.7
14.0	25.0	1000	26.8
12.0	21.4	857	23.0
10.0	17.9	714	19.2
8.0	14.3	571	15.3
6.0	10.7	429	11.5
4.0	7.1	286	7.7
2.0	3.6	143	3.8

Table 2.7 also illustrates another very important point. When a particular value of $S_{R_{st}}$ is reached, the value of stress range, S_R, at the extreme fiber of the beam is necessarily larger. Since the transverse stiffener-to-flange weld produces a Category C detail, it is conceivable that failure could be initiated in this region, rather than at the longitudinal-transverse stiffener intersection (a Category E detail at best). Preliminary calculations indicate that this will not be a problem, but the relationship should be studied in detail before the final design stage is reached.

The parameter which will likely be responsible for poor fatigue performance of the detail is the small gap between the longitudinal and transverse stiffeners. Since this gap is 1/2 in. in the full-scale girder, it would become 1/16 in. in the 1/4-scale model. Obviously, such a small gap is impossible to achieve. It must be remembered, however, that the critical parameter is actually the distance between the weld toes in the gap region. In the field, this distance varies from about 1/16 in. to a condition in which overlap of the welds occurs. It seems, then, that the welds of the 1/4-scale model should be designed such that little or no distance between welds exists. The resulting gap size will not be 1/16 in., but actual field conditions should be accurately reproduced.

CHAPTER 3

STRESS INTENSITY FACTORS

3.1 Introduction

The stress field ahead of a sharp crack is characterized by a single parameter, the stress intensity factor, K, which has units of ksi $\sqrt{in.}$. For Mode I crack extension, shown in Fig. 3.1 as the opening mode, the stress intensity factor is given by

$$K_I = F(a)\ \sigma \sqrt{\pi a} \tag{3.1}$$

where σ is the magnitude of the applied nominal stress and a is the crack length. The parameter F(a) varies depending on crack size, orientation, and shape, as well as loading conditions, and is given by

$$F(a) = F_g F_e F_s F_w \tag{3.2}$$

where F_g, F_e, F_s, and F_w are correction factors which are determined analytically. F_g, the stress gradient correction factor, is intended to account for a nonuniform applied stress or a stress concentration caused by detail geometry. The crack shape correction factor, F_e, adjusts the stress intensity to reflect the shape of the crack front, while F_s, the front free surface correction factor, accounts for a free surface at the crack origin. F_w, the back free surface correction factor, accounts for a free surface located at a finite crack length.

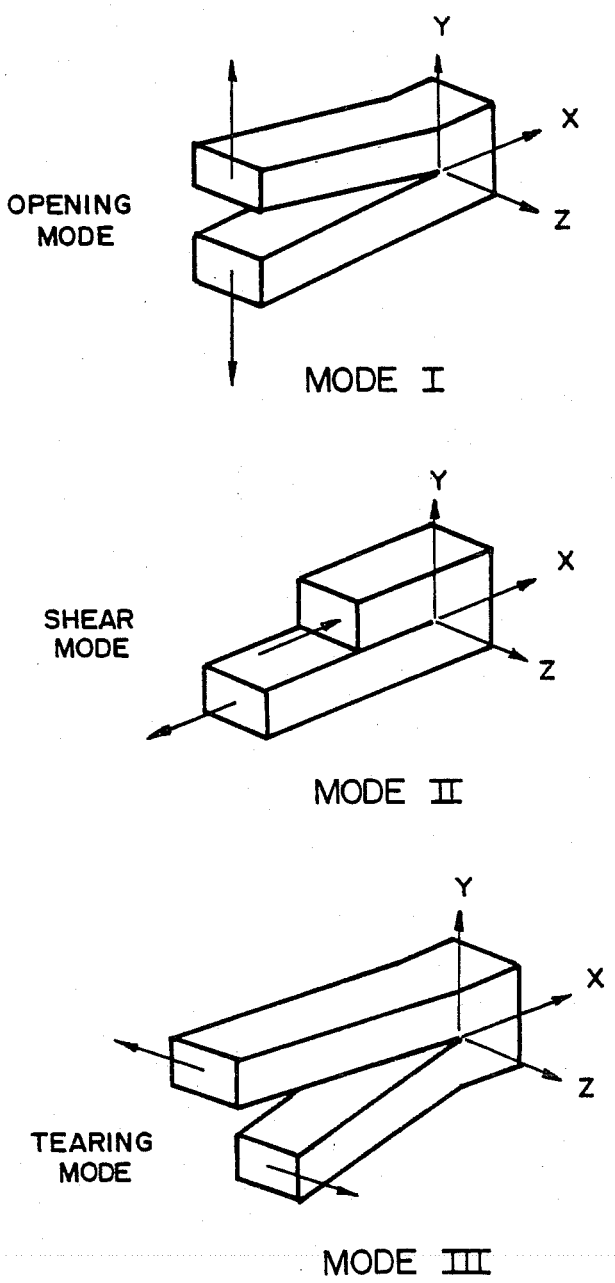

Fig. 3.1 Three basic modes of crack surface displacements

When studying welded bridge details, the range of stress intensity, ΔK_I, is of fundamental importance, and may be defined by modifying Eq. 3.1 such that

$$\Delta K_I = F(a)\ S_r \sqrt{\pi a} \tag{3.3}$$

where S_r is the nominal uniform stress range. This equation represents the solution of ΔK_I for a central through crack of length 2a in an infinite plate subjected to uniaxial tension modified by the correction function, F(a).

3.2 Longitudinal-Transverse Stiffener Intersection

Fatigue cracks normally encountered in welded bridge details such as the longitudinal-transverse stiffener intersection are surface cracks which possess semielliptical shaped crack fronts. Assuming this to be the case, and knowing the probable location of crack initiation, values for the correction factors F_g, F_e, F_s, and F_w may be estimated.

3.2.1 Stress Gradient Correction Factor, F_g. Changes in detail geometry may cause local stress concentrations which increase the stress intensity factor. The purpose of the finite element analysis conducted on the longitudinal-transverse stiffener intersection detail was to quantify these local stress conditions so that they may be accounted for by the stress gradient correction factor, F_g. F_g may be obtained for any crack length from the solution proposed by Albrecht [10] as:

$$F_g = \frac{2}{\pi} \sum_{i=1}^{n} \frac{\sigma_{b_i}}{\sigma} \left(\arcsin \frac{b_{i+1}}{a} - \arcsin \frac{b_i}{a}\right) \tag{3.4}$$

The variables in Eq. 3.4 are defined as follows:

$\frac{\sigma_{b_i}}{\sigma}$ = the average stress concentration factor, K_t, in element i.

n = the number of elements from the crack origin to the crack length a.

b_i = the distance from the crack origin to the near side of element i.

b_{i+1} = the distance from the crack origin to the far side of element i.

Use of the summation technique instead of the closed form integral solution results in an approximation which yields very good accuracy when the value of $(b_{i+1} - b_i)$ is sufficiently small in the vicinity of the crack origin. This condition has been satisfied by repeatedly refining the finite element grid in the critical region.

Equation (3.4) was used to determine the function, F_g, which accounts for the stress concentration caused by the local geometry of the longitudinal-transverse stiffener intersection detail. The results are displayed in tabular form in Table 3.1. Figure 3.2 illustrates the relationship between F_g and K_t as a function of a/T_w.

3.2.2 Crack Shape Correction Factor, F_e. Irwin [16] found that the stress intensity factor at any point along the perimeter of an elliptical crack imbedded in an infinite body subjected to uniform tensile stress is given by

$$K_I = \frac{\sigma\sqrt{\pi a}}{E_k}\left(\sin^2\beta + \frac{a^2}{c^2}\cos^2\beta\right)^{\frac{1}{4}} \qquad (3.5)$$

where K_I is the value of the stress intensity factor for a point on the perimeter whose location is defined by the angle, β, measured from the major axis. E_k is the elliptical integral given as

TABLE 3.1 CALCULATION OF F_g FOR THE LONGITUDINAL-TRANSVERSE STIFFENER INTERSECTION DETAIL

$\frac{a}{T_w}$	a	b_i	b_{i+1}	$\frac{\sigma_{b_i}}{\sigma}$	$\sum_{i=1}^{n}$	F_g
0.0053	0.002	0.0	0.002	15.0	23.6	15.0
0.0107	0.004	0.002	0.004	11.0	19.4	12.3
0.0187	0.007	0.004	0.007	9.40	16.9	10.8
0.0240	0.009	0.007	0.009	8.44	15.7	10.0
0.0293	0.011	0.009	0.011	7.78	14.8	9.45
0.0373	0.014	0.011	0.014	7.22	13.8	8.82
0.0453	0.017	0.014	0.017	6.73	13.1	8.32
0.0560	0.021	0.017	0.021	6.36	12.3	7.84
0.0640	0.024	0.021	0.024	6.05	11.8	7.53
0.0720	0.027	0.024	0.027	5.80	11.4	7.27
0.0827	0.031	0.027	0.031	5.54	11.0	6.97
0.0960	0.036	0.031	0.036	5.29	10.5	6.67
0.1070	0.040	0.036	0.040	5.06	10.1	6.45
0.1200	0.045	0.040	0.045	4.87	9.76	6.21
0.1310	0.049	0.045	0.049	4.69	9.49	6.04
0.1470	0.055	0.049	0.055	4.49	9.13	5.81
0.1630	0.061	0.055	0.061	4.28	8.80	5.60
0.1790	0.067	0.061	0.067	4.08	8.50	5.41
0.1950	0.073	0.067	0.073	3.91	8.23	5.24
0.2110	0.079	0.073	0.079	3.74	7.98	5.08
0.2350	0.088	0.079	0.088	3.54	7.68	4.89
0.2560	0.096	0.088	0.096	3.32	7.35	4.68
0.2800	0.105	0.096	0.105	3.12	7.05	4.49
0.3010	0.113	0.105	0.113	2.93	6.79	4.32
0.325	0.122	0.113	0.122	2.76	6.55	4.17

TABLE 3.1 (Cont.)

$\frac{a}{T_w}$	a	b_i	b_{i+1}	$\frac{\sigma_{b_i}}{\sigma}$	$\sum_{i=1}^{n}$	F_g
0.357	0.134	0.122	0.134	2.55	6.25	3.98
0.387	0.145	0.134	0.145	2.33	5.94	3.78
0.419	0.157	0.145	0.157	2.11	5.64	3.59
0.448	0.168	0.157	0.168	1.90	5.36	3.41
0.480	0.180	0.168	0.180	1.70	5.10	3.25
0.523	0.196	0.180	0.196	1.47	4.81	3.06
0.568	0.213	0.196	0.213	1.21	4.46	2.84
0.611	0.229	0.213	0.229	0.96	4.13	2.63
0.656	0.246	0.229	0.246	0.72	3.82	2.43
0.699	0.262	0.246	0.262	0.50	3.52	2.24
0.760	0.285	0.262	0.285	0.15	3.05	1.94
0.819	0.307	0.285	0.307	-0.16	2.67	1.70
0.880	0.330	0.307	0.330	-0.39	2.45	1.56
0.939	0.352	0.330	0.352	-0.77	2.04	1.30
1.000	0.375	0.352	0.375	-1.18	1.63	1.04

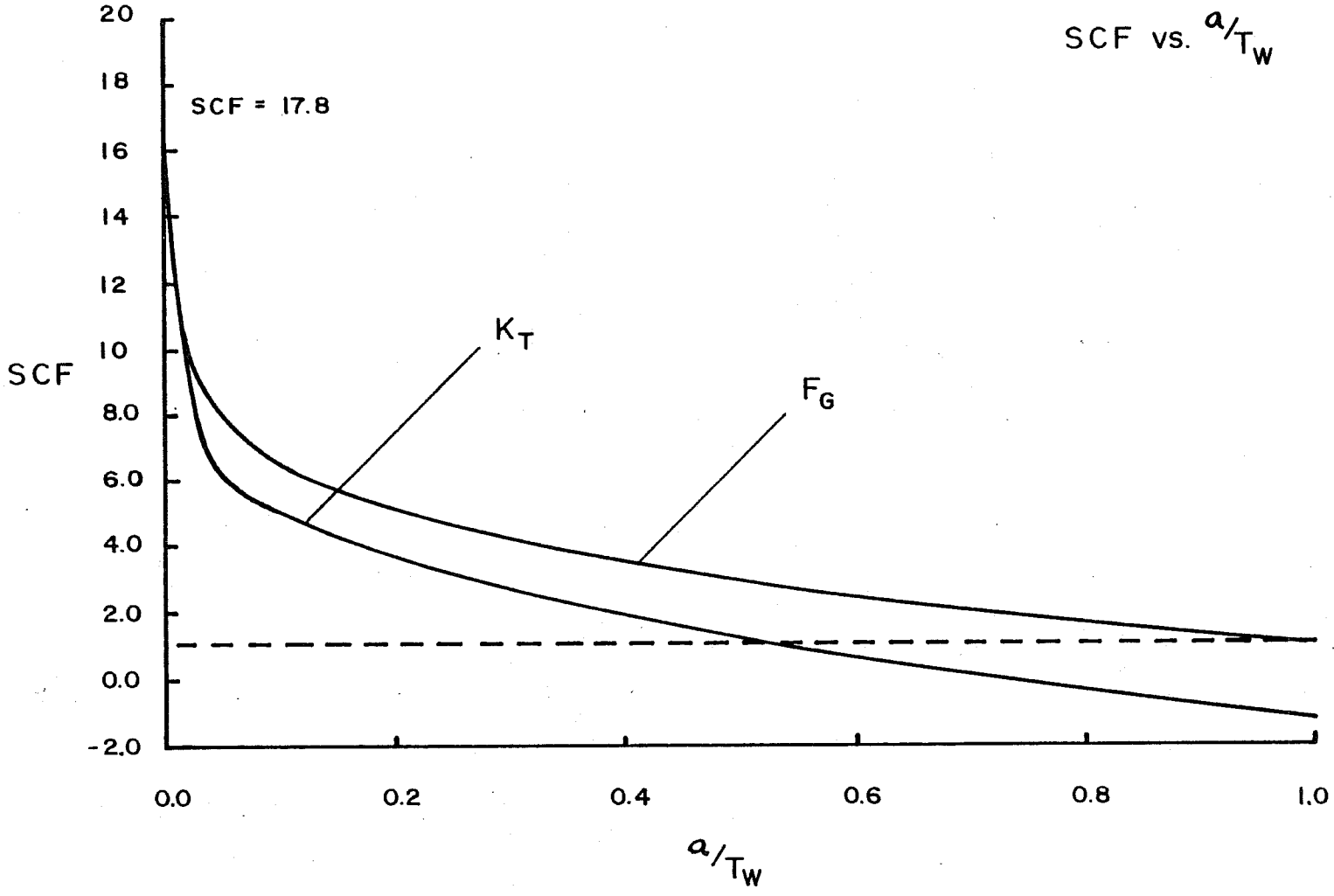

Fig. 3.2 Stress concentration (K_t) and stress gradient correction factor (F_g) decay curves for the longitudinal-transverse stiffener intersection

$$E_k = \int_0^{\pi/2} \left[1 - \left(\frac{c^2 - a^2}{c^2} \sin^2\theta\right)\right]^{\frac{1}{2}} d\theta \qquad (3.6)$$

where c is the major axis semidiameter and a is the minor axis semidiameter, as shown in Fig. 3.3. Equations (3.5) and (3.6) also apply to the solution of ΔK_I for the semielliptical surface crack shown in Fig. 3.4.

Since interest is usually directed toward estimating K_I at the leading edge of the crack front, the point on the semielliptical perimeter, shown in Fig. 3.4 and defined by $\beta = \pi/2$, is of particular interest. From Eq. (3.5), the stress intensity factor for this point becomes

$$K_I = \frac{\sigma_\Delta \sqrt{\pi a}}{E_k} \qquad (3.7)$$

The elliptical crack shape correction factor, F_e, may then be defined as

$$F_e = \frac{1}{E_k} \qquad (3.8)$$

The calculated values of F_e for various ratios of a/c are given in Table 3.2. Figure 3.5 illustrates the relationship between F_e and the ratio a/c. Values of the elliptical integral, E_k, were obtained from Ref. 17.

In selecting a value of F_e, the ratio a/c must be established. An a/c ratio of zero corresponds to an edge crack, while a/c equal to 1 implies a circular crack. Observed semi-elliptical cracks have been found to possess a/c ratios of approximately 0.6, a value which seems reasonable to use in solving the surface crack problem. This corresponds to a value of F_e equal to 0.79.

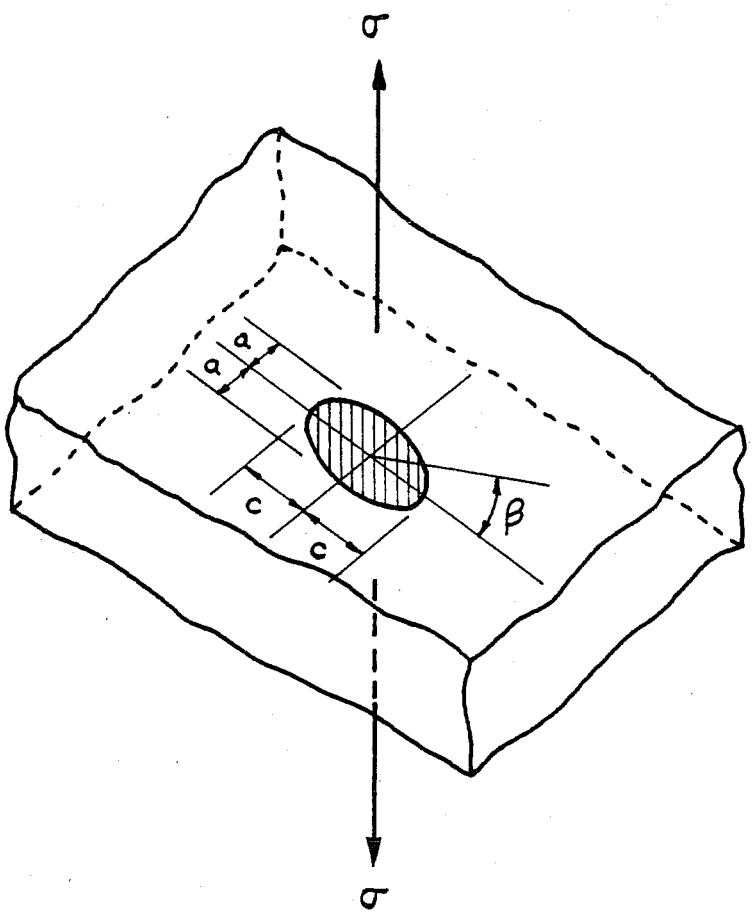

Fig. 3.3 Elliptical crack in an infinite body subjected to uniform tension

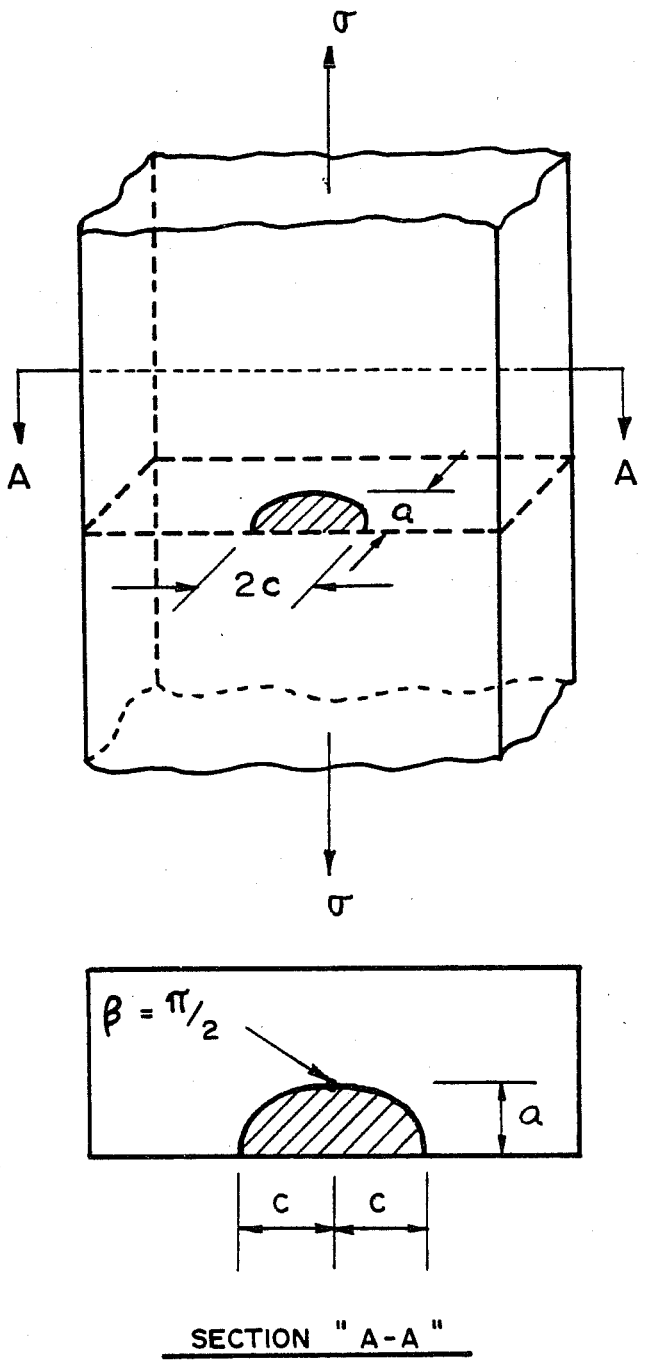

Fig. 3.4 Plate containing a semielliptical surface crack

TABLE 3.2 CALCULATION OF F_e FOR THE SEMI-ELLIPTICAL SURFACE CRACK

a/c	E_k	F_e
0.0	1.00	1.00
0.1	1.01	0.99
0.2	1.05	0.95
0.3	1.09	0.92
0.4	1.14	0.88
0.5	1.20	0.83
0.6	1.26	0.79
0.7	1.34	0.75
0.8	1.41	0.71
0.9	1.48	0.68
1.0	1.55	0.65

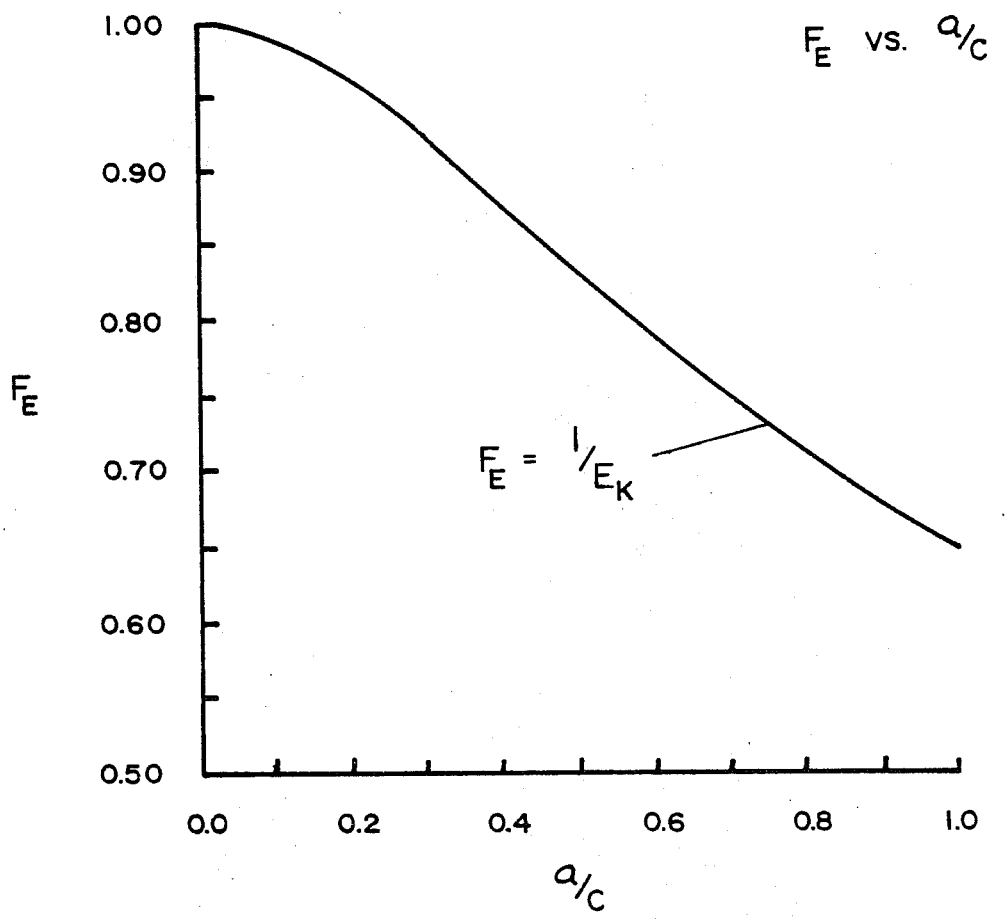

Fig. 3.5 Relationship between the crack shape correction factor, F_e, and a/c

3.2.3 Front Free Surface Correction Factor, F_s. The solution for an edge crack (a/c = 0) in a semi-infinite plate given by Irwin yields a front free surface correction factor, F_s, of 1.12. For a semielliptical crack in a semi-infinite plate, approximate solutions for F_s have been formulated by a number of researchers. Tada and Irwin [18] have tabulated values of F_s which vary with the stress distribution along the crack as well as the crack shape. These values are shown in Fig. 3.6. Paris and Sih [19] have suggested that F_s is merely a function of the crack shape and should be given by

$$F_s = 1 + 0.12\ (1 - a/c) \tag{3.9}$$

where a is the minor axis semidiameter (crack length) and c is the major axis semidiameter of the semielliptical crack. As shown in Fig. 3.7, Eq. (3.9) suggests a variation of F_s from 1.12 for an edge crack (a/c = 0) to 1.00 for a circular crack (a/c = 1).

It is interesting to note that the results of both approximate solutions are very much alike. Using Eq. (3.9) with a/c = 0.6, a value of F_s = 1.05 is obtained. In using the values given by Tada and Irwin, characteristics of stress distribution and crack shape must be evaluated. The stress distribution along the prospective crack path of the longitudinal-transverse stiffener intersection detail can be approximated by a uniform plus a linear stress distribution. Assuming a half-circular crack shape, a value for F_s of between 1.025 and 1.085 is suggested. Averaging these two values results in a value of F_s = 1.055, quite comparable to the value of 1.05 given by Eq. (3.9). A value of F_s = 1.05 will be assumed in this study.

CRACK SHAPE / STRESS DISTRIBUTION	THROUGH THICKNESS	HALF - CIRCULAR	QUARTER - CIRCULAR
UNIFORM 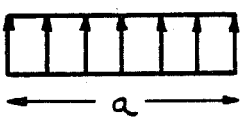	1.122	1.025	1.380
LINEAR 	1.210	1.085	1.067
CONCENTRATED 	1.300	1.145	0.754

Fig. 3.6 Front free surface correction factor, F_s, as a function of crack shape and stress distribution (from Ref. 18)

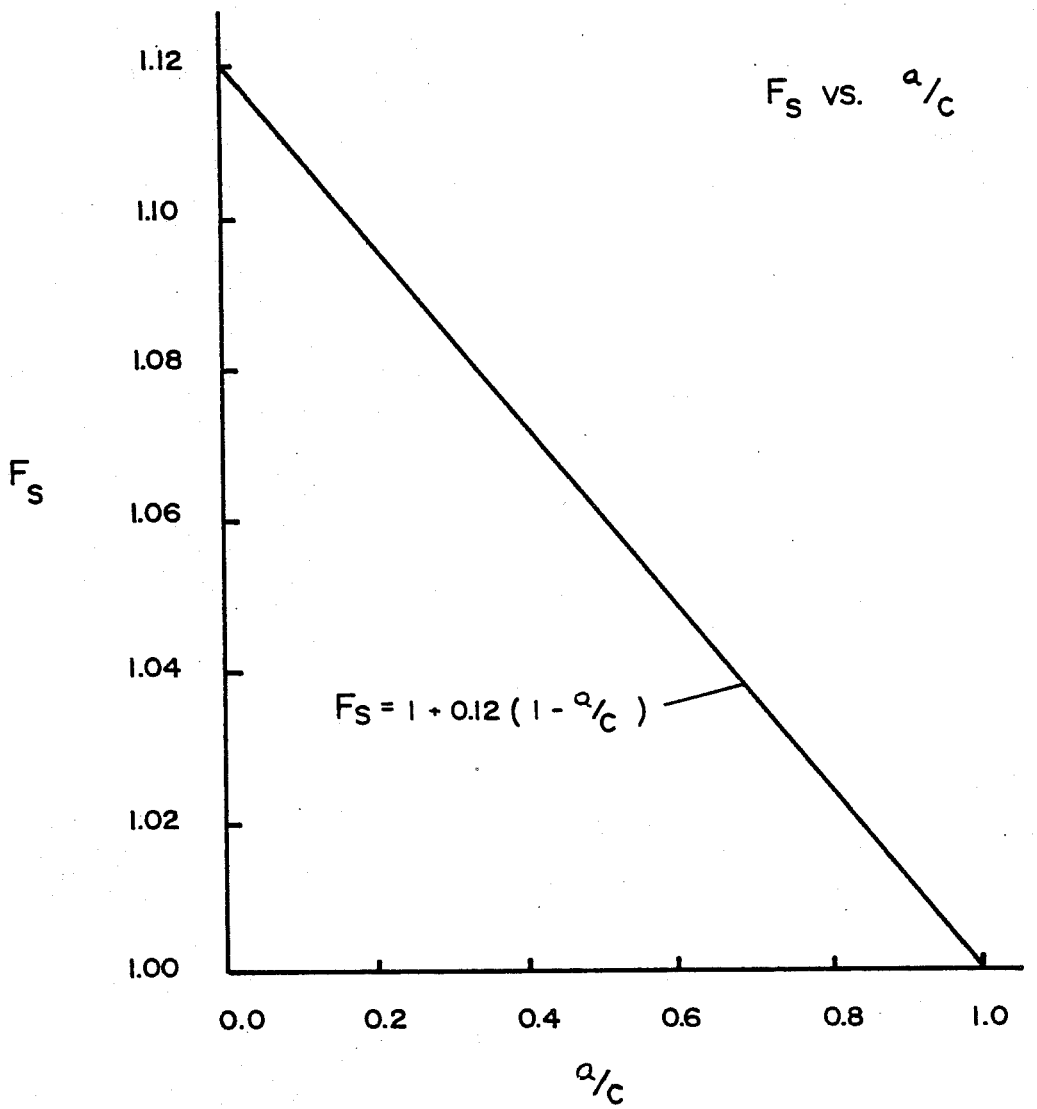

Fig. 3.7 Relationship between the front free surface correction, F_s, and a/c found in Ref. 19

3.2.4 Back Free Surface Correction Factor, F_w. Like F_s, F_w depends on stress distribution and crack shape, but not to a degree which warrants special attention. More importantly, F_w has been found to be sensitive to whether or not the section containing the crack is permitted to bend. Bending amplifies the back surface correction, particularly at high values of crack length to member thickness ratios (a/t).

For a plate not subjected to bending, the solution for finite width correction may be estimated by [20]

$$F_w = \left[\sec \frac{\pi a}{2t}\right]^{\frac{1}{2}} \tag{3.10}$$

where a is the crack length and t is the plate thickness. For cases in which plate bending occurs, the value of F_w may be taken as [20]

$$F_w = \left[\frac{0.752 + 2.02\alpha + 0.37\left[1 - \sin\left(\frac{\pi\alpha}{2}\right)\right]^3}{1.122\cos\left(\frac{\pi\alpha}{2}\right)}\right] \times \left[\left(\frac{2}{\pi\alpha}\right)\sin\left(\frac{\pi\alpha}{2}\right)\right]^{\frac{1}{2}} \times \left[\sec\left(\frac{\pi\alpha}{2}\right)\right]^{\frac{1}{2}} \tag{3.11}$$

where $\alpha = a/t$.

The nature of the structural detail must be considered to decide whether to use the bending or no bending solution for F_w. Typically, in welded bridge structures the no bending correction is applicable in cases where restraint is provided by common girder attachments [20]. This condition could be modeled by imposing roller support boundary conditions along the back surface of the cracked plate, as shown in Fig. 3.8. In the case of the longitudinal-transverse stiffener intersection detail, such

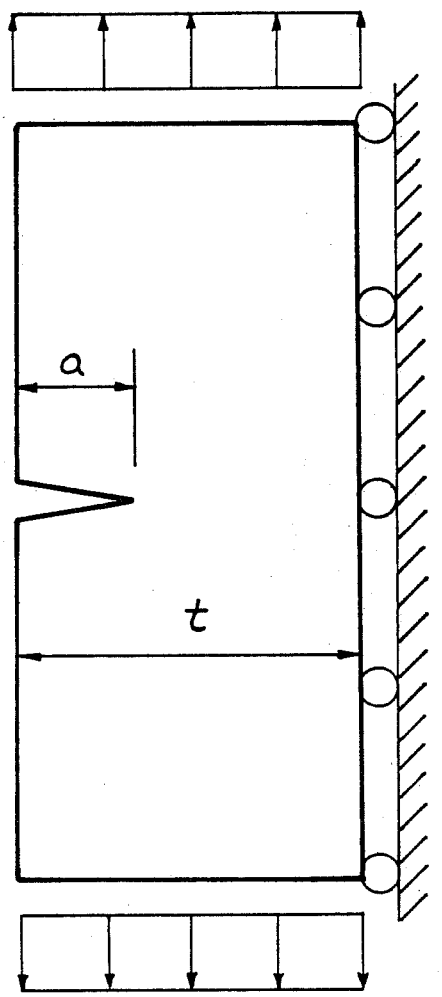

$$F_W = \left[\sec\left(\frac{\pi \alpha}{2}\right) \right]^{1/2}$$

Fig. 3.8 Back free surface correction factor with bending prevented

support is not provided to the web plate at the longitudinal stiffener end. It therefore seems likely that some bending may occur in the gap region between the longitudinal and transverse stiffeners. Rather than selecting either the bending or the no bending solution as being correct, it seems logical to estimate fatigue lives for both cases to determine the significance of choosing one solution over the other. Most of the useful fatigue life of a structural detail is expended at small values of a/t for which the two solutions for F_w do not differ to a great extent. As a result, fatigue life estimations should not depend heavily on the bending condition assumed.

Figure 3.9 illustrates the variation of F_w with a/t for both the bending and no bending cases. The values plotted in Fig. 3.9 are listed in Table 3.3.

3.3 Cope Detail

An estimation of the stress intensity factor for the proposed cope detail may be made using many of the same corrections presented for the existing detail. The major difference between the two details lies in the severity of the stress distributions along the prospective crack path through the girder web at the longitudinal stiffener termination. The less severe distribution found in the analysis of the cope detail can be expected to result in a more favorable fatigue life relationship.

3.3.1 Stress Gradient Correction Factor, F_g. Using Eq. (3.4), the stress gradient correction factor was obtained for the cope detail. Table 3.4 lists the calculated values of F_g which were subsequently plotted in Fig. 3.10.

3.3.2 Other Correction Factors. The relationship between the crack shape correction factor, F_e, and the ratio of minor axis semidiameter to major axis semidiameter, a/c, obtained for

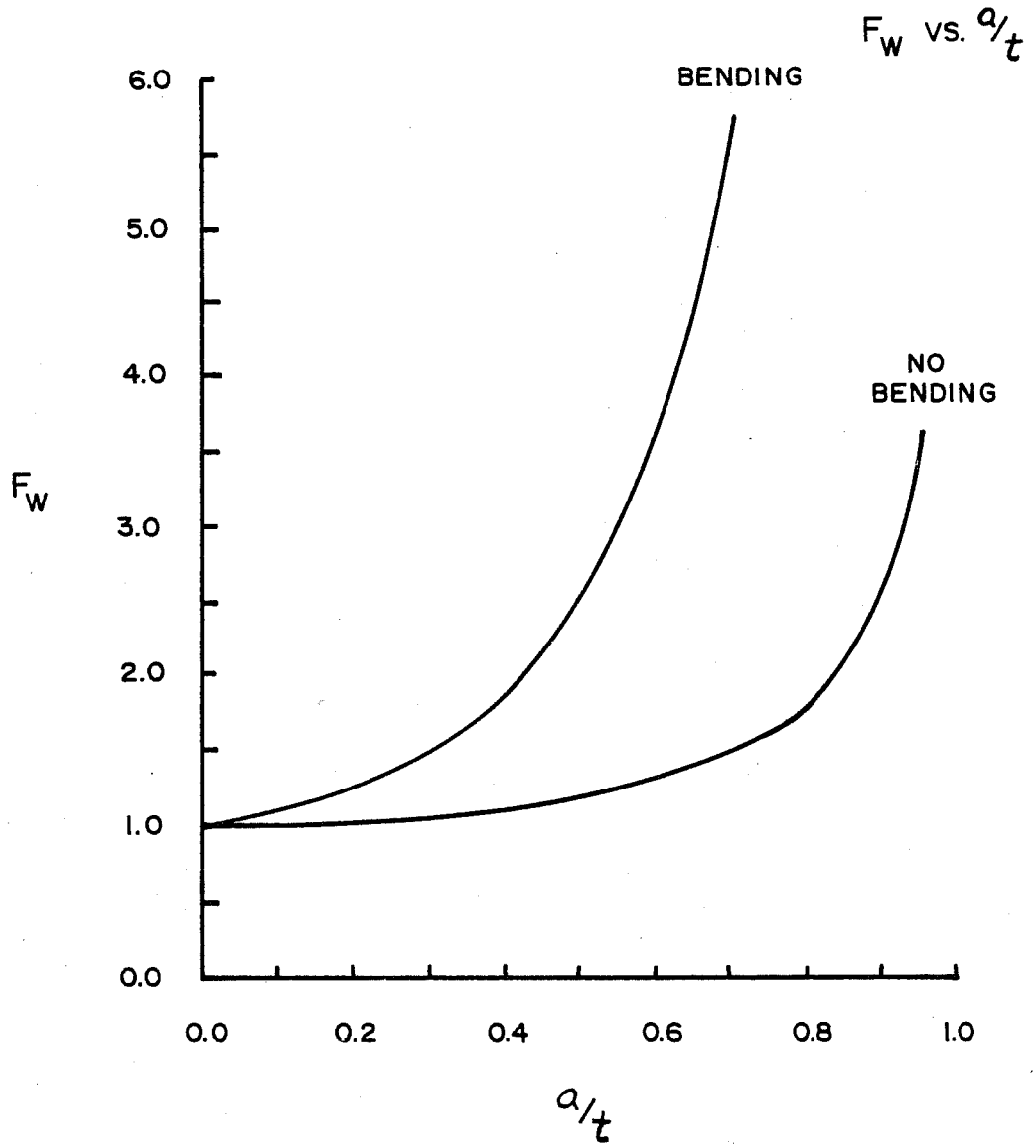

Fig. 3.9 Back free surface correction factor, F_w, for plate subjected to bending and for plate not subjected to bending

TABLE 3.3 BACK FREE SURFACE CORRECTION FACTOR, F_w, FOR BENDING AND NO BENDING

a/t	F_w (no bending)	F_w (bending)
0.00	1.00	1.00
0.05	1.00	1.02
0.10	1.01	1.07
0.15	1.01	1.13
0.20	1.03	1.22
0.25	1.04	1.33
0.30	1.06	1.48
0.35	1.08	1.65
0.40	1.11	1.88
0.45	1.15	2.16
0.50	1.19	2.52
0.55	1.24	2.98
0.60	1.30	3.60
0.65	1.38	4.46
0.70	1.48	5.68
0.75	1.62	7.56
0.80	1.80	10.70
0.85	2.07	16.60
0.90	2.53	40.00
0.95	3.57	88.50

TABLE 3.4 CALCULATION OF F_g FOR THE COPE DETAIL

$\frac{a}{T_w}$	a	b_i	b_{i+1}	$\frac{\sigma_{b_i}}{\sigma}$	$\sum_{i=1}^{n}$	F_g
0.0053	0.002	0.0	0.002	5.81	9.13	5.81
0.0107	0.004	0.002	0.004	4.72	7.99	5.08
0.0187	0.007	0.004	0.007	4.10	7.13	4.54
0.0240	0.009	0.007	0.009	3.71	6.70	4.27
0.0293	0.011	0.009	0.011	3.44	6.36	4.05
0.0373	0.014	0.011	0.014	3.22	5.99	3.81
0.0453	0.017	0.014	0.017	3.03	5.69	3.62
0.0560	0.021	0.017	0.021	2.88	5.40	3.44
0.0640	0.024	0.021	0.024	2.77	5.22	3.33
0.0720	0.027	0.024	0.027	2.68	5.07	3.23
0.0827	0.031	0.027	0.031	2.58	4.90	3.12
0.0960	0.036	0.031	0.036	2.50	4.72	3.00
0.1070	0.040	0.036	0.040	2.43	4.60	2.93
0.1200	0.045	0.040	0.045	2.37	4.47	2.85
0.1310	0.049	0.045	0.049	2.33	4.39	2.79
0.1470	0.055	0.049	0.055	2.26	4.27	2.72
0.1630	0.061	0.055	0.061	2.21	4.16	2.65
0.1790	0.067	0.061	0.067	2.16	4.07	2.59
0.1950	0.073	0.067	0.073	2.12	3.99	2.54
0.2110	0.079	0.073	0.079	2.08	3.92	2.49
0.2350	0.088	0.079	0.088	2.04	3.85	2.45
0.256	0.096	0.088	0.096	1.99	3.77	2.40
0.280	0.105	0.096	0.105	1.94	3.71	2.36
0.301	0.113	0.105	0.113	1.90	3.64	2.32
0.325	0.122	0.113	0.122	1.87	3.60	2.29

TABLE 3.4 (Cont.)

$\frac{a}{T_w}$	a	b_i	b_{i+1}	$\frac{\sigma_{b_i}}{\sigma}$	$\sum_{i=1}^{n}$	F_g
0.357	0.134	0.122	0.134	1.83	3.55	2.26
0.387	0.145	0.134	0.145	1.78	3.47	2.21
0.419	0.157	0.145	0.157	1.73	3.39	2.16
0.448	0.168	0.157	0.168	1.68	3.33	2.12
0.480	0.180	0.168	0.180	1.64	3.27	2.08
0.523	0.196	0.180	0.196	1.60	3.22	2.05
0.568	0.213	0.196	0.213	1.55	3.14	2.00
0.611	0.229	0.213	0.229	1.50	3.08	1.96
0.656	0.246	0.229	0.246	1.46	3.02	1.92
0.699	0.262	0.246	0.262	1.41	2.95	1.88
0.760	0.285	0.262	0.285	1.37	2.89	1.84
0.819	0.307	0.285	0.307	1.31	2.81	1.79
0.880	0.330	0.307	0.330	1.24	2.70	1.72
0.939	0.352	0.330	0.352	1.16	2.58	1.64
1.000	0.375	0.352	0.375	1.08	2.44	1.56

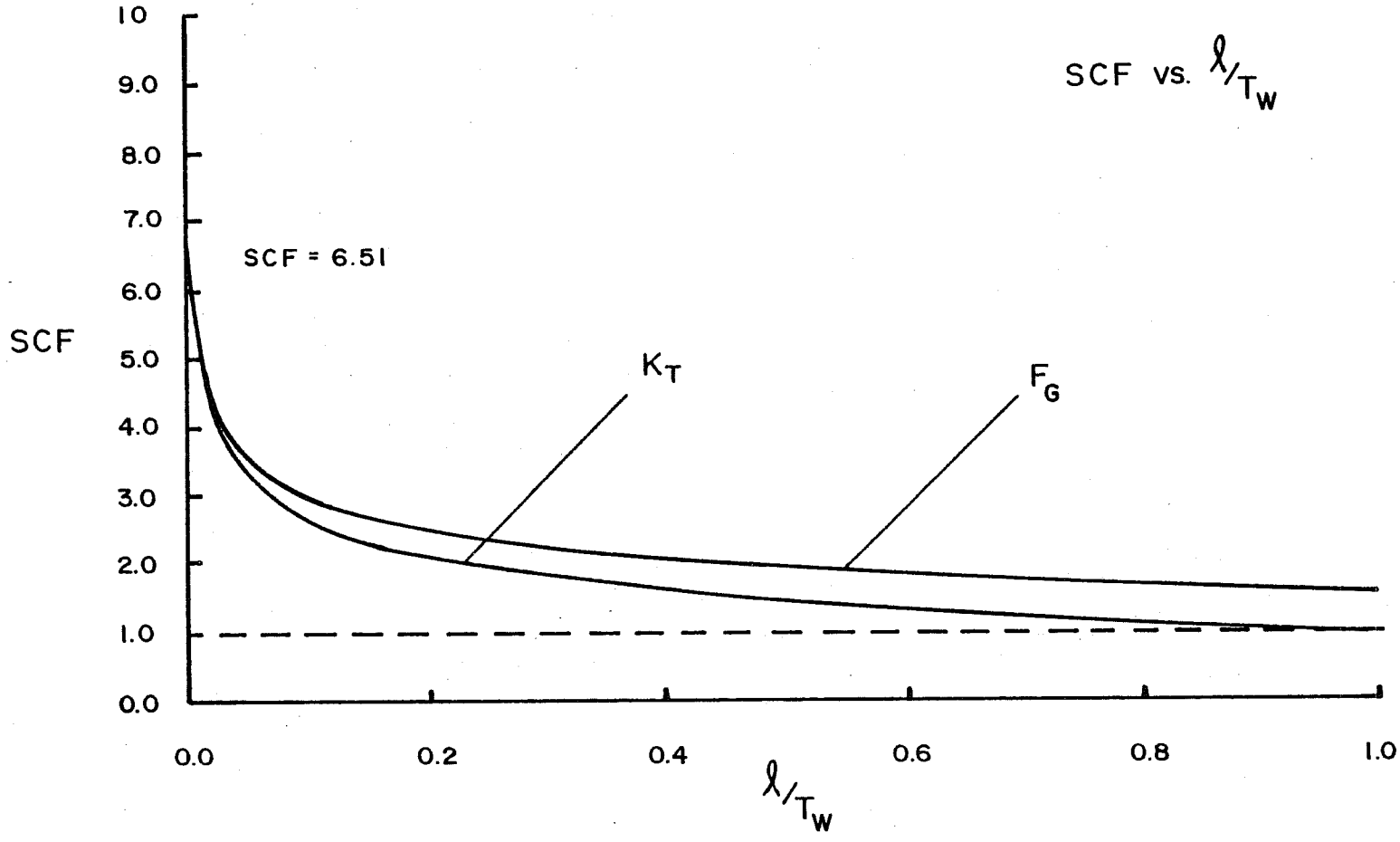

Fig. 3.10 Stress concentration (K_t) and stress gradient correction factor (F_g) decay curves for the cope detail

the existing detail also applies to the cope detail. This relationship has been shown in Fig. 3.5. Again, the value of a/c was taken as 0.6, corresponding to a value of F_e equal to 0.79.

A front free surface correction factor, F_s, is once again applied in estimating the stress intensity factor for the cope detail. The characteristics of stress distribution and crack shape were assumed to be similar to those of the longitudinal-transverse stiffener intersection detail. As a result, the value of F_s equal to 1.05 used for the existing detail will also be applied to the cope detail.

In determining a solution for F_w, the back free surface correction factor, the no bending correction factor plotted in Fig. 3.9 was assumed. This was done in the case of the cope detail due to the fact that the longitudinal stiffener is welded to the transverse stiffener. This connection prevents significant bending of the girder web at the longitudinal stiffener termination.

3.4 Discussion

It is important to understand that the correction factors, F_g, F_e, F_s, and F_w are determined not as exact solutions, but as estimates. Assumptions must be made in arriving at the estimated solutions. These assumptions are based on interpretation of a limited amount of research work. This, in turn, implies that differences of opinion are likely to be encountered, and that the means taken to arrive at the "correct solution" are surely open to discussion.

F_g, which is dependent upon detail geometry, is the most significant and well-defined correction factor. Using finite element codes in a manner similar to that given by Zettlemoyer [15], the correction for stress gradient along the prospective crack path can be determined. Little, if any, interpretation or judgment is required in applying this correction factor.

Most researchers believe that the back free surface correction factor, F_w, depends largely on whether or not the cracked plate is permitted to bend. F_w takes one of two possible forms, depending on one's judgment with regard to detail geometry. However, can all details be placed in one group (no bending) or the other (bending), or should an average of the two solutions be applied? In this study, an approach has been taken which demonstrates the differences involved by comparing the fatigue life relationships using both solutions. One may then obtain a feeling for the significance of any assumption made.

The factors considered to be the most controversial are the crack shape correction factor, F_e, and the front free surface correction factor, F_s. These factors depend largely on the a/c ratio assumed. This value, the ratio of minor axis semidiameter to major axis semidiameter of a given flaw or crack, is certainly not well defined for surface cracks. How is it possible to know how the crack will actually grow? The only answer seems to lie within the fact that a number of these situations have actually been observed in the laboratory. Based on these observations a value for a/c may be estimated, as was done in this study. But this is no guarantee that the value chosen will actually be accurate. For example, imagine an instance in which surface cracks are expected to grow at a certain location. It is possible for several small flaws in close proximity to one another to grow and coalesce. This coalescence will potentially result in a much greater "c" value than anticipated, significantly affecting the a/c ratio. The approach to the solution of F_e and F_s taken in this study is to estimate a value for a/c, and use that value to estimate fatigue life. Since the parameter $(1/F_sF_e)^{3.0}$ is a constant which can be removed from the fatigue life estimation, it becomes very easy to reestimate lives for different

values of F_s and F_e. Simply divide the estimated number of cycles, N, by the $(1/F_sF_e)^{3.0}$ parameter corresponding to that originally assumed. Then, multiply by the $(1/F_sF_e)^{3.0}$ parameter corresponding to the new estimates of F_s and F_e. This can be summarized in equation form as follows:

$$N_{new} = \frac{N_{original}}{(1/F_sF_e)^{3.0}_{original}} \times (1/F_sF_e)^{3.0}_{new} \qquad (3.12)$$

CHAPTER 4

FATIGUE LIFE ESTIMATIONS

4.1 Introduction

The fatigue life of a structural detail is determined by adding the number of cycles required to initiate a fatigue crack, to the number of cycles required to propagate the crack to its critical size. In structural components which have surface irregularities or small imperfections, the initiation portion of the fatigue life is reduced or eliminated entirely. The question of when does a crack initiate and become a propagating crack is difficult to answer. The fracture mechanics approach to the fatigue problem is to assume an initial flaw size, a_i, and calculate the number of cycles necessary to grow the crack to a critical size, a_{cr}, when rapid fracture occurs. The selection of a value for a_i is based on the type of inspection performed. Inspection techniques serve to establish an upper limit on undetectable defect size, a_d. This limit will be higher if inspection is conducted in the field ($a_{d_{field}}$), rather than in the shop ($a_{d_{shop}}$). The value of a_d then determines the maximum inspection interval necessary to maintain the integrity of the structure. Figure 4.1 illustrates the relationship between a_i, $a_{d_{shop}}$, $a_{d_{field}}$, and a_{cr}. The fatigue life is shown as the number of cycles necessary to grow the crack from a length of a_i to a_{cr}. The maximum inspection interval is established as the number of cycles necessary to grow the crack from a length of $a_{d_{field}}$ to a_{cr}. The rate of fatigue crack propagation, da/dN, is shown in Fig. 4.1 as the slope of the crack size vs. number of cycles curve. The rate of crack growth

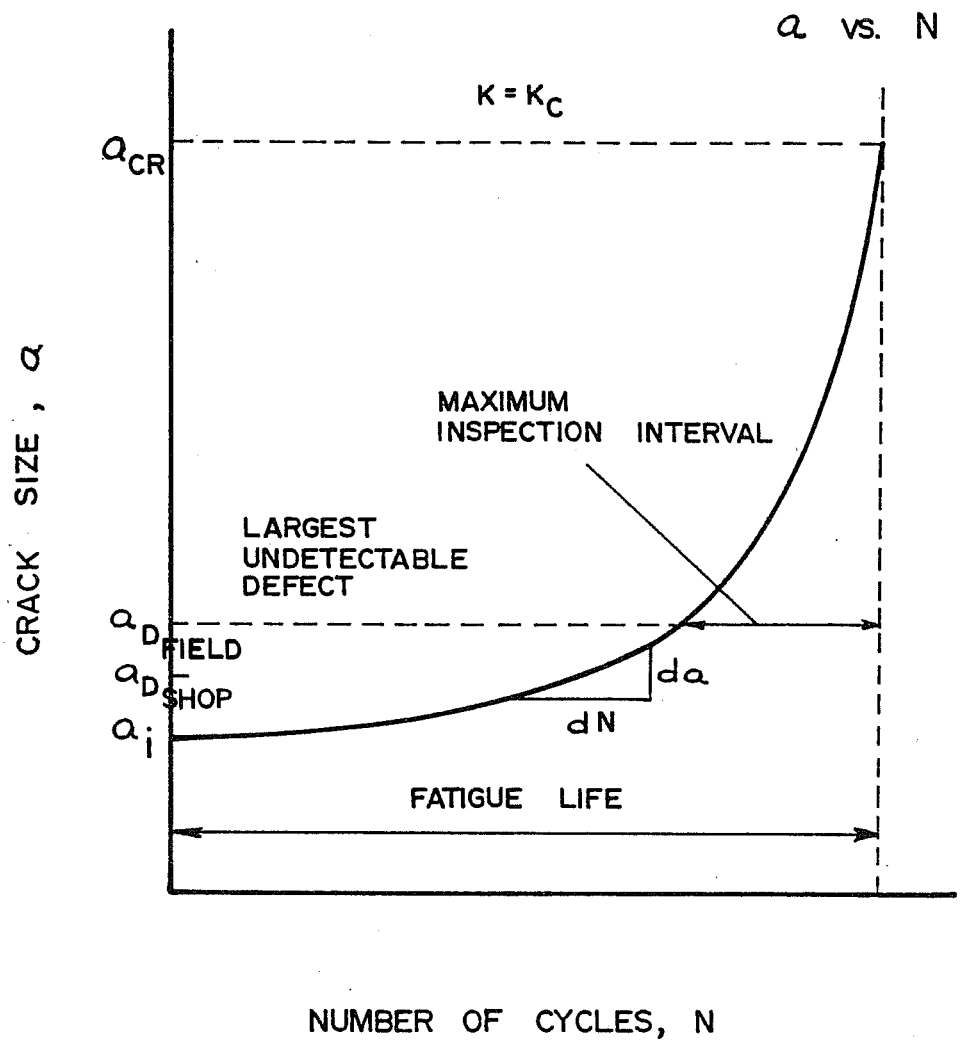

Fig. 4.1 Fatigue crack growth under constant amplitude cyclic loading showing the relationship between a_i, a_d (shop and field), and a_{cr}

is very important to the concept of fatigue life, and depends heavily on stress range.

The effect of stress range, S_r, on the rate of crack growth is illustrated in Fig. 4.2. For details having identical geometries, an increase in the cyclic stress range causes a decrease in fatigue life. Figure 4.3 shows that fatigue life decreases as the length of the initial crack increases. Furthermore, it can be seen that most of the useful cyclic life of a detail is expended when the crack length is very small.

The fracture toughness, K_c, of the material used in the structural detail also has an effect on fatigue life. An increase in fatigue life is realized if a material with a higher value of K_c is used, because the critical crack size, a_{cr}, becomes larger. Figure 4.4 shows the relative improvement of fatigue life which results from changing a_i, S_r, or K_c. The most improvement in life is realized by decreasing the initial crack size. This may be done by improving inspection procedures. Reducing the cyclic stress range also yields significant gains in terms of fatigue life. However, increasing material toughness, K_c, results in relatively small increases in fatigue life.

The range of stress intensity, ΔK_I, discussed previously, is the single parameter that incorporates the effect of changing crack length and stress range upon fatigue crack growth rate. Fatigue crack growth data are typically presented in a log-log plot of the rate of crack growth, da/dN, vs. ΔK_I, as shown in Fig. 4.5. Laboratory tests have shown that the crack growth behavior of metals can be divided into the three regions [17] depicted in Fig. 4.5. Region I behavior is characterized by a threshold value of ΔK_I, termed ΔK_{th}, below which cracks do not grow under cyclic loading. Above the level of ΔK_{th}, or in region II, crack growth occurs and can be represented mathematically by the expression

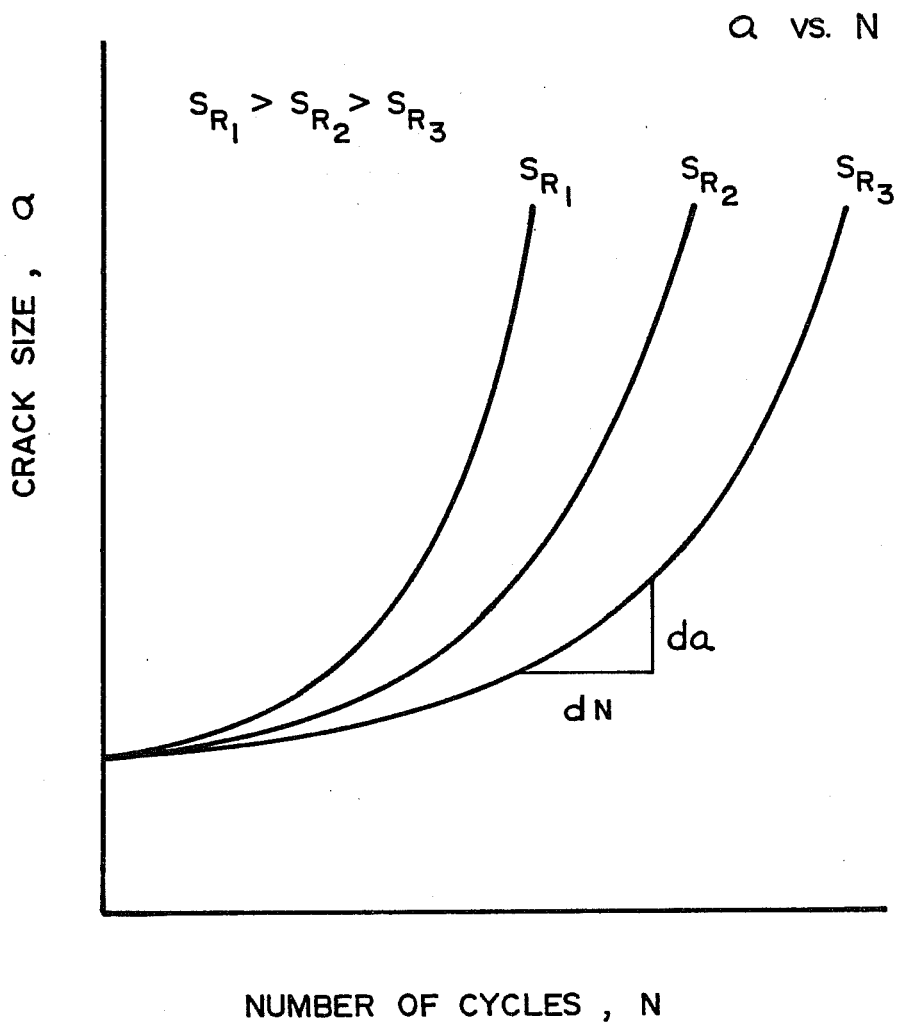

Fig. 4.2 Effect of stress range, S_r, on fatigue crack growth

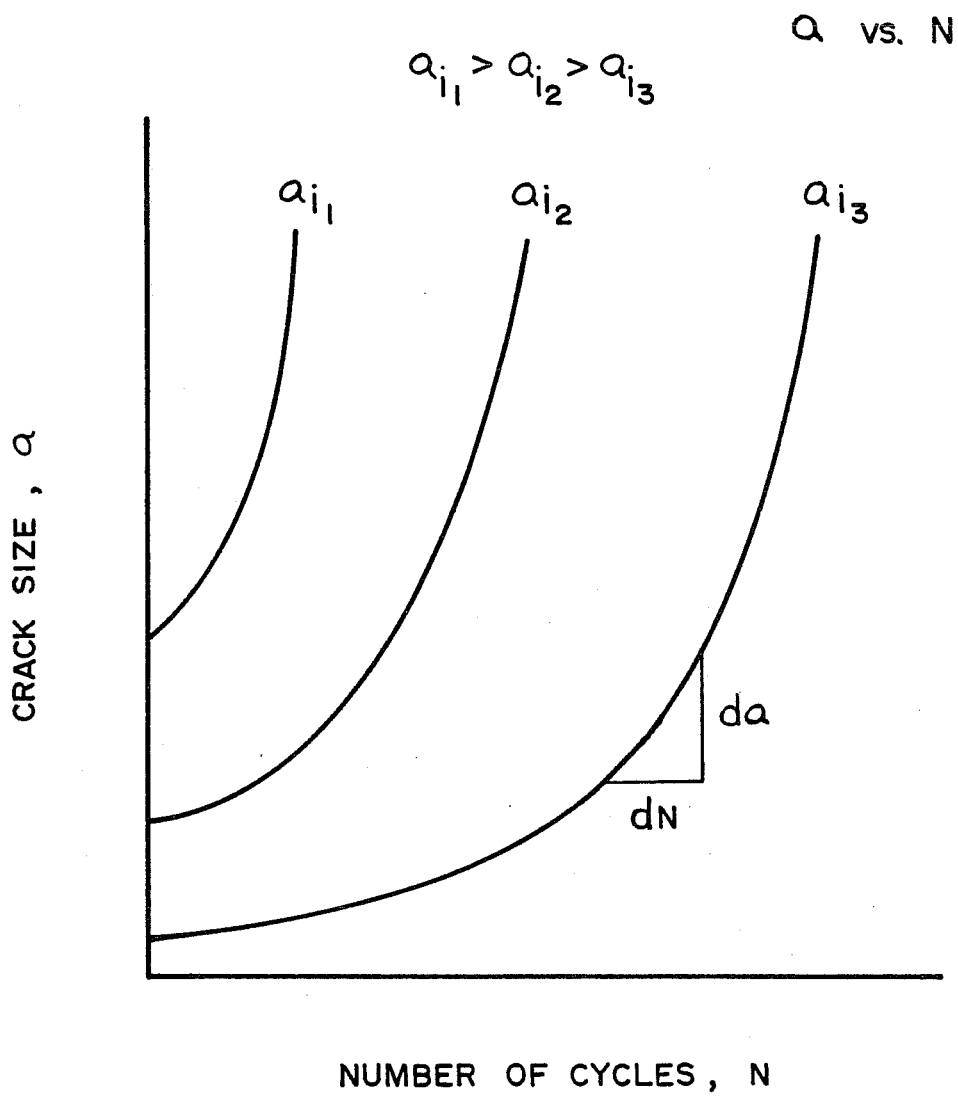

Fig. 4.3 Effect of initial crack size, a_i, on fatigue crack growth

I - IMPROVEMENT IN LIFE DUE TO SMALLER CRACK SIZE

II - IMPROVEMENT IN LIFE DUE TO LOWER STRESS RANGE

III - IMPROVEMENT IN LIFE DUE TO INCREASE IN MATERIAL TOUGHNESS

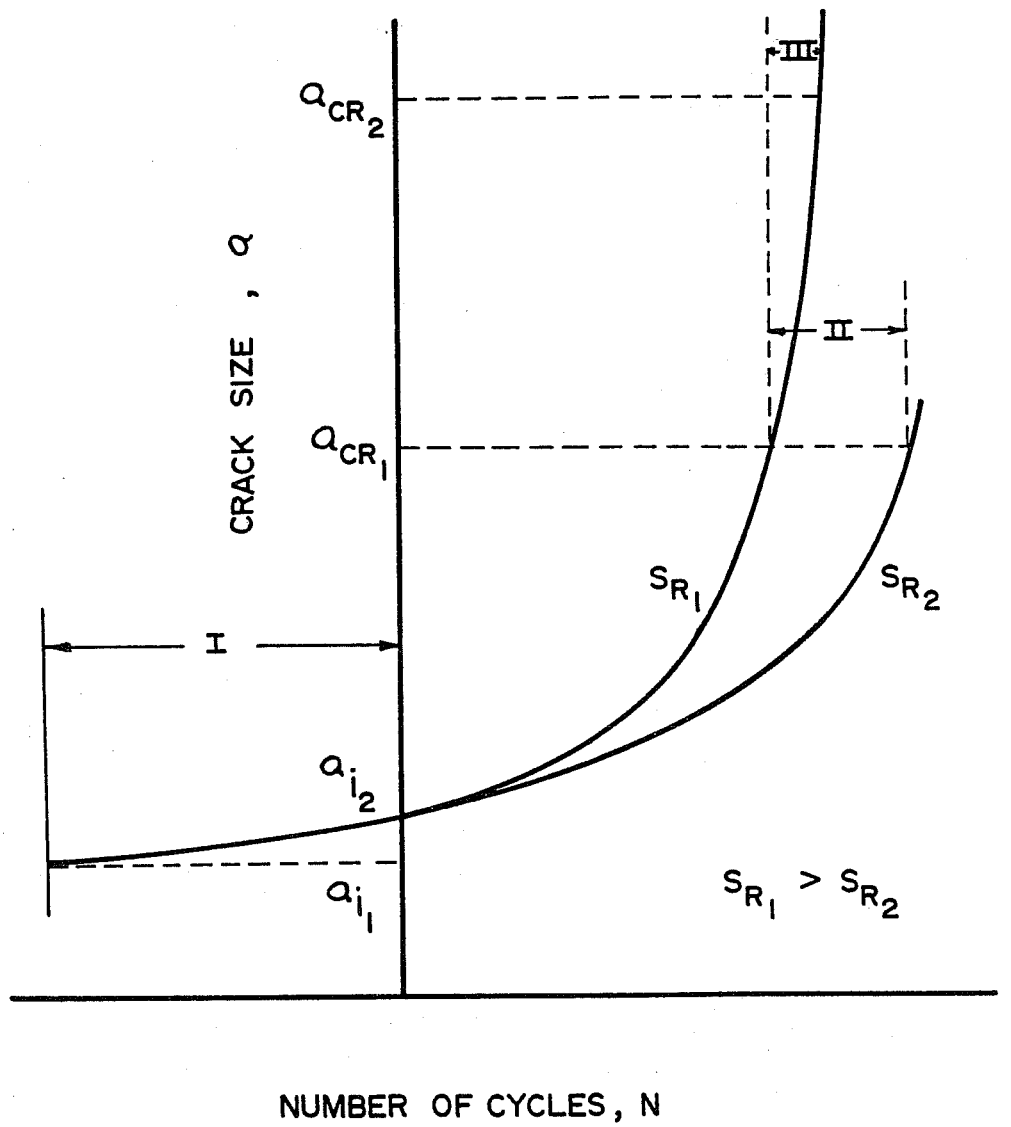

Fig. 4.4 Relative improvement of fatigue life realized by changing a_i, S_r, or K_c

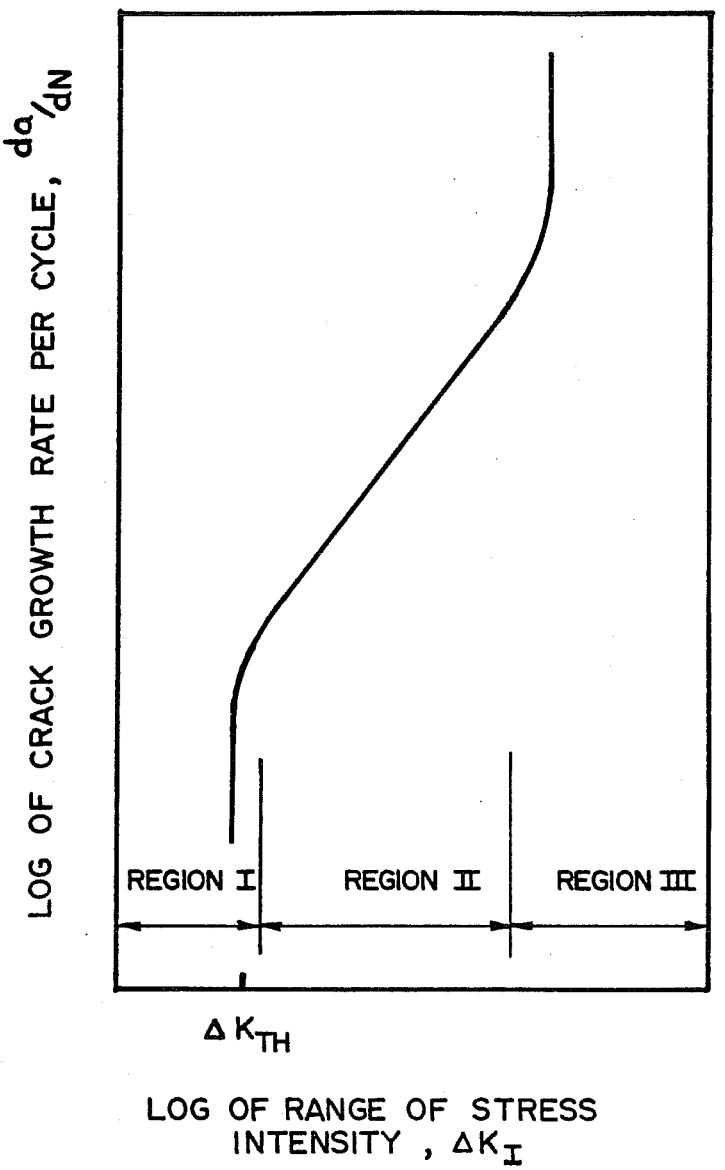

Fig. 4.5 Fatigue crack growth behavior

$$da/dN = C(\Delta K_I)^n \tag{4.1}$$

where C and n are material constants. Table 4.1 lists upper bound, fastest growth rate values of C and n for some common types of steel. Within region III, crack growth rate is accelerated above that of region II. This rapid growth occurs as the maximum stress intensity factor approaches the material's fracture toughness, K_c.

Equation (4.1) may be rearranged and integrated between the initial crack size, a_i, and final crack size, a_f. The resulting expression for fatigue life is

$$N = 1/C \int_{a_i}^{a_f} 1/(\Delta K_I)^n \, da \tag{4.2}$$

This relationship produces a straight line on a log-log plot of stress range, S_r, vs. number of cycles, N, and provides fatigue life information given the range of stress at a particular detail. The S-N relationship takes on the mathematical form

$$\text{Log}N = A - n\text{Log}S_r \tag{4.3}$$

where n is the material constant given in Table 4.1 and A is a constant which depends on the geometry of the detail. Furthermore, there exists a threshold stress range, S_{rth}, corresponding to the threshold stress intensity range, ΔK_{th}. That is, for stress ranges below S_{rth}, crack growth does not occur, and no damage to the structural detail can be expected. Figure 4.6 shows the S-N relationship along with the significance of the threshold stress range.

TABLE 4.1 VARIATION OF CRACK GROWTH RATE PARAMETERS, n AND C (FROM REF. 17)

Material	n	C
Martensitic Steels	2.25	6.6×10^{-9}
Ferrite-Pearlite Steels	3.0	3.6×10^{-10}
Austenitic Stainless Steels	3.25	3.0×10^{-10}

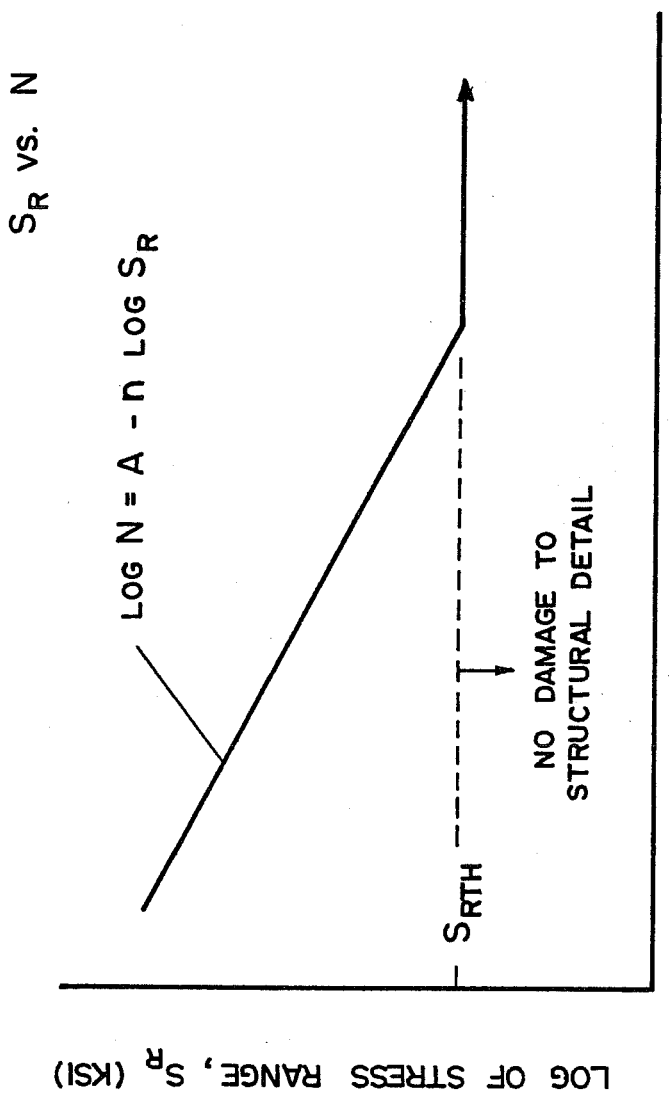

Fig. 4.6 S-N relationship with S_{rth} shown

4.2 Longitudinal-Transverse Stiffener Intersection

The procedure used to analyze the fatigue behavior of the longitudinal-transverse stiffener intersection detail using fracture mechanics principles was as follows:

(1) Estimate the initial crack size, a_i.

(2) Determine the critical crack size, a_{cr}.

(3) Select an expression for crack growth rate from Table 4.1.

(4) Determine the appropriate expression for ΔK_I.

(5) Determine the live load stress range, S_r.

(6) Integrate the crack growth rate expression between the limits of a_i and a_{cr} to obtain the fatigue life. This may be done by assuming an increment of crack growth, Δa, and solving for ΔN for each increment such that

$$\Delta N = \frac{\Delta a}{C\left[F(a) S_r \sqrt{\pi a_{avg}}\right]^n} \qquad (4.4)$$

where a_{avg} is the average crack size between two crack increments a_i and a_j.

In using the numerical technique described in step 6 above, greater accuracy is obtained (as compared to direct integration) for smaller and smaller crack increments.

Once the fatigue life of the existing detail is calculated, the corresponding S-N relationship and value of S_{rth} can be determined. Comparison may then be made with the current AASHTO fatigue categories shown in Figs. 1.1 and 1.2.

4.2.1 Life Estimate—No Bending. To determine the significance of whether or not bending is assumed to occur in the cracked plate, life estimates will be made first assuming no bending (below) and then assuming bending occurs (Sec. 4.2.2).

Since most useful fatigue life is expended at small crack sizes, the estimate of initial crack size, a_i, will significantly affect life calculations. In design applications, a_i is determined based on the inspection procedure and type of fabrication (shop vs. field). However, in the case of the existing longitudinal-transverse stiffener intersection detail, a_i at the weld toe is generally too small to find by inspection and must be estimated based on expected initial flaw sizes [15]. To demonstrate the effect of a_i on fatigue life, values of a_i, comparable to those used by Zettlemoyer [15], equal to 0.005 in., 0.010 in., and 0.020 in. were selected. S-N relationships were determined for each value of a_i.

The critical crack size is determined by solving for a_{cr} in the equation

$$K_c = F(a)S_r \sqrt{\pi a_{cr}} \tag{4.5}$$

where K_c is the fracture toughness of the girder web material. However, K_c for the existing detail is unknown. A value of final crack size, a_f, which constitutes failure, was assumed in a manner similar to that of Frank [7], Gurney [8], and Zettlemoyer [15]. Failure is assumed to occur when the crack at the longitudinal stiffener end grows to a length equal to the thickness of the girder web (3/8 in.).

Since the girder web is A36 steel, the expression for crack growth rate selected was

$$da/dN = 3.6 \times 10^{-10}(\Delta K_I)^{3.0} \tag{4.6}$$

The constants 3.6×10^{-10} and 3.0 were obtained from Table 4.1 and are applicable to all ferrite-pearlite (low-strength) steels.

The previously developed expression for ΔK_I given by

$$\Delta K_I = F_g F_e F_s F_w \times S_r \sqrt{\pi a} \qquad (4.7)$$

was used in the crack growth rate relationship defined by Eq. 4.6.

The magnitude of live load stress range, S_r, was determined based on field tests of the longitudinal-transverse stiffener intersection detail. Strain gages mounted on the longitudinal stiffener (gages 11, 12, 13, and 14 shown in Fig. 2.4) indicated live load stress ranges of approximately 2.0 ksi when the bridge structure was loaded with a 54.6 kip test truck. Figure 4.7 shows a computer plot of stress vs. time obtained from one of the longitudinal stiffener strain gages when the test truck was driven across the structure at a speed of 5 m.p.h.. The maximum stress range of 2.0 ksi is shown. This value was used in subsequent calculations. The integration to obtain fatigue life may also be performed removing S_r as a constant and multiplying the result by the appropriate S_r term.

Before integrating the crack growth rate expression, the correction function, F(a), to be applied to ΔK_I was determined for values of a_{avg}. These values are shown in Table 4.2. The crack shape correction factor, F_e, was taken as 0.79. F_s, the front free surface correction factor used, was 1.05. The back free surface correction factor, F_w, was obtained assuming no bending at the cracked plate region. F_g, the stress gradient correction factor, was determined based on finite element analysis.

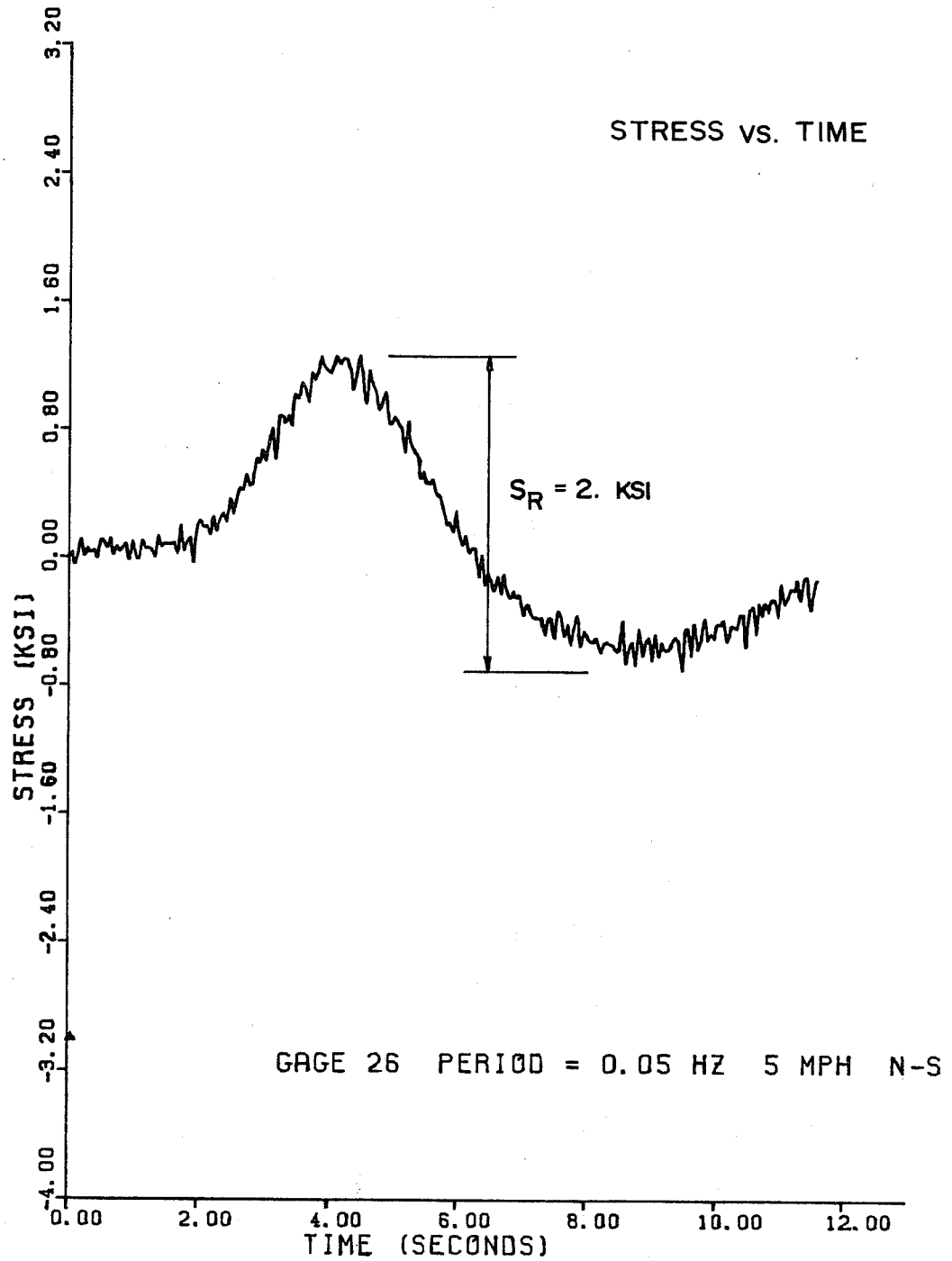

Fig. 4.7 Measured stress range at the longitudinal stiffener

TABLE 4.2 CALCULATION OF F(a) FOR THE LONGITUDINAL-TRANSVERSE STIFFENER INTERSECTION DETAIL ASSUMING NO BENDING

$F_e = 0.79$ $F_s = 1.05$ $F(a) = F_e F_s F_w F_g$

a_{avg} (in.)	a/t	F_w	F_g	F(a)
0.0075	0.020	1.00	10.6	8.79
0.015	0.040	1.00	8.65	7.18
0.025	0.053	1.00	7.44	6.17
0.035	0.093	1.01	6.73	5.64
0.045	0.120	1.01	6.21	5.20
0.055	0.147	1.01	5.81	4.87
0.065	0.173	1.02	5.47	4.63
0.075	0.200	1.03	5.19	4.43
0.085	0.227	1.03	4.95	4.23
0.095	0.253	1.04	4.70	4.05
0.105	0.280	1.05	4.49	3.91
0.115	0.307	1.06	4.28	3.76
0.125	0.333	1.07	4.12	3.66
0.135	0.360	1.09	3.96	3.58
0.145	0.387	1.10	3.78	3.45
0.155	0.413	1.12	3.61	3.35
0.165	0.440	1.14	3.47	3.28
0.175	0.467	1.16	3.31	3.18
0.185	0.493	1.18	3.19	3.12
0.195	0.520	1.21	3.07	3.08
0.205	0.547	1.24	2.95	3.03
0.215	0.573	1.27	2.86	3.01
0.225	0.600	1.30	2.67	2.88

TABLE 4.2 (Cont.)

a_{avg} (in.)	a/t	F_w	F_g	F(a)
0.235	0.627	1.34	2.56	2.85
0.245	0.653	1.39	2.43	2.80
0.255	0.680	1.44	2.32	2.77
0.265	0.707	1.50	2.22	2.76
0.275	0.733	1.57	2.02	2.63
0.285	0.760	1.65	1.94	2.66
0.295	0.787	1.75	1.83	2.66
0.305	0.813	1.86	1.72	2.65
0.315	0.840	2.01	1.65	2.75
0.325	0.867	2.20	1.60	2.92
0.335	0.893	2.44	1.51	3.06
0.345	0.920	2.82	1.36	3.18
0.355	0.947	3.47	1.27	3.66
0.365	0.973	4.89	1.15	4.66

The numerical integration of the crack growth rate expression was performed in Table 4.3 for $\Delta a = 0.01$ in. and $S_r = 2.0$ ksi. Similar calculations, not shown in this report, were made using $\Delta a = 0.002$ in. to determine the effect of increment size on fatigue life estimates. The difference in life estimates was found to be insignificant (less than 1 percent). For an initial crack size, a_i, of 0.010 in., a fatigue life of 10.2 million cycles was obtained. The mathematical equation representing the S-N relationship for $a_i = 0.010$ in. is given by

$$\text{Log}N = 7.91 - 3.0\text{Log}S_r \tag{4.8}$$

and is shown graphically in Fig. 4.8. Table 4.4 compares the fatigue lives obtained from assuming each of the three initial crack sizes, 0.005 in., 0.010 in., and 0.020 in. As expected, fatigue life decreases with an increase in a_i. The S-N relationships for $a_i = 0.005$ in. and 0.020 in. are also plotted in Fig. 4.8.

To determine the value of the threshold stress range, S_{rth}, the expression given by

$$S_{rth} = \Delta K_{th}/F(a)\sqrt{\pi a_i} \tag{4.9}$$

was used, where ΔK_{th} is the threshold range of stress intensity. As shown in Table 4.5, values of S_{rth} as a function of a_i were computed for three magnitudes of ΔK_{th}, 2.0, 3.5, and 5.0 ksi $\sqrt{\text{in.}}$ These values were then plotted in Fig. 4.9 as a family of S_{rth} vs. a_i curves. Using Fig. 4.9, S_{rth} may be obtained for any combination of initial flaw size and ΔK_{th}. For the initial flaw sizes of 0.005 in., 0.010 in., and 0.020 in., and assuming $\Delta K_{th} = 2.0$ ksi $\sqrt{\text{in.}}$ (a lower bound to most data), values of 1.50, 1.35, and 1.20 ksi were obtained, respectively, for S_{rth}. These are shown on the S-N plot of Fig. 4.8.

TABLE 4.3 CALCULATION OF FATIGUE LIFE FOR THE LONGITUDINAL-STIFFENER INTERSECTION DETAIL FOR S_r = 2.0 KSI AND ASSUMING NO BENDING

$$\Delta N = \frac{\Delta a}{\left[3.6 \times 10^{-10}\right]\left[F(a) S_r \sqrt{\pi a_{avg}}\right]^3}$$

S_r = 2.0 ksi Δa = 0.01 in.

a_o (in.)	a_f (in.)	a_{avg} (in.)	F(a)	ΔK (ksi$\sqrt{\text{in.}}$)	ΔN (cycles $\times 10^5$)	ΣN (cycles $\times 10^5$)
0.005	0.01	0.0075	8.79	2.70	7.07	7.07
0.01	0.02	0.015	7.18	3.12	9.17	16.2
0.02	0.03	0.025	6.17	3.46	6.72	23.0
0.03	0.04	0.035	5.64	3.74	5.31	28.3
0.04	0.05	0.045	5.20	3.91	4.65	32.9
0.05	0.06	0.055	4.87	4.05	4.19	37.1
0.06	0.07	0.065	4.63	4.18	3.79	40.9
0.07	0.08	0.075	4.43	4.30	3.49	44.4
0.08	0.09	0.085	4.23	4.37	3.32	47.7
0.09	0.10	0.095	4.05	4.43	3.21	50.9
0.10	0.11	0.105	3.91	4.49	3.07	54.0
0.11	0.12	0.115	3.76	4.52	3.01	57.0
0.12	0.13	0.125	3.66	4.59	2.88	59.9
0.13	0.14	0.135	3.58	4.66	2.74	62.6
0.14	0.15	0.145	3.45	4.66	2.75	65.4
0.15	0.16	0.155	3.35	4.68	2.72	68.1
0.16	0.17	0.165	3.28	4.72	2.64	70.7
0.17	0.18	0.175	3.18	4.72	2.65	73.4
0.18	0.19	0.185	3.12	4.76	2.58	76.0

TABLE 4.3 (Cont.)

a_o (in.)	a_f (in.)	a_{avg} (in.)	F(a)	ΔK (ksi$\sqrt{\text{in.}}$)	ΔN (cycles $\times 10^5$)	ΣN (cycles $\times 10^5$)
0.19	0.20	0.195	3.08	4.82	2.48	78.4
0.20	0.21	0.205	3.03	4.86	2.42	80.9
0.21	0.22	0.215	3.01	4.95	2.29	83.2
0.22	0.23	0.225	2.88	4.84	2.45	85.6
0.23	0.24	0.235	2.85	4.90	2.36	88.0
0.24	0.25	0.245	2.80	4.91	2.34	90.3
0.25	0.26	0.255	2.77	4.96	2.28	92.6
0.26	0.27	0.265	2.76	5.04	2.17	94.8
0.27	0.28	0.275	2.63	4.89	2.38	97.1
0.28	0.29	0.285	2.66	5.03	2.18	99.3
0.29	0.30	0.295	2.66	5.12	2.07	101.0
0.30	0.31	0.305	2.65	5.19	1.99	103.0
0.31	0.32	0.315	2.75	5.47	1.70	105.0
0.32	0.33	0.325	2.92	5.90	1.35	106.0
0.33	0.34	0.335	3.06	6.28	1.12	108.0
0.34	0.35	0.345	3.18	6.62	0.96	109.0
0.35	0.36	0.355	3.66	7.73	0.60	109.0
0.36	0.37	0.365	4.66	9.98	0.28	109.0

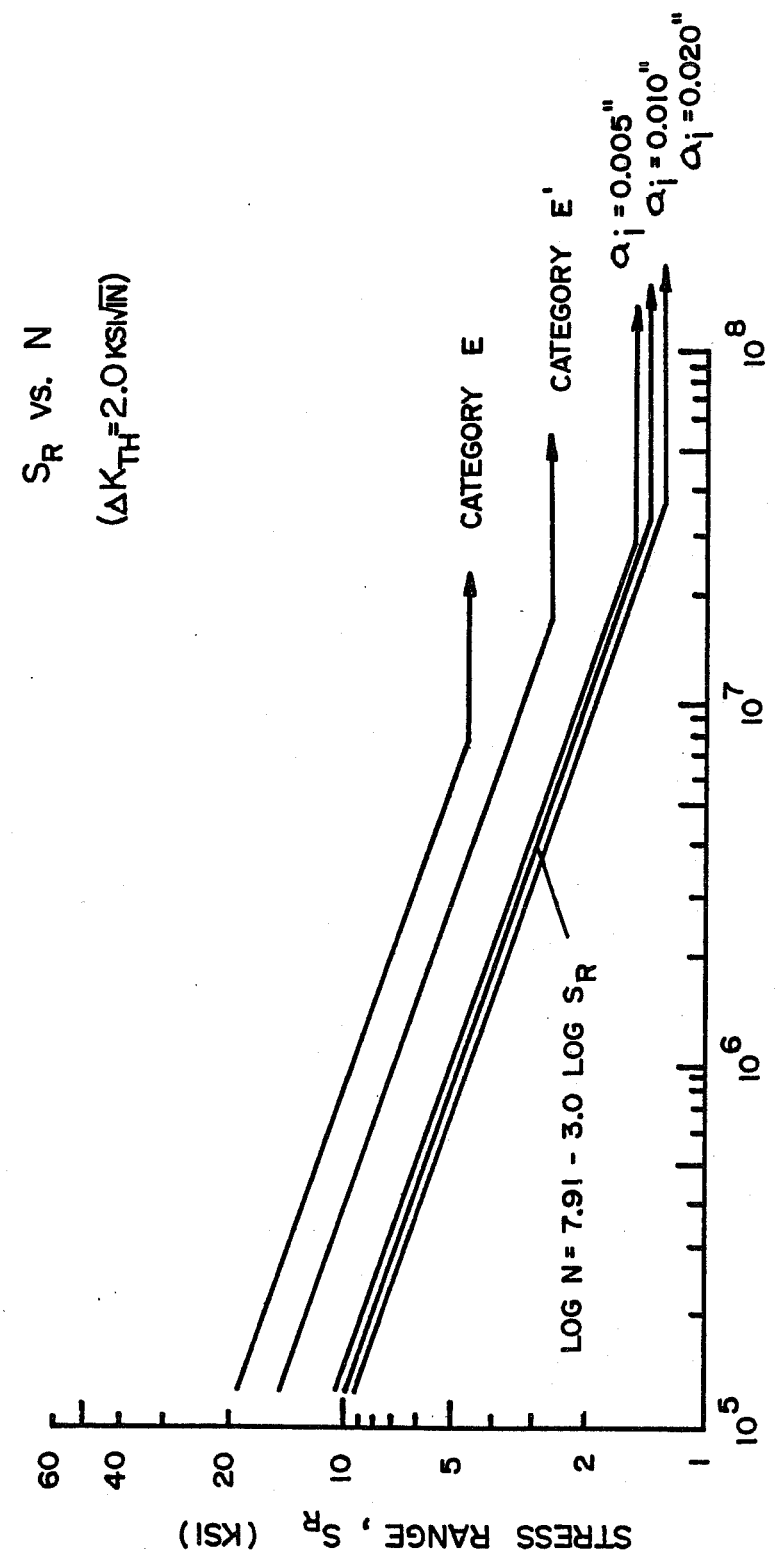

Fig. 4.8 S-N relationship for the longitudinal-transverse stiffener intersection detail assuming no bending

TABLE 4.4 VARIATION OF FATIGUE LIFE, N, WITH INITIAL CRACK SIZE, a_i, FOR S_r = 2.0 KSI, ASSUMING NO BENDING

S_r = 2.0 ksi	
a_i (in.)	N (cycles x 10^6)
0.005	10.9
0.010	10.2
0.020	9.3

TABLE 4.5 VALUES OF STRESS RANGE BELOW WHICH NO FATIGUE PROPAGATION WILL OCCUR—LONGITUDINAL-TRANSVERSE STIFFENER INTERSECTION DETAIL ASSUMING NO BENDING

$$S_{rth} = \Delta K_{th} / F(a)\sqrt{\pi a_i}$$

a_i (in.)	F(a)	ΔK_{th} (ksi$\sqrt{\text{in.}}$)		
		2.0	3.5	5.0
		S_{rth} (ksi)		
0.0075	8.79	1.48	2.59	3.71
0.015	7.18	1.28	2.25	3.21
0.035	5.64	1.07	1.87	2.67
0.055	4.87	0.99	1.73	2.47
0.075	4.43	0.93	1.63	2.33
0.095	4.05	0.90	1.58	2.26
0.115	3.76	0.88	1.55	2.21
0.135	3.58	0.86	1.50	2.14
0.155	3.35	0.86	1.50	2.14
0.175	3.18	0.85	1.48	2.12
0.195	3.08	0.83	1.45	2.07
0.235	2.85	0.82	1.43	2.04
0.275	2.63	0.82	1.43	2.05
0.315	2.75	0.73	1.28	1.83
0.355	3.66	0.52	0.91	1.29

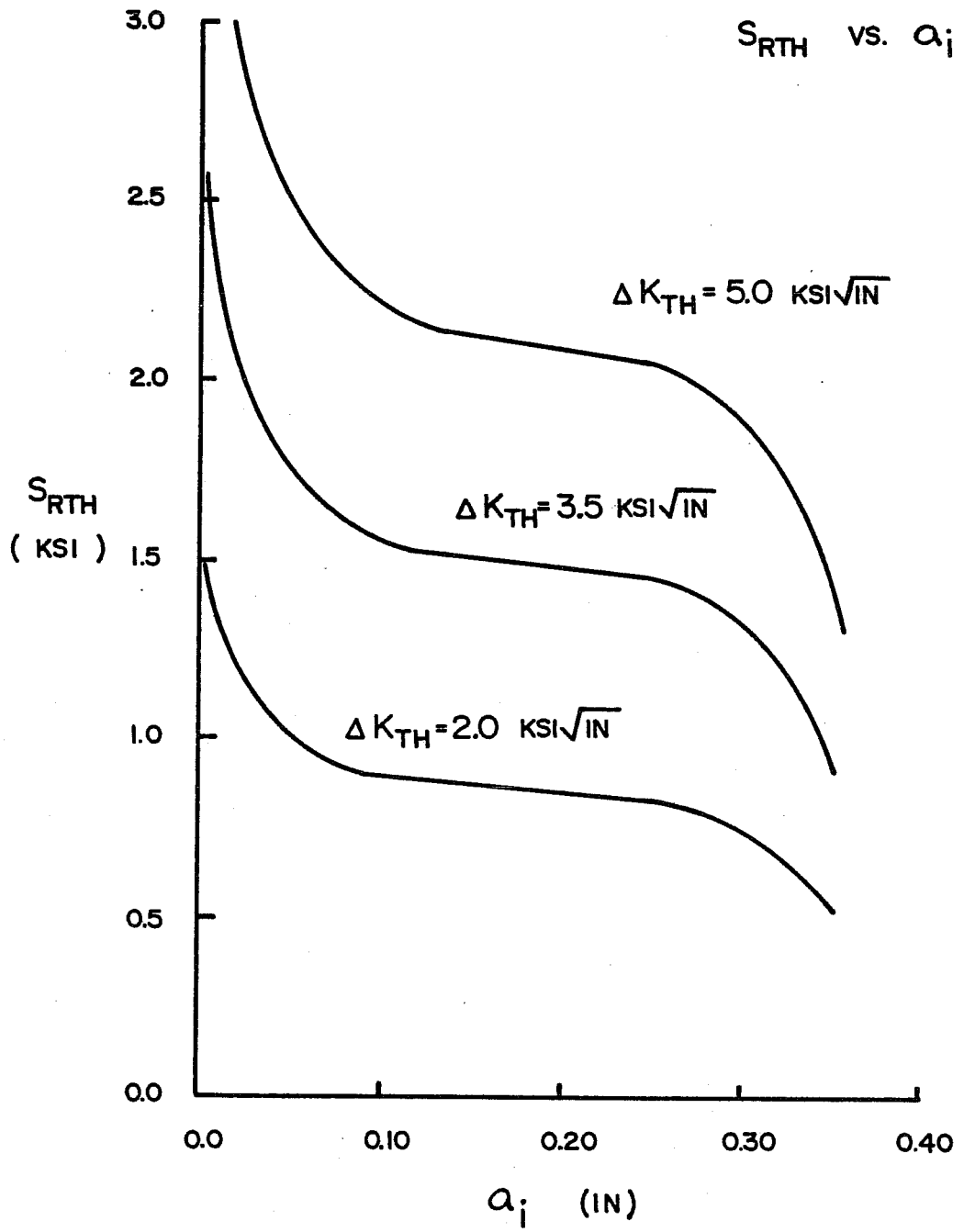

Fig. 4.9 S_{rth} vs. a_i—longitudinal-transverse stiffener intersection detail assuming no bending

Figure 4.8 compares the S-N relationships found for the existing detail, assuming no bending, to those of the AASHTO fatigue categories E and E′. It can be seen that the longitudinal-transverse stiffener intersection detail exhibits fatigue performance which is poorer than that of the worst AASHTO fatigue category, Category E′. Furthermore, for the live load stress range of 2.0 ksi observed in field tests, damage to the structure can be expected since S_{rth} for the normal range of a_i is less than 2.0 ksi.

4.2.2 Life Estimate—Bending. To determine the effect of using the back free surface correction factor, F_w, corresponding to bending of the cracked plate, the fatigue life was estimated using the same procedure as that used for the case of no bending.

Table 4.6 summarizes the calculations performed to establish the correction function, F(a), as a function of average crack size, a_{avg}.

The results of the numerical integration of the crack growth rate expression are shown in Table 4.7 for $\Delta a = 0.01$ in. and $S_r = 2.0$ ksi. For $a_i = 0.010$ in., a fatigue life of 4.14 million cycles was obtained. The resulting mathematical equation which represents the S-N relationship is given by

$$\text{Log}N = 7.52 - 3.0\text{Log}S_r \qquad (4.10)$$

and is shown graphically in Fig. 4.10. Table 4.8 compares the fatigue lives obtained assuming each of the three initial crack sizes, a_i, of 0.005 in., 0.010 in., and 0.020 in. The S-N relationships for $a_i = 0.005$ in. and $a_i = 0.020$ in. are also plotted in Fig. 4.10.

Table 4.9 lists values of S_{rth} as a function of a_i for values of ΔK_{th} equal to 2.0, 3.5, and 5.0 ksi $\sqrt{\text{in.}}$ The family

TABLE 4.6 CALCULATION OF F(a) FOR THE LONGITUDINAL-TRANSVERSE STIFFENER INTERSECTION DETAIL ASSUMING BENDING OCCURS

$F_e = 0.79$ $F_s = 1.05$ $F(a) = F_e F_s F_w F_g$

a_{avg} (in.)	a/t	F_w	F_g	F(a)
0.0075	0.020	1.00	10.6	8.79
0.015	0.040	1.01	8.65	7.25
0.025	0.053	1.03	7.44	6.36
0.035	0.093	1.06	6.73	5.92
0.045	0.120	1.09	6.21	5.61
0.055	0.147	1.13	5.81	5.45
0.065	0.173	1.17	5.47	5.31
0.075	0.200	1.22	5.19	5.25
0.085	0.227	1.27	4.95	5.21
0.095	0.253	1.34	4.70	5.22
0.105	0.280	1.42	4.49	5.29
0.115	0.307	1.50	4.28	5.33
0.125	0.333	1.58	4.12	5.40
0.135	0.360	1.67	3.96	5.49
0.145	0.387	1.78	3.78	5.58
0.155	0.413	1.90	3.61	5.69
0.165	0.440	2.09	3.47	6.02
0.175	0.467	2.28	3.31	6.26
0.185	0.493	2.48	3.19	6.56
0.195	0.520	2.70	3.07	6.88
0.205	0.547	2.95	2.95	7.22
0.215	0.573	3.30	2.86	7.83
0.225	0.600	3.60	2.67	7.97
0.235	0.627	4.04	2.56	8.58

TABLE 4.6 (Cont.)

a_{avg} (in.)	a/t	F_w	F_g	F(a)
0.245	0.653	4.50	2.43	9.07
0.255	0.680	5.19	2.32	9.99
0.265	0.707	5.94	2.22	10.9
0.275	0.733	6.94	2.02	11.6
0.285	0.760	8.19	1.94	13.2
0.295	0.787	8.41	1.83	12.8
0.305	0.813	12.3	1.72	17.5
0.315	0.840	15.4	1.65	21.1
0.325	0.867	24.6	1.60	32.6
0.335	0.893	36.7	1.51	46.0
0.345	0.920	59.4	1.36	67.0
0.355	0.947	85.6	1.27	90.2
0.365	0.973	--	1.15	--

TABLE 4.7 CALCULATION OF FATIGUE LIFE FOR THE LONGITUDINAL-TRANSVERSE STIFFENER INTERSECTION DETAIL FOR S_r = 2.0 KSI ASSUMING BENDING OCCURS

$$\Delta N = \frac{\Delta a}{\left[3.6 \times 10^{-10}\right]\left[F(a)S_r\sqrt{\pi a_{avg}}\right]^3}$$

S_r = 2.0 ksi Δa = 0.01 in.

a_o (in.)	a_f (in.)	a_{avg} (in.)	F(a)	ΔK (ksi$\sqrt{in.}$)	ΔN (cycles $\times 10^5$)	ΣN (cycles $\times 10^5$)
0.005	0.01	0.0075	8.79	2.70	7.07	7.07
0.01	0.02	0.015	7.25	3.15	8.91	16.0
0.02	0.03	0.025	6.36	3.56	6.13	22.1
0.03	0.04	0.035	5.92	3.93	4.59	26.7
0.04	0.05	0.045	5.61	4.22	3.70	30.4
0.05	0.06	0.055	5.45	4.53	2.99	33.4
0.06	0.07	0.065	5.31	4.80	2.51	35.9
0.07	0.08	0.075	5.25	5.10	2.10	38.0
0.08	0.09	0.085	5.21	5.38	1.78	39.8
0.09	0.10	0.095	5.22	5.70	1.50	41.3
0.10	0.11	0.105	5.29	6.08	1.24	42.5
0.11	0.12	0.115	5.33	6.41	1.06	43.6
0.12	0.13	0.125	5.40	6.77	0.90	44.5
0.13	0.14	0.135	5.49	7.15	0.76	45.2
0.14	0.15	0.145	5.58	7.53	0.65	45.9
0.15	0.16	0.155	5.69	7.94	0.55	46.4
0.16	0.17	0.165	6.02	8.67	0.43	46.9
0.17	0.18	0.175	6.26	9.28	0.35	47.2
0.18	0.19	0.185	6.56	10.0	0.28	47.5

TABLE 4.7 (Cont.)

a_o (in.)	a_f (in.)	a_{avg} (in.)	F(a)	ΔK (ksi$\sqrt{\text{in.}}$)	ΔN (cycles x 10^5)	ΣN (cycles x 10^5)
0.19	0.20	0.195	6.88	10.8	0.22	47.7
0.20	0.21	0.205	7.22	11.6	0.18	47.9
0.21	0.22	0.215	7.83	12.9	0.13	48.0
0.22	0.23	0.225	7.97	13.4	0.12	48.2
0.23	0.24	0.235	8.58	14.7	0.09	48.2
0.24	0.25	0.245	9.07	15.9	0.07	48.3
0.25	0.26	0.255	9.99	17.9	0.05	48.4
0.26	0.27	0.265	10.9	19.9	0.04	48.4
0.27	0.28	0.275	11.6	21.6	0.03	48.4
0.28	0.29	0.285	13.2	25.0	0.02	48.5
0.29	0.30	0.295	12.8	24.6	0.02	48.5
0.30	0.31	0.305	17.5	34.3	0.01	48.5
0.31	0.32	0.315	21.1	42.0	--	48.5
0.32	0.33	0.325	32.6	65.9	--	48.5
0.33	0.34	0.335	46.0	94.4	--	48.5
0.34	0.35	0.345	67.0	140.0	--	48.5
0.35	0.36	0.355	90.2	191.0	--	48.5
0.36	0.37	0.365	--	--	--	48.5

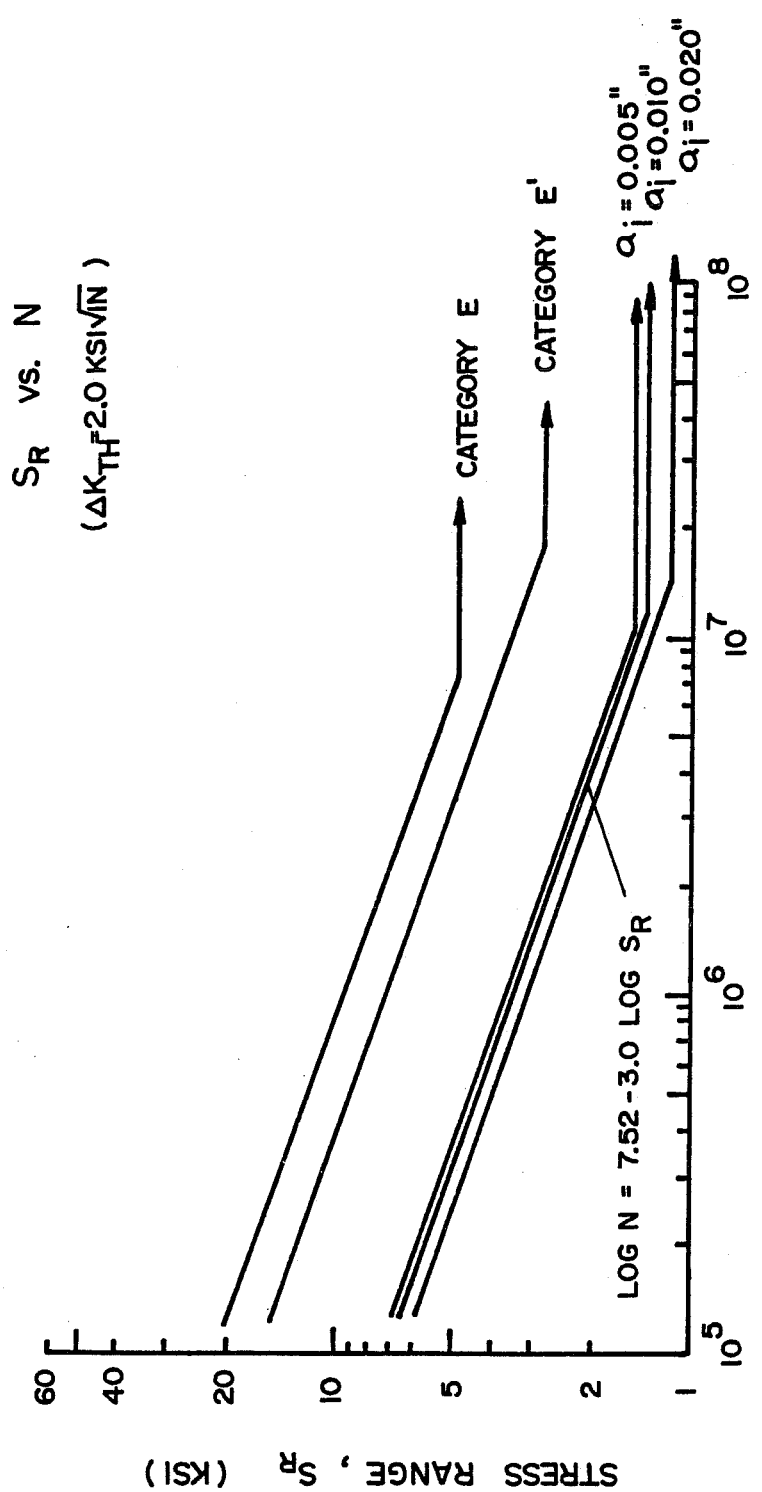

Fig. 4.10 S-N relationship for the longitudinal-transverse stiffener intersection detail assuming bending occurs

TABLE 4.8 VARIATION OF FATIGUE LIFE, N, WITH INITIAL CRACK SIZE, a_i, FOR S_r = 2.0 KSI, ASSUMING BENDING OCCURS

S_r = 2.0 ksi

a_i (in.)	N (cycles x 10^6)
0.005	4.85
0.010	4.14
0.020	3.25

TABLE 4.9 VALUES OF STRESS RANGE BELOW WHICH NO FATIGUE PROPAGATION WILL OCCUR--LONGITUDINAL-TRANSVERSE STIFFENER INTERSECTION DETAIL ASSUMING BENDING OCCURS

$S_{rth} = \Delta K_{th}/F(a)\sqrt{\pi a_i}$

a_i (in.)	F(a)	ΔK_{th} (ksi$\sqrt{\text{in.}}$)		
		2.0	3.5	5.0
		S_{rth} (ksi)		
0.0075	8.79	1.48	2.59	3.71
0.015	7.25	1.27	2.22	3.18
0.035	5.92	1.02	1.78	2.55
0.055	5.45	0.88	1.54	2.21
0.075	5.25	0.78	1.37	1.96
0.095	5.22	0.70	1.23	1.75
0.115	5.33	0.62	1.09	1.56
0.135	5.49	0.56	0.98	1.40
0.155	5.69	0.50	0.88	1.26
0.175	6.26	0.43	0.75	1.08
0.195	6.88	0.37	0.65	0.93
0.235	8.58	0.27	0.47	0.68
0.275	11.6	0.19	0.32	0.46
0.315	21.1	0.10	0.17	0.24
0.355	90.2	0.02	0.04	0.05

of three S_{rth} vs. a_i curves which these values represent is plotted in Fig. 4.11. Once again, S_{rth} may be obtained from Fig. 4.11 for any combination of a_i and ΔK_{th}. For the initial flaw sizes of 0.005 in., 0.010 in., and 0.020 in., and assuming ΔK_{th} = 2.0 ksi $\sqrt{in.}$, values of 1.50, 1.35, and 1.20 ksi were obtained, respectively, for S_{rth}. This is shown on the S-N plot of Fig. 4.10.

Figure 4.10 also compares the S-N relationship for the existing detail, assuming bending occurs, to those of the AASHTO fatigue categories E and E′. The fatigue performance of the longitudinal-transverse stiffener intersection detail, assuming bending occurs, is slightly worse than that seen for the existing detail assuming no bending (a direct comparison will be made later). Again, fatigue performance is seen to be worse than that of AASHTO Category E′ details.

4.3 Cope Detail

To determine the degree of improvement realized by modifying the existing longitudinal-transverse stiffener intersection detail with the cope, the same procedure was used to analyze fatigue behavior.

In addition to checking the fatigue performance of the cope detail through the girder web, the welds which connect the longitudinal stiffener to the transverse stiffener must be evaluated. These welds form a cruciform joint, as shown in Fig. 4.12. Design of the cruciform joint has recently been discussed in a paper by Frank [21]. The fatigue performance of such joints are found to be a function of weld size, weld penetration, and plate thickness. The cruciform detail is termed a Category C detail at best, and may be worse depending on the values of the above-mentioned parameters. Since the purpose of this study is to evaluate the fatigue performance of

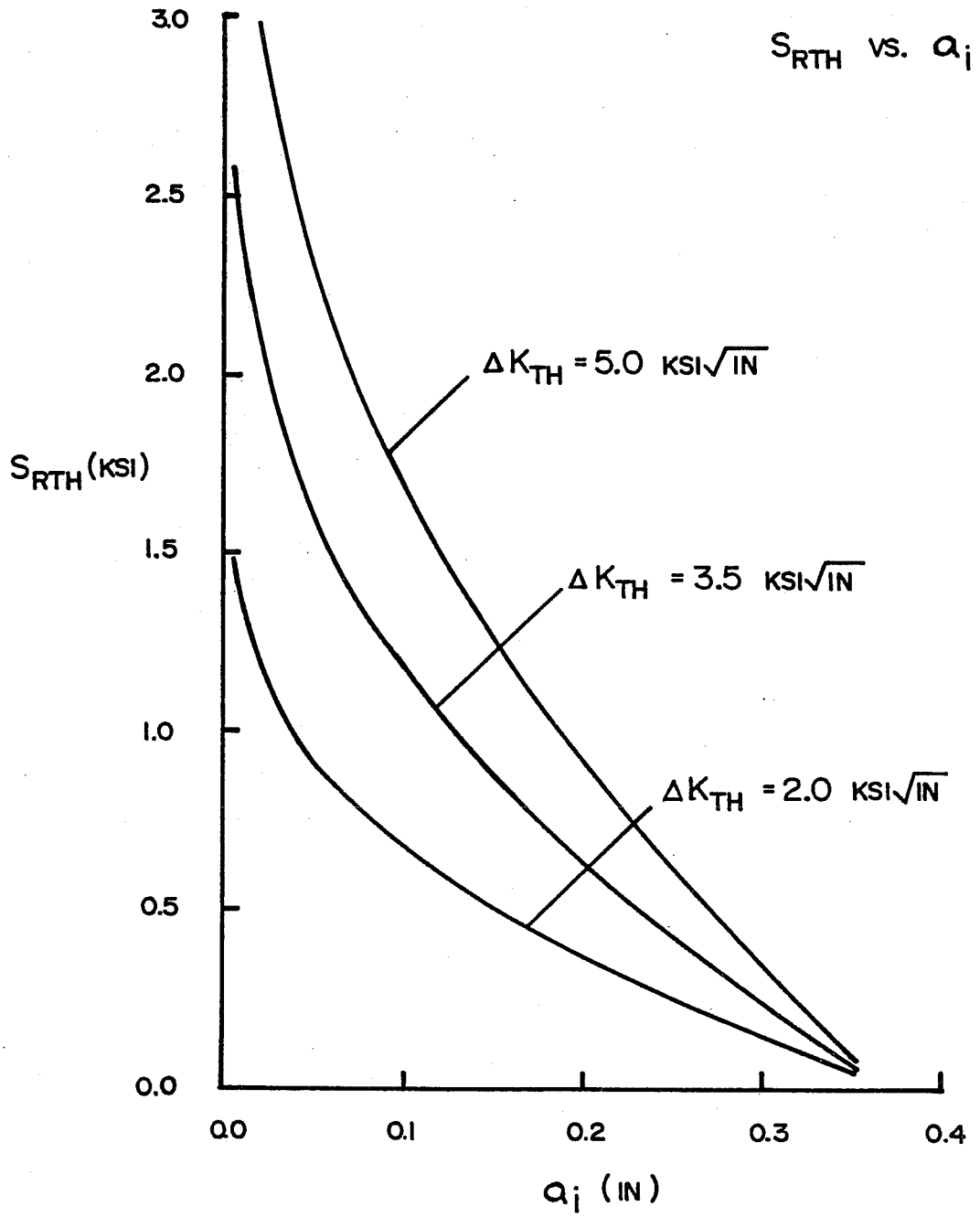

Fig. 4.11 S_{rth} vs. a_i —longitudinal-transverse stiffener intersection detail assuming bending occurs

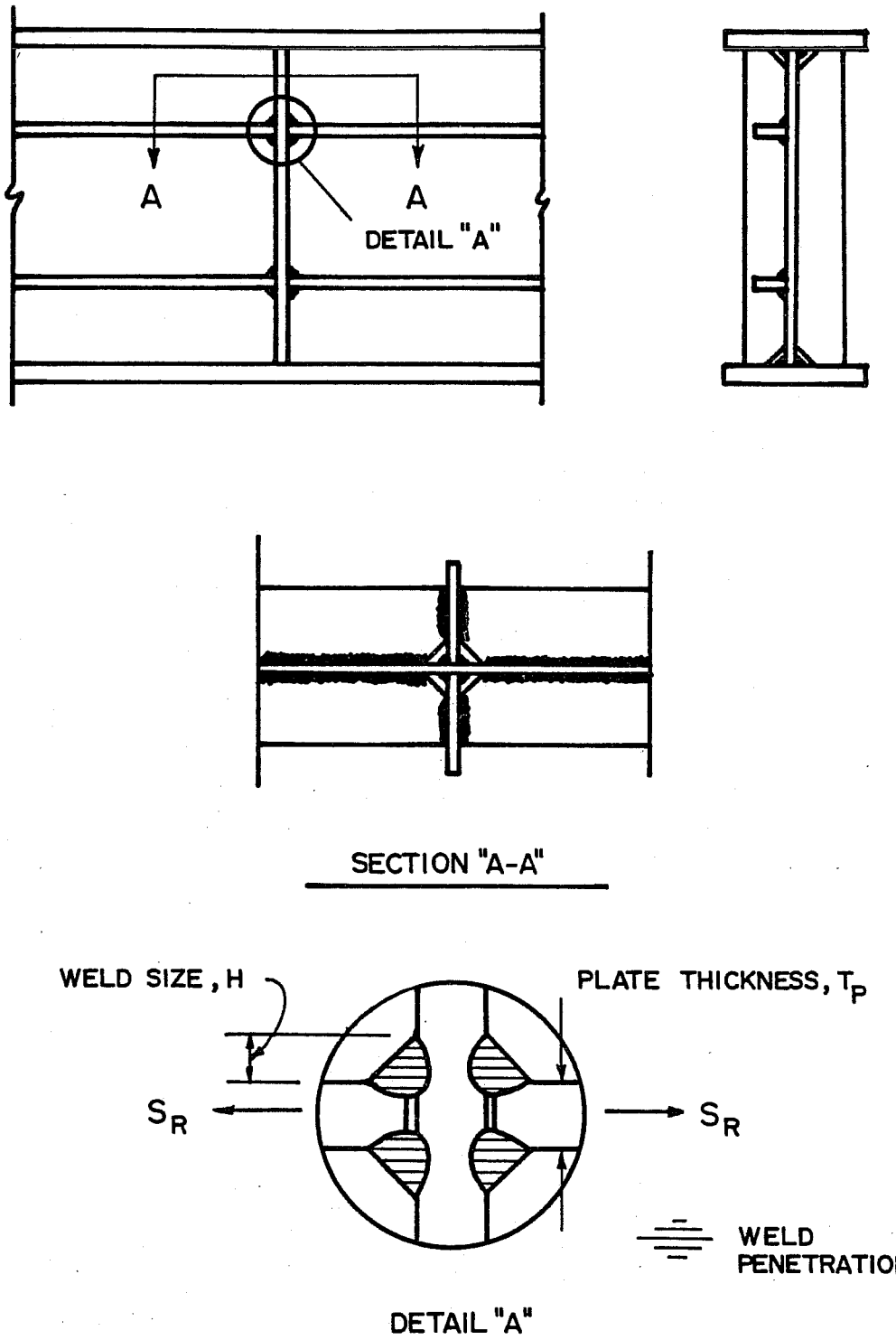

Fig. 4.12 Longitudinal-transverse stiffener intersection of the cope detail showing the resulting cruciform joint (detail "A")

the cope detail with regard to cracking through the girder web, a check of the cruciform joint is not performed. It should be noted, however, that this detail should be analyzed when designing a cope detail.

4.3.1 Life Estimate. Table 4.10 illustrates the calculations performed in determining the correction function, F(a), as a function of average crack size, a_{avg}.

The numerical integration of the crack growth rate expression was performed in Table 4.11 for $\Delta a = 0.01$ in. and $S_r = 2.0$ ksi. A stress range of 2.0 ksi for the cope detail was selected to facilitate comparison with previous calculations. For $a_i = 0.010$ in., a fatigue life of 63.3 million cycles was obtained. The mathematical equation which represents this detail is given by

$$\text{Log}N = 8.71 - 3.0\text{Log}S_r \qquad (4.11)$$

and is shown graphically in Fig. 4.13. Table 4.12 compares the fatigue lives obtained assuming each of the three initial crack sizes, a_i, of 0.005 in., 0.010 in., and 0.020 in. The S-N relationships for $a_i = 0.005$ in. and $a_i = 0.020$ in. are also plotted in Fig. 4.13.

Table 4.13 lists values of S_{rth} as a function of a_i for values of ΔK_{th} equal to 2.0, 3.5, and 5.0 ksi $\sqrt{\text{in.}}$ The family of three S_{rth} vs. a_i curves which these values represent is plotted in Fig. 4.14. S_{rth} may be obtained for any combination of a_i and ΔK_{th}. For the initial flaw sizes of 0.005 in., 0.010 in., and 0.020 in., and assuming $\Delta K_{th} =$ 2.0 ksi $\sqrt{\text{in.}}$, values of 3.8, 3.3, and 2.9 ksi were obtained, respectively, for S_{rth}. This is shown on the S-N plot of Fig. 4.13.

TABLE 4.10 CALCULATION OF F(a) FOR THE COPE DETAIL

$F_e = 0.79$ $F_s = 1.05$ $F(a) = F_e F_s F_w F_g$

a (in.)	a/t	F_w	F_g	F(a)
0.0075	0.020	1.00	4.47	3.71
0.015	0.040	1.00	3.75	3.11
0.025	0.053	1.00	3.29	2.73
0.035	0.093	1.01	3.02	2.53
0.045	0.120	1.01	2.85	2.39
0.055	0.147	1.01	2.72	2.28
0.065	0.173	1.02	2.56	2.17
0.075	0.200	1.03	2.52	2.15
0.085	0.227	1.03	2.46	2.10
0.095	0.253	1.04	2.41	2.08
0.105	0.280	1.05	2.36	2.06
0.115	0.307	1.06	2.31	2.03
0.125	0.333	1.07	2.28	2.02
0.135	0.360	1.09	2.25	2.03
0.145	0.387	1.10	2.21	2.02
0.155	0.413	1.12	2.17	2.02
0.165	0.440	1.14	2.13	2.01
0.175	0.467	1.16	2.09	2.01
0.185	0.493	1.18	2.07	2.03
0.195	0.520	1.21	2.05	2.06
0.205	0.547	1.24	2.03	2.09
0.215	0.573	1.27	2.00	2.11
0.225	0.600	1.30	1.97	2.12
0.235	0.627	1.34	1.94	2.16
0.245	0.653	1.39	1.92	2.21

TABLE 4.10 (Cont.)

a (in.)	a/t	F_w	F_g	F(a)
0.255	0.680	1.44	1.90	2.27
0.265	0.707	1.50	1.87	2.33
0.275	0.733	1.57	1.85	2.41
0.285	0.760	1.65	1.84	2.52
0.295	0.787	1.75	1.81	2.63
0.305	0.813	1.86	1.79	2.76
0.315	0.840	2.01	1.77	2.95
0.325	0.867	2.20	1.74	3.18
0.335	0.893	2.44	1.71	3.46
0.345	0.920	2.82	1.68	3.93
0.355	0.947	3.47	1.65	4.75
0.365	0.973	4.89	1.60	6.49

TABLE 4.11 CALCULATION OF FATIGUE LIFE FOR THE COPE DETAIL, S_r = 2.0 KSI

$$\Delta N = \frac{\Delta a}{\left[3.6 \times 10^{-10}\right]\left[F(a)S_r\sqrt{\pi a_{avg}}\right]^3}$$

S_r = 2.0 ksi Δa = 0.01 in.

a_o (in.)	a_f (in.)	a_{avg} (in.)	F(a)	ΔK (ksi$\sqrt{in.}$)	ΔN (cycles x 10^5)	ΣN (cycles x 10^5)
0.005	0.01	0.0075	3.71	1.14	94.0	94.0
0.01	0.02	0.015	3.11	1.35	112.8	207.0
0.02	0.03	0.025	2.73	1.53	77.5	284.0
0.03	0.04	0.035	2.53	1.81	46.8	331.0
0.04	0.05	0.045	2.39	1.80	47.8	379.0
0.05	0.06	0.055	2.28	1.90	40.8	420.0
0.06	0.07	0.065	2.17	1.96	36.8	456.0
0.07	0.08	0.075	2.15	2.09	30.5	487.0
0.08	0.09	0.085	2.10	2.17	27.2	514.0
0.09	0.10	0.095	2.08	2.27	23.7	538.0
0.10	0.11	0.105	2.06	2.37	21.0	559.0
0.11	0.12	0.115	2.03	2.44	19.1	578.0
0.12	0.13	0.125	2.02	2.53	17.1	595.0
0.13	0.14	0.135	2.03	2.64	15.0	610.0
0.14	0.15	0.145	2.02	2.73	13.7	624.0
0.15	0.16	0.155	2.02	2.82	12.4	636.0
0.16	0.17	0.165	2.01	2.91	11.3	648.0
0.17	0.18	0.175	2.01	2.98	10.5	658.0
0.18	0.19	0.185	2.03	3.10	9.37	667.0

TABLE 4.11 (Cont.)

a_o (in.)	a_f (in.)	a_{avg} (in.)	F(a)	ΔK (ksi$\sqrt{in.}$)	ΔN (cycles $\times 10^5$)	ΣN (cycles $\times 10^5$)
0.19	0.20	0.195	2.06	3.22	8.28	675.0
0.20	0.21	0.205	2.09	3.35	7.36	683.0
0.21	0.22	0.215	2.11	3.47	6.66	689.0
0.22	0.23	0.225	2.12	3.56	6.13	695.0
0.23	0.24	0.235	2.16	3.71	5.43	701.0
0.24	0.25	0.245	2.21	3.88	4.76	706.0
0.25	0.26	0.255	2.27	4.06	4.14	710.0
0.26	0.27	0.265	2.33	4.25	3.61	713.0
0.27	0.28	0.275	2.41	4.48	3.09	716.0
0.28	0.29	0.285	2.52	4.77	2.56	719.0
0.29	0.30	0.295	2.63	5.06	2.14	721.0
0.30	0.31	0.305	2.76	5.40	1.76	723.0
0.31	0.32	0.315	2.95	5.87	1.37	724.0
0.32	0.33	0.325	3.18	6.43	1.05	725.0
0.33	0.34	0.335	3.46	7.10	0.78	726.0
0.34	0.35	0.345	3.93	8.18	0.51	727.0
0.35	0.36	0.355	4.75	10.00	0.28	727.0
0.36	0.37	0.365	6.49	13.90	0.10	727.0

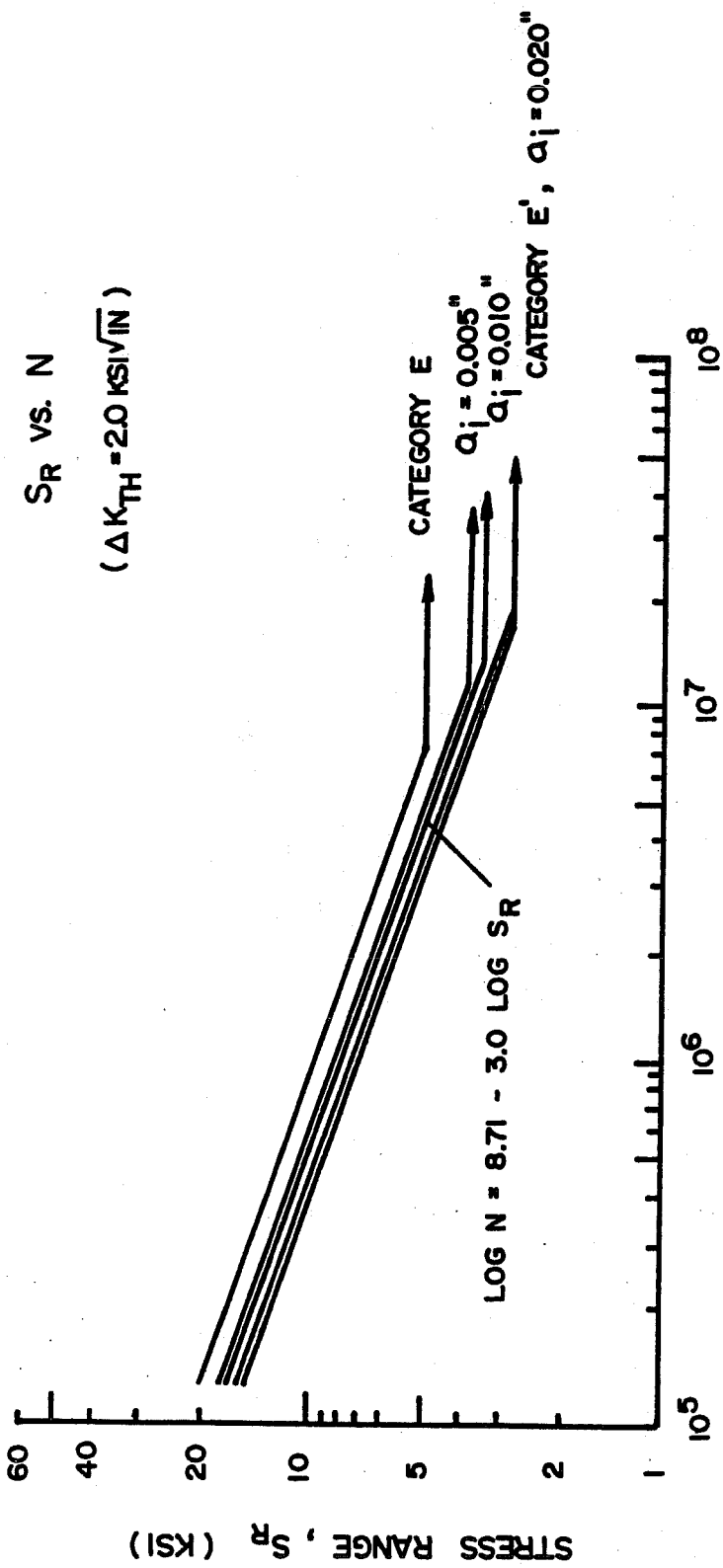

Fig. 4.13 S-N relationship for the cope detail

TABLE 4.12 VARIATION OF FATIGUE LIFE, N, WITH INITIAL CRACK SIZE, a_i, FOR S_r = 2.0 KSI, FOR THE COPE DETAIL

S_r = 2.0 ksi

a_i (in.)	N (cycles x 10^6)
0.005	72.7
0.010	63.3
0.020	52.0

TABLE 4.13 VALUES OF STRESS RANGE BELOW WHICH NO FATIGUE PROPAGATION WILL OCCUR--COPE DETAIL

$$S_{rth} = \Delta K_{th}/F(a)\sqrt{\pi a_i}$$

a_i (in.)	F(a)	ΔK_{th} (ksi$\sqrt{\text{in.}}$)		
		2.0	3.5	5.0
		S_{rth} (ksi)		
0.0075	3.71	3.51	6.15	8.78
0.015	3.11	2.96	5.18	7.41
0.035	2.53	2.38	4.17	5.96
0.055	2.28	2.11	3.69	5.28
0.075	2.15	1.92	3.35	4.79
0.095	2.08	1.76	3.08	4.40
0.115	2.03	1.64	2.89	4.10
0.135	2.03	1.51	2.65	3.78
0.155	2.02	1.42	2.48	3.55
0.175	2.01	1.34	2.35	3.35
0.195	2.06	1.24	2.17	3.10
0.235	2.16	1.08	1.89	2.69
0.275	2.41	0.89	1.56	2.23
0.315	2.95	0.68	1.19	1.70
0.355	4.75	0.40	0.70	1.00

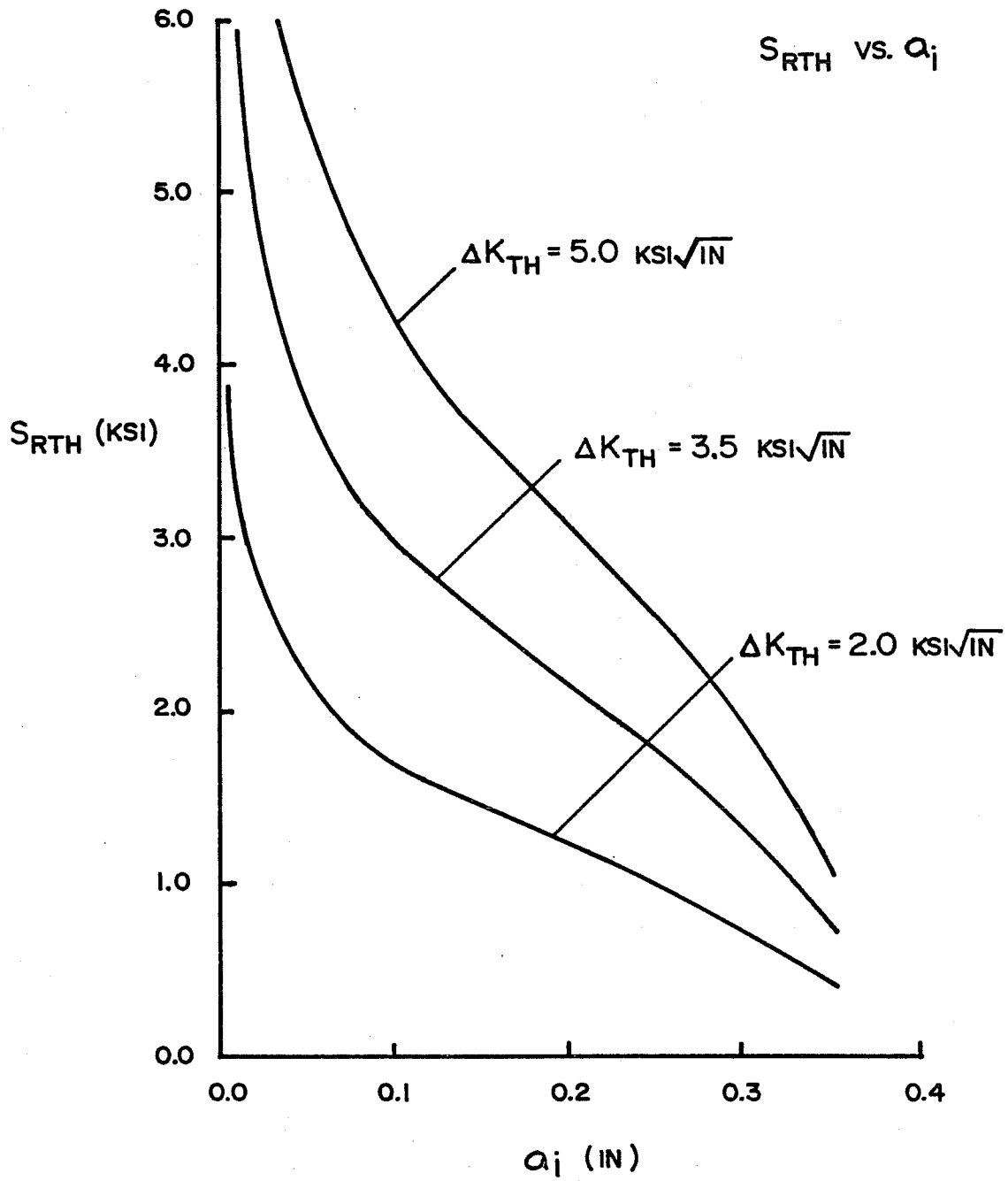

Fig. 4.14 S_{rth} vs. a_i—cope detail

Figure 4.13 also compares the S-N relationship for the cope detail to those of the AASHTO fatigue categories E and E′. The fatigue performance of the cope detail is slightly better than that of a Category E′ detail, but worse than a Category E detail. This poor performance may be due to the cope geometry used in the study. The author believes that if a smaller cope were used, fatigue performance may be enhanced.

4.4 Detail Comparisons

Figure 4.15 compares the S-N relationships for the longitudinal-transverse stiffener intersection detail and the cope detail assuming a_i = 0.010 in. and ΔK_{th} = 2.0 ksi $\sqrt{in.}$ S-N plots which describe AASHTO category E and E′ details are also shown for reference purposes.

A significant variation in S-N relationships seems to be present for the existing detail depending on whether or not the cracked plate is assumed to bend. The back free surface correction factor, F_w, is similar at small crack lengths assuming bending or assuming no bending. Since most useable fatigue life is expended at small crack lengths, it was originally expected that little difference in fatigue life would result. However, since the stress gradient correction factor, F_g, is so large, numerical integration of the crack growth rate expression indicates that significant life is obtained for larger crack lengths. At these crack lengths, the value of F_w becomes very large if bending is assumed to occur, and a significant decrease in fatigue life results.

In comparing the existing detail to the cope detail, a large difference is found in the values of threshold stress range, S_{rth}. In the case of the existing detail, values of S_{rth} are less than the observed live load stress range of 2.0 ksi. This implies that the structural detail can be damaged by the loads

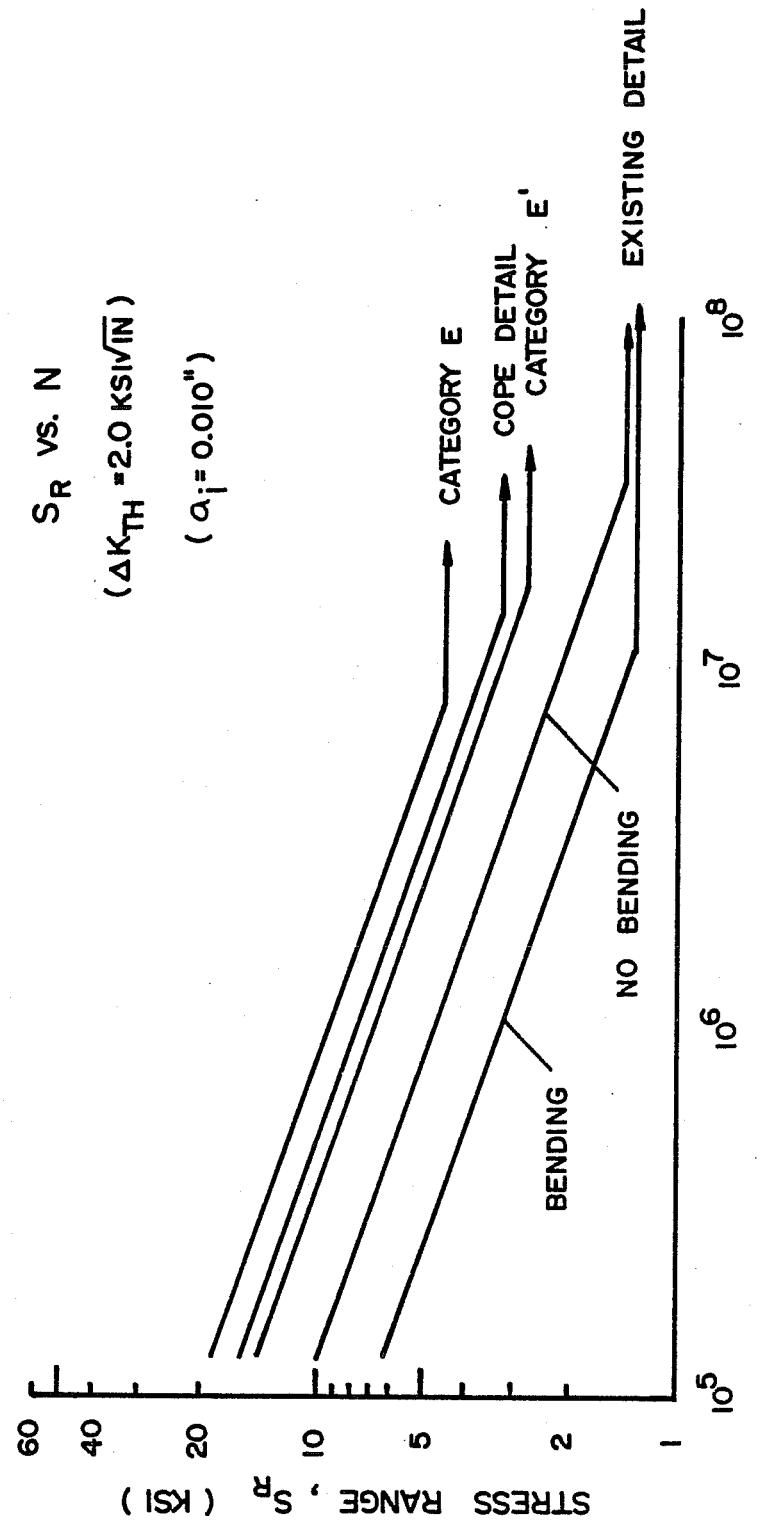

Fig. 4.15 Comparison of S-N relationships for the longitudinal-transverse stiffener intersection detail and the cope detail

currently being placed on the bridge structure. However, the S-N relationship for the cope detail indicates a value of S_{rth} of about 3.5 ksi, greater than the observed value of 2.0 ksi. Therefore, the cope detail should be considered as a possible means of retrofitting the existing detail.

4.5 Sources of Error

Although the fatigue life relationships for the existing detail and the cope detail seem to be exact and well-defined, they are not. Several assumptions were made in arriving at the results, which if made differently, could change the picture considerably. The assumptions enumerated below are discussed in what is believed to be an order of increasing significance.

It was assumed that useable fatigue life could be obtained for crack lengths approaching the girder web thickness in size. This may not be true if the fracture toughness of the A36 steel used in the bridge structure is very low. It seems, however, that fatigue life would only be affected slightly, since significant gains in life are not realized at large crack lengths.

The fracture mechanics approach to the fatigue problem conservatively ignores the existence of any initiation life which may actually be present. A crack must have a leading edge which is very sharp before crack growth may occur. Many cycles may be required to sharpen the crack front, and a resulting increase in estimated fatigue life could be realized.

Application of Albrecht's Green's Function in determining F_g required that the crack path be known. The path was assumed to extend from the longitudinal stiffener-to-web weld toe through the thickness of the girder web. Actual tests [15] have shown that during early stages of crack growth, slight deviations

from the expected crack path (a straight line) occur. If the exact crack path were used, F_g would be expected to increase slightly, causing a corresponding decrease in fatigue life.

The previously discussed problem of crack coalescence should be mentioned again. If such a phenomenon occurs, the a/c ratio would become very small. This results in an increase in the front free surface correction factor, F_s, as well as the crack shape correction factor, F_e. A small decrease in fatigue life could be expected.

The effect on fatigue life of the bending assumption made in calculating the back free surface correction factor, F_w, has been shown. In the case of the structural detail studied, a significant difference in fatigue life was found depending on whether or not the cracked plate was permitted to bend.

In the finite element analyses performed to characterize the stress gradient correction factor, F_g, fillet weld angles were assumed to be 45^o. Actually, the weld angle at the toe is often greater than 45^o, especially if the welds are made by hand. Gurney [8] found that the stress concentration at the weld toe increases with the weld angle, thereby increasing F_g local to the weld toe. This results in a loss of fatigue life during early stages of crack growth.

The value assumed for the initial crack size, a_i, in computing fatigue life has been shown to be significant. Since a sizeable portion of life is expended at small crack lengths, the choice of a_i can change the estimated fatigue life appreciably.

In comparing calculated values of threshold stress range, S_{rth}, to live load stress ranges found in field tests of the bridge structure, a value of $S_r = 2.0$ ksi was used for the

measured value. This value is probably high for several reasons. First, the test truck used weighed 55 kips, probably heavier than many trucks which use the structure. Also, a short dump truck was used to test, since computer analyses indicated that longer tractor-trailers of the same weight produced less severe conditions. Finally, the test truck was positioned on the bridge directly over one of the twin girders of the structure. This results in a maximum loading condition in one girder, with little load being transferred to the other girder. If the truck traveled in a different lane, a better load distribution between girders would be expected, and the severe condition created for testing purposes would not occur.

Perhaps the most important assumption made regarding the existing detail was the selection of the threshold range of stress intensity, ΔK_{th}, of 2.0 ksi $\sqrt{in.}$ This results in a lower bound value of S_{rth} which is itself affected by the initial crack size, a_i, and the weld angle. For ΔK_{th} = 2.0 ksi $\sqrt{in.}$, calculated values of threshold stress range, S_{rth}, fell below the observed live load stress range of 2.0 ksi. This implies that damage to the structural detail can occur. On the other hand, if a value of ΔK_{th} equal to 3.5 or 5.0 ksi $\sqrt{in.}$ were assumed, calculated values of S_{rth} would have been greater than 2.0 ksi. This would imply that the detail could be expected to perform under an infinite number of load cycles.

CHAPTER 5

SUMMARY, CONCLUSIONS, AND RECOMMENDED RESEARCH

(1) Stress concentration factors have been determined for the longitudinal stiffener-to-web weld toe of the longitudinal-transverse stiffener intersection detail using the finite element technique. The stress concentration at the weld toe increased as the size of the finite element mesh decreased. By reducing the mesh size local to the weld toe to a value less than the expected initial crack size, reasonable accuracy was obtained for the stress gradient correction at small crack lengths.

(2) The influence of detail geometry on the stress concentration at the longitudinal stiffener-to-web weld toe was investigated. Increasing the longitudinal stiffener width and/or thickness resulted in a more severe stress concentration at the weld toe. Increasing the girder web thickness decreased the stress concentration. The size of the gap between the longitudinal stiffener end and the transverse stiffener was found to affect the stress concentration. When the gap size was increased from 1/2 in. to 2 in., a drop in stress concentration at the weld toe of approximately 65 percent was realized.

(3) Using the results of finite element analyses performed on the longitudinal-transverse stiffener intersection detail, an experimental test specimen was proposed. A 1/4 scale model of the girder containing the existing detail was selected. By loading the girder at the one-third points,

constant moment in the region of the longitudinal-transverse stiffener intersection can be achieved. Actual conditions should be reproduced with reasonable accuracy using the scale model test specimen.

(4) Analytical solutions were obtained for F(a), the parameter which corrects the stress intensity factor for detail geometry. The stress gradient correction factor, F_g, was evaluated using the Green's Function approach proposed by Albrecht [10]. Values for the crack shape correction factor, F_e, the front free surface correction factor, F_s, and the back free surface correction factor, F_w, were determined in a manner similar to that used by Zettlemoyer [15].

(5) Fracture mechanics principles were used to estimate the fatigue life of the longitudinal-transverse stiffener intersection detail. The effect of changing the initial crack length, a_i, on the fatigue life estimate was demonstrated. In addition, relationships between initial crack length and threshold stress range, S_{rth}, were derived for values of ΔK_{th} equal to 2.0, 3.5, and 5.0 ksi $\sqrt{in.}$ Values for S_{rth} were found to be significantly affected by the value of ΔK_{th} assumed. For ΔK_{th} equal to 2.0 ksi $\sqrt{in.}$, S_{rth} fell below the measured live load stress range of 2.0 ksi, indicating that the existing detail could be damaged by cyclic loading. If a value of 3.5 ksi $\sqrt{in.}$ or greater was assumed, S_{rth} fell above 2.0 ksi, indicating no damage to the detail under cyclic loading. S-N relationships were shown for the existing detail, and were compared to current AASHTO Bridge Specifications. The longitudinal-transverse stiffener intersection detail fell below Category E′, the worst AASHTO fatigue category.

(6) Modification of the existing detail with a cope detail was investigated as a possible means of retrofitting the longitudinal-transverse stiffener intersection detail. The cope detail showed a considerable improvement in fatigue life over that of the existing detail. In comparing the S-N relationship established for the cope detail to AASHTO specifications, it was found that the detail fell in between Categories E and E′. Although the cope detail is a significant improvement over the existing detail, its use as a design detail is questionable. An equivalent improvement in fatigue life would likely result if the longitudinal stiffener were simply terminated at a greater distance from the transverse stiffener.

(7) The major recommendation of this study is to perform laboratory tests on the longitudinal-transverse stiffener intersection detail to establish a workable data base. Comparison of experimental data with the analytical results of this study should be made before making any final recommendations.

A P P E N D I X A

TEXGAP INPUT STRUCTURE

A.1 Introduction

The following pages describe the manner in which data are generated for processing by the TEXGAP series of computer programs. With the exception of the geometric variations, each problem analyzed as a part of this study is presented.

Generally, the preparation of each problem consists of several step-by-step operations. First, the problem is defined by establishing the coordinates of all locations of nodal points. This is conveniently done by drawing a picture of the model and dividing it into the desired number of finite elements. A convenient point, usually one corner of the model, is chosen as the origin of the global coordinate system. The nodal lines are then numbered, starting at the origin. Numerical dimensions are assigned to each nodel line, depending on the geometry of the desired grid, with the origin as reference. All nodal points may then be generated. Next, the elements which constitute the finite element model must be defined. Elements are defined based on the nodal point locations, but all nodal points will generally not be used to define elements. Only those points which lie within the boundaries of the model will be used. Lastly, boundary conditions are defined and the instructions to solve the problem are given.

The intent of the information presented above is to provide a general approach to the use of TEXGAP to solve finite element problems. Users manuals have been written for TEXGAP-3D and TEXGAP-2D and should be consulted to obtain details regarding input structure.

A.2 TEXGAP-3D

TEXGAP-3D is the three-dimensional finite element code. Examples of its use include the analysis of the full-scale model of the existing detail, the 1/4 symmetric model of the existing detail, and the 1/4 symmetric model of the cope detail.

A.2.1 Full-Scale Model. The drawings used to aid in the development of the input data are shown in Fig. A.1 and Fig. A.2. A complete listing of the input data is given in Fig. A.3.

A.2.2 Existing Detail 1/4 Symmetric Model. Figures A.4 and A.5 describe the grid definition for the model. The area local to the longitudinal stiffener end which was rezoned is defined in Fig. A.6. Figure A.7 presents a listing of the input data.

A.2.3 Cope Detail 1/4 Symmetric Model. The grid definition in the x-y plane for the cope detail model is the same as that for the existing detail model shown in Fig. A.4. Figure A.8 defines the grid in the x-z plane. The area local to the longitudinal stiffener end which was rezoned is defined in Fig. A.9. A listing of the input data used to analyze the cope detail 1/4 symmetric model is provided in Fig. A.10.

A.3 TEXGAP-2D

TEXGAP-2D is the two-dimensional finite element code. Examples of its use include analysis of the existing detail fine mesh and ultra-fine mesh, and the cope detail fine mesh and ultra-fine mesh.

A.3.1 Existing Detail Fine Mesh. The grid definition of the fine mesh is illustrated in Fig. A.11. Figure A.12 lists the input data used to solve the existing detail fine mesh.

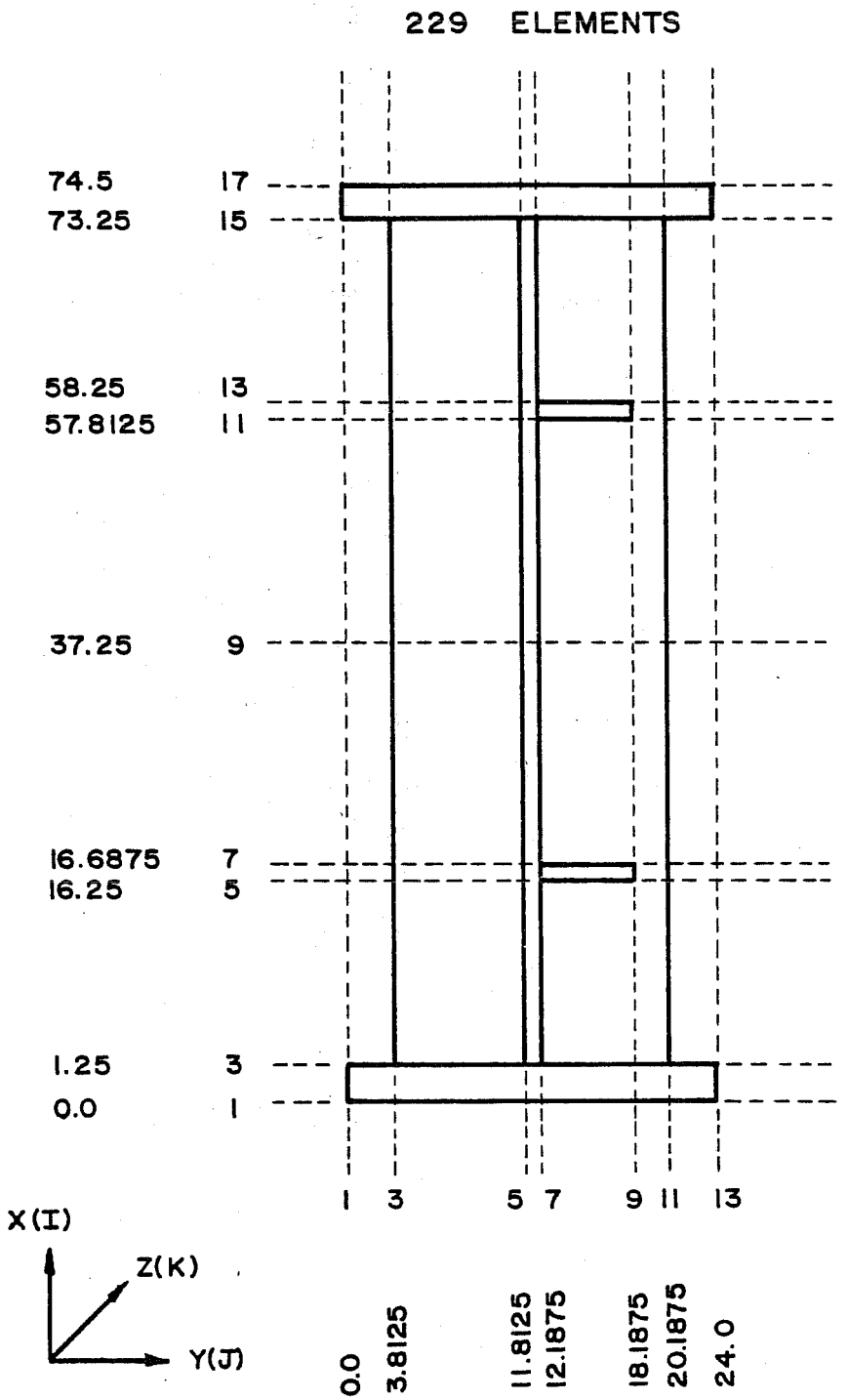

Fig. A.1 Full-scale finite element model grid definition in the x-y plane

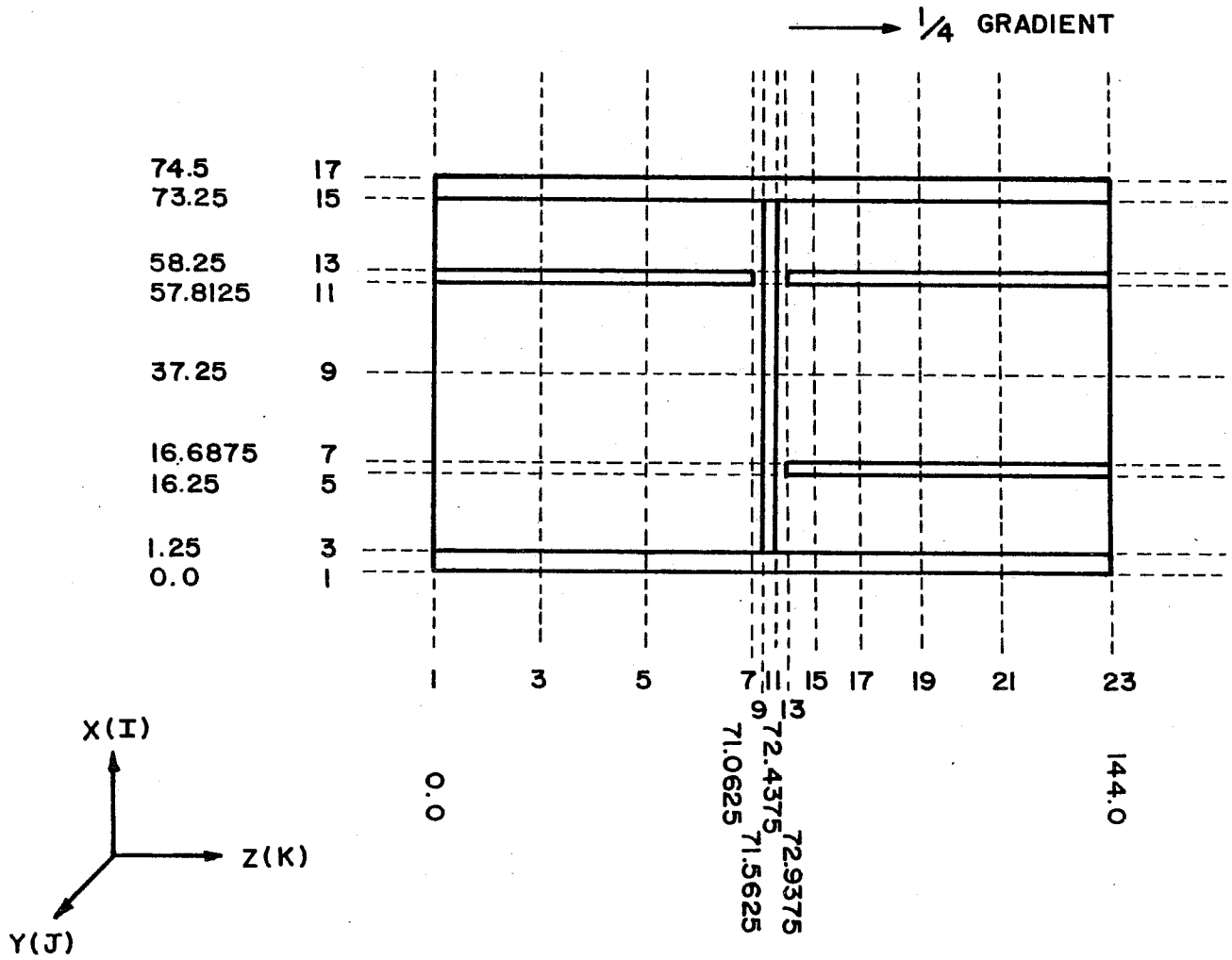

Fig. A.2 Full-scale finite element model grid definition in the x-z plane

```
$     STIFFENER INTERSECTION
SETUP,4,,17,13
ISO,STEEL,1,29E03,0.30
END,MATERIALS
BLOCK,1,1,1,1,3,3,7
0,0,0,1.25,0,0,1.25,3.8125,0,0,3.8125,0/
0,0,71.0625,1.25,0,71.0625,1.25,3.8125,71.0625,0,3.8125,71.0625
BLOCK,1,1,1,7,3,3,9
0,0,71.0625,1,25,0,71.0625,1.25,3.8125,71.0625,0,3.8125,71.0625/
0,0,71.5625,1.25,0,71.5625,1.25,3.8125,71.5625,0,3.8125,71.5625
BLOCK,1,1,1,9,3,3,11
0,0,71.5625,1,25,0,71.5625,1.25,3,8125,71.5625,0,3.8125,71.5625/
0,0,72.4375,1.25,0,72.4375,1.25,3.8125,72.4375,0,3.8125,72.4375
BLOCK,1,1,1,11,3,3,13
0,0,72.4375,1,25,0,72.4375,1.25,3,8125,72.4375,0,3.8125,72.4375/
0,0,72.9375,1.25,0,72.9375,1.25,3.8125,72.9375,0,3.8125,72.9375
BLOCK,1,1,1,13,3,3,23,9,0.25,10,0,25,11,0.25,12,0.25
0,0,72.9375,1.25,0,72.9375,1.25,3.8125,72.9375,0,3.8125,72.9375/
0,0,144.0,1.25,0,144.0,1.25,3.8125,144.0,0,3.8125,144.0
BLOCK,1,1,3,1,3,5,7
0,3,1825,0,1.25,3.8125,0,1.25,11.8125,0,0,11.8125,0/
0,3.8125,71.0625,1.25,3.8125,71.0625,1.25,11.8125,71.0625,0,11.8125,71.0625
BLOCK,1,1,3,7,3,5,9
0,3.8125,71.0625,1.25,3.8125,71,0625,1.25,11.8125,71.0625,0,11,8125,71.0625/
0,3.8125,71.5625,1.25,3.8125,71.5625,1.25,11.8125,71.5625,0,11.8125,71.5625
BLOCK,1,1,3,9,3,5,11
0,3.8125,71.5625,1.25,3.8125,71,5625,1.25,11.8125,71.5625,0,11,8125,71.5625/
0,3.8125,72.4375,1.25,3.8125,72.4375,1.25,11.8125,72.4375,0,11.8125,72.4375
BLOCK,1,1,3,11,3,5,13
0,3.8125,72.4375,1.25,3.8125,72.4375,1.25,11.8125,72.4375,0,11,8125,72.4375/
0,3.8125,72.9375,1.25,3.8125,72.9375,1.25,11.8125,72.9375,0,11.8125,72.9375
BLOCK,1,1,3,13,3,5,23,9,0.25,10,0.25,11,0.25,12,0.25
0,3.8125,72.9375,1.25,3.8125,72.9375,1.25,11.8125,72.9375,0,11.8125,72.9375/
0,3.8125,144.0,1.25,3.8125,144.0,1.25,11.8125,144.0,0,0,11.8125,144.0
BLOCK,1,1,5,1,3,7,7
0,11.8125,0,1.25,11.8125,0,1.25,12.1875,0,0,12.1875,0/
0,11.8125,71.0625,1.25,11.8125,71.0625,1.25,12.1875,71.0625,0,12.1875,71.0625
BLOCK,1,1,5,7,3,7,9
0,11.8125,71.0625,1.25,11,8125,71.0625,1.25,12.1875,71.0625,0,12,1875,71.0625/
0,11.8125,71.5625,1.25,11.8125,71.5625,1.25,12.1875,71.5625,0,12.1875,71.5625
BLOCK,1,1,5,9,3,7,11
0,11.8125,71.5625,1.25,11.8125,71,5625,1.25,12.1875,71.5625,0,12,1875,71.5625/
0,11.8125,72.4375,1.25,11.8125,72.4375,1.25,12.1875,72.4375,0,12.1875,72.4375
BLOCK,1,1,5,11,3,7,13
0,11.8125,72.4375,1.25,11,8125,72,4375,1.25,12.1875,72.4375,0,12,1875,72.4375/
0,11.8125,72.9375,1.25,11.8125,72.9375,1.25,12.1875,72.9375,0,12.1875,72.9375
BLOCK,1,1,5,13,3,7,23,9,0.25,10,0.25,11,0.25,12,0.25
0,11.8125,72.9375,1.25,11.8125,72.9375,1.25,12.1875,72.9375,0,12,1875,72.9375/
0,11.8125,144.0,1.25,11.8125,144.0,1.25,12.1875,144.0,0,0,12.1875,144.0
BLOCK,1,1,7,1,3,9,7
0,12.1875,0,1.25,12.1875,0,1.25,18.1875,0,0,18.1875,0/
0,12.1875,71.0625,1.25,12.1875,71.0625,1.25,18.1875,71.0625,0,18.1875,71.0625
BLOCK,1,1,7,7,3,9,9
0,12.1875,71.0625,1.25,12,1875,71,0625,1.25,18.1875,71.0625,0,18,1875,71.0625/
0,12.1875,71.5625,1.25,12.1875,71.5625,1.25,18.1875,71.5625,0,18.1875,71.5625
BLOCK,1,1,7,9,3,9,11
0,12.1875,71.5625,1.25,12,1875,71,5675,1.25,18.1875,71.5625,0,18,1875,71.5625/
0,12.1875,72.4375,1.25,12.1875,72.4375,1.25,18.1875,72.4375,0,18.1875,72.4375
BLOCK,1,1,7,11,3,9,13
0,12.1875,72.4375,1.25,12,1875,72,4375,1.25,18.1875,72.4375,0,18,1875,72.4375/
0,12.1875,72.9375,1.25,12.1875,72.9375,1.25,18.1875,72.9375,0,18.1875,72.9375
```

Fig. A.3 TEXGAP-3D input listing for full-scale model

```
BLOCK,1,1,7,13,3,9,23,9,0.25,10,0.25,11,0.25,12,0.25
0,12.1875,72.9375,1.25,12.1875,72.9375,1.25,18.1875,72.9375,0,18.1875,72.9375/
0,12.1875,144.0,1.25,12.1875,144.0,1.25,18.1875,144.0,0,18.1875,144.0
BLOCK,1,1,9,1,3,11,7
0,18.1875,0,1.25,18.1875,0,1.25,20.1875,0,0,20.1875,0/
0,18.1875,71.0625,1.25,18.1875,71.0625,1.25,20.1875,71.0625,0,20.1875,71.0625
BLOCK,1,1,9,7,3,11,9
0,18.1875,71.0625,1.25,18.1875,71.0625,1.25,20.1875,71.0625,0,20.1875,71.0625/
0,18.1875,71.5625,1.25,18.1875,71.5625,1.25,20.1875,71.5625,0,20.1875,71.5625
BLOCK,1,1,9,9,3,11,11
0,18.1875,71.5625,1.25,18.1875,71.5625,1.25,20.1875,71.5625,0,20.1875,71.5625/
0,18.1875,73.4375,1.25,18.1875,72.4375,1.25,20.1875,72.4375,0,20.1875,72.4375
BLOCK,1,1,9,11,3,11,13
0,18.1875,72.4375,1.25,18.1875,72.4375,1.25,20.1875,72.4375,0,20.1875,72.4375/
0,18.1875,72.9375,1.25,18.1875,72.9375,1.25,20.1875,72.9375,0,20.1875,72.9375
BLOCK,1,1,9,13,3,11,23,9,0.25,10,0.25,11,0.25,12,0.25
0,18.1875,72.9375,1.25,18.1875,72.9375,1.25,20.1875,72.9375,0,20.1875,72.9375/
0,18.1875,144.0,1.25,18.1875,144.0,1.25,20.1875,144.0,0,20.1875,144.0
BLOCK,1,1,11,1,3,13,7
0,20.1875,0,1.25,20.1875,0,1.25,24.0,0,0,0,24.0,0/
0,20.1875,71.0625,1.25,20.1875,71.0625,1.25,24.0,71.0625,0,24.0,71.0625
BLOCK,1,1,11,7,3,13,9
0,20.1875,71.0625,1.25,20.1875,71.0625,1.25,24.0,71.0625,0,24.0,71.0625/
0,20.1875,71.5625,1.25,20.1875,71.5625,1.25,24.0,71.5625,0,24.0,71.5625
BLOCK,1,1,11,9,3,13,11
0,20.1875,71.5625,1.25,20.1875,71.5625,1.25,24.0,71.5625,0,24.0,71.5625/
0,20.1875,72.4375,1.25,20.1875,72.4375,1.25,24.0,72.4375,0,24.0,72.4375
BLOCK,1,1,11,11,3,13,13
0,20.1875,72.4375,1.25,20.1875,72.4375,1.25,24.0,72.4375,0,24.0,72.4375/
0,20.1875,72.9375,1.25,20.1875,72.9375,1.25,24.0,72.9375,0,24.0,72.9375
BLOCK,1,1,11,13,3,13,23,9,0.25,10,0.25,11,0.25,12,0.25
0,20.1875,72.9375,1.25,20.1875,72.9375,1.25,24.0,72.9375,0,24.0,72.9375/
0,20.1875,144.0,1.25,20.1875,144.0,1.25,24.0,144.0,0,24.0,144.0
BLOCK,1,3,3,9,5,5,11
1.25,3.8125,71.5625,16.25,3.8125,71.5625,16.25,11.8125,71.5625/
1.25,11.8125,71.5625,1.25,3.8125,72.4375,16.25,3.8125,72.4375/
16.25,11.8125,72.4375,1.25,11.8125,72.4375
BLOCK,1,3,5,1,5,7,7
1.25,11.8125,0,16.25,11.8125,0,16.25,12.1875,0,1.25,12.1875,0/
1.25,11.8125,71.0625,16.25,11.8125,71.0625,16.25,12.1875,71.0625/
1.25,12.1875,71.0625
BLOCK,1,3,5,7,5,7,9
1.25,11.8125,71.0625,16.25,11.8125,71.0625,16.25,12.1875,71.0625/
1.25,12.1875,71.0625,1.25,11.8125,71.5625,16.25,11.8125,71.5625/
16.25,12.1875,71.5625,1.25,12.1875,71.5625
BLOCK,1,3,5,9,5,7,11
1.25,11.8125,71.5625,16.25,11.8125,71.5625,16.25,12.1875,71.5625/
1.25,12.1875,71.5625,1.25,11.8125,72.4375,16.25,11.8125,72.4375/
16.25,12.1875,72.4375,1.25,12.1875,72.4375
BLOCK,1,3,5,11,5,7,13
1.25,11.8125,72.4375,16.25,11.8125,72.4375,16.25,12.1875,72.4375/
1.25,12.1875,72.4375,1.25,11.8125,72.9375,16.25,11.8125,72.9375/
16.25,12.1875,72.9375,1.25,12.1875,72.9375
BLOCK,1,3,5,13,5,7,23,9,0.25,10,0.25,11,0.25,12,0.25
1.25,11.8125,72.9375,16.25,11.8125,72.9375,16.25,12.1875,72.9375/
1.25,12.1875,72.9375,1.25,11.8125,144.0,16.25,11.8125,144.0/
16.25,12.1875,144.0,1.25,12.1875,144.0
BLOCK,1,3,7,9,5,9,11
1.25,12.1875,71.5625,16.25,12.1875,71.5625,16.25,18.1875,71.5625/
1.25,18.1875,71.5625,1.25,12.1875,72.4375,16.25,12.1875,72.4375/
16.25,18.1875,72.4375,1.25,18.1875,72.4375
BLOCK,1,3,9,9,5,11,11
```

```
1.25,18.1875,71.5625,16.25,18.1875,71.5625,16.25,20.1875,71.5625/
1.25,20.1875,71.5625,1.25,18.1875,72.4375,16.25,18.1875,72.4375/
16.25,20.1875,72.4375,1.25,20.1875,72.4375
BLOCK,1,5,3,9,7,5,11
16.25,3.8125,71.5625,16.6875,3.8125,71.5625,16.6875,11.8125,71.5625/
16.25,11.8125,71.5625,16.25,3.8125,72.4375,16.6875,3.8125,72.4375/
16.6875,11.8125,72.4375,16.25,11.8125,72.4375
BLOCK,1,5,5,1,7,7,7
16.25,11.8125,0,16.6875,11.8125,0,16.6875,12.1875,0,16.25,12.1875,0/
16.25,11.8125,71.0625,16.6875,11.8125,71.0625,16.6875,12.1875,71.0625/
16.25,12.1875,71.0625
BLOCK,1,5,5,7,7,7,9
16.25,11.8125,71.0625,16.6875,11.8125,71.0625,16.6875,12.1875,71.0625/
16.25,12.1875,71.0625,16.25,11.8125,71.5625,16.6875,11.8125,71.5625/
16.6875,12.1875,71.5625,16.25,12.1875,71.5625
BLOCK,1,5,5,9,7,7,11
16.25,11.8125,71.5625,16.6875,11.8125,71.5625,16.6875,12.1875,71.5625/
16.25,12.1875,71.5625,16.25,11.8125,72.4375,16.6875,11.8125,72.4375/
16.6875,12.1875,72.4375,16.25,12.1875,72.4375
BLOCK,1,5,5,11,7,7,13
16.25,11.8125,72.4375,16.6875,11.8125,72.4375,16.6875,12.1875,72.4375/
16.25,12.1875,72.4375,16.25,11.8125,72.9375,16.6875,11.8125,72.9375/
16.6875,12.1875,72.9375,16.25,12.1875,72.9375
BLOCK,1,5,5,13,7,7,23,9,0,25,10,0.25,11,0.25,12,0.25
16.25,11.8125,72.9375,16.6875,11.8125,72.9375,16.6875,12.1875,72.9375/
16.25,12.1875,72.9375,16.25,11.8125,144.0,16.6875,11.8125,144.0/
16.6875,12.1875,144.0,16.25,12.1875,144.0
BLOCK,1,5,7,13,7,9,23,9,0,25,10,0.25,11,0.25,12,0.25
16.25,12.1875,72.9375,16.6875,12.1875,72.9375,16.6875,18.1875,72.9375/
16.25,18.1875,72.9375,16.25,12.1875,144.0,16.6875,12.1875,144.0/
16.6875,18.1875,144.0,16.25,18.1875,144.0
BLOCK,1,5,7,9,7,9,11
16.25,12.1875,71.5625,16.6875,12.1875,71.5625,16.6875,18.1875,71.5625/
16.25,18.1875,71.5625,16.25,12.1875,72.4375,16.6875,12.1875,72.4375/
16.6875,18.1875,72.4375,16.25,18.1875,72.4375
BLOCK,1,5,9,9,7,11,11
16.25,18.1875,71.5625,16.6875,18.1875,71.5625,16.6875,20.1875,71.5625/
16.25,20.1875,71.5625,16.25,18.1875,72.4375,16.6875,18.1875,72.4375/
16.6875,20.1875,72.4375,16.25,20.1875,72.4375
BLOCK,1,7,3,9,11,5,11
16.6875,3.8125,71.5625,57.8125,3.8125,71.5625,57.8125,11.8125,71.5625/
16.6875,11.8125,71.5625,16.6875,3.8125,72.4375,57.8125,3.8125,72.4375/
57.8125,11.8125,72.4375,16.6875,11.8125,72.4375
BLOCK,1,7,5,1,11,7,7
16.6875,11.8125,0,57.8125,11.8125,0,57.8125,12.1875,0,16.6875,12.1875,0/
16.6875,11.8125,71.0625,57.8125,11.8125,71.0625,57.8125,12.1875,71.0625/
16.6875,12.1875,71.0625
BLOCK,1,7,5,7,11,7,9
16.6875,11.8125,71.0625,57.8125,11.8125,71.0625,57.8125,12.1875,71.0625/
16.6875,12.1875,71.0625,16.6875,11.8125,71.5625,57.8125,11.8125,71.5625/
57.8125,12.1875,71.5625,16.6875,12.1875,71.5625
BLOCK,1,7,5,9,11,7,11
16.6875,11.8125,71.5625,57.8125,11.8125,71.5625,57.8125,12.1875,71.5625/
16.6875,12.1875,71.5625,16.6875,11.8125,72.4375,57.8125,11.8125,72.4375/
57.1825,12.1875,72.4375,16.6875,12.1875,72.4375
BLOCK,1,7,5,11,11,7,13
16.6875,11.8125,72.4375,57.8125,11.8125,72.4375,57.8125,12.1875,72.4375/
16.6875,12.1875,72.4375,16.6875,11.8125,72.9375,57.8125,11.8125,72.9375/
57.8125,12.1875,72.9375,16.6875,12.1875,72.9375
BLOCK,1,7,5,13,11,7,23,9,0.25,10,0.25,11,0.25,12,0.25
16.6875,11.8125,72.9375,57.8125,11.8125,72.9375,57.8125,12.1875,72.9375/
16.6875,12.1875,72.9375,16.6875,11.8125,144.0,57.8125,11.8125,144.0/
```

```
57.8125,12.1875,144.0,16.6875,12.1875,144.0
BLOCK,1,7,7,9,11,9,11
16.6875,12.1875,71.5625,57.8125,12.1875,71.5625,57.8125,18.1875,71.5625/
16.6875,18.1875,71.5625,16.6875,12.1875,72.4375,57.8125,12.1875,72.4375/
57.8125,18.1875,72.4375,16.6875,18.1875,72.4375
BLOCK,1,7,9,9,11,11,11
16.6875,18.1875,71.5625,57.8125,18.1875,71.5625,57.8125,20.1875,71.5625/
16.6875,20.1875,71.5625,16.6875,18.1875,72.4375,57.8125,18.1875,72.4375/
57.8125,20.1875,72.4375,16.6875,20.1875,72.4375
BLOCK,1,11,3,9,13,5,11
57.8125,3.8125,71.5625,58.25,3.8125,71.5625,58.25,11.8125,71.5625/
57.8125,11.8125,71.5625,57.8125,3.8125,72.4375,58.25,3.8125,72.4375/
58.25,11.8125,72.4375,57.8125,11.8125,72.4375
BLOCK,1,11,5,1,13,7,7
57.8125,11.8125,0,58.25,11.8125,0,58.25,12.1875,0,57.8125,12.1875,0/
57.8125,11.8125,71.0625,58.25,11.8125,71.0625,58.25,12.1875,71.0625/
57.8125,12.1875,71.0625
BLOCK,1,11,5,7,13,7,9
57.8125,11.8125,71.0625,58.25,11.8125,71.0625,58.25,12.1875,71.0625/
57.8125,12.1875,71.0625,57.8125,11.8125,71.5625,58.25,11.8125,71.5625/
58.25,12.1875,71.5625,57.8125,12.1875,71.5625
BLOCK,1,11,5,9,13,7,11
57.8125,11.8125,71.5625,58.25,11.8125,71.5625,58.25,12.1875,71.5625/
57.8125,12.1875,71.5625,57.8125,11.8125,72.4375,58.25,11.8125,72.4375/
58.25,12.1875,72.4375,57.8125,12.1875,72.4375
BLOCK,1,11,5,11,13,7,13
57.8125,11.8125,72.4375,58.25,11.8125,72.4375,58.25,12.1875,72.4375/
57.8125,12.1875,72.4375,57.8125,11.8125,72.9375,58.25,11.8125,72.9375/
58.25,12.1875,72.9375,57.8125,12.1875,72.9375
BLOCK,1,11,5,13,13,7,23,9,0.25,10,0.25,11,0.25,12,0.25
57.8125,11.8125,72.9375,58.25,11.8125,72.9375,58.25,12.1875,72.9375/
57.8125,12.1875,72.9375,57.8125,11.8125,144.0,58.25,11.8125,144.0/
58.25,12.1875,144.0,57.8125,12.1875,144.0
BLOCK,1,11,7,1,13,9,7
57.8125,12.1875,0,58.25,12.1875,0,58.25,18.1875,0,57.8125,18.1875,0/
57.8125,12.1875,71.0625,58.25,12.1875,71.0625,58.25,18.1875,71.0625/
57.8125,18.1875,71.0625
BLOCK,1,11,7,9,13,9,11
57.8125,12.1875,71.5625,58.25,12.1875,71.5625,58.25,18.1875,71.5625/
57.8125,18.1875,71.5625,57.8125,12.1875,72.4375,58.25,12.1875,72.4375/
58.25,18.1875,72.4375,57.8125,18.1875,72.4375
BLOCK,1,11,7,13,13,9,23,9,0.25,10,0.25,11,0.25,12,0.25
57.8125,12.1875,72.9375,58.25,12.1875,72.9375,58.25,18.1875,72.9375/
57.8125,18.1875,72.9375,57.8125,12.1875,144.0,58.25,12.1875,144.0/
58.25,18.1875,144.0,57.8125,18.1875,144.0
BLOCK,1,11,9,9,13,11,11
57.8125,18.1875,71.5625,58.25,18.1875,71.5625,58.25,20.1875,71.5625/
57.8125,20.1875,71.5625,57.8125,18.1875,72.4375,58.25,18.1875,72.4375/
58.25,20.1875,72.4375,57.8125,20.1875,72.4375
BLOCK,1,13,3,9,15,5,11
58.25,3.8125,71.5625,73.25,3.8125,71.5625,73.25,11.8125,71.5625/
58.25,11.8125,71.5625,58.25,3.8125,72.4375,73.25,3.8125,72.4375/
73.25,11.8125,72.4375,58.25,11.8125,72.4375
BLOCK,1,13,5,1,15,7,7
58.25,11.8125,0,73.25,11.8125,0,73.25,12.1875,0,58.25,12.1875,0/
58.25,11.8125,71.0625,73.25,11.8125,71.0625,73.25,12.1875,71.0625/
58.25,12.1875,71.0625
BLOCK,1,13,5,7,15,7,9
58.25,11.8125,71.0625,73.25,11.8125,71.0625,73.25,12.1875,71.0625/
58.25,12.1875,71.0625,58.25,11.8125,71.5625,73.25,11.8125,71.5625/
73.25,12.1875,71.5625,58.25,12.1875,71.5625
BLOCK,1,13,5,9,15,7,11
```

```
58.25,11.8125,71.5625,73.25,11.8125,71.5625,73.25,12.1875,71.5625/
58.25,12.1875,71.5625,58.25,11.8125,72.4375,73.25,11.8125,72.4375/
73.25,12.1875,72.4375,58.25,12.1875,72.4375
BLOCK,1,13,5,11,15,7,13
58.25,11.8125,72.4375,73.25,11.8125,72.4375,73.25,12.1875,72.4375/
58.25,12.1875,72.4375,58.25,11.8125,72.9375,73.25,11.8125,72.9375/
73.25,12.1875,72.9375,58.25,12.1875,72.9375
BLOCK,1,13,5,13,15,7,23,9,0.25,10,0.25,11,0.25,12,0.25
58.25,11.8125,72.9375,73.25,11.8125,72.9375,73.25,12.1875,72.9375/
58.25,12.1875,72.9375,58.25,11.8125,144.0,73.25,11.8125,144.0/
73.25,12.1875,144.0,58.25,12.1875,144.0
BLOCK,1,13,7,9,15,9,11
58.25,12.1875,71.5625,73.25,12.1875,71.5625,73.25,18.1875,71.5625/
58.25,18.1875,71.5625,58.25,12.1875,72.4375,73.25,12.1875,72.4375/
73.25,18.1875,72.4375,58.25,18.1875,72.4375
BLOCK,1,13,9,9,15,11,11
58.25,18.1875,71.5625,73.25,18.1875,71.5625,73.25,20.1875,71.5625/
58.25,20.1875,71.5625,58.25,18.1875,72.4375,73.25,18.1875,72.4375/
73.25,20.1875,72.4375,58.25,20.1875,72.4375
BLOCK,1,15,1,1,17,3,7
73.25,0,0,74.5,0,0,74.5,3.8125,0,73.25,3.8125,0/
73.25,0,71.0625,74.5,0,71.0625,74.5,3.8125,71.0625,73.25,3.8125,71.0625
BLOCK,1,15,1,7,17,3,9
73.25,0,71.0625,74.5,0,71.0625,74.5,3.8125,71.0625,73.25,3.8125,71.0625/
73.25,0,71.5625,74.5,0,71.5625,74.5,3.8125,71.5625,73.25,3.8125,71.5625
BLOCK,1,15,1,9,17,3,11
73.25,0,71.5625,74.5,0,71.5625,74.5,3.8125,71.5625,73.25,3.8125,71.5625/
73.25,0,72.4375,74.5,0,72.4375,74.5,3.8125,72.4375,73.25,3.8125,72.4375
BLOCK,1,15,1,11,17,3,13
73.25,0,72.4375,74.5,0,72.4375,74.5,3.8125,72.4375,73.25,3.8125,72.4375/
73.25,0,72.9375,74.5,0,72.9375,74.5,3.8125,72.9375,73.25,3.8125,72.9375
BLOCK,1,15,1,13,17,3,23,9,0.25,10,0.25,11,0.25,12,0.25
73.25,0,72.9375,74.5,0,72.9375,74.5,3.8125,72.9375,73.25,3.8125,72.9375/
73.25,0,144.0,74.5,0,144.0,74.5,3.8125,144.0,73.25,3.8125,144.0
BLOCK,1,15,3,1,17,5,7
73.25,3.8125,0,74.5,3.8125,0,74.5,11.8125,0,73.25,11.8125,0/
73.25,3.8125,71.0625,74.5,3.8125,71.0625,74.5,11.8125,71.0625/
73.25,11.8125,71.0625
BLOCK,1,15,3,7,17,5,9
73.25,3.8125,71.0625,74.5,3.8125,71.0625,74.5,11.8125,71.0625/
73.25,11.8125,71.0625,73.25,3.8125,71.5625,74.5,3.8125,71.5625/
74.5,11.8125,71.5625,73.25,11.8125,71.5625
BLOCK,1,15,3,9,17,5,11
73.25,3.8125,71.5625,74.5,3.8125,71.5625,74.5,11.8125,71.5625/
73.25,11.8125,71.5625,73.25,3.8125,72.4375,74.5,3.8125,72.4375/
74.5,11.8125,72.4375,73.25,11.8125,72.4375
BLOCK,1,15,3,11,17,5,13
73.25,3.8125,72.4375,74.5,3.8125,72.4375,74.5,11.8125,72.4375/
73.25,11.8125,72.4375,73.25,3.8125,72.9375,74.5,3.8125,72.9375/
74.5,11.8125,72.9375,73.25,11.8125,72.9375
BLOCK,1,15,3,13,17,5,23,9,0.25,10,0.25,11,0.25,12,0.25
73.25,3.8125,72.9375,74.5,3.8125,72.9375,74.5,11.8125,72.9375/
73.25,11.8125,72.9375,73.25,3.8125,144.0,74.5,3.8125,144.0/
74.5,11.8125,144.0,73.25,11.8125,144.0
BLOCK,1,15,5,1,17,7,7
73.25,11.8125,0,74.5,11.8125,0,74.5,12.1875,0,73.25,12.1875,0/
73.25,11.8125,71.0625,74.5,11.8125,71.0625,74.5,12.1875,71.0625/
73.25,12.1875,71.0625
BLOCK,1,15,5,7,17,7,9
73.25,11.8125,71.0625,74.5,11.8125,71.0625,74.5,12.1875,71.0625/
73.25,12.1875,71.0625,73.25,11.8125,71.5625,74.5,11.1825,71.5625/
74.5,12.1875,71.5625,73.25,12.1875,71.5625
```

```
BLOCK,1,15,5,9,17,7,11
73.25,11.8125,71.5625,74.5,11.8125,71.5625,74.5,12.1875,71.5625/
73.25,12.1875,71.5625,73.25,11.8125,72.4375,74.5,11.8125,72.4375/
74.5,12.1875,72.4375,73.25,12.1875,72.4375
BLOCK,1,15,5,11,17,7,13
73.25,11.8125,72.4375,74.5,11.8125,72.4375,74.5,12.1875,72.4375/
73.25,12.1875,72.4375,73.25,11.8125,72.9375,74.5,11.8125,72.9375/
74.5,12.1875,72.9375,73.25,12.1875,72.9375
BLOCK,1,15,5,13,17,7,23,9,0,.25,10,0,.25,11,0,.25,12,0,.25
73.25,11.8125,72.9375,74.5,11.8125,72.9375,74.5,12.1875,72.9375/
73.25,12.1875,72.9375,73.25,11.8125,144.0,74.5,11.8125,144.0/
74.5,12.1875,144.0,73.25,12.1875,144.0
BLOCK,1,15,7,1,17,9,7
73.25,12.1875,0,74.5,12.1875,0,74.5,18.1875,0,73.25,18.1875,0/
73.25,12.1875,71.0625,74.5,12.1875,71.0625,74.5,18.1875,71.0625/
73.25,18.1875,71.0625
BLOCK,1,15,7,7,17,9,9
73.25,12.1875,71.0625,74.5,12.1875,71.0625,74.5,18.1875,71.0625/
73.25,18.1875,71.0625,73.25,12.1875,71.5625,74.5,12.1875,71.5625/
74.5,18.1875,71.5625,73.25,18.1875,71.5625
BLOCK,1,15,7,9,17,9,11
73.25,12.1875,71.5625,74.5,12.1875,71.5625,74.5,18.1875,71.5625/
73.25,18.1875,71.5625,73.25,12.1875,72.4375,74.5,12.1875,72.4375/
74.5,18.1875,72.4375,73.25,18.1875,72.4375
BLOCK,1,15,7,11,17,9,13
73.25,12.1875,72.4375,74.5,12.1875,72.4375,74.5,18.1875,72.4375/
73.25,18.1875,72.4375,73.25,12.1875,72.9375,74.5,12.1875,72.9375/
74.5,18.1875,72.9375,73.25,18.1875,72.9375
BLOCK,1,15,7,13,17,9,23,9,0,.25,10,0,.25,11,0,.25,12,0,.25
73.25,12.1875,72.9375,74.5,12.1875,72.9375,74.5,18.1875,72.9375/
73.25,18.1875,72.9375,73.25,12.1875,144.0,74.5,12.1875,144.0/
74.5,18.1875,144.0,73.25,18.1875,144.0
BLOCK,1,15,9,1,17,11,7
73.25,18.1875,0,74.5,18.1875,0,74.5,20.1875,0,73.25,20.1875,0/
73.25,18.1875,71.0625,74.5,18.1875,71.0625,74.5,20.1875,71.0625/
73.25,20.1875,71.0625
BLOCK,1,15,9,7,17,11,9
73.25,18.1875,71.0625,74.5,18.1875,71.0625,74.5,20.1875,71.0625/
73.25,20.1875,71.0625,73.25,18.1875,71.5625,74.5,18.1875,71.5625/
74.5,20.1875,71.5625,73.25,20.1875,71.5625
BLOCK,1,15,9,9,17,11,11
73.25,18.1875,71.5625,74.5,18.1875,71.5625,74.5,20.1875,71.5625/
73.25,20.1875,71.5625,73.25,18.1875,72.4375,74.5,18.1875,72.4375/
74.5,20.1875,72.4375,73.25,20.1875,72.4375
BLOCK,1,15,9,11,17,11,13
73.25,18.1875,72.4375,74.5,18.1875,72.4375,74.5,20.1875,72.4375/
73.25,20.1875,72.4375,73.25,18.1875,72.9375,74.5,18.1875,72.9375/
74.5,20.1875,72.9375,73.25,20.1875,72.9375
BLOCK,1,15,9,13,17,11,23,9,0,.25,10,0,.25,11,0,.25,12,0,.25
73.25,18.1875,72.9375,74.5,18.1875,72.9375,74.5,20.1875,72.9375/
73.25,20.1875,72.9375,73.25,18.1875,144.0,74.5,18.1875,144.0/
74.5,20.1875,144.0,73.25,20.1875,144.0
BLOCK,1,15,11,1,17,13,7
73.25,20.1875,0,74.5,20.1875,0,74.5,24.0,0,73.25,24.0,0/
73.25,20.1875,71.0625,74.5,20.1875,71.0625,74.5,24.0,71.0625/
73.25,24.0,71.0625
BLOCK,1,15,11,7,17,13,9
73.25,20.1875,71.0625,74.5,20.1875,71.0625,74.5,24.0,71.0625/
73.25,24.0,71.0625,73.25,20.1875,71.5625,74.5,20.1875,71.5625/
74.5,24.0,71.5625,73.25,24.0,71.5625
BLOCK,1,15,11,9,17,13,11
73.25,20.1875,71.5625,74.5,20.1875,71.5625,74.5,24.0,71.5625/
```

```
73.25,24.0,71.5625,73.25,20.1875,72.4375,74.5,20.1875,72.4375/
74.5,24.0,72.4375,73.25,24.0,72.4375
BLOCK,1,15,11,11,17,13,13
73.25,20.1875,72.4375,74.5,20.1875,72.4375,74.5,24.0,72.4375/
73.25,24.0,72.4375,73.25,20.1875,72.9375,74.5,20.1875,72.9375/
74.5,24.0,72.9375,73.25,24.0,72.9375
BLOCK,1,15,11,13,17,13,23,9,0,25,10,0,25,11,0,25,12,0,25
73.25,20.1875,72.9375,74.5,20.1875,72.9375,74.5,24.0,72.9375/
73.25,24.0,72.9375,73.25,20.1875,144.0,74.5,20.1875,144.0/
74.5,24.0,144.0,73.25,24.0,144.0
END,GRID
JLOOP,6
KLOOP,11
BRICK,1,1,1,1
KEND
JEND
KLOOP,5
BRICK,1,5,7,13
KEND
ILOOP,6
KLOOP,11
BRICK,1,3,5,1
KEND
IEND
JLOOP,6
KLOOP,11
BRICK,1,15,1,1
KEND
JEND
KLOOP,3
BRICK,1,11,7,1
KEND
KLOOP,5
BRICK,1,11,7,13
KEND
ILOOP,6
BRICK,1,3,3,9
IEND
ILOOP,6
BRICK,1,3,7,9
IEND
ILOOP,6
BRICK,1,3,9,9
IEND
JLOOP,6
BC,PRESSURE,15,1,1,6,173.96,180.0,180.0,173.96
JEND
BC,PRESSURE,13,5,1,6,101.48,173.96,173.96,101.48
JLOOP,2
BC,PRESSURE,11,5,1,6,99.36,101.48,101.48,99.36
JEND
BC,PRESSURE,9,5,1,6,0.,99.36,99.36,0.
BC,PRESSURE,7,5,1,6,-99.36,0.,0.,-99.36
BC,PRESSURE,5,5,1,6,-101.48,-99.36,-99.36,-101.48
BC,PRESSURE,3,5,1,6,-173.96,-101.48,-101.48,-173.96
JLOOP,6
BC,PRESSURE,1,1,1,6,-180.0,-173.96,-173.96,-180.0
JEND
JLOOP,6
BC,SLOPE,1,1,21,3
JEND
ILOOP,6
```

```
BC,SLOPE,3,5,21,3
IEND
JLOOP,6
BC,SLOPE,15,1,21,3
JEND
BC,SLOPE,11,7,21,3
BC,SLOPE,5,7,21,3
JLOOP,6
BC,UX,1,1,21,5
JEND
BC,UX,1,11,21,8
BC,SLOPE,9,9,9,2
JLOOP,6
BC,UX,1,1,21,20
JEND
END,ELEMENTS
SOLVE
POST
BLOCK,,4
OPTION,2
END,STRESS
STOP
```

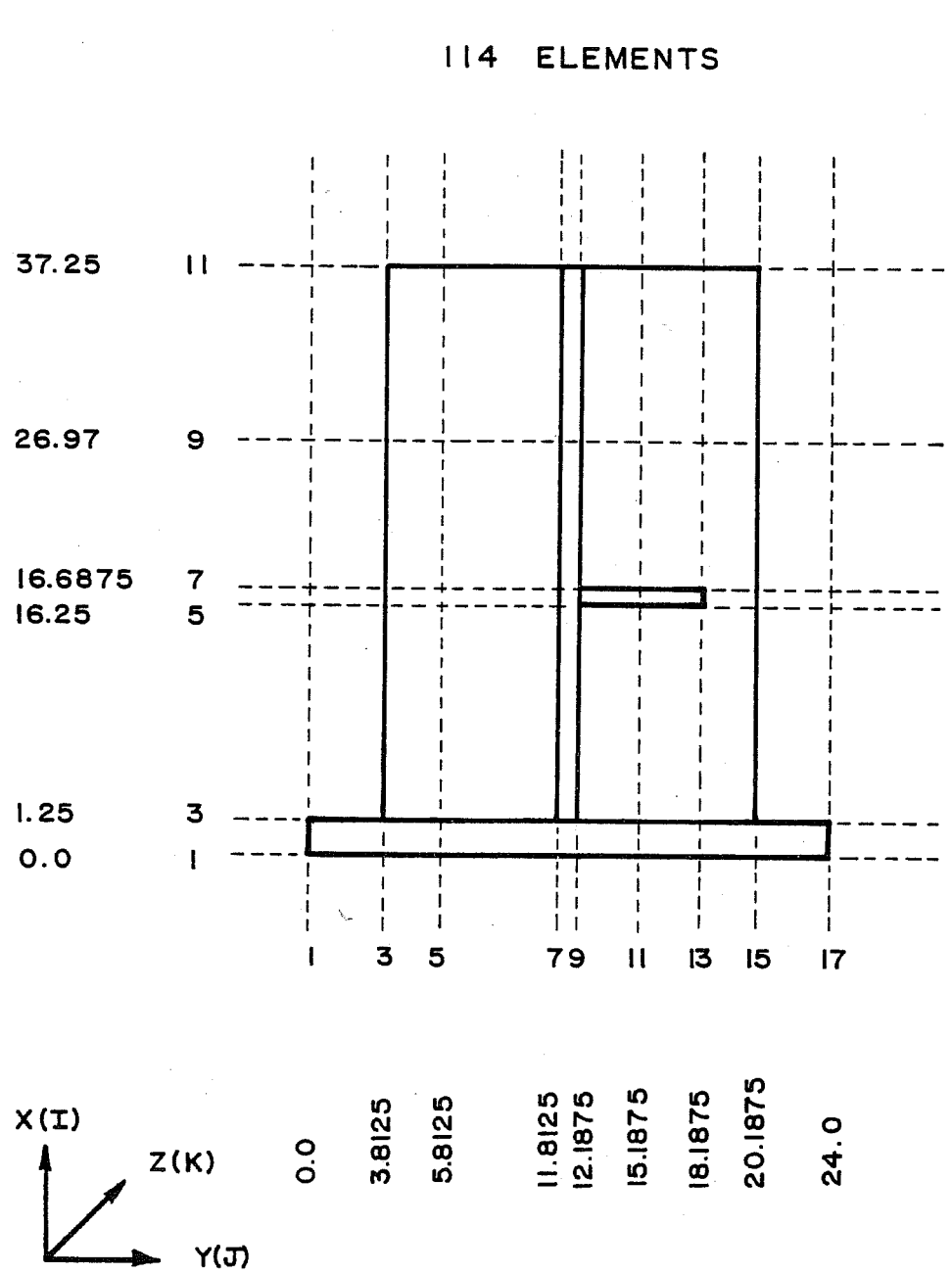

Fig. A.4 One-quarter symmetric finite element model grid definition in the x-y plane

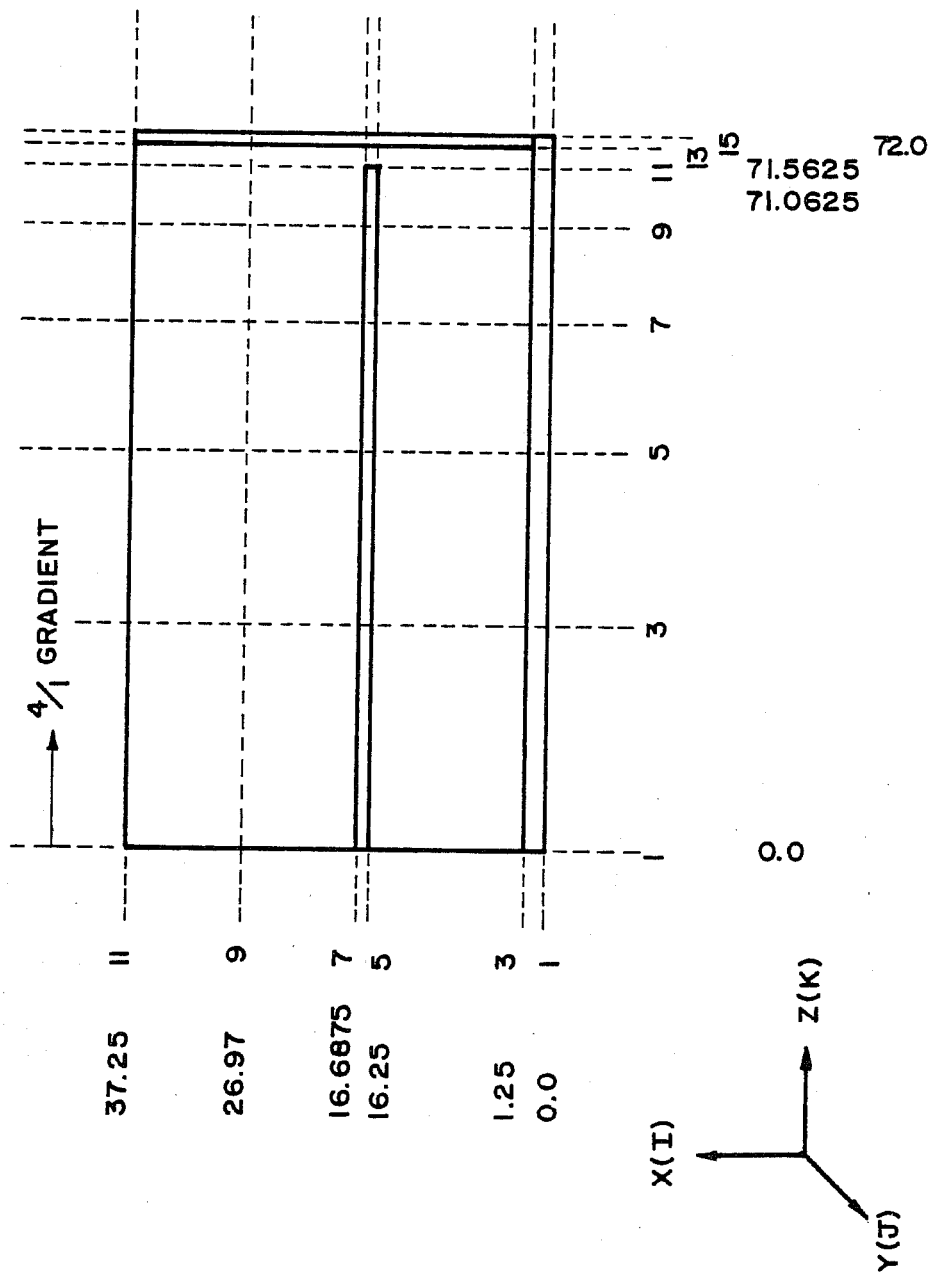

Fig. A.5 One-quarter symmetric finite element model grid definition in the x-z plane

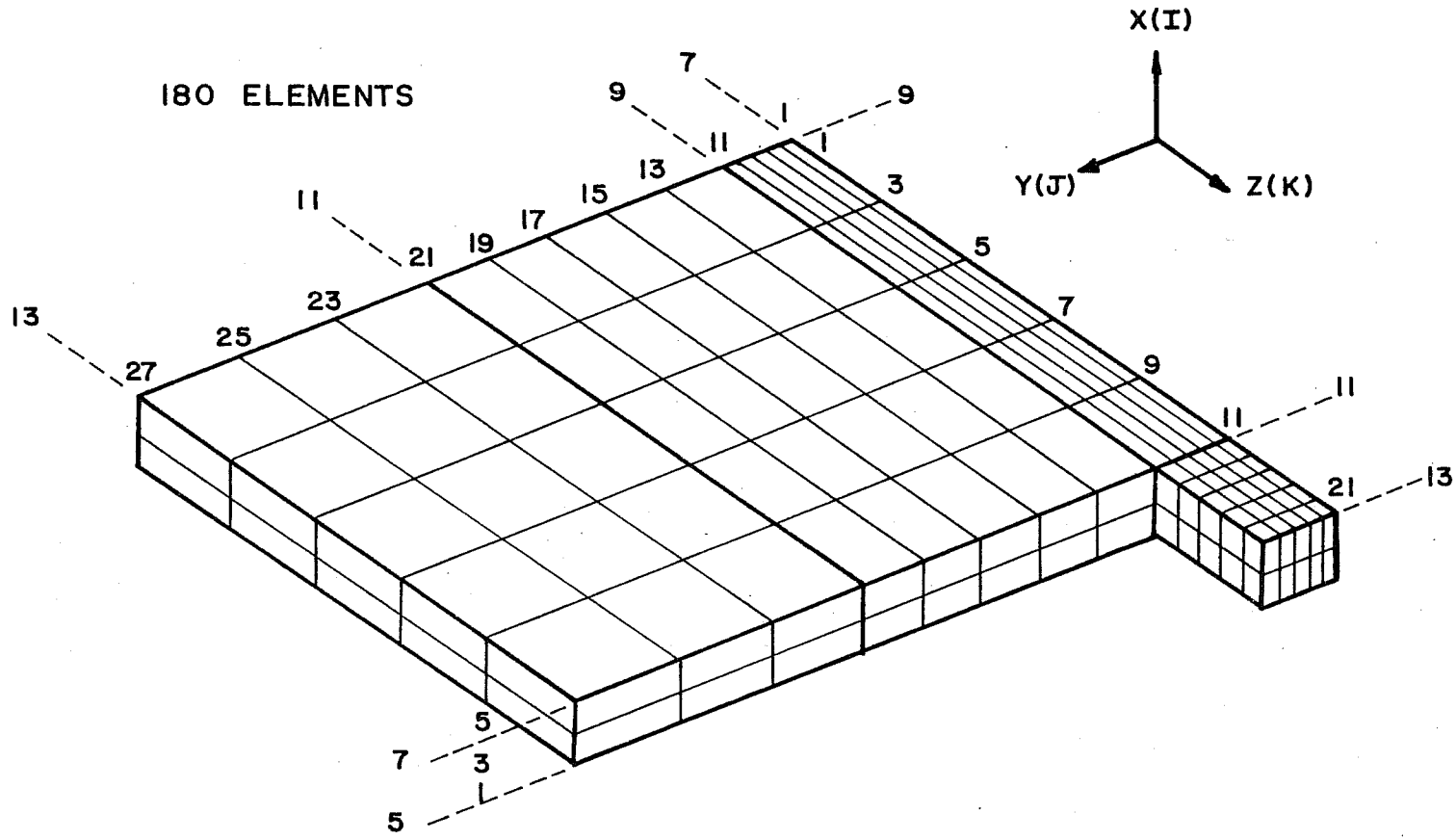

Fig. A.6 One-quarter symmetric finite element model grid definition of rezoned area

```
$ STIFFENER INTERSECTION
SETUP,4,,11,17
ISO,STEEL,1,29E03,0.30
END,MATERIALS
BLOCK,1,1,1,1,3,3,11,9,4.0,10,4.0,11,4.0,12,4.0
0,0,0,1.25,0,0,1.25,3.8125,0,0,3.8125,0/
0,0,71.0625,1.25,0,71.0625,1.25,3.8125,71.0625,0,3.8125,71.0625
BLOCK,1,1,1,11,3,3,13
0,0,71.0625,1.25,0,71.0625,1.25,3.8125,71.0625,0,3.8125,71.0625/
0,0,71.5625,1.25,0,71.5625,1.25,3.8125,71.5625,0,3.8125,71.5625
BLOCK,1,1,1,13,3,3,15
0,0,71.5625,1.25,0,71.5625,1.25,3.8125,71.5625,0,3.8125,71.5625/
0,0,72.0,1.25,0,72.0,1.25,3.8125,72.0,0,3.8125,72.0
BLOCK,1,1,3,1,3,5,11,9,4.0,10,4.0,11,4.0,12,4.0
0,3,8125,0,1.25,3.8125,0,1.25,5.8125,0,0,5.8125,0/
0,3.8125,71.0625,1.25,3.8125,71.0625,1.25,5.8125,71.0625,0,5.8125,71.0625
BLOCK,1,1,3,11,3,5,13
0,3.8125,71.0625,1.25,3.8125,71.0625,1.25,5.8125,71.0625,0,5.8125,71.0625/
0,3.8125,71.5625,1.25,3.8125,71.5625,1.25,5.8125,71.5625,0,5.8125,71.5625
BLOCK,1,1,3,13,3,5,15
0,3.8125,71.5625,1.25,3.8125,71.5625,1.25,5.8125,71.5625,0,5.8125,71.5625/
0,3.8125,72.0,1.25,3.8125,72.0,1.25,5.8125,72.0,0,0,5.8125,72.0
BLOCK,1,1,5,1,3,7,11,9,4.0,10,4.0,11,4.0,12,4.0
0,5,8125,0,1.25,5.8125,0,1.25,11.8125,0,0,11.8125,0/
0,5.8125,71.0625,1.25,5.8125,71.0625,1.25,11.8125,71.0625,0,11.8125,71.0625
BLOCK,1,1,5,11,3,7,13
0,5.8125,71.0625,1.25,5.8125,71.0625,1.25,11.8125,71.0625,0,11.8125,71.0625/
0,5.8125,71.5625,1.25,5.8125,71.5625,1.25,11.8125,71.5625,0,11.8125,71.5625
BLOCK,1,1,5,13,3,7,15
0,5.8125,71.5625,1.25,5.8125,71.5625,1.25,11.8125,71.5625,0,11.8125,71.5625/
0,5.8125,72.0,1.25,5.8125,72.0,1.25,11.8125,72.0,0,0,11.8125,72.0
BLOCK,1,1,7,1,3,9,11,9,4.0,10,4.0,11,4.0,12,4.0
0,11.8125,0,1.25,11.8125,0,1.25,12.1875,0,0,12.1875,0/
0,11.8125,71.0625,1.25,11.8125,71.0625,1.25,12.1875,71.0625,0,12.1875,71.0625
BLOCK,1,1,7,11,3,9,13
0,11.8125,71.0625,1.25,11.8125,71.0625,1.25,12.1875,71.0625,0,12.1875,71.0625/
0,11.8125,71.5625,1.25,11.8125,71.5625,1.25,12.1875,71.5625,0,12.1875,71.5625
BLOCK,1,1,7,13,3,9,15
0,11.8125,71.5625,1.25,11.8125,71.5625,1.25,12.1875,71.5625,0,12.1875,71.5625/
0,11.8125,72.0,1.25,11.8125,72.0,1.25,12.1875,72.0,0,0,12.1875,72.0
BLOCK,1,1,9,1,3,13,11,9,4.0,10,4.0,11,4.0,12,4.0
0,12.1875,0,1.25,12.1875,0,1.25,18.1875,0,0,18.1875,0/
0,12.1875,71.0625,1.25,12.1875,71.0625,1.25,18.1875,71.0625,0,18.1875,71.0625
BLOCK,1,1,9,11,3,13,13
0,12.1875,71.0625,1.25,12.1875,71.0625,1.25,18.1875,71.0625,0,18.1875,71.0625/
0,12.1875,71.5625,1.25,12.1875,71.5625,1.25,18.1875,71.5625,0,18.1875,71.5625
BLOCK,1,1,9,13,3,13,15
0,12.1875,71.5625,1.25,12.1875,71.5625,1.25,18.1875,71.5625,0,18.1875,71.5625/
0,12.1875,72.0,1.25,12.1875,72.0,1.25,18.1875,72.0,0,0,18.1875,72.0
BLOCK,1,1,13,1,3,15,11,9,4.0,10,4.0,11,4.0,12,4.0
0,18.1875,0,1.25,18.1875,0,1.25,20.1875,0,0,20.1875,0/
0,18.1875,71.0625,1.25,18.1875,71.0625,1.25,20.1875,71.0625,0,20.1875,71.0625
BLOCK,1,1,13,11,3,15,13
0,18.1875,71.0625,1.25,18.1875,71.0625,1.25,20.1875,71.0625,0,20.1875,71.0625/
0,18.1875,71.5625,1.25,18.1875,71.5625,1.25,20.1875,71.5625,0,20.1875,71.5625
BLOCK,1,1,13,13,3,15,15
0,18.1875,71.5625,1.25,18.1875,71.5625,1.25,20.1875,71.5625,0,20.1875,71.5625/
0,18.1875,72.0,1.25,18.1875,72.0,1.25,20.1875,72.0,0,0,20.1875,72.0
BLOCK,1,1,15,1,3,17,11,9,4.0,10,4.0,11,4.0,12,4.0
0,20.1875,0,1.25,20.1875,0,1.25,24.0,0,0,0,24.0,0/
0,20.1875,71.0625,1.25,20.1875,71.0625,1.25,24.0,71.0625,0,24.0,71.0625
```

Fig. A.7 TEXGAP-3D input listing for 1/4 symmetric model of existing detail

```
BLOCK,1,1,15,11,3,17,13
0,20.1875,71.0625,1.25,20.1875,71.0625,1.25,24.0,71.0625,0,24.0,71.0625/
0,20.1875,71.5625,1.25,20.1875,71.5625,1.25,24.0,71.5625,0,24.0,71.5625
BLOCK,1,1,15,13,3,17,15
0,20.1875,71.5625,1.25,20.1875,71.5625,1.25,24.0,71.5625,0,24.0,71.5625/
0,20.1875,72.0,1.25,20.1875,72.0,1.25,24.0,72.0,0,24.0,72.0
BLOCK,1,3,3,13,5,5,15
1.25,3.8125,71.5625,16.25,3.8125,71.5625,16.25,5.8125,71.5625/
1.25,5.8125,71.5625,1.25,3.8125,72.0,16.25,3.8125,72.0/
16.25,5.8125,72.0,1.25,5.8125,72.0
BLOCK,1,3,5,13,5,7,15
1.25,5.8125,71.5625,16.25,5.8125,71.5625,16.25,11.8125,71.5625/
1.25,11.8125,71.5625,1.25,5.8125,72.0,16.25,5.8125,72.0/
16.25,11.8125,72.0,1.25,11.8125,72.0
BLOCK,1,3,7,1,5,9,11,9,4.0,10,4.0,11,4.0,12,4.0
1.25,11.8125,0,16.25,11.8125,0,16.25,12.1875,0,1.25,12.1875,0/
1.25,11.8125,71.0625,16.25,11.8125,71.0625,16.25,12.1875,71.0625/
1.25,12.1875,71.0625
BLOCK,1,3,7,13,5,9,15
1.25,11.8125,71.5625,16.25,11.8125,71.5625,16.25,12.1875,71.5625/
1.25,12.1875,71.5625,1.25,11.8125,72.0,16.25,11.8125,72.0/
16.25,12.1875,72.0,1.25,12.1875,72.0
BLOCK,1,3,9,13,5,13,15
1.25,12.1875,71.5625,16.25,12.1875,71.5625,16.25,18.1875,71.5625/
1.25,18.1875,71.5625,1.25,12.1875,72.0,16.25,12.1875,72.0/
16.25,18.1875,72.0,1.25,18.1875,72.0
BLOCK,1,3,7,11,5,9,13
1.25,11.8125,71.0625,16.25,11.8125,71.0625,16.25,12.1875,71.0625/
1.25,12.1875,71.0625,1.25,11.8125,71.5625,16.25,11.8125,71.5625/
16.25,12.1875,71.5625,1.25,12.1875,71.5625
BLOCK,1,3,13,13,5,15,15
1.25,18.1875,71.5625,16.25,18.1875,71.5625,16.25,20.1875,71.5625/
1.25,20.1875,71.5625,1.25,18.1875,72.0,16.25,18.1875,72.0/
16.25,20.1875,72.0,1.25,20.1875,72.0
BLOCK,1,5,3,13,7,5,15
16.25,3.8125,71.5625,16.6875,3.8125,71.5625,16.6875,5.8125,71.5625/
16.25,5.8125,71.5625,16.25,3.8125,72.0,16.6875,3.8125,72.0/
16.6875,5.8125,72.0,16.25,5.8125,72.0
BLOCK,1,5,5,13,7,7,15
16.25,5.8125,71.5625,16.6875,5.8125,71.5625,16.6875,11.8125,71.5625/
16.25,11.8125,71.5625,16.25,5.8125,72.0,16.6875,5.8125,72.0/
16.6875,11.8125,72.0,16.25,11.8125,72.0
BLOCK,1,5,7,1,7,9,11,9,4.0,10,4.0,11,4.0,12,4.0
16.25,11.8125,0,16.6875,11.8125,0,16.6875,12.1875,0,16.25,12.1875,0/
16.25,11.8125,71.0625,16.6875,11.8125,71.0625,16.6875,12.1875,71.0625/
16.25,12.1875,71.0625
BLOCK,1,5,7,11,7,9,13
16.25,11.8125,71.0625,16.6875,11.8125,71.0625,16.6875,12.1875,71.0625/
16.25,12.1875,71.0625,16.25,11.8125,71.5625,16.6875,11.8125,71.5625/
16.6875,12.1875,71.5625,16.25,12.1875,71.5625
BLOCK,1,5,7,13,7,9,15
16.25,11.8125,71.5625,16.6875,11.8125,71.5625,16.6875,12.1875,71.5625/
16.25,12.1875,71.5625,16.25,11.8125,72.0,16.6875,11.8125,72.0/
16.6875,12.1875,72.0,16.25,12.1875,72.0
BLOCK,1,5,9,1,7,13,11,9,4.0,10,4.0,11,4.0,12,4.0
16.25,12.1875,0,16.6875,12.1875,0,16.6875,18.1875,0,16.25,18.1875,0/
16.25,12.1875,71.0625,16.6875,12.1875,71.0625,16.6875,18.1875,71.0625/
16.25,18.1875,71.0625
BLOCK,1,5,9,13,7,13,15
16.25,12.1875,71.5625,16.6875,12.1875,71.5625,16.6875,18.1875,71.5625/
16.25,18.1875,71.5625,16.25,12.1875,72.0,16.6875,12.1875,72.0/
16.6875,18.1875,72.0,16.25,18.1875,72.0
```

```
BLOCK,1,5,13,13,7,15,15
16.25,18.1875,71.5625,16.6875,18.1875,71.5625,16.6875,20.1875,71.5625/
16.25,20.1875,71.5625,16.25,18.1875,72.0,16.6875,18.1875,72.0/
16.6875,20.1875,72.0,16.25,20.1875,72.0
BLOCK,1,7,3,13,11,5,15
16.6875,3.8125,71.5625,37.25,3.8125,71.5625,37.25,5.8125,71.5625/
16.6875,5.8125,71.5625,16.6875,3.8125,72.0,37.25,3.8125,72.0/
37.25,5.8125,72.0,16.6875,5.8125,72.0
BLOCK,1,7,5,13,11,7,15
16.6875,5.8125,71.5625,37.25,5.8125,71.5625,37.25,11.8125,71.5625/
16.6875,11.8125,71.5625,16.6875,5.8125,72.0,37.25,5.8125,72.0/
37.25,11.8125,72.0,16.6875,11.8125,72.0
BLOCK,1,7,7,1,11,9,11,9,4.0,10,4.0,11,4.0,12,4.0
16.6875,11.8125,0,37.25,11.8125,0,37.25,12.1875,0,16.6875,12.1875,0/
16.6875,11.8125,71.0625,37.25,11.8125,71.0625,37.25,12.1875,71.0625/
16.6875,12.1875,71.0625
BLOCK,1,7,7,11,11,9,13
16.6875,11.8125,71.0625,37.25,11.8125,71.0625,37.25,12.1875,71.0625/
16.6875,12.1875,71.0625,16.6875,11.8125,71.5625,37.25,11.8125,71.5625/
37.25,12.1875,71.5625,16.6875,12.1875,71.5625
BLOCK,1,7,7,13,11,9,15
16.6875,11.8125,71.5625,37.25,11.8125,71.5625,37.25,12.1875,71.5625/
16.6875,12.1875,71.5625,16.6875,11.8125,72.0,37.25,11.8125,72.0/
37.25,12.1875,72.0,16.6875,12.1875,72.0
BLOCK,1,7,9,13,11,13,15
16.6875,12.1875,71.5625,37.25,12.1875,71.5625,37.25,18.1875,71.5625/
16.6875,18.1875,71.5625,16.6875,12.1875,72.0,37.25,12.1875,72.0/
37.25,18.1875,72.0,16.6875,18.1875,72.0
BLOCK,1,7,13,13,11,15,15
16.6875,18.1875,71.5625,37.25,18.1875,71.5625,37.25,20.1875,71.5625/
16.6875,20.1875,71.5625,16.6875,18.1875,72.0,37.25,18.1875,72.0/
37.25,20.1875,72.0,16.6875,20.1875,72.0
END,GRID
JLOOP,8
KLOOP,7
BRICK,1,1,1,1
KEND
JEND
ILOOP,4
KLOOP,7
BRICK,1,3,7,1
KEND
IEND
JLOOP,2
KLOOP,5
BRICK,1,5,9,1
KEND
JEND
JLOOP,2
ILOOP,4
BRICK,1,3,3,13
IEND
JEND
JLOOP,3
ILOOP,4
BRICK,1,3,9,13
IEND
JEND
JLOOP,8
BC,PRESSURE,1,1,1,6,-180.0,-173.96,-173.96,-180.0
JEND
BC,PRESSURE,3,7,1,6,-173.96,-101.48,-101.48,-173.96
```

```
JLOOP,3
BC,PRESSURE,5,7,1,6,-101.48,-99.36,-99.36,-101.48
JEND
BC,PRESSURE,7,7,1,6,-99.36,-49.68,-49.68,-99.36
BC,PRESSURE,9,7,1,6,-49.68,0.0,0.0,0.0,-49.68
JLOOP,8
BC,SLOPE,1,1,13,3
JEND
ILOOP,4
JLOOP,6
BC,SLOPE,3,3,13,3
JEND
IEND
ILOOP,4
BC,SLOPE,3,3,13,5
IEND
ILOOP,4
BC,SLOPE,3,13,13,2
IEND
JLOOP,8
BC,UX,1,1,13,5
BC,UX,1,1,13,20
JEND
BC,UX,1,15,13,8
KLOOP,7
BC,UZ,9,7,1,2
BC,UZ,9,7,1,10
BC,UZ,9,7,1,3
BC,UZ,9,7,1,14
BC,UZ,9,7,1,15
KEND
END,ELEMENTS
SOLVE
REZONE,5,7,9,7,13,13
REFINE,GRIDS,5,7,9,2,5,5
BCR,REZONE,5,7,9,2,0,0,2,0,2,1,1,1
REFINE,GRIDS,5,9,9,2,5,5
BCR,REZONE,5,9,9,0,0,0,0,0,2,1,11,1
REFINE,GRIDS,5,11,9,2,3,5
BCR,REZONE,5,11,9,0,0,0,0,0,2,1,21,1
REFINE,GRIDS,5,7,11,2,5,5
BCR,REZONE,5,7,11,2,0,2,2,0,0,1,1,11
END
SOLVE
POST
BLOCK,,4
OPTION,2
END,STRESS
STOP
```

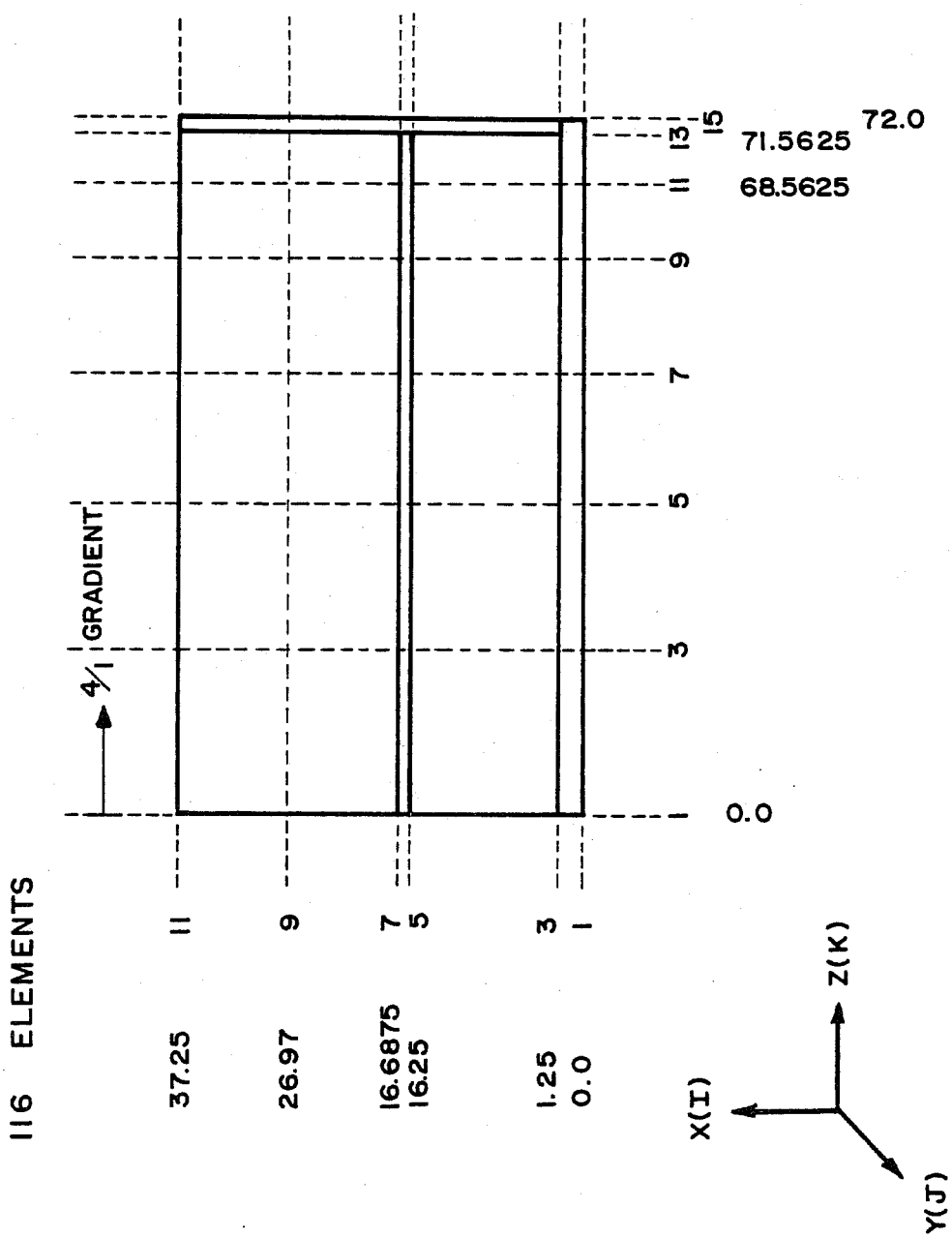

Fig. A.8 Cope detail one-quarter symmetric finite element model grid definition in the x-z plane

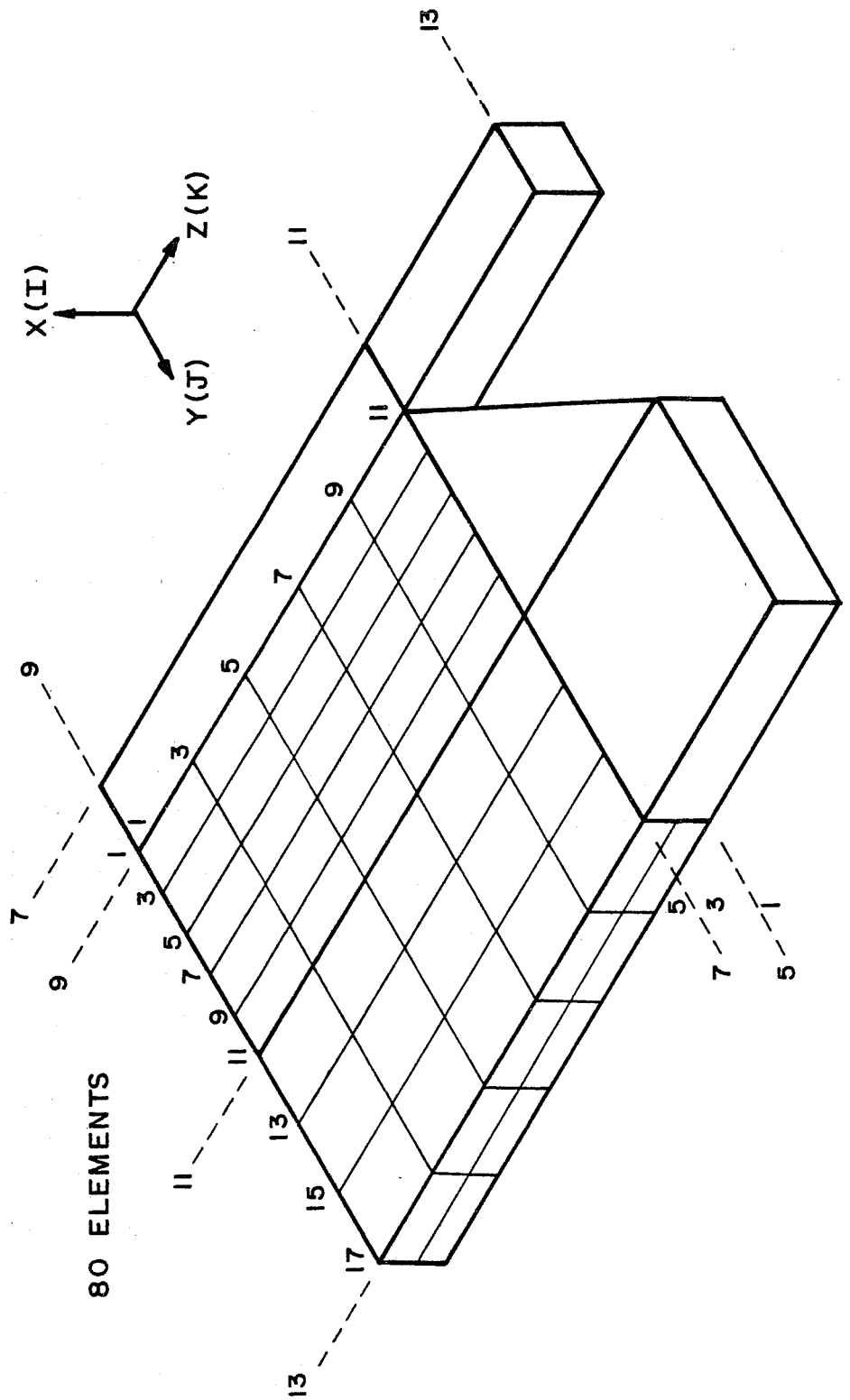

Fig. A.9 Finite element model grid definition of rezoned area of cope detail

```
$ STIFFENER INTERSECTION
SETUP,4,,11,17
ISO,STEEL,1,29E03,0.30
END,MATERIALS
BLOCK,1,1,1,1,3,3,11,9,4.0,10,4.0,11,4.0,12,4.0
0,0,0,1.25,0,0,1.25,3.8125,0,0,3.8125,0/
0,0,68.5625,1.25,0,68.5625,1.25,3.8125,68.5625,0,3.8125,68.5625
BLOCK,1,1,1,11,3,3,13
0,0,68.5625,1.25,0,68.5625,1.25,3.8125,68.5625,0,3.8125,68.5625/
0,0,71.5625,1.25,0,71.5625,1.25,3.8125,71.5625,0,3.8125,71.5625
BLOCK,1,1,1,13,3,3,15
0,0,71.5625,1.25,0,71.5625,1.25,3.8125,71.5625,0,3.8125,71.5625/
0,0,72.0,1.25,0,72.0,1.25,3.8125,72.0,0,3.8125,72.0
BLOCK,1,1,3,1,3,5,11,9,4.0,10,4.0,11,4.0,12,4.0
0,3.8125,0,1.25,3.8125,0,1.25,5.8125,0,0,5.8125,0/
0,3.8125,68.5625,1.25,3.8125,68.5625,1.25,5.8125,68.5625,0,5.8125,68.5625
BLOCK,1,1,3,11,3,5,13
0,3.8125,68.5625,1.25,3.8125,68.5625,1.25,5.8125,68.5625,0,5.8125,68.5625/
0,3.8125,71.5625,1.25,3.8125,71.5625,1.25,5.8125,71.5625,0,5.8125,71.5625
BLOCK,1,1,3,13,3,5,15
0,3.8125,71.5625,1.25,3.8125,71.5625,1.25,5.8125,71.5625,0,5.8125,71.5625/
0,3.8125,72.0,1.25,3.8125,72.0,1.25,5.8125,72.0,0,5.8125,72.0
BLOCK,1,1,5,1,3,7,11,9,4.0,10,4.0,11,4.0,12,4.0
0,5.8125,0,1.25,5.8125,0,1.25,11.8125,0,0,11.8125,0/
0,5.8125,68.5625,1.25,5.8125,68.5625,1.25,11.8125,68.5625,0,11.8125,68.5625
BLOCK,1,1,5,11,3,7,13
0,5.8125,68.5625,1.25,5.8125,68.5625,1.25,11.8125,68.5625,0,11.8125,68.5625/
0,5.8125,71.5625,1.25,5.8125,71.5625,1.25,11.8125,71.5625,0,11.8125,71.5625
BLOCK,1,1,5,13,3,7,15
0,5.8125,71.5625,1.25,5.8125,71.5625,1.25,11.8125,71.5625,0,11.8125,71.5625/
0,5.8125,72.0,1.25,5.8125,72.0,1.25,11.8125,72.0,0,11.8125,72.0
BLOCK,1,1,7,1,3,9,11,9,4.0,10,4.0,11,4.0,12,4.0
0,11.8125,0,1.25,11.8125,0,1.25,12.1875,0,0,12.1875,0/
0,11.8125,68.5625,1.25,11.8125,68.5625,1.25,12.1875,68.5625,0,12.1875,68.5625
BLOCK,1,1,7,11,3,9,13
0,11.8125,68.5625,1.25,11.8125,68.5625,1.25,12.1875,68.5625,0,12.1875,68.5625/
0,11.8125,71.5625,1.25,11.8125,71.5625,1.25,12.1875,71.5625,0,12.1875,71.5625
BLOCK,1,1,7,13,3,9,15
0,11.8125,71.5625,1.25,11.8125,71.5625,1.25,12.1875,71.5625,0,12.1875,71.5625/
0,11.8125,72.0,1.25,11.8125,72.0,1.25,12.1875,72.0,0,12.1875,72.0
BLOCK,1,1,9,1,3,13,11,9,4.0,10,4.0,11,4.0,12,4.0
0,12.1875,0,1.25,12.1875,0,1.25,18.1875,0,0,18.1875,0/
0,12.1875,68.5625,1.25,12.1875,68.5625,1.25,18.1875,68.5625,0,18.1875,68.5625
BLOCK,1,1,9,11,3,13,13
0,12.1875,68.5625,1.25,12.1875,68.5625,1.25,18.1875,68.5625,0,18.1875,68.5625/
0,12.1875,71.5625,1.25,12.1875,71.5625,1.25,18.1875,71.5625,0,18.1875,71.5625
BLOCK,1,1,9,13,3,13,15
0,12.1875,71.5625,1.25,12.1875,71.5625,1.25,18.1875,71.5625,0,18.1875,71.5625/
0,12.1875,72.0,1.25,12.1875,72.0,1.25,18.1875,72.0,0,18.1875,72.0
BLOCK,1,1,13,1,3,15,11,9,4.0,10,4.0,11,4.0,12,4.0
0,18.1875,0,1.25,18.1875,0,1.25,20.1875,0,0,20.1875,0/
0,18.1875,68.5625,1.25,18.1875,68.5625,1.25,20.1875,68.5625,0,20.1875,68.5625
BLOCK,1,1,13,11,3,15,13
0,18.1875,68.5625,1.25,18.1875,68.5625,1.25,20.1875,68.5625,0,20.1875,68.5625/
0,18.1875,71.5625,1.25,18.1875,71.5625,1.25,20.1875,71.5625,0,20.1875,71.5625
BLOCK,1,1,13,13,3,15,15
0,18.1875,71.5625,1.25,18.1875,71.5625,1.25,20.1875,71.5625,0,20.1875,71.5625/
0,18.1875,72.0,1.25,18.1875,72.0,1.25,20.1875,72.0,0,20.1875,72.0
BLOCK,1,1,15,1,3,17,11,9,4.0,10,4.0,11,4.0,12,4.0
0,20.1875,0,1.25,20.1875,0,1.25,24.0,0,0,24.0,0/
0,20.1875,68.5625,1.25,20.1875,68.5625,1.25,24.0,68.5625,0,24.0,68.5625
```

Fig. A.10 TEXGAP-3D input listing for 1/4 symmetric model of cope detail

```
BLOCK,1,1,15,11,3,17,13
0,20.1875,68.5625,1.25,20.1875,68.5625,1.25,24.0,68.5625,0,24.0,68.5625/
0,20.1875,71.5625,1.25,20.1875,71.5625,1.25,24.0,71.5625,0,24.0,71.5625
BLOCK,1,1,15,13,3,17,15
0,20.1875,71.5625,1.25,20.1875,71.5625,1.25,24.0,71.5625,0,24.0,71.5625/
0,20.1875,72.0,1.25,20.1875,72.0,1.25,24.0,72.0,0,24.0,72.0
BLOCK,1,3,3,13,5,5,15
1.25,3.8125,71.5625,16.25,3.8125,71.5625,16.25,5.8125,71.5625/
1.25,5.8125,71.5625,1.25,3.8125,72.0,16.25,3.8125,72.0/
16.25,5.8125,72.0,1.25,5.8125,72.0
BLOCK,1,3,5,13,5,7,15
1.25,5.8125,71.5625,16.25,5.8125,71.5625,16.25,11.8125,71.5625/
1.25,11.8125,71.5625,1.25,5.8125,72.0,16.25,5.8125,72.0/
16.25,11.8125,72.0,1.25,11.8125,72.0
BLOCK,1,3,7,1,5,9,11,9,4.0,10,4.0,11,4.0,12,4.0
1.25,11.8125,0,16.25,11.8125,0,16.25,12.1875,0,1.25,12.1875,0/
1.25,11.8125,68.5625,16.25,11.8125,68.5625,16.25,12.1875,68.5625/
1.25,12.1875,68.5625
BLOCK,1,3,7,13,5,9,15
1.25,11.8125,71.5625,16.25,11.8125,71.5625,16.25,12.1875,71.5625/
1.25,12.1875,71.5625,1.25,11.8125,72.0,16.25,11.8125,72.0/
16.25,12.1875,72.0,1.25,12.1875,72.0
BLOCK,1,3,9,13,5,13,15
1.25,12.1875,71.5625,16.25,12.1875,71.5625,16.25,18.1875,71.5625/
1.25,18.1875,71.5625,1.25,12.1875,72.0,16.25,12.1875,72.0/
16.25,18.1875,72.0,1.25,18.1875,72.0
BLOCK,1,3,7,11,5,9,13
1.25,11.8125,68.5625,16.25,11.8125,68.5625,16.25,12.1875,68.5625/
1.25,12.1875,68.5625,1.25,11.8125,71.5625,16.25,11.8125,71.5625/
16.25,12.1875,71.5625,1.25,12.1875,71.5625
BLOCK,1,3,13,13,5,15,15
1.25,18.1875,71.5625,16.25,18.1875,71.5625,16.25,20.1875,71.5625/
1.25,20.1875,71.5625,1.25,18.1875,72.0,16.25,18.1875,72.0/
16.25,20.1875,72.0,1.25,20.1875,72.0
BLOCK,1,5,3,13,7,5,15
16.25,3.8125,71.5625,16.6875,3.8125,71.5625,16.6875,5.8125,71.5625/
16.25,5.8125,71.5625,16.25,3.8125,72.0,16.6875,3.8125,72.0/
16.6875,5.8125,72.0,16.25,5.8125,72.0
BLOCK,1,5,5,13,7,7,15
16.25,5.8125,71.5625,16.6875,5.8125,71.5625,16.6875,11.8125,71.5625/
16.25,11.8125,71.5625,16.25,5.8125,72.0,16.6875,5.8125,72.0/
16.6875,11.8125,72.0,16.25,11.8125,72.0
BLOCK,1,5,7,1,7,9,11,9,4.0,10,4.0,11,4.0,12,4.0
16.25,11.8125,0,16.6875,11.8125,0,16.6875,12.1875,0,16.25,12.1875,0/
16.25,11.8125,68.5625,16.6875,11.8125,68.5625,16.6875,12.1875,68.5625/
16.25,12.1875,68.5625
BLOCK,1,5,7,11,7,9,13
16.25,11.8125,68.5625,16.6875,11.8125,68.5625,16.6875,12.1875,68.5625/
16.25,12.1875,68.5625,16.25,11.8125,71.5625,16.6875,11.8125,71.5625/
16.6875,12.1875,71.5625,16.25,12.1875,71.5625
BLOCK,1,5,7,13,7,9,15
16.25,11.8125,71.5625,16.6875,11.8125,71.5625,16.6875,12.1875,71.5625/
16.25,12.1875,71.5625,16.25,11.8125,72.0,16.6875,11.8125,72.0/
16.6875,12.1875,72.0,16.25,12.1875,72.0
BLOCK,1,5,9,1,7,13,11,9,4.0,10,4.0,11,4.0,12,4.0
16.25,12.1875,0,16.6875,12.1875,0,16.6875,18.1875,0,16.25,18.1875,0/
16.25,12.1875,68.5625,16.6875,12.1875,68.5625,16.6875,18.1875,68.5625/
16.25,18.1875,68.5625
BLOCK,1,5,9,13,7,13,15
16.25,12.1875,71.5625,16.6875,12.1875,71.5625,16.6875,18.1875,71.5625/
16.25,18.1875,71.5625,16.25,12.1875,72.0,16.6875,12.1875,72.0/
16.6875,18.1875,72.0,16.25,18.1875,72.0
```

```
BLOCK,1,5,13,13,7,15,15
16.25,18.1875,71.5625,16.6875,18.1875,71.5625,16.6875,20.1875,71.5625/
16.25,20.1875,71.5625,16.25,18.1875,72.0,16.6875,18.1875,72.0/
16.6875,20.1875,72.0,16.25,20.1875,72.0
BLOCK,1,7,3,13,11,5,15
16.6875,3.8125,71.5625,37.25,3.8125,71.5625,37.25,5.8125,71.5625/
16.6875,5.8125,71.5625,16.6875,3.8125,72.0,37.25,3.8125,72.0/
37.25,5.8125,72.0,16.6875,5.8125,72.0
BLOCK,1,7,5,13,11,7,15
16.6875,5.8125,71.5625,37.25,5.8125,71.5625,37.25,11.8125,71.5625/
16.6875,11.8125,71.5625,16.6875,5.8125,72.0,37.25,5.8125,72.0/
37.25,11.8125,72.0,16.6875,11.8125,72.0
BLOCK,1,7,7,1,11,9,11,9.4.0,10,4.0,11,4.0,12,4.0
16.6875,11.8125,0.37.25,11.8125,0,37.25,12.1875,0,16.6875,12.1875,0/
16.6875,11.8125,68.5625,37.25,11.8125,68.5625,37.25,12.1875,68.5625/
16.6875,12.1875,68.5625
BLOCK,1,7,7,11,11,9,13
16.6875,11.8125,68.5625,37.25,11.8125,68.5625,37.25,12.1875,68.5625/
16.6875,12.1875,68.5625,16.6875,11.8125,71.5625,37.25,11.8125,71.5625/
37.25,12.1875,71.5625,16.6875,12.1875,71.5625
BLOCK,1,7,7,13,11,9,15
16.6875,11.8125,71.5625,37.25,11.8125,71.5625,37.25,12.1875,71.5625/
16.6875,12.1875,71.5625,16.6875,11.8125,72.0,37.25,11.8125,72.0/
37.25,12.1875,72.0,16.6875,12.1875,72.0
BLOCK,1,7,9,13,11,13,15
16.6875,12.1875,71.5625,37.25,12.1875,71.5625,37.25,18.1875,71.5625/
16.6875,18.1875,71.5625,16.6875,12.1875,72.0,37.25,12.1875,72.0/
37.25,18.1875,72.0,16.6875,18.1875,72.0
BLOCK,1,7,13,13,11,15,15
16.6875,18.1875,71.5625,37.25,18.1875,71.5625,37.25,20.1875,71.5625/
16.6875,20.1875,71.5625,16.6875,18.1875,72.0,37.25,18.1875,72.0/
37.25,20.1875,72.0,16.6875,20.1875,72.0
BLOCK,1,5,9,11,7,13,13
16.25,12.1875,68.5625,16.6875,12.1875,68.5625,16.6875,18.1875,68.5625/
16.25,18.1875,68.5625,16.25,12.1875,71.5625,16.6875,12.1875,71.5625/
16.6875,18.1875,71.5625,16.25,18.1875,71.5625
END,GRID
BRICK,1,5,11,11
PRISM,1,7,11,11,7,9,11,7,11,13,5,11,11,5,9,11/
5,11,13,7,10,11,7,10,12,7,11,12,6,11,11/
6,9,11,6,11,13,5,10,11,5,10,12,5,11,12
JLOOP,8
KLOOP,7
BRICK,1,1,1,1
KEND
JEND
ILOOP,4
KLOOP,7
BRICK,1,3,7,1
KEND
IEND
JLOOP,2
KLOOP,5
BRICK,1,5,9,1
KEND
JEND
JLOOP,2
ILOOP,4
BRICK,1,3,3,13
IEND
JEND
JLOOP,3
```

```
ILOOP,4
BRICK,1,3,9,13
IEND
JEND
JLOOP,8
BC,PRESSURE,1,1,1,6,-180.0,-173.96,-173.96,-180.0
JEND
BC,PRESSURE,3,7,1,6,-173.96,-101.48,-101.48,-173.96
JLOOP,3
BC,PRESSURE,5,7,1,6,-101.48,-99.36,-99.36,-101.48
JEND
BC,PRESSURE,7,7,1,6,-99.36,-49.68,-49.68,-99.36
BC,PRESSURE,9,7,1,6,-49.68,0.0,0.0,0.0,-49.68
JLOOP,8
BC,SLOPE,1,1,13,3
JEND
ILOOP,4
JLOOP,6
BC,SLOPE,3,3,13,3
JEND
IEND
ILOOP,4
BC,SLOPE,3,3,13,5
IEND
ILOOP,4
BC,SLOPE,3,13,13,2
IEND
JLOOP,8
BC,UX,1,1,13,5
BC,UX,1,1,13,20
JEND
BC,UX,1,15,13,8
KLOOP,7
BC,UZ,9,7,1,2
BC,UZ,9,7,1,10
BC,UZ,9,7,1,3
BC,UZ,9,7,1,14
BC,UZ,9,7,1,15
KEND
END,ELEMENTS
SOLVE
REZONE,5,9,9,7,13,11
REFINE,GRIDS,5,9,9,2,5,5
BCR,REZONE,5,9,9,0,0,2,0,2,2,1,1,1
REFINE,GRIDS,5,11,9,2,3,5
BCR,REZONE,5,11,9,0,0,2,0,0,2,1,11,1
END
SOLVE
POST
BLOCK,,4
OPTION,2
END,STRESS
STOP
```

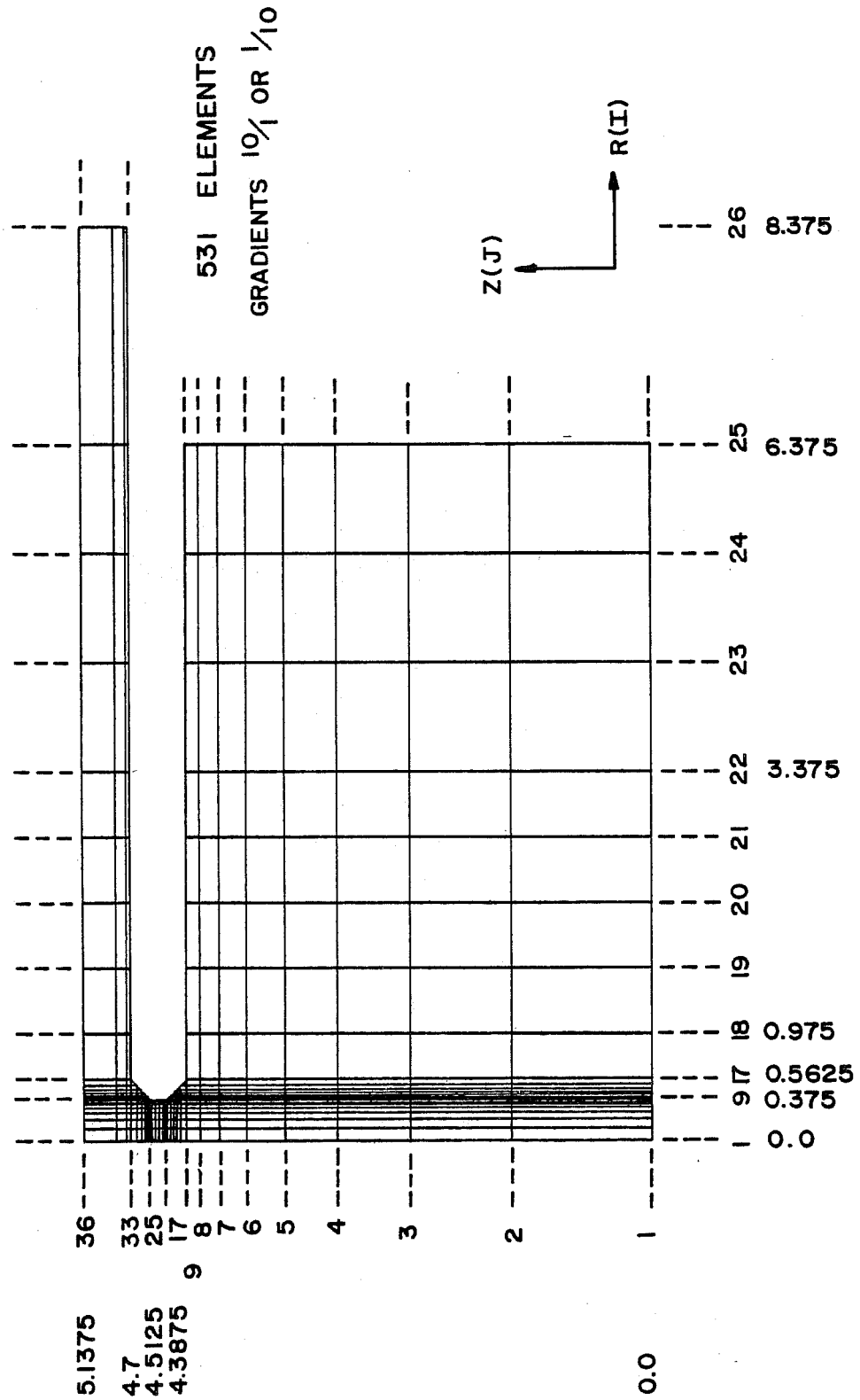

Fig. A.11 Two-dimensional finite element model grid definition of existing detail

```
$ STIFFENER INTERSECTION
SETUP,,,26
STEEL,1,29.E03,0.3
END,MATERIALS
1,1,9,9,10.0,10.0,10.0,10.0
0.0,0.375,0.375,0.0
0.0,0.0,4.2,4.2
9,1,17,9,0.10,10.0,0.0,10,10.0
0.375,0.5625,0.5625,0.375
0.0,0.0,4.2,4.2
17,1,18,9,1.0,10.0,1.0,10.0
0.5625,0.975,0.975,0.5625
0.0,0.0,4.2,4.2
18,1,22,9,1.0,10.0,1.0,10.0
0.975,3.375,3.375,0.975
0.0,0.0,4.2,4.2
22,1,25,9,1.0,10.0,1.0,10.0
3.375,6.375,6.375,3.375
0.0,0.0,4.2,4.2
1,9,9,17,10.0,10.0,10.0,10.0
0.0,0.375,0.375,0.0
4.2,4.2,4.3875,4.3875
9,9,17,17,0.10,10.0,0.0,10,10.0
0.375,0.5625,0.5625,0.375
4.2,4.2,4.3875,4.3875
1,17,9,21,10.0,0.10,10.0,0.0.10
0.0,0.375,0.375,0.0
4.3875,4.3875,4.45,4.45
1,21,9,25,10.0,10.0,10.0,10.0
0.0,0.375,0.375,0.0
4.45,4.45,4.5125,4.5125
1,25,9,33,10.0,0.10,10,10.0,0.10
0.0,0.375,0.375,0.0
4.5125,4.5125,4.7,4.7
9,25,17,33,0.10,0.10,0.10,0.10
0.375,0.5625,0.5625,0.375
4.5125,4.5125,4.7,4.7
1,33,9,36,10.0,0.10,10,10.0,0.10
0.0,0.375,0.375,0.0
4.7,4.7,5.1375,5.1375
9,33,17,36,0.10,0.10,0.10,0.10
0.375,0.5625,0.5625,0.375
4.7,4.7,5.1375,5.1375
17,33,18,36,1.0,0.10,1.0,0.10
0.5625,0.975,0.975,0.5625
4.7,4.7,5.1375,5.1375
18,33,22,36,1.0,0.10,1.0,0.10
0.975,3.375,3.375,0.975
4.7,4.7,5.1375,5.1375
22,33,25,36,1.0,0.10,1.0,0.10
3.375,6.375,6.375,3.375
4.7,4.7,5.1375,5.1375
25,33,26,36,1.0,0.10,1.0,0.10
6.375,8.375,8.375,6.375
4.7,4.7,5.1375,5.1375
END,GRID
ILOOP,8,1
JLOOP,35,1
QUAD8,1,1,1
JEND
IEND
```

Fig. A.12 TEXGAP-2D input listing for fine mesh of existing detail

```
ILOOP,16,1
JLOOP,8,1
QUAD8,1,9,1
JEND
IEND
ILOOP,17,1
JLOOP,3,1
QUAD8,1,9,33
JEND
IEND
JLOOP,7,1
QUAD8,1,9,9
QUAD8,1,9,26
JEND
JLOOP,6,1
QUAD8,1,10,9
QUAD8,1,10,27
JEND
JLOOP,5,1
QUAD8,1,11,9
QUAD8,1,11,28
JEND
JLOOP,4,1
QUAD8,1,12,9
QUAD8,1,12,29
JEND
JLOOP,3,1
QUAD8,1,13,9
QUAD8,1,13,30
JEND
JLOOP,2,1
QUAD8,1,14,9
QUAD8,1,14,31
JEND
QUAD8,1,15,9
QUAD8,1,15,32
TRI,1,9,16,10,16,9,17
TRI,1,10,15,11,15,10,16
TRI,1,11,14,12,14,11,15
TRI,1,12,13,13,13,12,14
TRI,1,13,12,14,12,13,13
TRI,1,14,11,15,11,14,12
TRI,1,15,10,16,10,15,11
TRI,1,16,9,17,9,16,10
TRI,1,9,25,10,26,9,26
TRI,1,10,26,11,27,10,27
TRI,1,11,27,12,28,11,28
TRI,1,12,28,13,29,12,29
TRI,1,13,29,14,30,13,30
TRI,1,14,30,15,31,14,31
TRI,1,15,31,16,32,15,32
TRI,1,16,32,17,33,16,33
ILOOP,25,1
BC,SLOPE,1,35,3
IEND
JLOOP,3,1
BC,SLOPE,25,33,2
JEND
BC,UR,1,1,1,-0.082330
BC,UZ,1,1,1,-0.015256
BC,UR,9,1,1,-0.082916
BC,UZ,9,1,1,-0.022712
```

```
BC,UR,18,1,1,-0.083651
BC,UZ,18,1,1,-0.035358
BC,UR,19,1,1,-0.084282
BC,UZ,19,1,1,-0.048021
BC,UR,20,1,1,-0.084753
BC,UZ,20,1,1,-0.060619
BC,UR,21,1,1,-0.085079
BC,UZ,21,1,1,-0.073098
BC,UR,22,1,1,-0.085291
BC,UZ,22,1,1,-0.085436
BC,UR,23,1,1,-0.085478
BC,UZ,23,1,1,-0.105690
BC,UR,24,1,1,-0.085517
BC,UZ,24,1,1,-0.125660
BC,UR,24,1,2,-0.085426
BC,UZ,24,1,2,-0.145540
END,ELEMENTS
PLANE,STRESS
PLOT,ELEMENTS,0.0,4.3,0.5625,4.45
END,PLOT
STOP
```

A.3.2 Existing Detail Ultra-Fine Mesh. Figure A.13 defines the grid in the gap region of the existing detail. The ultra-fine mesh is obtained by rezoning this grid along the prospective crack path. A listing of the input data is presented in Fig. A.14.

A.3.3 Cope Detail Fine Mesh. The cope detail fine mesh grid definition is given in Fig. A.15. A complete listing of the input used to analyze the fine mesh is presented in Fig. A.16.

A.3.4 Cope Detail Ultra-Fine Mesh. Figure A.17 defines the grid in the region of the web-to-longitudinal stiffener weld toe of the cope detail. This grid is rezoned along the prospective crack path to obtain the ultra-fine mesh. Figure A.18 lists the input data.

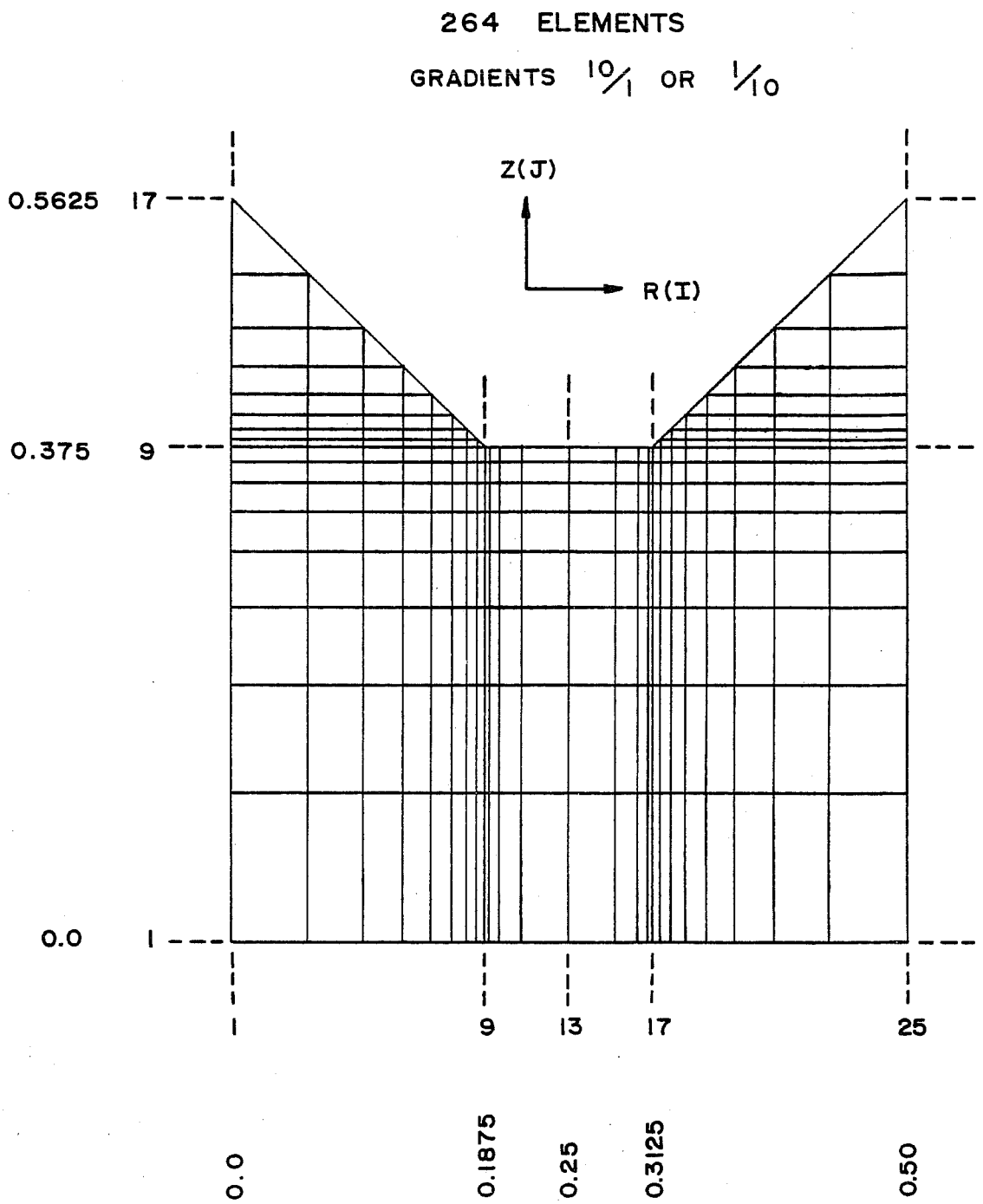

Fig. A.13 Existing detail grid definition for 1/2 in. gap region

```
$ STIFFENER INTERSECTION
SETUP,,,25
STEEL,1,29.E03,0.3
END,MATERIALS
1,1,9,9,10.0,10.0,10.0,10.0
0.0,0.1875,0.1875,0.0
0.0,0.0,0.375,0.375
9,1,13,9,0.10,10.0,0.0,10,10.0
0.1875,0.25,0.25,0.1875
0.0,0.0,0.375,0.375
13,1,17,9,10.0,10.0,10.0,10.0
0.25,0.3125,0.3125,0.25
0.0,0.0,0.375,0.375
17,1,25,9,0.10,10.0,0.10,10.0
0.3125,0.5,0.5,0.3125
0.0,0.0,0.375,0.375
1,9,9,17,10.0,0.10,10.0,0.10
0.0,0.1875,0.1875,0.0
0.375,0.375,0.5625,0.5625
17,9,25,17,0.10,0.10,0.10,0.10
0.3125,0.5,0.5,0.3125
0.375,0.375,0.5625,0.5625
END,GRID
ILOOP,24,1
JLOOP,8,1
QUAD8,1,1,1
JEND
IEND
ILOOP,7,1
QUAD8,1,1,9
QUAD8,1,18,9
IEND
ILOOP,6,1
QUAD8,1,1,10
QUAD8,1,19,10
IEND
ILOOP,5,1
QUAD8,1,1,11
QUAD8,1,20,11
IEND
ILOOP,4,1
QUAD8,1,1,12
QUAD8,1,21,12
IEND
ILOOP,3,1
QUAD8,1,1,13
QUAD8,1,22,13
IEND
ILOOP,2,1
QUAD8,1,1,14
QUAD8,1,23,14
IEND
QUAD8,1,1,15
QUAD8,1,24,15
TRI,1,1,16,2,16,1,17
TRI,1,2,15,3,15,2,16
TRI,1,3,14,4,14,3,15
TRI,1,4,13,5,13,4,14
TRI,1,5,12,6,12,5,13
TRI,1,6,11,7,11,6,12
TRI,1,7,10,8,10,7,11
```

Fig. A.14 TEXGAP-2D input listing for ultra-fine mesh of existing detail

```
TRI,1,8,9,9,9,8,10
TRI,1,17,9,18,9,18,10
TRI,1,18,10,19,10,19,11
TRI,1,19,11,20,11,20,12
TRI,1,20,12,21,12,21,13
TRI,1,21,13,22,13,22,14
TRI,1,22,14,23,14,23,15
TRI,1,23,15,24,15,24,16
TRI,1,24,16,25,16,25,17
BC,UZ,24,1,2,-0.0023408
BC,UR,24,1,2,0.0017786
BC,UZ,24,2,2,-0.0024418
BC,UR,24,2,2,0.0042435
BC,UZ,24,3,2,-0.0025981
BC,UR,24,3,2,0.0059122
BC,UZ,24,4,2,-0.0027586
BC,UR,24,4,2,0.0071828
BC,UZ,24,5,2,-0.0028948
BC,UR,24,5,2,0.0081813
BC,UZ,24,6,2,-0.0029971
BC,UR,24,6,2,0.0089599
BC,UZ,24,7,2,-0.0030690
BC,UR,24,7,2,0.0095551
BC,UZ,24,8,2,-0.0031179
BC,UR,24,8,2,0.010002
BC,UZ,24,9,2,-0.0031509
BC,UR,24,9,2,0.010332
BC,UZ,24,10,2,-0.0031665
BC,UR,24,10,2,0.010500
BC,UZ,24,11,2,-0.0031873
BC,UR,24,11,2,0.010736
BC,UZ,24,12,2,-0.0032141
BC,UR,24,12,2,0.011070
BC,UZ,24,13,2,-0.0032469
BC,UR,24,13,2,0.011542
BC,UZ,24,14,2,-0.0032835
BC,UR,24,14,2,0.012213
BC,UZ,24,15,2,-0.0033169
BC,UR,24,15,2,0.013166
BC,UZ,24,16,2,-0.0033353
BC,UR,24,16,2,0.014511
BC,UZ,24,16,3,-0.0033309
BC,UR,24,16,3,0.016403
BC,UZ,1,1,1,0.0031072
BC,UR,1,1,1,0.0023828
BC,UZ,1,2,1,0.0029820
BC,UR,1,2,1,0.0024627
BC,UZ,1,3,1,0.0028094
BC,UR,1,3,1,0.0026485
BC,UZ,1,4,1,0.0026371
BC,UR,1,4,1,0.0027231
BC,UZ,1,5,1,0.0024928
BC,UR,1,5,1,0.0026985
BC,UZ,1,6,1,0.0023849
BC,UR,1,6,1,0.0026245
BC,UZ,1,7,1,0.0023092
BC,UR,1,7,1,0.0025389
BC,UZ,1,8,1,0.0022578
BC,UR,1,8,1,0.0024604
BC,UZ,1,9,1,0.0022229
BC,UR,1,9,1,0.0023956
BC,UZ,1,10,1,0.0022063
```

```
BC,UR,1,10,1,0.0023608
BC,UZ,1,11,1,0.0021843
BC,UR,1,11,1,0.0023099
BC,UZ,1,12,1,0.0021557
BC,UR,1,12,1,0.0022345
BC,UZ,1,13,1,0.0021204
BC,UR,1,13,1,0.0021219
BC,UZ,1,14,1,0.0020803
BC,UR,1,14,1,0.0019533
BC,UZ,1,15,1,0.0020412
BC,UR,1,15,1,0.0017044
BC,UZ,1,16,1,0.0020134
BC,UR,1,16,1,0.0013481
BC,UZ,1,16,3,0.0019917
BC,UR,1,16,3,0.0008615
END,ELEMENTS
PLANE,STRESS
REZONE,,,,,1,5,,14,1,20,12
PLOT,ELEMENTS,0.0,0.0,0.0,0.5,0.5625
END,PLOT
STOP
```

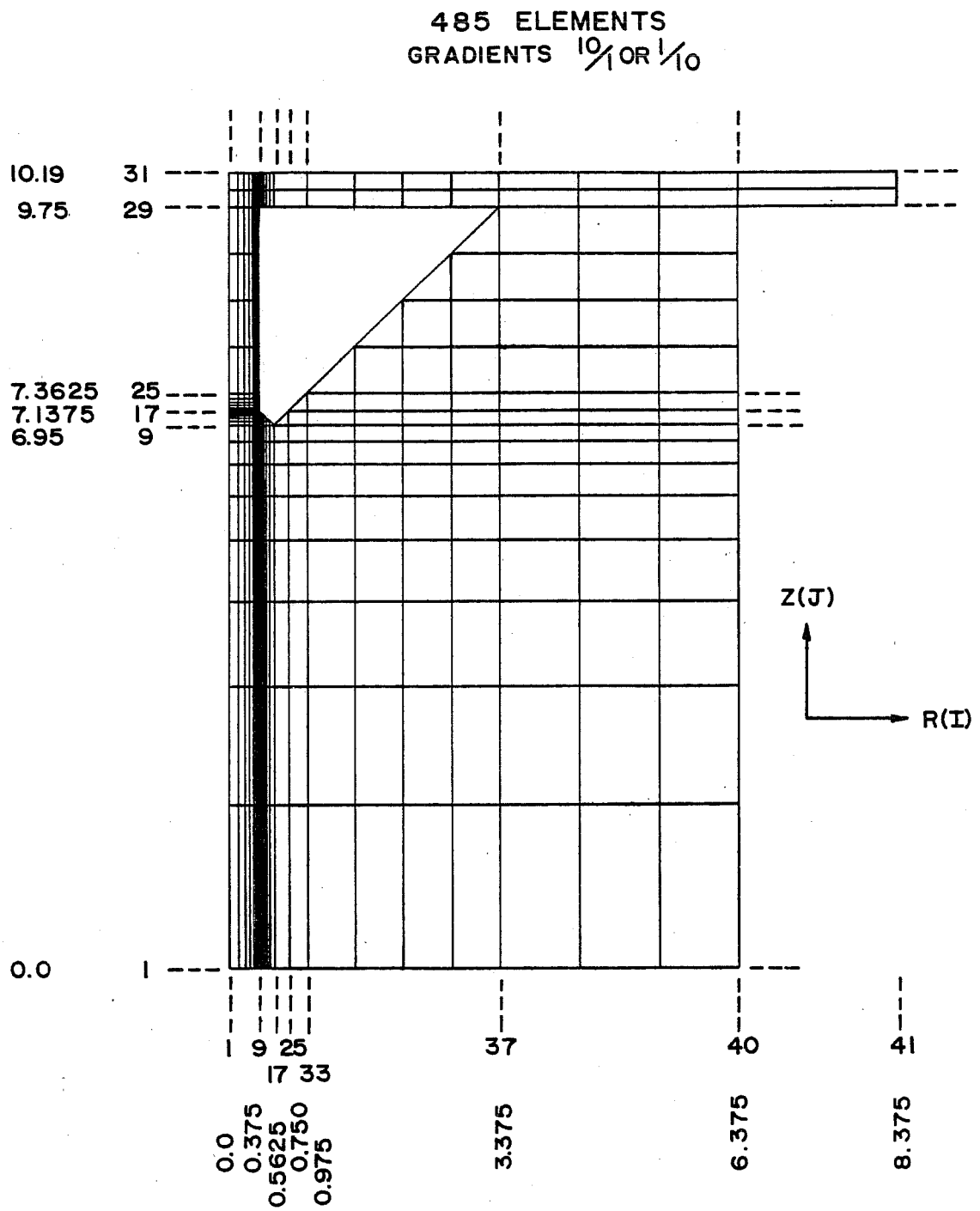

Fig. A.15 Two-dimensional finite element model grid definition of cope detail

```
$ STIFFENER  INTERSECTION
SETUP,,,41
STEEL,1,29.E03,0.3
END,MATERIALS
1,1,9,9,10.0,10.0,10.0,10.0,10.0
0,0,0.375,0.375,0.0
0.0,0.0,6.95,6.95
9,1,17,9,0.10,10.0,0,0.10,10.0
0.375,0.5625,0.5625,0.375
0.0,0.0,6.95,6.95
17,1,25,9,10.0,10.0,10.0,10.0,10.0
0.5625,0.750,0.750,0.5625
0.0,0.0,6.95,6.95
25,1,33,9,0.10,10.0,0,0.10,10.0
0.750,0.975,0.975,0.750
0.0,0.0,6.95,6.95
33,1,37,9,1.0,10.0,1.0,10.0
0.975,3.375,3.375,0.975
0.0,0.0,6.95,6.95
37,1,40,9,1.0,10.0,1.0,10.0
3.375,6.375,6.375,3.375
0.0,0.0,6.95,6.95
1,9,9,17,10.0,10.0,10.0,10.0,10.0
0.0,0.375,0.375,0.0
6.95,6.95,7.1375,7.1375
9,9,17,17,0.10,10.0,0,0.10,10.0
0.375,0.5625,0.5625,0.375
6.95,6.95,7.1375,7.1375
17,9,25,17,10.0,10.0,10.0,10.0,10.0
0.5625,0.750,0.750,0.5625
6.95,6.95,7.1375,7.1375
25,9,33,17,0.10,10.0,0,0.10,10.0
0.750,0.975,0.975,0.750
6.95,6.95,7.1375,7.1375
33,9,37,17,1.0,10.0,1.0,10.0
0.975,3.375,3.375,0.975
6.95,6.95,7.1375,7.1375
37,9,40,17,1.0,10.0,1.0,10.0
3.375,6.375,6.375,3.375
6.95,6.95,7.1375,7.1375
1,17,9,25,10.0,0,10,10.0,0.10
0.0,0.375,0.375,0.0
7.1375,7.1375,7.3625,7.3625
25,17,33,25,0,10,0,10,0.10,0.10
0.750,0.975,0.975,0.750
7.1375,7.1375,7.3625,7.3625
33,17,37,25,1.0,0.0,10,1.0,0,0.10
0.975,3.375,3.375,0.975
7.1375,7.1375,7.3625,7.3625
37,17,40,25,1.0,0.0,10,1.0,0,0.10
3.375,6.375,6.375,3.375
7.1375,7.1375,7.3625,7.3625
1,25,9,26,10.0,1.0,10.0,1.0
0.0,0.375,0.375,0.0
7.3625,7.3625,7.95,7.95
33,25,37,26
0.975,3.375,3.375,0.975
7.3625,7.3625,7.95,7.95
37,25,40,26
3.375,6.375,6.375,3.375
7.3625,7.3625,7.95,7.95
```

Fig. A.16 TEXGAP-2D input listing for fine mesh of cope detail

```
1,26,9,29,10.0,1.0,10.0,1.0
0.0,0.375,0.375,0.0
7.95,7.95,9.75,9.75
33,26,37,29
0.975,3.375,3.375,0.975
7.95,7.95,9.75,9.75
37,26,40,29
3.375,6.175,6.375,3.375
7.95,7.95,9.75,9.75
1,29,9,31,10.0,1.0,10.0,1.0
0.0,0.375,0.375,0.0
9.75,9.75,10.19,10.19
9,29,17,31,0.10,1.0,0,10,1.0
0.375,0.5625,0.5625,0.375
9.75,9.75,10.19,10.19
17,29,25,31,10.0,1.0,10.0,1.0
0.5625,0.750,0.750,0.5625
9.75,9.75,10.19,10.19
25,29,33,31,0.10,1.0,0.10,1.0
0.750,0.975,0.975,0.750
9.75,9.75,10.19,10.19
33,29,37,31
0.975,3.375,3.375,0.975
9.75,9.75,10.19,10.19
37,29,40,31
3.375,6.375,6.375,3.375
9.75,9.75,10.19,10.19
40,29,41,31
6.375,8.375,8.375,6.375
9.75,9.75,10.19,10.19
END,GRID
ILOOP,8,1
JLOOP,30,1
QUAD8,1,1,1
JEND
IEND
ILOOP,8,1
JLOOP,8,1
QUAD8,1,9,1
JEND
IEND
JLOOP,7,1
QUAD8,1,9,9
JEND
JLOOP,6,1
QUAD8,1,10,9
JEND
JLOOP,5,1
QUAD8,1,11,9
JEND
JLOOP,4,1
QUAD8,1,12,9
JEND
JLOOP,3,1
QUAD8,1,13,9
JEND
JLOOP,2,1
QUAD8,1,14,9
JEND
QUAD8,1,15,9
TRI,1,9,16,10,16,9,17
TRI,1,10,15,11,15,10,16
```

```
TRI,1,11,14,12,14,11,15
TRI,1,12,13,13,13,12,14
TRI,1,13,12,14,12,13,13
TRI,1,14,11,15,11,14,12
TRI,1,15,10,16,10,15,11
TRI,1,16,9,17,9,16,10
JLOOP,2,1
ILOOP,8,1
QUAD8,1,9,29
IEND
JEND
QUAD8,1,17,29,33,29,33,30,17,30
QUAD8,1,17,30,33,30,33,31,17,31
QUAD8,1,17,1,25,1,25,2,17,2
QUAD8,1,17,2,25,2,25,3,17,3
QUAD8,1,17,3,25,3,25,4,17,4
QUAD8,1,17,4,25,4,25,5,17,5
QUAD8,1,17,5,25,5,25,6,17,6
QUAD8,1,17,6,25,6,25,7,17,7
QUAD8,1,17,7,25,7,25,8,17,8
QUAD8,1,17,8,25,8,25,9,17,9
TRI,1,17,9,25,9,25,17
QUAD8,1,25,1,33,1,33,2,25,2
QUAD8,1,25,2,33,2,33,3,25,3
QUAD8,1,25,3,33,3,33,4,25,4
QUAD8,1,25,4,33,4,33,5,25,5
QUAD8,1,25,5,33,5,33,6,25,6
QUAD8,1,25,6,33,6,33,7,25,7
QUAD8,1,25,7,33,7,33,8,25,8
QUAD8,1,25,8,33,8,33,9,25,9
QUAD8,1,25,9,33,9,33,17,25,17
TRI,1,25,17,33,17,33,25
JLOOP,8,1
ILOOP,4,1
QUAD8,1,33,1
IEND
JEND
QUAD8,1,33,9,34,9,34,17,33,17
QUAD8,1,34,9,35,9,35,17,34,17
QUAD8,1,35,9,36,9,36,17,35,17
QUAD8,1,36,9,37,9,37,17,36,17
QUAD8,1,33,17,34,17,34,25,33,25
QUAD8,1,34,17,35,17,35,25,34,25
QUAD8,1,35,17,36,17,36,25,35,25
QUAD8,1,36,17,37,17,37,25,36,25
QUAD8,1,34,25,35,25,35,26,34,26
QUAD8,1,35,25,36,25,36,26,35,26
QUAD8,1,36,25,37,25,37,26,36,26
QUAD8,1,35,26
QUAD8,1,36,26,37,26,37,27,36,27
QUAD8,1,36,27,37,27,37,28,36,28
TRI,1,33,25,34,25,34,26
TRI,1,34,26,35,26,35,27
TRI,1,35,27,36,27,36,28
TRI,1,36,28,37,28,37,29
JLOOP,2,1
ILOOP,4,1
QUAD8,1,33,29
IEND
JEND
JLOOP,8,1
ILOOP,3,1
```

```
QUAD8,1,37,1
IEND
JEND
QUAD8,1,37,9,38,9,38,17,37,17
QUAD8,1,38,9,39,9,39,17,38,17
QUAD8,1,39,9,40,9,40,17,39,17
QUAD8,1,37,17,38,17,38,25,37,25
QUAD8,1,38,17,39,17,39,25,38,25
QUAD8,1,39,17,40,17,40,25,39,25
JLOOP,6,1
ILOOP,3,1
QUAD8,1,37,25
IEND
JEND
JLOOP,2,1
QUAD8,1,40,29
JEND
ILOOP,16,1
BC,SLOPE,1,30,3
IEND
BC,SLOPE,17,30,3
ILOOP,8,1
BC,SLOPE,33,29,3
IEND
JLOOP,2,1
BC,SLOPE,40,29,2
JEND
BC,UR,1,1,1,0.0055856
BC,UZ,1,1,1,-0.033993
BC,UR,9,1,1,0.0051921
BC,UZ,9,1,1,-0.034119
BC,UR,33,1,1,0.0045951
BC,UZ,33,1,1,-0.034230
BC,UR,34,1,1,0.0040245
BC,UZ,34,1,1,-0.034424
BC,UR,35,1,1,0.0034802
BC,UZ,35,1,1,-0.034702
BC,UR,36,1,1,0.0029624
BC,UZ,36,1,1,-0.035062
BC,UR,37,1,1,0.0024710
BC,UZ,37,1,1,-0.035504
BC,UR,38,1,1,0.0014613
BC,UZ,38,1,1,-0.035773
BC,UR,39,1,1,0.00041161
BC,UZ,39,1,1,-0.036012
BC,UR,39,1,2,-0.0006781
BC,UZ,39,1,2,-0.036219
END,ELEMENTS
PLOT,ELEMENTS,0.0,6.9,0.5625,7.4
PLANE,STRESS
END,PLOT
STOP
```

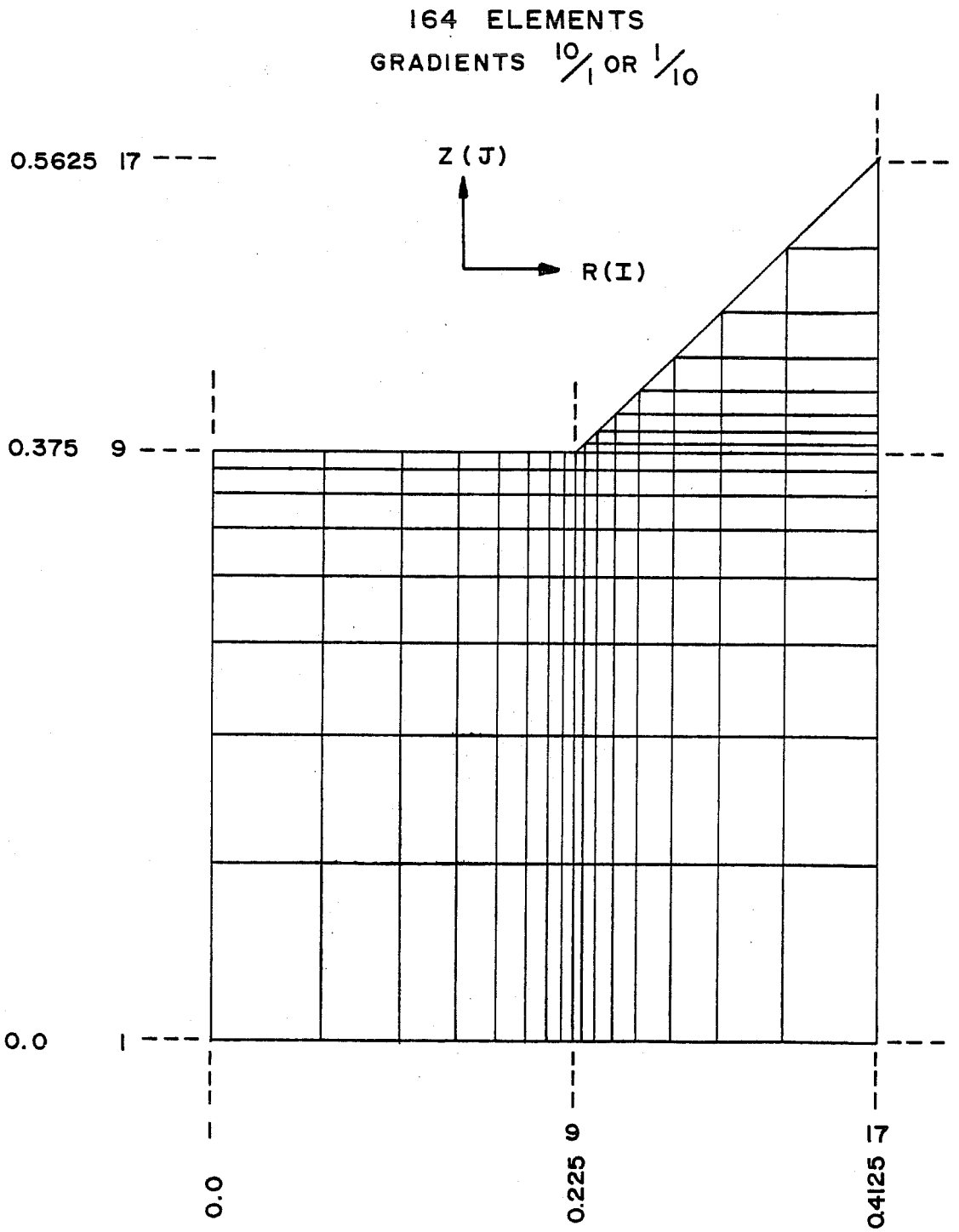

Fig. A.17 Cope detail grid definition which is rezoned to obtain an ultra-fine mesh in an area local to the weld toe

```
$ STIFFENER INTERSECTION
SETUP
STEEL,1,29.E03,0.3
END,MATERIALS
1,1,9,9,10.0,10.0,10.0,10.0
0,0,0.225,0.225,0.0
0.0,0.0,0.375,0.375
9,1,17,9,0.10,10.0,0.0,10,10.0
0.225,0.4125,0.4125,0.225
0.0,0.0,0.375,0.375
9,9,17,17,0.10,0.10,0,10,0.10
0.225,0.4125,0.4125,0.225
0.375,0.375,0.5625,0.5625
END,GRID
ILOOP,16,1
JLOOP,8,1
QUAD8,1,1,1
JEND
IEND
ILOOP,7,1
QUAD8,1,10,9
IEND
ILOOP,6,1
QUAD8,1,11,10
IEND
ILOOP,5,1
QUAD8,1,12,11
IEND
ILOOP,4,1
QUAD8,1,13,12
IEND
ILOOP,3,1
QUAD8,1,14,13
IEND
ILOOP,2,1
QUAD8,1,15,14
IEND
QUAD8,1,16,15
TRI,1,9,9,10,9,10,10
TRI,1,10,10,11,10,11,11
TRI,1,11,11,12,11,12,12
TRI,1,12,12,13,12,13,13
TRI,1,13,13,14,13,14,14
TRI,1,14,14,15,14,15,15
TRI,1,15,15,16,15,16,16
TRI,1,16,16,17,16,17,17
BC,UZ,16,1,2,0.0077910
BC,UR,16,1,2,0.017306
BC,UZ,16,2,2,0.0076054
BC,UR,16,2,2,0.017885
BC,UZ,16,3,2,0.0074581
BC,UR,16,3,2,0.018289
BC,UZ,16,4,2,0.0073383
BC,UR,16,4,2,0.018613
BC,UZ,16,5,2,0.0072453
BC,UR,16,5,2,0.018878
BC,UZ,16,6,2,0.0071764
BC,UR,16,6,2,0.019091
BC,UZ,16,7,2,0.0071271
BC,UR,16,7,2,0.019255
BC,UZ,16,8,2,0.0070921
```

Fig. A.18 TEXGAP-2D input listing for ultra-fine mesh of cope detail

```
BC,UR,16,8,2,0,.0193A0
BC,UZ,16,9,2,0,.0070637
BC,UR,16,9,2,0,.019473
BC,UZ,16,10,2,0,.0070551
BC,UR,16,10,2,0,.019520
BC,UZ,16,11,2,0,.0070382
BC,UR,16,11,2,0,.019587
BC,UZ,16,12,2,0,.0070152
BC,UR,16,12,2,0,.019681
BC,UZ,16,13,2,0,.0069839
BC,UR,16,13,2,0,.019814
BC,UZ,16,14,2,0,.0069410
BC,UR,16,14,2,0,.020003
BC,UZ,16,15,2,0,.0068806
BC,UR,16,15,2,0,.020270
BC,UZ,16,16,2,0,.0067810
BC,UR,16,16,2,0,.020646
BC,UZ,16,16,3,0,.0065475
BC,UR,16,16,3,0,.021169
BC,UZ,1,1,1,0,.0097125
BC,UR,1,1,1,0,.015595
BC,UZ,1,2,1,0,.0095682
BC,UR,1,2,1,0,.015863
BC,UZ,1,3,1,0,.0094412
BC,UR,1,3,1,0,.016067
BC,UZ,1,4,1,0,.0093357
BC,UR,1,4,1,0,.016213
BC,UZ,1,5,1,0,.0092518
BC,UR,1,5,1,0,.016314
BC,UZ,1,6,1,0,.0091873
BC,UR,1,6,1,0,.016385
BC,UZ,1,7,1,0,.0091388
BC,UR,1,7,1,0,.016433
BC,UZ,1,8,1,0,.0091031
BC,UR,1,8,1,0,.016466
BC,UZ,1,8,4,0,.0090769
BC,UR,1,8,4,0,.016489
END,ELEMENTS
PLANE,STRESS
REZONE,,,,,1,5,,6,1,12,12
PLOT,ELEMENTS,0.0,0.0,0.0,0.4125,0.5625
END,PLOT
STOP
```

N O T A T I O N

a = crack size, minor axis semidiameter of elliptical crack, in.

A = constant which is a function of detail geometry

Δa = increment of crack growth, in.

a_{avg} = average crack size, in.

a_{cr} = critical crack size, in.

$a_{d_{field}}$ = largest undetectable defect size using field inspection, in.

$a_{d_{shop}}$ = largest undetectable defect size using shop inspection, in.

a_f = final crack size, in.

a_i = initial crack size, in.

b_i = distance from the crack origin to the near side of element i, in.

b_{i+1} = distance from the crack origin to the far side of element i, in.

B_s = longitudinal stiffener width, in.

c = major axis semidiameter of elliptical crack, in.

C = material constant

D = unsupported distance between girder flange components, in.

d_o = distance between transverse stiffeners, in.

d_s = distance along longitudinal stiffener measured from stiffener end, in.

E_k = complete elliptical integral

$F(a)$ = geometry correction function

f_b = flange bending stress, psi

F_e = crack shape correction factor

F_g = stress gradient correction factor

F_s = free surface correction factor

F_w = finite width correction factor

G = gap between longitudinal and transverse stiffeners, in.

H = weld size, in.

I = moment of inertia, $in.^4$

K = stress intensity factor, $ksi\sqrt{in.}$

K_I = mode I stress intensity factor, $ksi\sqrt{in.}$

ΔK = range of stress intensity, $ksi\sqrt{in.}$

K_C = fracture toughness, $ksi\sqrt{in.}$

K_t = stress concentration factor

ΔK_{th} = threshold stress intensity range, $ksi\sqrt{in.}$

ℓ = distance along crack path from weld toe, in.

n = material constant

N = number of cycles

ΔN = increment of number of cycles

P = fixed load, kips

S = section modulus, $in.^3$

SCF = maximum stress concentration factor at crack origin

S_R = stress range, ksi

S_{rth} = threshold stress range, ksi

t = plate thickness, in.

T_s = longitudinal stiffener thickness, in.

T_w = girder web thickness, in.

da/dN = rate of crack propagation

dC/da = rate of change of the compliance vs. crack size curve

α = nondimensionalized crack length, a/t

β = parametric angle measured from major axis of ellipse, radians

σ = nominal stress, ksi

B I B L I O G R A P H Y

1. Fisher, J. W., Frank, K. H., Hirt, M. A., and McNamee, B. M., "Effect of Weldments on the Fatigue Strength of Steel Beams," NCHRP Report 102, Highway Research Board, 1970.

2. Fisher, J. W., Albrecht, P. A., Yen, B. T., Klingerman, D. J., and McNamee, B. M., "Fatigue Strength of Steel Beams with Transverse Stiffeners and Attachments," NCHRP Report 147, Highway Research Board, 1974.

3. Fisher, J. W., Hausammann, H., Sullivan, M. D., and Pense, A. W., "Detection and Repair of Fatigue Damage in Welded Highway Bridges," NCHRP Report 206, Highway Research Board, 1979.

4. Irwin, G. R., "Analysis of Stresses and Strains Near the End of a Crack Traversing a Plate," Transactions, American Society of Mechanical Engineers, Series E, Vol. 24, No. 3, Sept. 1957.

5. Lubahn, J. D., "Experimental Determination of Energy Release Rate for Notch Bending and Notch Tension," Proceedings, American Society Testing Materials, Vol. 59, 1959, p. 885

6. Sprawley, J. E., Jones, M. H., and Gross, B., "Experimental Determination of the Dependence of Crack Extension Force on Crack Length for a Single-Edge-Notch Tension Specimen," Technical Note D-2396, NASA, August, 1964.

7. Frank, K. H., "The Fatigue Strength of Fillet Welded Connections," unpublished Ph.D. dissertation, Lehigh University, Bethlehem, Pa., October 1971.

8. Gurney, T. R., "Finite Element Analysis of Some Joints with the Welds Transverse to the Direction of Stress," Welding Institute Report No. R/RB/E 62/74, Cambridge, England, December 1974.

9. Kobayashi, A. S., "A Simple Procedure for Estimating Stress Intensity Factor in Region of High Stress Gradient," Significance of Defects in Welded Structures, Proceedings of the 1973 Japan-U.S. Seminar, University of Tokyo Press, Tokyo, Japan, 1974, p. 127.

10. Albrecht, P., and Yamada, K., "Rapid Calculation of Stress Intensity Factors," Journal of the Structural Division, ASCE, Vol. 103, No. ST2, Proc. Paper 12742, February 1977, pp. 377-389.

11. Zettlemoyer, N., and Fisher, J. W., "Stress Gradient Correction Factor for Stress Intensity at Welded Stiffeners and Cover Plates," Welding Journal, 56(12), December 1977, Research Suppl., pp. 393-s to 398-s.

12. Zettlemoyer, N., and Fisher, J. W., "Stress Gradient Correction Factor for Stress Intensity at Welded Gusset Plates," Welding Journal, 57(2), February 1978, Research Suppl., pp. 57-s to 62-s.

13. Signes, E. G., Baker, R. G., Harrison, J. D., and Burdekin, F. M., "Factors Affecting the Fatigue Strength of Welded High Strength Steels," British Welding Journal, Vol. 14, No. 3, March 1967, p. 108

14. Watkinson, F., Bodger, P. H., and Harrison, J. D., "The Fatigue Strength of Welded Joints in High Strength Steels and Methods for its Improvement," Proceedings, Fatigue of Welded Structures Conference, Welding Institute, Brighton, England, 1971.

15. Zettlemoyer, N., "Stress Concentration and Fatigue of Welded Details," unpublished Ph.D. dissertation, Lehigh University, Bethlehem, Pa., October 1976.

16. Irwin, G. R., "The Crack Extension Force for a Part Through Crack in a Plate," Transactions, ASME, Journal of Applied Mechanics, Vol. 29, No. 4, 1962.

17. Rolfe, S. T., and Barsom, J. M., Fracture and Fatigue Control in Structures—Applications of Fracture Mechanics, Prentice-Hall, Inc., Englewood Cliffs, N. J., 1977.

18. Tada, H., and Irwin, G. R., "K-Value Analysis for Cracks in Bridge Structures," Fritz Engineering Laboratory Report No. 399.1, Lehigh University, Bethlehem, Pa., June 1975.

19. Paris, C. P., and Sih, G. C., "Stress Analysis of Cracks," Fracture Toughness Testing and Its Applications, ASTM STP No. 381, 1965.

20. Zettlemoyer, N., and Fisher, J. W., "Stress Gradient and Crack Shape Effects on Stress Intensity at Welded Details," Welding Journal, 57(8), August 1978, Research Suppl., pp. 246-s to 250-s.

21. Frank, K. H., and Fisher, J. W., "Fatigue Strength of Fillet Welded Cruciform Joints," Journal of the Structural Division ASCE, Vol. 105, No. ST9, September 1979, pp. 1727-1740.

22. Dunham, R. S., and Becker, E. B., "Texas Grain Analysis Program (TEXGAP)," Texas Institute for Computation Mechanics, The University of Texas at Austin, 1973.

V I T A

David Alan Platten was born in Milwaukee, Wisconsin, on March 14, 1955, the son of Dolly Marie Platten and Jack Randall Platten. In 1973, after completing his work at Fairmont East High School, Kettering, Ohio, he enrolled in the College of Engineering at the University of Cincinnati, Cincinnati, Ohio. He received the degree of Bachelor of Science in Civil Engineering from the University of Cincinnati in June 1978. In August 1978, he entered The Graduate School of The University of Texas at Austin and worked as a Research Assistant at the Phil M. Ferguson Structural Engineering Laboratory.

Permanent address: 4939 Harwich Court
Kettering, Ohio 45440

This thesis was typed by Maxine R. DeButts and Tina Robinson.